



National Library
of Canada

Bibliothèque nationale
du Canada

Canadian Theses Service

Service des thèses canadiennes

Ottawa, Canada
K1A 0N4

NOTICE

The quality of this microform is heavily dependent upon the quality of the original thesis submitted for microfilming. Every effort has been made to ensure the highest quality of reproduction possible.

If pages are missing, contact the university which granted the degree.

Some pages may have indistinct print especially if the original pages were typed with a poor typewriter ribbon or if the university sent us an inferior photocopy.

Reproduction in full or in part of this microform is governed by the Canadian Copyright Act, R.S.C. 1970, c. C-30, and subsequent amendments.

AVIS

La qualité de cette microforme dépend grandement de la qualité de la thèse soumise au microfilmage. Nous avons tout fait pour assurer une qualité supérieure de reproduction.

S'il manque des pages, veuillez communiquer avec l'université qui a conféré le grade.

La qualité d'impression de certaines pages peut laisser à désirer, surtout si les pages originales ont été dactylographiées à l'aide d'un ruban usé ou si l'université nous a fait parvenir une photocopie de qualité inférieure.

La reproduction, même partielle, de cette microforme est soumise à la Loi canadienne sur le droit d'auteur, SRC 1970, c. C-30, et ses amendements subséquents.

UNIVERSITY OF ALBERTA

**ANALYSIS OF THE PERMEABILITY AND BEHAVIOUR OF
DISSOCIABLE SPECIES IN ION-SELECTIVE MEMBRANES**

by



ELISABETH M. J. VERPOORTE

A THESIS SUBMITTED TO
THE FACULTY OF GRADUATE STUDIES AND RESEARCH
IN PARTIAL FULFILLMENT OF
THE REQUIREMENTS FOR THE DEGREE OF
DOCTOR OF PHILOSOPHY

DEPARTMENT OF CHEMISTRY

EDMONTON, ALBERTA

FALL, 1990



National Library
of Canada

Bibliothèque nationale
du Canada

Canadian Theses Service Service des thèses canadiennes

Ottawa, Canada
K1A 0N4

The author has granted an irrevocable non-exclusive licence allowing the National Library of Canada to reproduce, loan, distribute or sell copies of his/her thesis by any means and in any form or format, making this thesis available to interested persons.

The author retains ownership of the copyright in his/her thesis. Neither the thesis nor substantial extracts from it may be printed or otherwise reproduced without his/her permission.

L'auteur a accordé une licence irrévocable et non exclusive permettant à la Bibliothèque nationale du Canada de reproduire, prêter, distribuer ou vendre des copies de sa thèse de quelque manière et sous quelque forme que ce soit pour mettre des exemplaires de cette thèse à la disposition des personnes intéressées.

L'auteur conserve la propriété du droit d'auteur qui protège sa thèse. Ni la thèse ni des extraits substantiels de celle-ci ne doivent être imprimés ou autrement reproduits sans son autorisation.

ISBN 0-315-64775-2

Canada

UNIVERSITY OF ALBERTA

RELEASE FORM

NAME OF AUTHOR: **Elisabeth M. J. Verpoorte**

TITLE OF THESIS: **Analysis of the Permeability and Behaviour of Dissociable
Species in Ion-Selective Membranes**

DEGREE FOR WHICH THESIS WAS PRESENTED: **Doctor of Philosophy**

YEAR THIS DEGREE GRANTED: **1990**

Permission is hereby granted to

THE UNIVERSITY OF ALBERTA LIBRARY

to reproduce single copies of this thesis, and to lend or sell such copies for private, scholarly or scientific research purposes only.

The author reserves other publication rights and neither the thesis, nor extensive extracts from it, may be printed or otherwise reproduced without the author's written permission.

AUTHOR'S SIGNATURE:

Elisabeth Verpoorte

PERMANENT ADDRESS: **11 Westgate Drive**

Halifax, Nova Scotia

B3P 1T7

DATE: *June 26, 1990*

UNIVERSITY OF ALBERTA

FACULTY OF GRADUATE STUDIES AND RESEARCH

The undersigned certify that they have read, and recommend to the Faculty of Graduate Studies and Research for acceptance, a thesis entitled

ANALYSIS OF THE PERMEABILITY AND BEHAVIOUR OF DISSOCIABLE SPECIES IN ION-SELECTIVE MEMBRANES

Submitted by

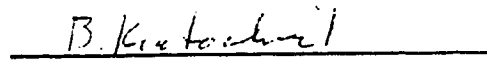
ELISABETH M. J. VERPOORTE

in partial fulfillment of the requirements for the degree of

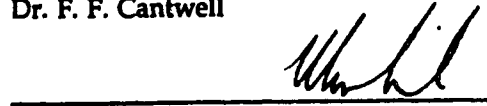
DOCTOR OF PHILOSOPHY

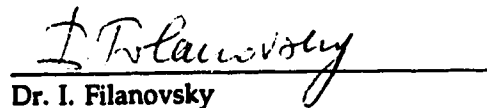
SUPERVISOR:


Dr. D. J. Harrison

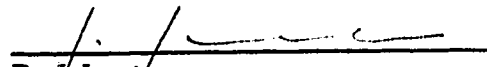

Dr. B. Kratochvil


Dr. F. F. Cantwell


Dr. M. Keil


Dr. I. Filanovsky

EXTERNAL EXAMINER:


Dr. J. Janata

DATE: June 14, 1990

ABSTRACT

The main objective of the research presented in this work was to obtain a better understanding of the response properties of a liquid K^+ -selective membrane which has found wide application in both ion-selective electrodes (ISE) and ion-sensitive field-effect transistors (ISFET). Of particular interest were the interference phenomena observed at ISE's and ISFET's in the presence of lipophilic anionic species and, in the latter case, neutral acidic species.

To facilitate studies of ISFET response, a membrane-coated silicon electrode was proposed as a model for the ISFET gate. Characterization of the impedance response of this electrode was made possible through an equivalent circuit model consisting of simple circuit elements. This allowed utilization of the AC impedance technique to gain information about the response properties of both the membrane itself and the silicon/insulator/membrane structure.

In studies examining the interference of benzoic acid at K^+ -selective ISFET's, capacitance-voltage and UV spectroscopic measurements verified the hypothesis that this neutral acid was capable of permeating the membrane and undergoing acid-base chemistry at the insulator interface, causing a change in the interfacial charge state. Passivation of the insulator surface was accomplished through interposition of a Ag/AgCl layer between the membrane and the insulator, resulting in elimination of this neutral species interference on electrode potential response.

The effect of permeation by benzoic acid and benzoate on the membrane itself was considered, and it was shown that ingress of both these species leads to decreased membrane resistivity being observed, though

neither species interferes with ISE response. Studies of the temperature dependence of membrane conductivity indicated that the acid contributed to membrane charge carrier concentration through acid dissociation. A detailed analysis of membrane conductance as a function of concentration enabled the determination of values of dissociation constants, K_d , and limiting conductances, Λ_0 , for benzoic acid, as well as for various benzoate salts and NaClO_4 . The acid dissociation constant for benzoic acid was found to be anomalously high, clearly demonstrating the effect that the presence of water in the membrane has on membrane properties and on chemical equilibria within this phase.

ACKNOWLEDGEMENTS

During my studies in the chemistry department at the University of Alberta, I have had the pleasure of meeting and working with many talented and wonderful people. The work presented in this thesis would have proven to be very difficult, if not impossible, without the varied help and support I have received from faculty, colleagues, and friends. I would like to express my appreciation to them all, in particular the following:

Dr. D. Jed Harrison, my Ph.D. supervisor, who has been the guiding force behind the research I've done throughout the course of the program. His encouragement and support have proven to be invaluable.

The members of the Harrison research group, all of whom have been great to work with. In particular, I'd like to thank Paul Glavina and Rob Turner for their friendship and support. I'd also like to acknowledge Xizhong Li, Andrew Chan, and Alebachew Demoz, all of whom I've collaborated with at one time or another, and whose work is mentioned in portions of this thesis.

Dr. Kratochvil, Dr. Cantwell, and other members of my examining committee, whose comments and suggestions were very useful in the preparation of this thesis.

The various shops and secretarial offices within the department, all of whom have been most helpful at one time or another. In particular, I'd like to thank Mr. E. Young, who was our consultant in the design of the cell used in many of the membrane studies.

Gordon Kennedy, whose typing and computer graphics skills are demonstrated in the lists of references and several figures in Chapters 1 and 2.

And last but not least...my gratitude is extended to my family and friends, both in and outside the department, who have provided moral support and encouragement during the difficult times, and made the good times so much fun.

The financial support provided by the Natural Sciences and Engineering Research Council of Canada during 1985-1986 is hereby also acknowledged.

TABLE OF CONTENTS

CHAPTER	PAGE
1. Introduction.....	1
1.1 The Ion-Selective Electrode.....	3
1.2 The ISFET	6
1.3 AC Impedance Analysis	17
1.4 Conductance of Electrolyte Solutions.....	26
1.5 References.....	38
2. A Semiconductor Electrode for Use in Studies of ISFET Structures	42
2.1 Introduction.....	42
2.2 The Model	43
2.3 Equivalent Circuit Analysis of the MIS Electrode	55
2.4 Experimental.....	62
2.5 Results and Discussion	69
2.6 Conclusion	100
2.7 References.....	103
3. A Characterization of Neutral Species Interference at the Ion-Sensitive Membrane/Semiconductor Interface.....	105
3.1 Introduction.....	105
3.2 Experimental.....	107
3.3 Results and Discussion.....	110

3.4	Conclusion	134
3.5	References.....	136
4.	A Study of Membrane Permeability by AC Impedance Analysis.....	138
4.1	Introduction.....	138
4.2	Experimental.....	141
4.3	Results and Discussion.....	147
4.4	Conclusion	170
4.5	References.....	173
5.	Behaviour of Dissociable Species in Liquid Ion-Selective Membranes	175
5.1	Introduction.....	175
5.2	Experimental.....	180
5.3	Calculation of Λ_0 and K_d	183
5.4	Results and Discussion.....	195
	5.4.1 Evaluation of Dissociation Constants (K_d) and Limiting Ionic Conductances (Λ_0) for Salts in the Membrane.....	195
	5.4.2 Dependence of Conductivity on Temperature	221
	5.4.3 Membrane Resistance as a Function of Benzoic Acid Concentration : Matrix	

	Effects.....	233
	5.4.4 Evaluation of Λ Data for Benzoic Acid.....	241
	5.5 Conclusion	248
	5.6 References.....	251
6.	Conclusions.....	253
	6.1 Summary of Progress.....	253
	6.2 Directions for Future Work.....	256
	6.3 References.....	260

LIST OF TABLES

TABLE	PAGE
2.1	Flatband potentials, V_{fb} , and flatband shifts, ΔV_{fb} , determined as a function of KCl concentration for two functional MIS electrodes87
2.2	Bulk membrane resistance, R_g , and capacitance, C_g , determined at each KCl concentration from the Nyquist plots for a n-Si/SiO ₂ /membrane electrode.....92
2.3	Flatband potentials, V_{fb} , and flatband shifts, ΔV_{fb} , determined as a function of KCl concentration for the MIS electrode whose C_{eq} -V curves are given in Figure 2.13.....96
2.4	Theoretical flatband potentials, V_{fb} , and flatband shifts, ΔV_{fb} , determined for R_s , C_g , and C_e values of 100 Ω , 100 pF, and 1 nF, respectively, with R_g assuming values given in Table 2.299
3.1	Changes in R_g and C_g as a function of added benzoate at pH 4.5 and pH 8.6, determined from Nyquist plots for a n-Si/SiO ₂ /Si ₃ N ₄ /membrane electrode..... 123
3.2	Flatband potentials, V_{fb} , and flatband shifts, ΔV_{fb} , determined from C-V curves which were measured as a function of Cl ⁻ concentration for a bare n-Si/SiO ₂ /Si ₃ N ₄ /Ag/AgCl electrode..... 126
3.3	Flatband potentials, V_{fb} , and flatband shifts, ΔV_{fb} , determined from C-V curves which were measured as a function of K ⁺ concentration for a n-Si/SiO ₂ /Si ₃ N ₄ /Ag/AgCl/membrane electrode..... 129
3.4	Changes in R_g and C_g measured as a function of added benzoate at pH 4.5 and pH 8.6 for a n-Si/SiO ₂ /Si ₃ N ₄ /Ag/AgCl/membrane electrode 133

4.1	Results of potentiometric response measurements in KCl, potassium benzoate and KClO ₄ solutions, maintained at a μ of 0.1	148
4.2	Bulk resistances, R_g , of membranes before and after a one hour exposure to a 0.01 M benzoate-containing solution, for membranes with and without KB(C ₆ H ₅) ₄	157
5.1	R_g and Λ_{cor} data measured for tetraethylammonium benzoate (TEAB) in normal membranes.....	196
5.2	R_g and Λ_{cor} data measured for potassium benzoate (KBz) (Series 1) in normal membranes.....	196
5.3	R_g and Λ_{cor} data measured for KBz (Series 2) in normal membranes.....	199
5.4	R_g and Λ_{cor} data measured for sodium benzoate (NaBz) in normal membranes.....	199
5.5	R_g and Λ_{cor} data measured for NaClO ₄ in normal membranes.....	202
5.6	R_g and Λ_{cor} data measured for TEAB in PVC/DOA membranes.....	202
5.7	R_g and Λ_{cor} data measured for KBz in PVC/DOA membranes.....	205
5.8	Dissociation constants (K_d) and limiting ionic conductances (Λ_0) from Λ data analysis for data sets given in Tables 5.1 through 5.7	207
5.9	Variation of experimentally determined K_d 's and Λ_0 's with λ for KBz and TEAB in normal and PVC/DOA matrices.....	215
5.10	Values of K_d predicted using Equation (35), at $\epsilon_r = 8$ for the membrane	216
5.11	A comparison of the relative magnitudes of the J_{ac} and $K_a \Lambda f^2 \alpha c$ terms of the Fuoss equation over a range of concentrations	217

5.12	Conductivity as a function of temperature for benzoic acid in PVC/DOA.....	225
5.13	Conductivity as a function of temperature for benzoic acid and methyl benzoate in PVC/DOA/KB(C ₆ H ₅) ₄	231
5.14	Bulk membrane resistances measured for benzoic acid in PVC/DOA/KB(C ₆ H ₅) ₄	234
5.15	Bulk membrane resistances, R_g , measured for benzoic acid in two series of normal membranes.....	234
5.16	R_g and Λ_{cor} data measured for benzoic acid in PVC/DOA/KB(C ₆ H ₅) ₄ membranes.....	242
5.17	R_g and Λ_{cor} data measured for benzoic acid in normal membranes (Series 2).....	244

LIST OF FIGURES

FIGURE	PAGE
1.1 Cross-sectional view of a MOS capacitor	11
1.2 Cross-sectional view of a MOSFET	13
1.3 Cross-sectional view of an ISFET	15
1.4 Representation of the impedance vector, Z , in the impedance plane	21
1.5 Nyquist plots for some simple circuit elements: a) a pure resistor, R ; b) a pure capacitor, C ; c) a resistor, R_s , and capacitor, C_s , in series; d) a resistor, R_p , and capacitor, C_p , in parallel.....	23
2.1 Interfacial structure of a MIS electrode	44
2.2 Energy band diagrams of an n-type Si-based MIS electrode at thermal equilibrium and no applied bias potential: a) ideal MIS electrode b) non-ideal electrode.....	46
2.3 Energy level diagrams of a MIS electrode under 4 different biasing conditions.....	52
2.4 Equivalent circuit model for the MIS electrode.....	56
2.5 Instrumental set-up used in capacitance-voltage (C_{eq} - V) and impedance measurements.....	64
2.6 The Nyquist plot expected for the equivalent circuit of Fig. 2.4	68
2.7(a) Nyquist plot of an n-Si/SiO ₂ /membrane electrode over a frequency range of 25 Hz to 40 kHz, measured in a solution containing 10 ⁻³ M KCl and buffered at pH 4.5	71
2.7(b) Plot of Z_{real}^{-1} vs ω^2 for the Nyquist plot of Figure 2.7(a).....	72

2.8(a)	Nyquist plot of the membrane-coated Pt electrode over a frequency range of 25 Hz to 40 kHz, measured in 0.1M KCl.....	73
2.8(b)	Plot of Z_{real}^{-1} vs ω^2 for the Nyquist plot of Fig. 2.8(a).....	74
2.9(a)	C_{eq} -V curves for an n-Si/SiO ₂ /membrane electrode obtained at 100 Hz and 10 kHz in 0.1 M KCl.....	76
2.9(b)	Model C_{eq} -V curves calculated for the MIS electrode of Figure 2.9(a) at 100 Hz and 10 kHz, using Equations (8)-(10)	77
2.10(a)	Quadrature-voltage curves for an n-Si/SiO ₂ /membrane electrode, obtained at 25, 40, 50, and 100 Hz in 0.1 M KCl.....	79
2.10(b)	Model C_{eq} -V curves calculated for the MIS electrode of Figure 2.10(a) at 25, 40, 50, and 100 Hz from Equations (8)-(10).....	81
2.11(a)	C_{eq} -V curves for an n-Si/SiO ₂ /membrane electrode acquired at 25 Hz as a function of K ⁺ concentration	83
2.11(b)	Mott-Schottky plots of C_{eq}^{-2} vs V for the C_{eq} -V curves of Figure 2.11(a) acquired at 25 Hz.....	84
2.12(a)	C_{eq} -V curves for an n-Si/SiO ₂ /Si ₃ N ₄ /membrane electrode acquired at 25 Hz as a function of K ⁺ concentration.....	85
2.12(b)	Mott-Schottky plots of C_{eq}^{-2} vs V for the C_{eq} -V curves of Figure 2.12(a) acquired at 25 Hz.....	86
2.13	C_{eq} -V curves for an n-Si/SiO ₂ /membrane electrode acquired at 100 Hz as a function of K ⁺ concentration	89
2.14	Nyquist plots for the MIS electrode of Figure 2.13 recorded over the frequency range 25 Hz to 20 kHz as a function of K ⁺ concentration.....	91
2.15	Theoretical C_{eq} -V curves calculated for the MIS electrode of Figure 2.13 as a function of R_g at a frequency of 100 Hz	93

2.16	Mott-Schottky plots of C_{eq}^{-2} vs V for the C_{eq} - V curves of Figure 2.13, recorded at 100 Hz.....	95
3.1	Absorbance spectra of K^+ sensitive PVC membranes following a 90-h immersion in solutions containing 0.1 M HCl, 0.1 M NaCl, and 10^{-3} M KCl, both with and without 0.01 M benzoic acid present.....	113
3.2	Calibration curve of absorbance change as a function of benzoic acid in the membrane, measured at 274 nm.....	114
3.3	Effect of added benzoate on the capacitance-voltage (C-V) curves of a bare n-Si/SiO ₂ /Si ₃ N ₄ electrode in solutions containing 10^{-3} M KCl and 0.1 M trisodium citrate adjusted to pH 4.5 and 8.6.....	118
3.4	Effect of added benzoate on the capacitance-voltage (C-V) curves of a n-Si/SiO ₂ /Si ₃ N ₄ / K^+ -membrane electrode in solutions containing 10^{-3} M KCl and 0.1 M trisodium citrate adjusted to a) pH 4.5 or b) 8.6.....	119
3.5	Nyquist plots recorded over frequencies ranging from 25 Hz to 40 kHz for the MIS electrode of Figure 3.4, showing the effect of added benzoate at a) pH4.5 and b) pH 8.6.....	121
3.6	C_{eq} - V curves for a bare n-Si/SiO ₂ /Si ₃ N ₄ /Ag/AgCl electrode acquired at 1000 Hz as a function of Cl^- concentration.....	125
3.7	C_{eq} - V curves for an n-Si/SiO ₂ /Si ₃ N ₄ /Ag/AgCl/membrane electrode acquired at 25 Hz as a function of K^+ concentration.....	128
3.8	Effect of added benzoate on the capacitance-voltage (C-V) curves of an n-Si/SiO ₂ /Si ₃ N ₄ / K^+ -membrane electrode in solutions containing 10^{-3} M KCl and 0.1 M trisodium citrate adjusted to a) pH 4.5 or b) 8.6.....	131

3.9	Nyquist plots recorded over frequencies ranging from 25 Hz to 40 kHz for the MIS electrode of Figure 3.4, showing the effect of added benzoate at a) pH 4.5 and b) pH 8.6.....	132
4.1	Side and end views of one half of the cell used in impedance measurements of free-standing membranes.....	144
4.2	Experimental set-up used in impedance measurements.....	146
4.3	Potentiometric response of ISE D-1 as a function of K^+ concentration in solutions containing KCl, KBz, and $KClO_4$	151
4.4	Effect of added ClO_4^- on the potentiometric response of ISE's D1, D2, and D3 in 0.01 M KCl at a constant μ of 0.1 (NaCl)	153
4.5	Nyquist plot for a portion of normal membrane over the frequency range 50 Hz to 40 kHz, showing the effect of added ClO_4^- on R_g	155
4.6	Calibration curve of % change in R_g ($\% \Delta R_g$) as a function of KBz concentration in a normal membrane matrix.....	163
4.7	Calibration curve of % change in R_g ($\% \Delta R_g$) as a function of $NaClO_4$ concentration in a normal membrane matrix.....	165
4.8	Calibration curve of % change in R_g ($\% \Delta R_g$) as a function of benzoic acid concentration in a normal membrane matrix.....	167
5.1	Curves of membrane resistance (R_g) vs concentration and corrected conductance (Λ_{COR}) vs the square root of concentration for TEAB in a normal membrane	197
5.2	Curves of membrane resistance (R_g) vs concentration and corrected conductance (Λ_{COR}) vs the square root of concentration for a series of normal membranes containing KBz at concentrations up to 0.005 M (Series 1).....	198

5.3	Curves of membrane resistance (R_g) vs concentration and corrected conductance (Λ_{cor}) vs the square root of concentration for a series of normal membranes containing KBz at concentrations up to 0.002 M (Series 2).....	200
5.4	Curves of membrane resistance (R_g) vs concentration and corrected conductance (Λ_{cor}) vs the square root of concentration for a series of normal membranes containing NaBz	201
5.5	Curves of membrane resistance (R_g) vs concentration and corrected conductance (Λ_{cor}) vs the square root of concentration for a series of normal membranes containing NaClO ₄	203
5.6	Curves of membrane resistance (R_g) vs concentration and corrected conductance (Λ_{cor}) vs the square root of concentration for a series of PVC/DOA membranes containing TEAB.....	204
5.7	Curves of membrane resistance (R_g) vs concentration and corrected conductance (Λ_{cor}) vs the square root of concentration for a series of PVC/DOA membranes containing KBz.....	206
5.8	Nyquist plot showing the effect of temperature on membrane impedance in a 10 ⁻³ M KCl ($\mu = 0.1$ (NaCl)) for a PVC/DOA membrane containing 0.0667 M benzoic acid.....	227
5.9	ln σ vs 1/T plots for the benzoic acid-containing PVC/DOA membrane of Figure 5.8 and the corresponding blank membrane.....	228
5.10	Plot of R_g vs concentration for benzoic acid in PVC/DOA/KTPB, showing the effect of benzoic acid on membrane impedance in this matrix	235

5.11	Plot of R_g vs concentration for benzoic acid in the normal matrix, showing the effect of benzoic acid on membrane impedance in this matrix.....	236
5.12	Plot of Λ_{cor} vs the square root of concentration for benzoic acid in PVC/DOA/KTPB for the R_g data of Figure 5.10.....	243
5.13	Plot of Λ_{cor} vs the square root of concentration for benzoic acid in the normal membranes for the R_g data of Figure 5.11.....	245

CHAPTER 1

INTRODUCTION

The study of chemical sensors comprises a broad field in the science of analytical chemistry. Very generally, a chemical sensor may be defined as any device which can convert a chemical signal into an electronic one. As such, chemical sensors function as interfaces between the chemical world and the electronic world, allowing the properties of chemical systems to be probed in an analytically useful manner through measurement of electrical signals. Much attention continues to be paid to the development of sensors for the determination of ionic species in solution. Sensors designed with this purpose in mind generally fall into two categories, that of ion-selective electrodes (ISE) and of chemically sensitive solid-state devices. Of particular importance in the latter group is a device known as the ion-sensitive field-effect-transistor (ISFET). The electrical signals of devices in both categories is determined by the response of an ion-sensitive material to the species of interest in solution. However, the manner in which this material or membrane is deployed in the sensor differentiates ISE's from their solid state counterparts. In ISE's, the membrane is exposed to solution at both interfaces, with one of these solutions serving as a reference. In ISFET's, one of the membrane/solution interfaces is replaced with a membrane/solid interface, with the result that these sensors are characterized by a response mechanism which is different from that of the ISE.

Because of the difference in interfacial structure, the ISE and ISFET each have some unique problems associated with their usage. Many of these problems stem from the necessity of making determinations of ion concentrations in solutions containing additional neutral and ionic species besides the species of interest. While many species adversely affect the response of both ISE's and ISFET's, ISFET's do suffer from certain interferences not observed for ISE's, and vice versa. In both cases, however, the origins of the interference phenomena observed lie in the response of the ion-selective membrane itself. Development of more selective and versatile ISE's and ISFET's requires a more fundamental knowledge of the response mechanisms of the ion-sensitive materials employed, and in the case of solid state devices, how this response affects the membrane/solid interface.

The work presented in this thesis is directed towards obtaining a better understanding of the response properties of a liquid K^+ -selective membrane, and how these properties are affected by certain interfering species. The liquid membrane examined consists of a 2:1 ratio of plasticizer (a water immiscible organic solvent) to poly(vinylchloride) and contains a neutral carrier, valinomycin, specific for K^+ . Since this membrane has found wide application in both K^+ -ISE's and K^+ -ISFET's, its response behaviour was considered with respect to both types of sensors, using the electrochemical method known as AC impedance analysis. In order to address certain interference phenomena observed in the presence of organic acids and CO_2 for K^+ -ISFET's coated with this membrane, a membrane-coated silicon electrode was proposed and subsequently employed as a model for ISFET response. The results of these studies, presented in Chapters 2 and 3, motivated the closer examination of membrane permeability undertaken in Chapter 4. An analysis of ion and neutral species behaviour within the

membrane proper, through measurement of membrane conductance, is described in Chapter 5. Since these studies were all carried out with the ISE and ISFET in mind, a brief description of these sensors is presented below. Also included is some background on the AC impedance method, which has proven to be a powerful tool for the investigation of membrane properties. In the last section, an overview of the conductance of non-aqueous solutions is given, with a brief discussion of the application of this type of analysis to liquid membrane systems.

1.1 THE ION-SELECTIVE ELECTRODE [1-7]

A conventional ion-selective electrode (ISE) consists of an ion-selective membrane in contact with solution at both interfaces, where one solution contains the ion to be determined and the other solution contains the same ion at known activity in contact with a Ag/AgCl wire or some other suitable internal reference. The membrane may take one of several forms. Glass membrane electrodes, which are based upon a fixed charge ion exchanging glass membrane and are most commonly used in the measurement of pH, have the longest history in the field of ion-selective electrode technology. The membrane may also consist of a sparingly soluble salt of the ion of interest, such as LaF_3 for F^- or AgCl for Cl^- . Increasingly popular are the liquid membrane electrodes based upon hydrophobic organic solvents. These derive their ion selectivity from a charged ion exchanger or neutral ion carrier (ionophore) dissolved in the solvent. This discussion will be concerned primarily with liquid membranes containing a neutral ion carrier.

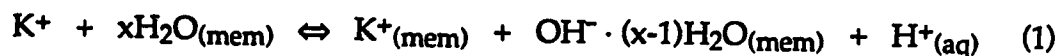
The membranes examined throughout this work are commonly used for K^+ -ISEs and consist of a 2:1 ratio of plasticizer to poly(vinylchloride) (PVC), where the plasticizer is the long chain ester, dioctyladipate (DOA). The PVC lends structural strength to the membrane. The ionophoric cyclic polyamide valinomycin, which imparts K^+ selectivity to the membrane, is incorporated into this matrix. ISE's based on these membranes respond to K^+ in a Nernstian manner, exhibiting slopes of close to 59.2mV per decade change in K^+ concentration. Response of the membrane to K^+ is determined by the reversible exchange of K^+ across the membrane-solution interface, which occurs to satisfy the requirement that the electrochemical potential of K^+ , μ_{K^+} , be equal in both phases. This exchange is facilitated by valinomycin, which forms a very stable complex with K^+ .

While valinomycin is highly selective for K^+ , it has been found that this ion carrier need not be present in the matrix for the membrane to show some response to K^+ , albeit sub-Nernstian (less than 59.2 mV per decade change in K^+ concentration) [8]. Plasticized PVC-based membranes in general respond to cations rather than anions, thereby exhibiting a property known as permselectivity, by which ions of one charge are admitted into the membrane with the almost total exclusion of ions of the opposite charge.

There have been essentially two schools of thought as to the mechanism for cation permselectivity in neutral carrier membranes. One model, which could be called the "space charge model", is based on the fundamental thin membrane model put forth by Ciani, Eisenman, and Szabo (CES) [9]. They viewed the potential difference across the membrane as consisting of two interfacial and an internal potential contribution. The model assumes exclusive solubilization of cationic carrier complexes, and in fact defines the internal potential difference in terms of concentrations at the

inner side of the membrane surfaces within the diffuse space charge regions. Accordingly, permselectivity for cations arises through the total exclusion of hydrophilic anions from the membrane, and the membrane cannot be characterized as electrically neutral. The other model, introduced by Kedem, Perry, and Bloch [10], suggests that the membrane is actually an electroneutral entity, containing fixed sites associated with the membrane matrix. The membrane can then be treated as a low density, low capacity ion exchanger, with preferential extraction of the ion of interest into the membrane from the bathing solution due to the presence of the neutral complexing agent for that ion within the membrane. Donnan exclusion of hydrophilic anions ensures membrane permselectivity for cations.

It is now generally agreed that the model proposed by Kedem et al., and variations of it, provide the more accurate description of neutral carrier membranes. In fact, there is substantial evidence for the presence of weakly dissociable ion exchange sites within these membranes, obtained using a variety of electrochemical techniques. Several sources for these sites have been postulated. One study has suggested that water immobilized in clusters in the membrane is a prime source of these sites, through the following reaction [11]:



The OH^- ions that result remain immobilized in these water clusters because of the extreme hydrophilicity of the OH^- ion. Others [12,13] regard the sites as originating mainly from impurities and leftover additives used in the manufacture of the PVC used as the membrane matrix; one type of PVC would then yield a membrane having different electrical characteristics than

another manufacturer's PVC. This latter view is now more generally accepted.

Due to the presence of ion exchange sites, the potential which develops across the membrane of an ISE can be viewed as consisting of three components, two of which arise at the membrane-solution interfaces and one due to diffusion [2]. The diffusion potential is the result of differences in ion mobilities in the membrane phase, in much the same way as a liquid junction potential. The membrane's ability to preferentially extract cations from solution gives rise to a charge separation in the membrane's interfacial regions with the formation of a potential difference across these interfaces as a consequence. These potentials are referred to as the Donnan potentials. The observed potentiometric response to K^+ concentration of ISE's based on this is due mostly to changes in the Donnan potential at the membrane-test solution interface.

1.2 THE ISFET [14-18]

Research in the field of ion-sensing technology over the past two decades has resulted in a proliferation of new sensors for a variety of species. Much of this interest has centred on a family of solid-state devices known as ion-sensitive field effect transistors, or ISFET's. Often regarded as a second generation ion-selective electrode (ISE), the ISFET is based on two established technologies, namely solid-state integrated circuits and ISE's. Like the ISE, the response of an ISFET to the species of interest in solution is determined by an ion-selective membrane of some kind. Unlike the ISE, however, this membrane is deposited directly onto the solid surface of the ISFET, with the

result that the internal membrane/solution interface of the ISE has been replaced with a membrane/solid interface. The mechanism by which an ISFET operates is therefore quite different from an ISE, and has been the subject of some study [16-18]. The presence of the internal membrane/solid interface also gives rise both to some unique advantages and problems not encountered with ISE's [16-19].

To date, most of the research involving ISFET's has been directed primarily towards application of this device in the biomedical field, for measurements of the ionic constituents in various physiological fluids such as blood and urine. The small size of the ISFET makes it an ideal candidate for *in vivo* determinations of these fluids, determinations which are not possible with conventional ISE's. While other applications in analytical chemistry are also of interest, the availability of ISE's which are adequate for these tasks has resulted in ISFET's being applied less often for non-biomedical ion determinations.

Chapters 2 and 3 examine the properties of a membrane-coated silicon electrode, in conjunction with its use as a model for the ISFET in studies of factors affecting ISFET response. Since much of the work in this thesis was carried out with the ISFET in mind, a brief explanation of its characteristics and operation is presented below. Mention will also be made of some of the advantages and disadvantages associated with use of the device.

ISFET's are based on the semiconductor silicon, as are most solid-state electronic devices. Silicon has supplanted other semiconductors, in particular germanium, as the material of choice in semiconductor fabrication for a number of reasons. Chief among these are the more acceptable temperature behaviour of devices made from silicon, and its relatively low cost. Silicon is

a crystalline solid, with a diamond lattice structure in which each atom is covalently bonded to four equidistant neighbours in a tetrahedral arrangement. The electrons in these bonds occupy a band of continuous energy levels known as the valence band. The bonds themselves are only moderately strong, so that thermal vibrations at any finite temperature will break some bonds, resulting in free electrons capable of participating in electrical conduction. A corresponding number of positively charged remnant holes are created in the valence band. The free electrons occupy a band of energies known as the conduction band, which lies above the valence band. The energy gap separating the valence and conduction bands is known as the bandgap. Electrons may not possess energies that fall within this region, so that this gap is also referred to as the forbidden gap.

An intrinsic semiconductor is one in which the number of thermally generated holes and electrons exceeds the number of impurities (i.e. electron-rich or electron-poor sites in the lattice) so that the presence of the latter proves to be insignificant. At thermal equilibrium, the number of holes per unit volume, p , is then equal to the number of electrons per unit volume, n , which in turn is equal to the intrinsic carrier density, n_i . Through a relationship often called the mass action law [15] :

$$n p = n_i^2 \quad (1)$$

Equation (1) is also valid for semiconductors at thermal equilibrium that have been doped either with an element having a fifth valence electron, such as arsenic (so that $n > p$), or with an element having only three valence electrons, such as boron (so that $p > n$). Doped semiconductors are termed extrinsic semiconductors. If $n > p$, the semiconductor is referred to as being n-type, whereas if $p > n$ the semiconductor is referred to as being p-type.

The current-passing ability of silicon is characterized by its conductivity, σ_{Si} :

$$\sigma_{Si} = q n u_n + q p u_p \quad (2)$$

u_n and u_p are mobilities of the electrons and holes, respectively, and q is electronic charge. The corresponding resistivity, ρ_{Si} , of silicon is defined as

$$\rho_{Si} = \frac{1}{\sigma_{Si}} = \frac{1}{q (n u_n + p u_p)} \quad (3)$$

In doped silicon, one of the terms in Equations (2) and (3) will dominate, because of the many orders-of-magnitude difference between carrier densities. For n-type silicon, then, Equations (2) and (3) reduce to

$$\sigma_{Si} = q n u_n \quad (4)$$

and
$$\rho_{Si} = \frac{1}{q n u_n} \quad (5)$$

while for p-type silicon, they become

$$\sigma_{Si} = q p u_p \quad (6)$$

and
$$\rho_{Si} = \frac{1}{q p u_p} \quad (7)$$

Basically, the operation of ISFET's, and of field effect transistors (FET) in general, depends on the modulation of σ_{Si} by means of an electric field perpendicular to the silicon surface. To understand how this might be accomplished, consideration of changes that occur in the silicon substrate of a metal-oxide-semiconductor (MOS) capacitor as a function of applied voltage should prove useful.

A cross-sectional view of a MOS capacitor based on p-type silicon is given in Figure 1.1. The structure consists of an insulating layer, in this case SiO_2 , sandwiched between a metal contact and the p-type substrate. An ohmic contact to the back face of the substrate completes the structure.

If a negative voltage is applied to the contact at the oxide, holes are attracted from the silicon bulk to the Si/SiO_2 interface, resulting in an accumulation of positive charges at the silicon surface. This particular biasing condition for the MOS capacitor of Figure 1.1 is thus termed the accumulation case. The positive charge layer that is formed at the silicon surface is equal and opposite to the charge layer existing on the field plate, and is of negligible thickness. The conductivity of this layer is much greater than that of the silicon bulk, due to the presence of an excess number of mobile charge carriers.

If the situation is reversed and a slightly positive voltage is applied to the oxide contact, holes will be repelled from the interface, leaving behind negatively charged acceptor ions confined to the silicon lattice. This layer of exposed acceptor ions, which extends a relatively long way into the bulk, is called the depletion layer, in reference to the fact that it has been depleted of holes. This bias condition is therefore known as the depletion case. The absence of mobile carriers in the depletion layer causes the region at the silicon surface to be characterized by a much lower conductivity than the silicon bulk.

Should the positive voltage being applied be increased further, a substantial number of generated electrons will eventually accumulate at the silicon surface. The result is the formation of the inversion layer, so called because the electrons, or minority carriers, far outnumber the holes, or majority carriers, in this region. Hence, this bias condition is referred to as the

Figure 1.1 Cross-sectional view of a MOS capacitor. This diagram was adapted from ref. [15], but has been removed due to the unavailability of copyright permission.

inversion case. The inversion layer has a width of 10 to 100 Å, and is always much narrower than the depletion layer. The latter reaches a maximum width once an inversion layer is formed. Under this bias condition, three distinct regions of varying conductivity exist in the silicon substrate, namely the inversion layer, the depletion layer, and the bulk substrate. The region generally having the greatest ability to pass charge is the inversion layer, due to the presence of excess, mobile, minority carriers, whereas the depletion layer is characterized by the lowest conductivity.

From the foregoing discussion, it is clear that application of varying voltages perpendicular to the MOS capacitor structure has a profound effect on the conductivity in the surface region of the silicon substrate. This surface charge phenomenon is utilized in the metal-oxide-semiconductor field effect transistor (MOSFET), a FET which is based on the MOS capacitor. Figure 1.2 shows a cross-sectional view of a MOSFET based on a p-type silicon substrate. Two heavily doped n-type regions, labelled the source and drain, have been created next to one another in the substrate, separated by a distance that is typically on the order of several micrometers. A thin layer of SiO₂ covers the surface of the device between the source and the drain. This layer is itself covered by a conductive layer of metal or polycrystalline silicon, known as the gate. Accordingly, the structure of this central section of the device is simply that of a MOS capacitor. The MOSFET is a four terminal device, meaning that voltage is controlled at four contacts during device operation, namely the source, drain, gate, and back face of the substrate. Generally, the source contact is used as the voltage reference, with the substrate contact being held at this same voltage or a voltage that is slightly positive with respect to the source.

As with the MOS capacitor of Figure 1.1, application of a sufficiently large positive voltage to the gate of the MOSFET causes the formation of an

Figure 1.2 Cross-sectional view of a MOSFET. This diagram was adapted from ref. [16], but has been removed due to the unavailability of copyright permission.

inversion layer or channel at the silicon surface between the source and drain. The source and drain are then effectively connected by an n-type channel, the conductivity of which is a function of applied gate voltage, V_G . If a small positive drain voltage, V_{DS} , is applied with respect to the source, electrons will flow from the source to the drain, with the corresponding drain current, I_D , flowing from drain to source. Since the magnitude of I_D is dependent on the conductivity of the channel, I_D is also a function of applied V_G .

In an ISFET, the conductive layer of the gate is replaced by a layer of ion-sensitive membrane, a solution containing the ion of interest, and a reference electrode, as shown in Figure 1.3. The V_G applied to the device is now determined by the response of the membrane to the species of interest. Response of the ISFET to changes in ion concentration may then be monitored in one of two ways. The first method involves measuring I_D as a function of ion concentration, thereby exploiting the dependence of I_D on V_G . More commonly, however, the ISFET is operated in a constant current mode. This mode requires that I_D be maintained at a constant level, so that changes in V_G arising from changes in ion concentration are compensated by application of a second voltage of sufficient magnitude to ensure constant n-channel conductivity. The response measured is then the magnitude of this second voltage at each ion concentration. This is the preferred mode of operation for an ISFET, since non-ideal device characteristics which could affect I_D in a non-linear fashion, such as the development of potential differences across the source-channel and drain-channel interfaces, are compensated for.

The types of membrane which have been used as gate material fall into several categories. The first ISFET, introduced by Bergveld [20], employed the

Figure 1.3 Cross-sectional view of an ISFET. This diagram was adapted from ref. [17] and an original diagram by Paul Glavina of our group, but has been removed due to the unavailability of copyright permission.

bare SiO_2 insulating layer of the gate to obtain a pH-responsive device. Silicon nitride (Si_3N_4) has also been used in this regard. To make devices selective for ions other than H^+ , the bare gate insulator is coated with a second ion-selective film to obtain a composite gate ISFET [16]. Membranes which have been employed in this capacity have been borrowed from ISE technology, and include films which consist of liquid phases containing a dissolved hydrophobic anion exchanger, as well as solid-state membranes consisting of non-porous, sparingly soluble salts. An example of the former type is a membrane selective for Ca^{2+} , which is comprised of calcium dialkylphosphate (the ion-exchanger) in dioctylphenylphosphonate [21]. As an example of the latter case, the paper by Buck and Hackleman is cited [22], in which is described use of an AgBr film coated onto the insulator of a silicon structure to impart sensitivity to halogen anions. Of direct relevance to this work is a third class of membranes, which are generally based on plasticized poly(vinylchloride) (PVC) in which is dissolved a neutral ion carrier. A commonly employed example of this type of membrane is the K^+ -selective membrane examined throughout this thesis, whose matrix consists of PVC plasticized with a long chain ester such as dioctyladipate (DOA), and contains the K^+ -selective ionophore, valinomycin. In fact the first composite gate device to be reported in the literature, the K^+ -responsive ISFET of Moss et al. [23], featured the membrane described above.

ISFET's and related devices possess several advantages over today's conventional ion-sensing technology, in that they are much smaller and well suited to mass production using established microfabrication techniques. Much of the signal processing circuitry may also be incorporated onto the device chip, thereby minimizing the need for extraneous transducing instrumentation. Despite their inherent advantages, however, ISFET's have

been slow in achieving commercial viability because they are subject to a number of problems, both in terms of manufacture and lifetime. For instance, the electrolyte solutions in which ISFET's are used present a very harsh environment to electronic devices. Device encapsulation therefore becomes very important, and has proven to be a more difficult problem to solve than first thought. Adhesion of the membrane to the silicon of the gate may become a problem, as does long term drift in response. It has been observed that the response of composite gate ISFET's suffer from certain interferences that do not affect the response behaviour of their conventional ion-selective electrode (ISE) counterparts, because the internal membrane/solution interface of the ISE has been replaced by the membrane/oxide interface. For instance, Fogt and co-workers [19] have shown that the presence of carbon dioxide and organic acids in solution can adversely affect the response of a K^+ -ISFET coated with a liquid polymeric membrane containing valinomycin. This particular interference phenomenon is examined more closely in Chapter 3, using K^+ -selective membrane coated silicon electrodes as models for the ISFET gate.

1.3 AC IMPEDANCE ANALYSIS [24-27]

Kinetic and mechanistic information about a chemical system may be obtained using a variety of available electrochemical techniques. Generally, these involve the imposition of a perturbation upon the system, with measurement of the resulting current or potential response. The size and nature of the perturbation imposed varies from one technique to the next. For instance, cyclic voltammetry, chronoamperometry, and

chronopotentiometry employ perturbations in the form of potential sweeps, potential steps, and current steps, respectively, to drive the system to a condition far from equilibrium. The measured current or potential response is then transient in nature, because it depicts the system's return to equilibrium after being disturbed. Other techniques use a second approach, in which the system is subjected to an alternating signal of small amplitude. In this case, the measured response reflects the way the system follows the perturbation at steady state. AC impedance analysis falls into this category of electrochemical methods, as does AC voltammetry. An important advantage of using this second approach to study an electrochemical system lies in the time-invariant nature of the response, as this allows measurements to be averaged over time to achieve better precision. The current-potential (I-E) characteristics of the system's response are also more easily interpreted, since the data is obtained with the system at a state close to equilibrium.

AC impedance analysis has been employed in a wide variety of applications, including studies of corrosion [28-30], biological membranes [31], conducting solids [32], and electrode processes [25,33]. Use of the method for the study of ion-selective membranes was first proposed by Buck [34]. It has since found wide application in this regard, as demonstrated by various investigators who have used AC impedance analysis in tandem with other techniques to understand more fully the response mechanisms of both solid and liquid membranes [35-37]. A brief discussion of AC impedance analysis will now be undertaken. For more comprehensive treatments of the subject, the reader is referred to references [24-27].

The electrical behaviour of an electrochemical cell is determined by the manner in which the various current conducting elements are

interconnected, in much the same way as an electronic circuit. This allows the cell to be represented by an equivalent electrical circuit consisting of resistances (R), capacitances (C), and inductances (L) in various combinations. Herein lies the usefulness of AC impedance analysis, since the cell's response may be interpreted in terms of its equivalent circuit model, using established AC circuit theory.

In an impedance measurement, a sinusoidal AC voltage of small amplitude is applied to the cell, and the resulting sinusoidal AC current output is measured. The input signal may be expressed in terms of its amplitude, ΔE , and angular frequency, ω :

$$E = \Delta E \sin \omega t \quad (8)$$

where $\omega = 2\pi f$, f is the sinusoidal frequency in Hz, and t is time in seconds. The output current, which has the same ω as the input voltage, may be expressed in terms of its amplitude, ΔI , and the phase angle, θ , where θ is equal to the phase difference between the applied voltage and the resultant current :

$$I = \Delta I \sin (\omega t + \theta) \quad (9)$$

Because they have both magnitude and direction, the input and output signals can be characterized as vector quantities. As such, they may be employed to define a third vector, AC impedance or Z , such that

$$Z = \frac{E}{I} \quad (10)$$

Z has a magnitude of $|Z| = \Delta E/\Delta I$, and the same phase angle, θ , as the output current. Equation (10) is the AC equivalent of the Ohm's law definition of resistance, R , in direct current (DC) theory, where $R = E/I$. R is a measure of the resistance to current flow that is observed when a DC voltage (i.e. one that does not vary with time) is applied across a resistor. Z is the AC analogue of

R, in that it is also a measure of the obstruction to current flow; however, unlike R, Z consists of capacitance, inductance, and resistance.

Because Z is a vector, it may be conveniently represented in the complex plane, as shown in Figure 1.4. In this coordinate system, the horizontal axis is labelled as real, while the vertical axis is labelled as imaginary. The mathematical convention is to multiply imaginary coordinate values, Z_{imag} in this case, by $i=\sqrt{-1}$. The vector Z can be described in terms of its real and imaginary components, Z_{real} and Z_{imag} , as

$$Z(\omega) = Z_{real}(\omega) - iZ_{imag}(\omega) \quad (11)$$

Though the imaginary component of the vector Z is actually $-Z_{imag}$, it is shown to be positive in Figure 1.4. This convention of plotting negative Z_{imag} values along the positive imaginary axis shall be employed throughout this work. The real and imaginary components of Z are defined using the input voltage waveform, $E = \Delta E \sin \omega t$, as a reference. Z_{real} is in phase with E, while Z_{imag} , which is often termed the "quadrature" component, is exactly 90° out of phase with E. As Equation (11) indicates, Z is dependent on the frequency of the input (and output) signal. From the complex plane plot of Z in Figure 1.4, the magnitude of Z can be expressed as

$$|Z| = \sqrt{Z_{real}^2 + Z_{imag}^2} \quad (12)$$

while the phase angle, θ , is

$$\theta = \arctan\left(\frac{Z_{imag}}{Z_{real}}\right) \quad (13)$$

Figure 1.4 Representation of the impedance vector, Z , in the impedance plane. This diagram was adapted from ref. [27], but has been removed due to the unavailability of copyright permission.

In order to facilitate interpretation of information provided by AC impedance analysis of real systems, it is useful to consider the impedance response of some simple circuit elements. Impedance spectra measured as a function of input voltage frequency are generally presented as complex plane plots known as impedance plane or Nyquist plots. In the ensuing discussion, the appearance of the Nyquist plots for some simple circuit elements will be examined.

The Nyquist plot of a pure resistance is presented in Figure 1.5(a). Simple resistors always obey Ohm's law, so that under AC conditions, current flowing through the resistor is proportional to the instantaneous applied voltage at all frequencies. Therefore, application of a sinusoidal voltage, $E = \Delta E \sin \omega t$, across a resistor R gives rise to a current, I , which may be simply stated as $I = (\Delta E/R) \sin \omega t$. This current is in phase with the input signal, so that the measured Z consists only of an in-phase, or real, component R , which is independent of frequency. As a result, the Nyquist plot of the resistor's impedance spectrum consists of a single point on the real axis, at which $Z_{\text{real}} = R$.

Figure 1.5(b) shows the Nyquist plot for a pure capacitance. The fundamental relation that defines the behaviour of a capacitor is $Q = CE$, where Q denotes the quantity of charge stored in the capacitor. Varying the voltage as a function of time gives rise to a corresponding variation in Q , dQ/dt . By definition, $I = dQ/dt$, so that $I = dQ/dt = C (dE/dt)$. Differentiating Equation (8) with respect to t , I becomes

$$I = \omega C \Delta E \cos \omega t \quad (14)$$

$$= \omega C \Delta E \sin \left(\omega t + \frac{\pi}{2} \right) \quad (15)$$

Figure 1.5 Nyquist plots for some simple circuit elements: a) a pure resistor, R ; b) a pure capacitor, C ; c) a resistor, R_s , and capacitor, C_s , in series; d) a resistor, R_p , and capacitor, C_p , in parallel. This figure was adapted from ref. [27], but has been removed due to the unavailability of copyright permission.

Z , also referred to as "capacitive reactance" in this case, is now equal to $1/\omega C$. Since the current now leads the voltage input by 90° , Z will also be 90° out of phase with the input. For this reason, Z consists only of an imaginary component, Z_{imag} , and is defined by $Z = -iZ_{imag}$. The Nyquist plot consists of a series of frequency-dependent points on the Z_{imag} axis, with points obtained at high frequency occurring at low Z_{imag} , and vice versa.

Generally speaking, the equivalent circuits related to electrochemical cells consist of serial and parallel RC networks. It has been shown that liquid PVC-based membranes are well represented by an equivalent circuit consisting of two parallel R-C networks, one corresponding to the bulk membrane, the other to the solution/membrane interface [27]. On the other hand, silicon structures in which a silicon substrate is coated with an insulating SiO_2 layer may be described as consisting of two capacitances in series, with one C due to the silicon substrate and the other due to the oxide layer [38-40]. An ability to recognize the impedance spectra of serial and parallel R-C networks is thus a necessary prerequisite for AC impedance analysis of real systems.

Figure 1.5(c) gives the Nyquist plot for a resistance and capacitance in series. As with resistances in series, impedances in series may be summed directly, so that Z of this combination is

$$Z = R - \frac{i}{\omega C} \quad (16)$$

$Z_{real} = R$ and $Z_{imag} = 1/\omega C$, in accordance with Equation (11). Z_{real} is independent of frequency, while Z_{imag} increases with decreasing frequency. As a result, the Nyquist plot in Figure 1.5(c) resembles that of a pure capacitance, with each point having a real coordinate of R in this case.

The Nyquist plot of a parallel R-C network is quite distinctive, as illustrated by Figure 1.5(d). Z of this circuit is found by adding together the reciprocals of the individual impedances, so that

$$\frac{1}{Z} = \frac{1}{R} + i\omega C = \frac{1 + i\omega CR}{R} \quad (17)$$

Z is then
$$Z = \frac{R}{1 + i\omega CR} \quad (18)$$

Multiplying by the complex conjugate of $(1 - i\omega CR)$ yields

$$Z = \frac{R - i\omega CR^2}{1 + (\omega CR)^2} \quad (19)$$

Accordingly,
$$Z_{\text{real}} = \frac{R}{1 + (\omega CR)^2} \quad (20)$$

and
$$Z_{\text{imag}} = \frac{-\omega CR^2}{1 + (\omega CR)^2} \quad (21)$$

Elimination of ω from Equations (20) and (21) may be carried out as follows.

From Equation (20)

$$(\omega CR)^2 = \frac{R - Z_{\text{real}}}{Z_{\text{real}}} \quad (22)$$

and
$$\omega CR = \sqrt{\frac{R - Z_{\text{real}}}{Z_{\text{real}}}} \quad (23)$$

Substituting these expressions into Equation (21) yields

$$Z_{\text{imag}} = -\sqrt{(R - Z_{\text{real}}) Z_{\text{real}}} \quad (24)$$

so that
$$Z_{\text{imag}}^2 - R Z_{\text{real}} + Z_{\text{real}}^2 = 0 \quad (25)$$

If $\frac{R^2}{4}$ is added to both sides, Equation (25) becomes

$$Z_{\text{imag}}^2 + \left(Z_{\text{real}} - \frac{R}{2} \right)^2 = \left(\frac{R}{2} \right)^2 \quad (26)$$

Hence, Equations (20) and (21) predict a semicircle in the impedance plane, centred at $Z_{\text{real}} = R/2$, and with a radius of $R/2$. From Equation (20), Z_{real} increases as frequency decreases to a maximum value of R when ω is 0. Consequently, R may be evaluated by finding the low frequency intercept of the semicircle in Figure 1.5(d). C may be determined from ω_{max} , the angular frequency at which Z_{imag} attains its maximum value, through the relationship $\omega_{\text{max}} = 1/(RC)$. The time constant, τ , of this R-C network is simply the reciprocal of ω_{max} i.e. $\tau = RC$. If the equivalent circuit model of a real system consists of two or more parallel R-C circuits in series, a corresponding number of semicircles will appear in the Nyquist plot, provided the ratio of the time constants of these networks is greater than 10. If this should prove not to be the case, the respective semicircles will be overlapped.

Alternative methods of analyzing impedance data exist, but as they were not employed in any of the following studies, they will not be discussed here. More detailed treatments on this aspect of impedance analysis may be found in references [24-27].

1.4 CONDUCTANCE OF ELECTROLYTE SOLUTIONS [41-44]

Conductance is a measure of the current-carrying ability of a given amount of electrolyte in solution, and is defined as

$$\Lambda = \frac{\sigma 1000}{c} \quad (\text{cm}^2 \cdot \text{mole}^{-1} \cdot \Omega^{-1}) \quad (27)$$

where Λ is equivalent conductance, σ is specific conductivity, and c is the nominal solute concentration in equivalents/L. If concentration has units of moles/L, then Λ is referred to as molar conductance. When dealing with 1 : 1 electrolytes, the molar conductance and the equivalent conductance are the same. σ is dependent on the number and mobility of ions, as shown in Equation (28) :

$$\sigma = \sum n_i u_i q_i \quad (28)$$

where n_i , u_i , and q_i denote the number, mobility, and charge of the i^{th} current-carrying species, respectively. Since the magnitude of Λ is determined by these ionic parameters, the conductance method is a useful tool for the study of electrolytes in solution. The development of expressions that successfully describe the dependence of Λ on solute concentration in solution has led to the clarification of a number of aspects of ion behaviour in a wide variety of solvents. Generally, the solutes examined fall into two categories, ionophores and ionogens. Ionophores, sometimes referred to as true electrolytes, are those compounds which exist as ionic crystals, while ionogens, molecules like the carboxylic acids, form ions through chemical reaction with the solvent.

Of particular relevance to this thesis is the work which has been carried out in non-aqueous solvents of low dielectric strength. Using conductance measurements, estimates of ion-pairing for ionophores or dissociation for ionogens may be obtained in these solvents. Evaluation of single ion mobilities is also possible, allowing characterization of ion-solvent interactions.

AC impedance analysis of ion-selective membranes provides a measure of membrane σ through the related quantity membrane resistance. Measured resistance depends on the geometric properties of the membrane, as well as specific resistivity, ρ , through

$$R = \frac{\rho l}{A} \quad (29)$$

where l is membrane thickness, and A is surface area. ρ is related to σ by

$$\sigma = \frac{1}{\rho} \quad (\Omega \cdot \text{cm})^{-1} \quad (30)$$

NMR and impedance measurements show that liquid membranes may be viewed as very viscous, non-aqueous solutions characterized by a low dielectric strength [35,45]. Therefore, an insight into the behaviour of an electrolyte in the liquid membrane matrix may be gained through investigation of the variation of membrane conductance as a function of electrolyte concentration [35]. In the case of liquid membranes, conductance can be effectively determined using AC impedance.

A conductance function derived by Fuoss [43] for associated electrolytes in solvents of low and moderate dielectric strength can be used to interpret conductance data obtained for membranes containing both ionophores and ionogens. This type of data analysis allows characterization of the solute's behaviour in the membrane through estimation of ion-pair or ionogen dissociation. Ion mobilities may also be qualitatively estimated through determination of the conductance at infinite dilution, Λ_0 . A brief review of the steps leading up to the derivation of this function, as well as a description of the function itself, follows.

The study of the conductance of electrolytic solutions as a means of elucidating the properties of these solutions has a long history. Researchers in the mid to late nineteenth century, Ostwald and Kohlrausch [46] primary among them, reported the concentration dependence exhibited by the conductance curves of a variety of aqueous electrolyte solutions. It was with the appearance of the ionic theory of Arrhenius in about 1887 [47] that the first attempts were made to quantitatively describe this dependence. Arrhenius' hypothesis for the behaviour of electrolytes in solutions is summarized in Equation (31), where



AB denotes a neutral molecule of the electrolyte, and A^+ and B^- represent the ions into which the electrolyte dissociates. Letting α represent the degree of dissociation, the ionic concentrations, $[A^+]$ and $[B^-]$, become (αc) , where c is the stoichiometric concentration of AB. Similarly, $[AB]$ becomes $(1 - \alpha)c$. Using the mass action hypothesis, Arrhenius derived an expression for the equilibrium constant, K , governing the dissociation of AB in solution, where

$$K = \frac{c\alpha^2}{1 - \alpha} \quad (32)$$

He further proposed that α at any given concentration was equal to the ratio of the equivalent conductance, Λ , to the limiting conductance at infinite dilution, Λ_0 :

$$\alpha = \frac{\Lambda}{\Lambda_0} \quad (33)$$

As a result, Arrhenius' dissociation theory predicted that at low concentrations Λ should vary linearly with concentration. Ostwald used

Equations (32) and (33) to derive an expression relating Λ to c , appropriately called the Ostwald dilution law [48], which is stated below :

$$\frac{1}{\Lambda} = \frac{1}{\Lambda_0} + \frac{c\Lambda}{K\Lambda_0^2} \quad (34)$$

Applying this law to the solutions of organic acids he had been studying, Ostwald found that plots of $1/\Lambda$ versus $c\Lambda$ produced the predicted straight line plots, so that Arrhenius' ionic theory held for these systems. However, precise conductance measurements at low electrolyte concentrations made by Kohlrausch between 1860 and 1880 indicated that aqueous solutions of mineral acids, alkalis, and inorganic salts, all strong electrolytes, simply did not obey the Ostwald dilution law. His data led him to conclude that conductance was more aptly described as a linear function of the square root of concentration for these systems. It appeared that the Arrhenius dissociation theory could only be applied to the so-called weak electrolytes, which were for the most part carboxylic acids and amines. The confusion was further compounded with the first conductance measurements in non-aqueous solvents, since solutes which behaved as strong electrolytes in water exhibited conductance curves in non-aqueous solvents which were characteristic of weak electrolytes in water.

This contradiction between theory and experiment for the conductance of many systems arose for two reasons. First, there was a lack of understanding of the fundamental structural difference between compounds now known as ionophores and ionogens. This difference became clear with the advent of X-ray diffraction measurements in the early part of this century, which showed that salts such as NaCl were made up solely of ions arranged in a periodic lattice, whereas ionogens existed as neutral molecules. The

second reason lies in the Arrhenius theory itself, which had assumed that all of the change in Λ with concentration was due to a change in α , thereby neglecting altogether the occurrence of ion-ion interactions in solution.

It was not until 1923 that a workable model of electrolytes in solution, which took into account electrostatic forces between ions, was proposed in the form of the now-famous Debye-Hückel theory [49]. The first result of this theory was that the activity coefficients of dilute solutions of ionophores should be a linear function of the square root of ionic strength. Turning to the Λ of these solutions, Debye and Hückel also showed that Λ at low concentration should be a linear function of the square root of concentration, which was in direct agreement with Kohlrausch's observations.

With the Debye-Hückel theory, the groundwork was laid for the development of expressions which described the dependence of Λ on concentration by taking into account both concentration and mobility of ions. These expressions have all taken the form

$$\Lambda = \Lambda_0 - \Lambda_I(c; \Lambda_0, a, \epsilon, T) - \Lambda_{II}(c; a, \epsilon, \eta, T) \quad (35)$$

Λ_I is a term which arises from the unsymmetrical charge distribution about a migrating ion. Every ion in solution has associated with it an "ionic atmosphere", consisting of other ions in solution. In a solution at equilibrium, this "ionic atmosphere" is distributed on average with spherical symmetry around the central ion. When the central ion moves to an off-centre position under the influence of an external field, the spherical distribution of charge around it is disturbed and it experiences a restoring force which inhibits its movement. This force rapidly dies away as the atmosphere rearranges through thermal motions of its constituent ions to reattain its spherical distribution. The restoring force experienced by the

migrating ion is known as the relaxation effect, and Λ_I is referred to the relaxation term. Besides concentration, Λ_I is also dependent on Λ_0 ; a , the ion size parameter, which is generally taken to be the distance of closest approach of two ions of opposite charge; ϵ , the dielectric constant; and T , the absolute temperature.

Λ_{II} in Equation (35) is known as the electrophoretic term, and is due to displacement of solvent by the migrating ion and its accompanying ion cloud. This term shows a dependence on solvent viscosity, η , as well as on a , ϵ , and T .

The first conductance function having a form like that of Equation (35) was proposed by Onsager in 1927 [50]. His result can be summarized by the formula

$$\Lambda = \Lambda_0 - (S_1\Lambda_0 + S_2)\sqrt{c} \quad (36)$$

$S_1 \Lambda_0 \sqrt{c}$ corresponds to the Λ_I term of Equation (35) whereas $S_2 \sqrt{c}$ is the Λ_{II} term. Together, $(S_1 \Lambda_0 + S_2)$ define the Onsager slope, S , which is completely determined by solvent properties and universal constants. A test of Equation (36) against a large body of data for ionophores in solvents of high dielectric strength showed that it was an exact expression for the limiting tangent to the observed conductance curves. Equation (36) is therefore often called the Onsager limiting law. In the model used by Onsager to derive his theoretical result, ions are represented as point charges moving through a continuum. As a consequence, the parameter a does not appear in either S_1 or S_2 , and the Onsager law is only applicable to data recorded at very dilute solute concentrations where ion size does not have to be taken into account. Furthermore, Onsager assumed complete dissociation of the ionophore in solution in his derivation, so that this conductance function cannot explain

the behaviour of ionophores in solvents of low dielectric strength, or of ionogens in most solvents, including water.

In 1955, Fuoss and Onsager derived a more accurate conductance function for completely dissociated electrolytes [43], based on a model in which the ion in solution is represented as a sphere moving through a continuum. This equation has the form given below :

$$\Lambda = \Lambda_0 - S\sqrt{c} + E c \log(c) + Jc \quad (37)$$

The coefficients S (the Onsager slope), E , and J all contain components due to both the relaxation and electrophoretic effects. The exact expressions for each of these coefficients will be presented later. Equation (37) is an obvious extension of the Onsager limiting law, with the E and J terms arising from the integration of differential equations describing ionic motion at boundary conditions corresponding to ions of finite size (see reference [43] for a complete discussion of this). The appearance of the logarithmic term in the Fuoss-Onsager derivation was consistent with earlier observations that no reasonable combination of algebraic terms could fully describe the shape of most conductance curves. Because of the model on which it is based, Equation (37) is valid over a reasonable range of dilute concentrations in most cases. The upper concentration limit of this range for a given solvent corresponds to [51]

$$\kappa a = 0.2 \quad (38)$$

where κ , the Debye-Hückel term is defined as

$$\kappa = \sqrt{\frac{8 \pi e N \mu}{1000 \epsilon k T}} \quad (39)$$

μ equals ionic strength, and the other symbols have their usual meanings.

Fuoss extended Equation (37) in 1958 to consider the case of associated electrolytes, to obtain Equation (40) :

$$\Lambda = \Lambda_0 - S\sqrt{c\alpha} + E c\alpha \log(c\alpha) + Jc\alpha - K_a \Lambda f^2 c\alpha \quad (40)$$

This conductance function is similar to that derived for completely dissociated electrolytes, but includes an additional term which contains K_a , the constant describing association of ionic species into ion pairs. As well, concentrations, c , have all been replaced with αc , since the ion concentrations which determine conductivity are now dependent on the degree of dissociation of ion pairs (for ionophores) or molecules (for ionogens). The mean activity coefficient, f , has been included in the last term of Equation (40), to account for long range ion interactions, and may be computed using the Debye-Hückel theory. The full expressions for the coefficients S , E , and J , which are the same as in Equation (37) are given below [43].

S is the sum of two terms, as illustrated in Equation (41), where

$$S = S_1 \Lambda_0 + S_2 \quad (41)$$

where

$$S_1 = \frac{e^2 \kappa}{6 \epsilon k T (1 + q) \mu^{1/2}} \quad (42)$$

and

$$S_2 = \frac{\mathcal{F} e \kappa 10^8}{3 \pi \eta C \mu^{1/2}} \quad (43)$$

where : κ = Debye-Hückel constant, defined in Equation (39)

e = electronic charge = 4.803×10^{-10} esu

k = Boltzmann constant = 1.3807×10^{-16} erg K⁻¹

N = Avogadro's number = 6.022×10^{23} mol⁻¹

\mathcal{F} = Faraday constant = 96,485 C mol⁻¹

C = speed of light = 2.9979×10^{10} cm s⁻¹

η = viscosity (in Poise)

ϵ = relative dielectric constant

μ = ionic strength

q' = mobility function in the theory of the relaxation effect [43]; q'^2 is equal to 1/2 for symmetrical electrolytes, so that $q' = \sqrt{1/2} = 0.7071$

Though both S_1 and S_2 appear to show a dependence on μ , incorporation of the full expression for κ in the numerator of both these terms results in the disappearance of this quantity, and S_1 and S_2 being independent of ionic strength. As shown, evaluation of the coefficients in the Fuoss function are generally carried out using the Gaussian system of units. E shows a dependence on S_2 , as shown below

$$E = E_1 \Lambda_0 - E_2 \quad (44)$$

where

$$0.4343 E_1 = \frac{\kappa^2 a^2 b^2}{24 \mu} \quad (45)$$

and

$$0.4343 E_2 = \frac{\kappa a b S_2}{16 \mu^{1/2}} \quad (46)$$

where : a = ion size parameter (in cm)
 $b = \frac{e^2}{a \epsilon k T}$

Again, incorporation of the full expression for κ reveals that both the E_1 and E_2 terms are independent of μ . As with E and S , J is also a combination of two terms :

$$J = \sigma_1 \Lambda_0 + \sigma_2 \quad (47)$$

where

$$\sigma_1 = \left(\frac{\kappa^2 a^2 b^2}{12 \mu} \right) \left[h(b) + 0.9074 + \ln \left(\frac{\kappa a}{\mu^{1/2}} \right) \right] \quad (48)$$

and

$$\sigma_2 = S_1 S_2 + \left(\frac{11 S_2 \kappa a}{12 \mu^{1/2}} \right) - \left(\frac{\kappa a b S_2}{8 \mu^{1/2}} \right) \left[1.0170 + \ln \left(\frac{\kappa a}{\mu^{1/2}} \right) \right] \quad (49)$$

The function $h(b)$ is defined as

$$h(b) = \frac{(2b^2 + 2b - 1)}{b^3} \quad (50)$$

As with S and E , J is actually independent of μ .

In all three cases, the terms subscripted by 1 account for the relaxation effect, whereas the terms subscripted by 2 account for the electrophoretic effect. As in the fully dissociated electrolyte case, the highest ionic concentration at which Equation (40) is valid is defined by Equations (38) and (39). However, when dealing with associated electrolytes, ionic concentration is determined by α , so that associated electrolytes can generally be studied over a wider range of nominal concentrations in a given solvent than completely dissociated electrolytes.

Though several modified versions of the conductance functions given in Equations (37) and (40) have appeared in the literature [44,52], these functions have proven to be quite similar to those proposed by Fuoss and Onsager, and Fuoss. As a result, it was decided that application of the

conductance function for associated electrolytes given in Equation (40) would provide a sufficiently accurate interpretation of Λ data obtained for liquid membranes using AC impedance analysis. The highest membrane concentration at which Equation (40) is valid was calculated to be about 2 mM for strong electrolytes, using Equations (38) and (39), and assuming an ϵ of 8 for the membrane (determined using AC impedance analysis) and a typical value of a of 4 Å. This meant that Λ data obtained at membrane solute concentrations up to and slightly exceeding 2 mM could be analyzed, since ion association is expected to a significant extent in a solvent of such low dielectric strength.

1.5 REFERENCES

1. Harris, W.E., Kratochvil, B., *An Introduction To Chemical Analysis*, Saunders College Publishing: New York, 1981
2. Lakshminarayanaiah, N., *Membrane Electrodes*, Academic Press: New York, 1976
3. Koryta, J., "Theory And Applications Of Ion-Selective Electrodes (Review)", *Anal. Chem. Acta*, 1972, 61, 329
4. Koryta, J., "Theory And Applications Of Ion-Selective Electrodes, Part II (Review)", *Anal. Chem. Acta*, 1977, 91, 1
5. Koryta, J., "Theory And Applications Of Ion-Selective Electrodes, Part III (Review)", *Anal. Chem. Acta*, 1979, 111, 1
6. Koryta, J., "Theory And Applications Of Ion-Selective Electrodes, Part IV (Review)", *Anal. Chem. Acta*, 1982, 139, 1
7. Koryta, J., "Theory And Applications Of Ion-Selective Electrodes, Part V (Review)", *Anal. Chem. Acta*, 1984, 159, 1
8. Fiedler, U., Ruzicka, J., *Anal. Chem. Acta*, 1973, 67, 179
9. Ciani, S., Eisenman, G., Szabo, G., *J. Membrane Biol.*, 1969, 1, 1
10. Kedem, O., Perry, M., Bloch, R., IUPAC Int. Symp. On Selective Ion-Sensitive Electrodes, Univ. Of Wales, April 12, 1973
11. Morf, W.E., Simon, W., *Helvetica Chim. Acta*, 1986, 69, 1120
12. Horvai, G., Graf, E., Toth, K., Pungor, E., Buck, R.P., *Anal. Chem.*, 1986, 58, 2735
13. Thoma, A.P., Viviani-Nauer, A., Arvanitis, S., Morf, W.E., Simon, W., *Anal. Chem.*, 1977, 49, 1567
14. Sze, S.M., *Semiconductor Devices: Physics And Technology*; J. Wiley and Sons: New York, 1985

15. Sze, S.M., *Semiconductor Devices: Physics And Technology*; Wiley - Interscience: New York, 1967
16. Bergveld, P., Sibbald, A., *Analytical And Biomedical Applications Of Ion-Selective Field-Effect Transistors*; Elsevier: Amsterdam, 1988
17. Janata, J., Huber, R.J., in *Ion-Selective Electrodes In Analytical Chemistry*, vol.2; Plenum Press, 1980
18. Janata, J., in *Solid State Chemical Sensors*; Janata, J., Huber, R.J., Ed.; Academic: London, 1985
19. Fogt, E.J., Unterecker, D.F., Norenberg, M.S., Meyerhoff, M.E., *Anal. Chem.*, 1985, 57, 1995
20. Bergveld, P., *I.E.E.E. Trans. Biomed. Eng.*, 1972, BME-19, 342
21. Moody, G.J., Nassory, N.S., Thomas, J.D.R., *Analyst*, 1978, 103, 68
22. Buck, R.P., Hackleman, D.E., *Anal. Chem.*, 1977, 49, 2315
23. Moss, S.D., Janata, J., Johnson, C.C., *Anal. Chem.*, 1975, 47, 2238
24. E.G. and G. Princeton Applied Research Company, Application Note AC-1, "Basics of AC Impedance Measurements"
25. Sluyters-Rehbach, M., Sluyters, J.H., in *Electroanalytical Chemistry*, vol.4; Bard, A.J., Ed.; Marcel Dekker: New York, 1969, ch.1
26. Bard, A.J., Faulkner, L.R., *Electrochemical Methods: Fundamentals And Applications*; J. Wiley And Sons: New York, 1980, ch.9
27. Lindner, E., Toth, K., Pungor, E., *Dynamic Characteristics Of Ion-Selective Electrodes*; CRC Press: Boca Raton, Fla., 1988
28. Brasher, D.M., Kingsbury, A.H., *J. Appl. Chem.*, 1954, 4, 62
29. Mansfeld, F., Kendig, M.W., Tsai, S., *Corrosion*, 1982, 38, 478
30. Padget, J.C., Moreland, P.J., *J. Coatings Tech.*, 1983, 55, 39
31. Clausen, C., Reinach, P.S., Marcus, D.C., *J. Membrane Biol.*, 1986, 91, 213

32. Macdonald, J.R., in *Superionic Conductors*; Maha, G.D., Roth, W.L., Eds.; Plenum Press: New York, 1976, p81
33. Armstrong, R.D., Henderson, M.J., *J. Electroanal. Chem. Interfacial Electrochem.*, 1972, 39, 81
34. Buck, R.P., *Ion-Selective Electrode Rev.*, 1982, 4, 3
35. Armstrong, R.D., Horvai, G., *Electrochem. Acta*, 1990, 35, 1
36. Li, X., Verpoorte, E.M.J., Harrison, D.J., *Anal. Chem.*, 1988, 60, 493
37. Horvai, G., Graf, E., Toth, K., Pungor, E., Buck, R.P., *Anal. Chem.*, 1986, 58, 2735
38. Lindner, R., *Bell Sys. Tech. J.*, 1962, 41, 803
39. Terman, L.M., *Solid State Electron.*, 1962, 5, 285
40. Grove, A.S., Deal, B.E., Snow, E.H., Sah, L.T., *Solid State Electron.*, 1965, 8, 145
41. Robinson, R.A., Stokes, R.H., *Electrolyte Solutions*; Butterworths Scientific Publications: London, 1955
42. Nancollas, G.H., *Interactions In Electrolyte Solutions*; Elsevier: Amsterdam, 1966
43. Fuoss, R.M., Accasina, F., *Electrolyte Conductance*; Interscience: New York, 1959
44. Barthel, J., *Angew. Chem. Int. Ed. Engl.*, 1968, 7, 260
45. Büchi, R., Pretsch, E., Simon, W., *Helvetica Chim. Acta*, 1976, 59, 2327
46. Kohlrausch, F., *Ann. Physik.*, 1855, 26, 108
47. Arrhenius, S., *Z. Physik. Chem.*, 1887, 1, 631
48. Ostwald, W., *Z. Physik. Chem.*, 1888, 2, 36
49. Debye, P., Hückel, E., *Physik. Z.*, 1923, 24, 185, 305
50. Onsager, L., *Physik. Z.*, 1927, 28, 277
51. Kratochvil, B., Yeager, H., in *Topics In Current Chemistry*, 1972, 27, 1

52. Fuoss, R.M., *J.Phys.Chem.*, 1978, 82, 2427

CHAPTER 2

A SEMICONDUCTOR ELECTRODE FOR USE IN STUDIES OF ISFET STRUCTURES

2.1 INTRODUCTION

Since Bergveld first exposed the insulator gate of a field effect transistor to an electrolyte solution to obtain a pH-responsive solid state device [1], much time and effort has been expended on the development of usable ion-sensitive field effect transistors (ISFET), and on better understanding the mechanism(s) of response of these devices [2-5]. In this chapter, we propose the use of semiconductor electrodes as models for the study of ISFET response behaviour. Similar systems have been reported in the literature, where they have been employed in the characterization of the electrolyte/insulator/semiconductor structure (EOS) [6] and the metal/oxide/semiconductor (MOS) capacitor [7,8,9]. In the case of the former study, the EOS structure was used as a model for the gate of a pHFET. It was noted that this structure, because of its simplicity, would not suffer from the non-ideal behaviour often exhibited by full-fledged transistor structures, hence facilitating the study of the electrolyte/oxide interface. This statement should hold true for the electrodes of interest in this chapter, though they differ from the EOS structures mentioned above in that a plasticized polyvinylchloride (PVC) membrane selective for K^+ has been introduced between the electrolyte and the oxide. Other characteristics of these electrodes

favouring their use as ISFET gate models are the ease with which they may be constructed in a lab, and their larger size. These electrodes are easily handled, and may be studied using standard electrochemical techniques. An equivalent circuit model describing the impedance response of semiconductor electrodes is developed in the following pages. Its validity is tested by comparing the measured AC impedance response of several electrodes to that predicted by this model.

2.2 THE MODEL

Figure 2.1 is a representation of the interfacial structure of the electrodes under consideration. The insulator in this case is sandwiched between a K^+ -selective membrane and an n-type silicon substrate, to give a membrane/insulator/silicon (MIS) electrode. The membrane is a plasticized polyvinylchloride (PVC) membrane based on the neutral ion carrier, valinomycin. It belongs to that class of membranes which is assumed to be electroneutral, and may be described as low capacity, low density ion exchangers [10]. The reversible exchange of K^+ from the aqueous phase into the membrane phase, made favourable because the valinomycin stabilizes K^+ through complexation in the latter phase, is the mechanism by which a potential difference is established across the electrolyte/membrane interface. The insulating layer may either be a thin native layer of SiO_2 (about 20 to 100 Å thick), a thicker (about 500 Å) layer of pyrolytic SiO_2 , or a layer of pyrolytic SiO_2 (about 500 Å) covered by Si_3N_4 (about 500 Å). The two interfaces formed by the insulator with the membrane and the silicon substrate, respectively,

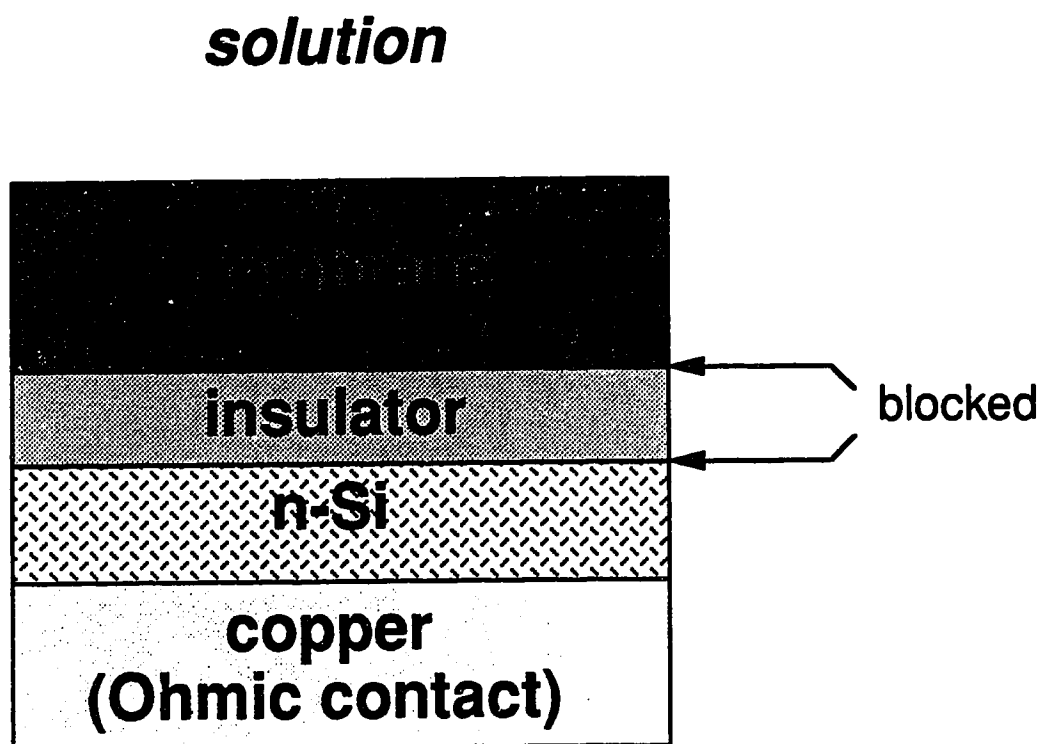


Figure 2.1 Interfacial structure of a MIS electrode.

are labelled "blocked" in Figure 2.1, referring to the fact that no net charge transfer can occur there. A change in the charge distribution at one side of the interface will be compensated by a change in the charge distribution at the other side of the interface through processes such as transient external current flow and chemical generation of charged surface species [11]. The presence of these two blocked, polarizable interfaces places the MIS electrode in the category of polarizable electrodes. An ohmic metal contact is made to the back face of the silicon. Bias potential applied to the electrode may be varied at this contact with respect to a non-polarizable reference electrode.

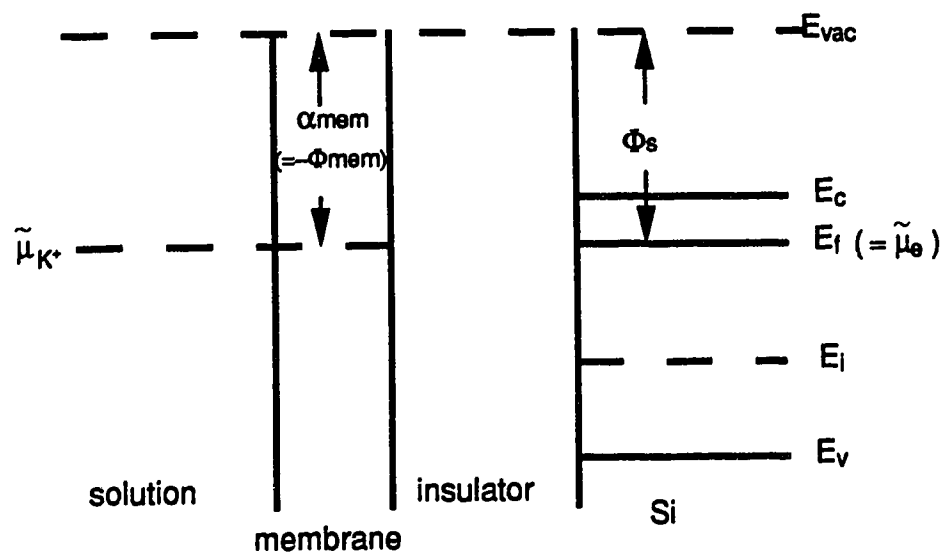
In Figure 2.2(a) is presented the energy band diagram for an ideal MIS electrode at thermal equilibrium when the applied bias is 0 V. The diagram is representative of those commonly used to depict the energy levels of MOS capacitors, except that now a liquid membrane has replaced the metal over the insulator. The diagram has been adapted from Janata et. al. [12] and Lauks [13]. The symbols used for various parameters stem from either the semiconductor physics or electrochemistry literature.

The first thing to note is that the electrochemical potential of K^+ in solution, $\tilde{\mu}_{K^+}$, is the same as that of K^+ in the membrane, since the reversible exchange of K^+ across this interface will ensure that equilibrium exists between phases. $\tilde{\mu}_{K^+,mem}$ consists of two terms, one chemical and one electrostatic, as shown in equation (1) for the membrane phase :

$$\tilde{\mu}_{K^+,mem} = \mu_{K^+,mem} + e\phi_{mem} \quad (1)$$

If one regards the membrane as being separated conceptually into an excess charge and dipole-free bulk, an outer ring of charge, and an outer ring of dipoles, then ϕ_{mem} is defined as the electrostatic inner potential of the phase, the total electrical work required to place a charge in the membrane phase.

a) ideal MIS



b) non-ideal MIS

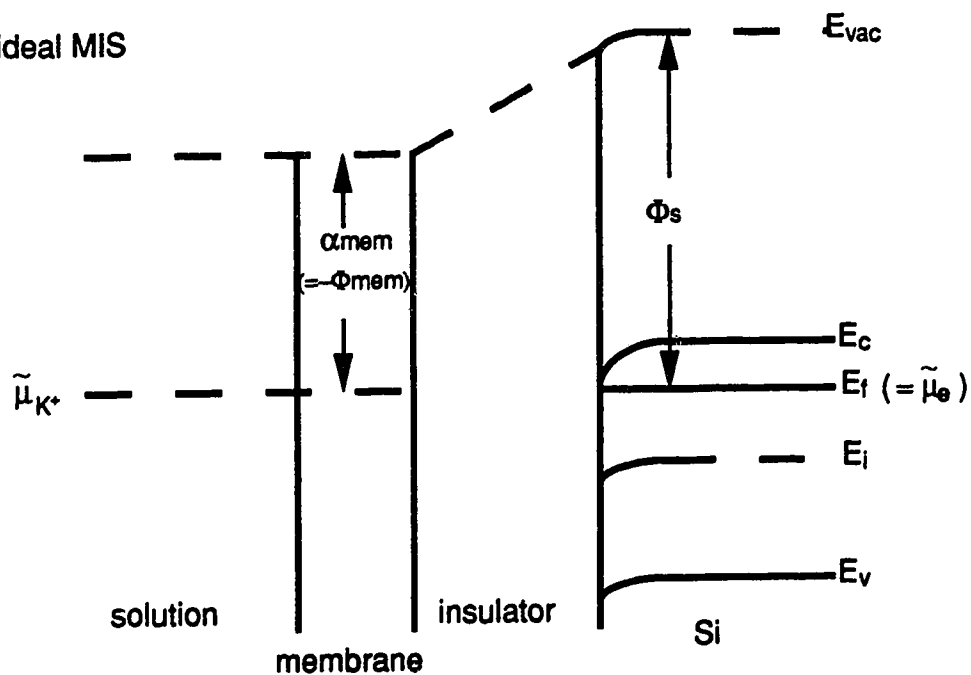


Figure 2.2 Energy band diagrams of an n-type Si-based MIS electrode at thermal equilibrium and no applied bias potential: a) ideal MIS electrode b) non-ideal electrode. The energy levels are defined in the text.

$\mu_{K^+,mem}$ is the absolute chemical potential, the energy required to place a charge inside a charge and dipole-free membrane [13]. e has its usual meaning of electronic charge. $\mu_{K^+,mem}$ may be related to the activity of K^+ in solution, $a_{K^+,soln}$, through the usual thermodynamic relationship :

$$\mu_{K^+,mem} = \mu_{K^+,soln} = \mu_{K^+,soln}^\circ + RT \ln a_{K^+} \quad (2)$$

E_c , E_v , E_i , and E_f mark four significant energy levels in the semiconductor. E_v indicates the uppermost boundary of the valence band, a band of essentially continuous energy levels, any of which may be occupied by electrons involved in the covalent Si-Si bonds of the semiconductor. E_c is the lowest energy level of the so-called conduction band, which is the band of allowed energies for free electrons. Electrons may not possess energies above the valence band less than that designated by E_c , so that the gap between E_v and E_c is referred to as the forbidden gap, or bandgap. E_i in Figure 2.2 may be thought of as the energy level in an intrinsic semiconductor at which the probability of occupation by an electron is exactly one half. It falls very close to the middle of the semiconductor bandgap.

Increasing the number of free electrons in a semiconductor through doping naturally increases the probability with which any one particular energy level in the conduction band may be occupied by an electron. The corresponding Fermi level of electrons in the n-type silicon, E_f , the energy level at which the probability of occupation by an electron is again one half, increases, so that it lies between E_i and E_c . E_f is the semiconductor equivalent of electrochemical potential for electrons in the n-type silicon substrate; note that in Figure 2.2, E_f has the alternate label, $\bar{\mu}_e$, to emphasize this fact. When the bias potential applied to the MIS electrode is 0 V, as in Figure 2.2, $\bar{\mu}_{K^+,mem}$ and E_f are equal.

The membrane and silicon are each characterized by an energy level known as the work function, which remains unchanged upon contact of these materials with any other phase. Φ_s is the semiconductor work function, which may be regarded as the energy required to remove an electron from the Fermi level of the semiconductor to a vacuum level just outside the silicon [14], here represented by E_{vac} . α_{mem} , the real potential of the membrane, is the electrochemical equivalent of the work function, except for the reversal in sign. α_{mem} consists of two terms, as indicated by equation (3):

$$\alpha_{mem} = \mu_{K^+,mem} + e\chi \quad (3)$$

χ is the surface bipolar potential, the energy required to transport a charge from just outside the membrane across the surface bipolar ring into the membrane. $\mu_{K^+,mem}$ again is the absolute chemical potential. In this ideal MIS electrode case, it has been assumed that Φ_s and α_{mem} are of equal magnitude, so that the vacuum level just outside the membrane falls at the same height as that of the silicon.

The assumptions that have been made in order to make the MIS electrode shown in Figure 2.2(a) "ideal" may now be described. Firstly, the difference in the work functions (or real potentials) of the membrane and semiconductor is 0. In general, this will not be the case. Secondly, it has been assumed that the insulator is ideal, meaning it contains no trapped charge states, which is also not true in most circumstances. Thirdly, the semiconductor itself, silicon in our case, is assumed to have no surface states. These are fixed charge states at the silicon/insulator interface that are due purportedly to dangling Si bonds and ionic silicon [15], left over after the oxide formation step of the wafer manufacturing process. The density of these states can be minimized with today's technology.

Should the difference between membrane and semiconductor work functions be non-zero, and/or either of the other above conditions for ideality not be satisfied, the situation shown in the semiconductor band diagram of Figure 2.2(b) will be observed. The difference between Φ_s and α_{mem} leads to the vacuum levels just outside these phases being different [14], and to a potential developing across the oxide. The flatband condition of the ideal MIS electrode of Figure 2.2(a), so called because the energy bands in the silicon are flat throughout the substrate, no longer exists, though the bias potential is still 0 V and the system is at thermal equilibrium. The semiconductor bands have bent downward at the n-Si/insulator interface, in order to accommodate the work function difference. If the flatband condition of Figure 2.2(a) is to be re-attained, a potential equal to the work function difference plus any potentials arising from insulator and silicon surface states would have to be applied to the electrode. This potential is known as the flatband potential, V_{fb} .

The downward bending of bands at the silicon surface results in excess negative charge collecting in this region due to a lowering of electron energy. The opposite could also be true under certain circumstances : that the upward bending of bands results in excess positive charge collecting in the silicon surface. This region at the silicon surface at which excess charge accumulates is known as the space charge region. It has associated with it a space charge capacitance, C_{sc} , whose magnitude depends on the region's width. This dimension is in turn dependent on applied potential, so that the behaviour of the space charge region of the MIS electrode under various bias conditions parallels that of the p-n junction on which ISFET's and other types of chemically sensitive solid state devices are based. This is the fundamental premise underlying the use of the MIS electrode as a model in the study of

ISFET response. The voltage sensitivity of C_{sc} is a feature which may be gainfully exploited in studies employing the MIS electrode, as measurement of electrode capacitance as a function of applied voltage effectively replaces measurement of current changes between the source and drain of a transistor.

The interfacial structure of the MIS electrode is such that its response is determined not only by potential differences over reversible interfaces allowing charge transfer but also by charge distributions associated with the blocked interfaces. The MIS electrode is therefore said to respond via a field effect mechanism. Because membrane potential is integrally related to the electric field and charge density gradient existing in this phase, a change in membrane potential will be compensated by adjustments in the latter two quantities. Since the membrane forms part of a multiphase structure, thermodynamic considerations demand that changes in the three membrane quantities be reflected as changes in potentials, fields, and charge density gradients across the insulator and silicon substrate. The discussion of Figure 2.2 centered on the energy band diagrams of a MIS electrode when $\tilde{\mu}_{K^+,mem}$ is the same as E_f (or $\tilde{\mu}_e$). Attention will now focus primarily on the behaviour of energy bands within the silicon substrate, and the changes in the capacitance of the silicon/insulator substrate structure that result as $\tilde{\mu}_{K^+,mem}$ in the membrane bulk changes. The discussion will be somewhat simplified, as it will not provide a detailed explanation of changes occurring over the entire charge and potential profiles of the MIS electrode. For the purposes of this chapter, however, the simplified discussion will suffice. Should a more detailed discussion of polarizable electrodes of the MIS type be desired, the reader is referred to articles by Lauks [13] and Buck and Hackleman [11], among others.

The effects of three different biasing conditions on band-bending in the space charge region of the silicon substrate are clearly illustrated in Figure 2.3, where $\tilde{\mu}_{K^+,mem}$ has been shifted up or down relative to E_f by applying a bias voltage at a constant concentration of K^+ . Figure 2.3(a) corresponds to the zero applied bias case of Figure 2.2(b), and has been included as a reference for the other three diagrams depicting three different bias conditions. Figure 2.3(b) is the energy band diagram for the situation that results when the $\tilde{\mu}_{K^+,mem}$ level in the membrane (and solution) is shifted downward with respect to E_f . The energy bands in the silicon bend downward in the space charge region in order to accommodate this change in bias potential. Majority carriers, electrons in this case, are attracted to the n-Si/insulator interface, so that an increased concentration of these carriers finds itself in the space charge region relative to the semiconductor bulk. This bias condition is then referred to, not surprisingly, as accumulation. A high density of electrons near the edge of the conduction band is allowed, so that the space charge region is narrow and C_{sc} is large, very much larger, in fact, than the capacitance associated with the insulator (C_{ox}). The capacitance of the silicon/insulator structure consists of the silicon and insulator capacitances in series, so that the capacitance observed for the silicon electrode, C_e , is equal to

$$C_e = \frac{C_{ox} C_{sc}}{(C_{ox} + C_{sc})} \quad (4)$$

Under accumulation, then, C_e will approach a value corresponding to C_{ox} alone.

Figure 2.3(c) depicts the so-called depletion condition, when the $\tilde{\mu}_{K^+,mem}$ level in the membrane is shifted upward

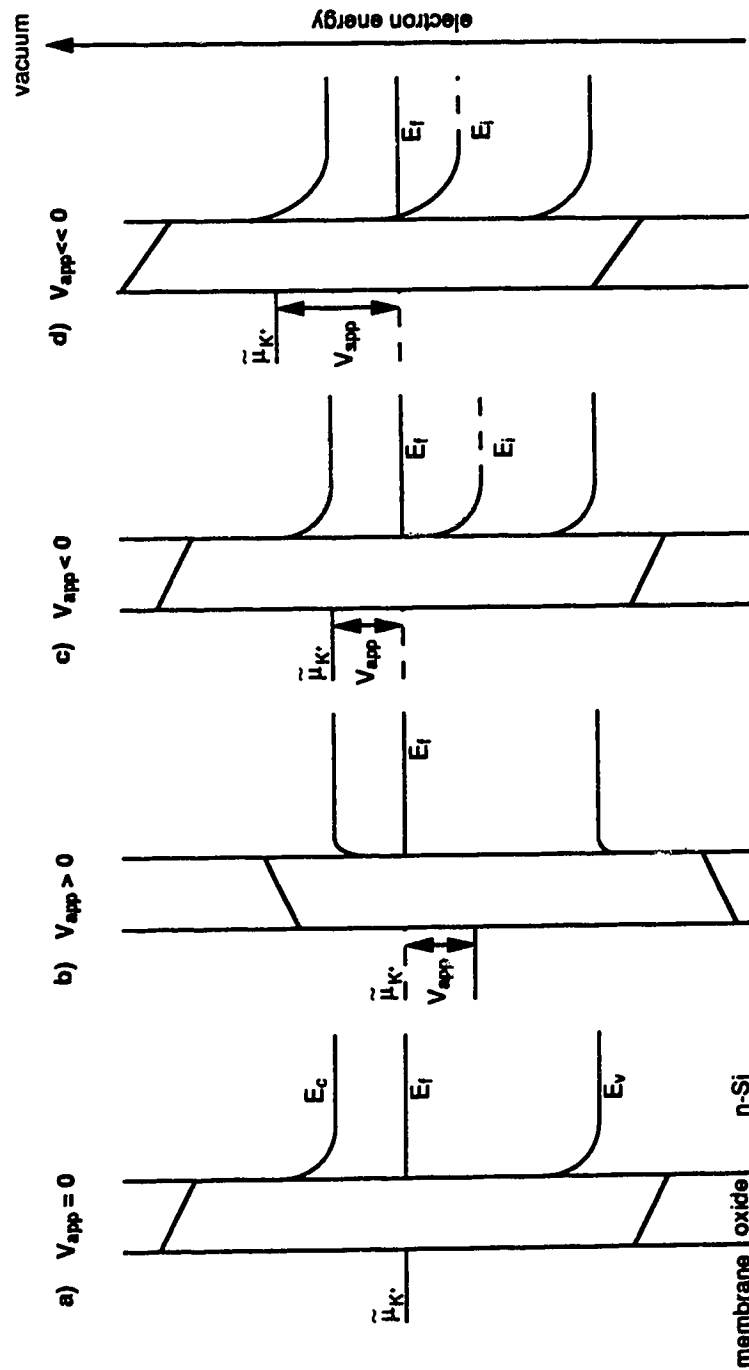


Figure 2.3: Energy level diagrams of a MIS electrode under 4 different biasing conditions: a) no applied bias b) accumulation c) depletion d) inversion

with respect to E_f . To accommodate this change, the semiconductor bands bend upward in the space charge region, causing majority carriers to be repelled from this area to leave behind immobilized ionized donor ions that are positively charged. The space charge region is now depleted of electrons, so that it becomes the surface depletion region, an area of positive space charge extending a relatively long way into the semiconductor bulk. C_{sc} is small, and C_e falls from its maximum value of C_{ox} .

The situation in 2.3(d) results when $\tilde{\mu}_{K^+,mem}$ has been shifted sufficiently upward with respect to E_f that E_i crosses over E_f in the surface depletion region, as shown. When this crossover occurs, the number of minority carriers, holes in this case, becomes larger than the number of majority carriers, or electrons, in a narrow region adjacent to the silicon/insulator interface, so that this region is said to be inverted. This bias condition is therefore referred to as the inversion case, and the narrow region of increased positive charge at the silicon surface known as the inversion layer. Once this layer is formed, the surface depletion region as a whole reaches its maximum width, since any additional positive charge resulting from further upward bending of the semiconductor bands will reside in the inversion layer. The density of space charge in the surface depletion region is now governed by the processes by which holes are generated (or emitted) and recombined (or captured) in the lattice, as well as by the existence of ionized donor atoms immobilized in the lattice. Whereas majority carriers can be removed from the semiconductor bulk with a time constant on the order of 10^{-12} seconds [9] generation/recombination processes occur at slower rates and are characterized by time constants on the order of 10^{-9} seconds or larger [7]. The magnitude of C_e is therefore dependent on the frequency at which the

capacitance measurement is carried out when the electrode is in inversion. At low frequencies, typically 100 Hz or less, generation/recombination rates are equal to or faster than the variation of the AC input signal, so that variations in the hole concentration can in essence follow fluctuations in that signal, leading to charge exchange with the inversion layer occurring in step with the measurement. The measurable C_{sc} is then very large, so that the C_e will again approach that of the insulator, C_{ox} . At high frequencies, these variations in hole concentration due to generation and recombination processes become inaccessible to the overall capacitance measurement. This means that all the incremental charge that results from the oscillating input signal appears at the edge of the depletion region. Since the width of this region is fixed at a relatively large value, the observed C_{sc} will be small and C_e will reach a minimum.

In Figure 2.3, the bias potentials may have been changed simply by varying the potential applied between the back contact of the MIS electrode and the reference electrode, or by changing the activity of K^+ , a_{K^+} , in solution. From the foregoing discussion, it is evident that a change in $a_{K^+,soln}$ will cause a redistribution of charge in the space charge region of the electrode by changing the degree of bandbending over this region. As a result, the magnitude of the associated flatband potential, V_{fb} , should also be changed. A functional MIS electrode, one which exhibits a shift in open circuit potential, V_{oc} , as $a_{K^+,soln}$ is varied, is thus expected to show a corresponding variation in measured V_{fb} . For MIS electrodes coated with plasticized membranes which are based on a neutral carrier and which may be considered to be electroneutral, this variation of V_{oc} and V_{fb} with $a_{K^+,soln}$ is predicted to be Nernstian [13].

2.3 EQUIVALENT CIRCUIT ANALYSIS OF THE MIS ELECTRODE

It is evident from the above discussion that the characteristics associated with the semiconductor of the MIS electrode are quite well understood, thanks in large part to the efforts of several groups to investigate the silicon/insulator interface and the response behaviour of the MOS capacitor [6-9]. In these earlier studies, it was recognized that the existence of charge densities in the insulator and at the silicon/insulator interface would give rise to characteristic capacitances for the oxide and the semiconductor space charge regions. Measurement of the impedance response of a structure like the MOS capacitor as a function of both frequency and applied potential yielded much information on how these capacitances, particularly C_{sc} , varied as a function of both variables, thus allowing for a better understanding of these structures and their response mechanism. Of course, the MIS electrode differs from the MOS capacitor in that a membrane has replaced the metal over the insulator, but as it turns out, valinomycin-based PVC membranes have been analyzed for their impedance response as a function of frequency as well [16-18]. These studies have led to a greater understanding of the nature of the potential determining mechanism of these membranes and the role of various membrane constituents.

On the basis of a knowledge of the membrane impedance and the semiconductor electrode characteristics, an equivalent circuit of the MIS electrodes we have examined is proposed in Figure 2.4. The semiconductor electrode introduces a space charge capacitance, C_{sc} , in series with the geometric capacitance of the insulator, C_{ox} [6-9], as mentioned above. As already seen in Equation (4), total electrode capacitance, C_e , is

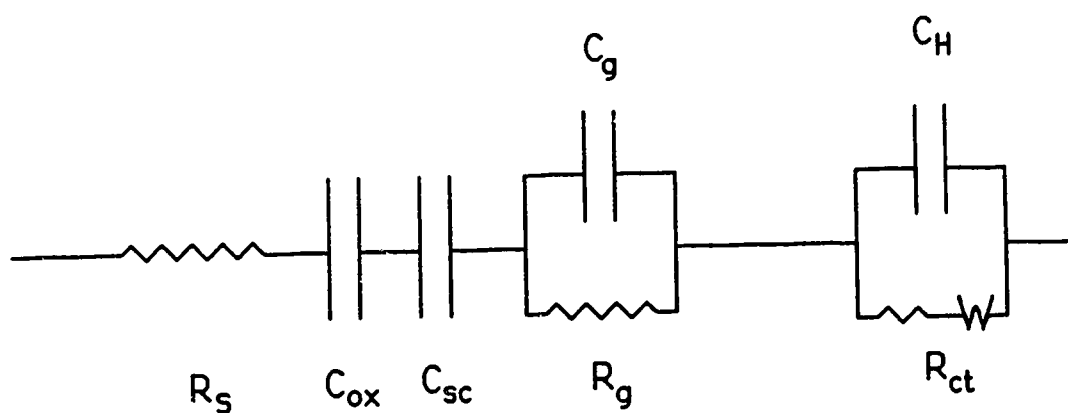


Figure 2.4: Equivalent circuit model for the MIS electrode. R_s is the series resistance of the solution and the Si electrode; C_{sc} and C_{ox} are the space charge and oxide capacitance, respectively, for the Si electrode; R_g and C_g are the geometric resistance and capacitance, respectively, associated with the membrane; C_H is the Helmholtz capacitance; R_{ct} is the charge transfer resistance; W is the diffusional or Warburg impedance.

$$C_e = \frac{C_{ox} C_{sc}}{(C_{ox} + C_{sc})} \quad (5)$$

The bulk membrane and membrane/solution interfacial impedances can be modelled as two lumped impedance networks [18]. The bulk membrane properties lead to a geometric resistance, R_g , and capacitance, C_g , in parallel. The solution/membrane interface leads to a network consisting of the double layer or Helmholtz capacitance, C_H , the charge-transfer resistance at the interface, R_{ct} , and the diffusional, or Warburg, impedance, W [18-20]. The impedance for a MIS electrode may then be written as follows :

$$Z_r = R_s + \frac{R_g}{1 + (\omega R_g C_g)^2} + \frac{R_{ct}}{1 + (\omega R_{ct} C_H)^2} \quad (6)$$

$$Z_{im} = \frac{1}{\omega C_e} + \frac{\omega C_g R_g^2}{1 + (\omega R_g C_g)^2} + \frac{\omega C_H R_{ct}^2}{1 + (\omega C_H R_{ct})^2} \quad (7)$$

where Z_r is the real or resistive component of the impedance and Z_{im} is the imaginary or capacitive component, and ω is the frequency term and is equal to $2\pi f$. Series resistance of the solution and the Si electrode, R_s , is small at 100 Ω , which, when compared to typical membrane resistances of $10^5 \Omega$ or more, allows it to be neglected in the overall analysis of the circuit. The elements arising from the membrane/solution interface are observed at frequencies below 5 Hz [21], indicating a long time constant. This circuit element will show high frequency limiting behaviour over the 25 Hz to 40 kHz range used in this study and so is not observed in our data. Equations (6) and (7) then reduce to the following :

$$Z_r = \frac{R_g}{1 + (\omega C_g R_g)^2} \quad (8)$$

$$\begin{aligned}
Z_{im} &= \frac{1}{\omega C_e} + \frac{\omega C_g R_g^2}{1 + (\omega C_g R_g)^2} \\
&= \frac{(1 + (\omega C_g R_g)^2) + (\omega C_e R_g)(\omega C_g R_g)}{\omega C_e (1 + (\omega C_g R_g)^2)} \quad (9)
\end{aligned}$$

These equations predict a semicircle at higher frequencies when Z_{im} is plotted versus Z_r in an impedance plane or Nyquist plot, since bulk membrane properties will dominate the impedance response. When ω is sufficiently low, the impedance response will be determined by electrode capacitance, C_e . Accordingly, a rapidly rising tail will be observed at these lower frequencies in the Nyquist plot because one is measuring a variation in $(\omega C_e)^{-1}$ for the most part; this usually occurs at frequencies less than 100 Hz. Viewing electrode impedance in terms of the related quantity, admittance (Y), this amounts to the imaginary component of Y being given by $Y_{im} = \omega C_e$. The direct proportionality of Y_{im} to C_e proved to be very useful to those researchers involved in the study of the Si/insulator interface in MOS capacitors and related structures, as it allowed a direct measurement of the dependence of C_e , or more precisely, C_{sc} , on applied voltage through measurement of Y_{im} . In the same way, Y_{im} measured for MIS electrodes at sufficiently low frequencies will be proportional to the electrode's C_{sc} and show a functional dependence on voltage.

At higher frequencies, however, the K^+ -selective membrane over the insulator plays a significant role in determining the magnitude of the measured Y_{im} , and the relationship $Y_{im} = \omega C_e$ no longer holds true. In order

to examine the higher frequency case more closely, first recall that the transformation of Z_{im} to Y_{im} may be accomplished using the relation below

$$Y_{im} = \frac{Z_{im}}{Z_r^2 + Z_{im}^2} \quad (10)$$

From Equations (8), (9), and (10), then, Y_{im} becomes

$$\begin{aligned} Y_{im} &= \frac{\frac{(1 + (\omega C_g R_g)^2) + (\omega C_e R_g)(\omega C_g R_g)}{\omega C_e (1 + (\omega C_g R_g)^2)}}{\frac{R_g^2}{(1 + (\omega C_g R_g)^2)^2} + \frac{[(1 + (\omega C_g R_g)^2) + (\omega C_e R_g)(\omega C_g R_g)]^2}{\omega C_e^2 (1 + (\omega C_g R_g)^2)^2}} \\ &= \frac{[(1 + (\omega C_g R_g)^2) + (\omega C_e R_g)(\omega C_g R_g)] [\omega C_e (1 + (\omega C_g R_g)^2)]}{(\omega C_e R_g)^2 + [(1 + (\omega C_g R_g)^2) + (\omega C_e R_g)(\omega C_g R_g)]^2} \end{aligned} \quad (11)$$

Since C_g tends to fall anywhere between 10 and 100 pF, and R_g is usually on the order of $M\Omega$'s, the assumption that $(\omega C_g R_g)^2 \ll 1$ may be made. This yields the expression for Y_{im} given in Equation (12) :

$$Y_{im} = \frac{\omega C_e + \omega C_g (\omega C_e R_g)^2}{(\omega C_e R_g)^2 + [1 + (\omega C_e R_g)(\omega C_g R_g)]^2} \quad (12)$$

For a typical "higher frequency" of 1000 Hz, and if C_e is 10 nF or so (as expected for MIS electrodes in the accumulation state having a surface area of about .05 cm²), Equation (12) may be treated in the limit where $(\omega C_g R_g)(\omega C_e R_g) \leq 1$ and $(\omega C_e R_g) > 10$, to yield

$$Y_{im} = \frac{1}{\omega C_e R_g^2} + \omega C_g \quad (13)$$

Y_{im} is now inversely proportional to C_e , the total electrode capacitance, and directly proportional to C_g . Y_{im} represents neither a pure electrode capacitance nor a pure membrane capacitance, so that measurement of this quantity at higher frequencies yields what may only be termed an equivalent capacitance, C_{eq} . Equation (13) shows that at sufficiently high frequencies, bulk membrane properties will dominate, and the equivalent capacitance, Y_{im}/ω , will be independent of applied voltage, provided that C_g is voltage independent.

Expected impedance response curves and equivalent capacitance-voltage curves for the MIS electrode may be calculated from equations (8) and (9). The modelling process is straightforward for the most part since all the parameters in these equations are voltage-independent except for C_{sc} . This latter capacitance may be calculated as a function of applied voltage using an equation derived by Garrett and Brattain for the space charge capacitance in n-type silicon [8,22]:

$$C_{sc} = \sqrt{\frac{q\epsilon_s\epsilon_0 N_0 \beta}{2}} \frac{\exp(\beta(-\Delta V)) - 1}{[\exp(\beta(-\Delta V)) - \beta(-\Delta V) - 1]^{1/2}} \left(\frac{F}{m^2}\right) \quad (14)$$

where : q = electronic charge

ϵ_s = silicon dielectric constant ≈ 12 [15]

ϵ_0 = permittivity of free space = 8.854×10^{-12} F/m

N_0 = carrier density $\approx 10^{21}$ m⁻³ (for the n-Si used in this study)

$\beta = \frac{q}{kT}$, where k and T have their usual meanings

$\Delta V = V_{applied} - V_{fb}$

Equation (14) accurately describes the C_{sc} when the electrode is in accumulation or depletion, but only deals with the high frequency case where inversion in the space charge region is not considered [8]. In other words, Equation (14) predicts that C_e will continue to decrease slowly upon transition of the electrode from depletion to inversion biases. At $\Delta V = 0$, Equation (14) reduces to the value of C_{sc} at V_{fb} , which is

$$C_{fb} = \sqrt{e\epsilon_s\epsilon_0 N_0 \beta} \quad (15)$$

Determination of V_{fb} , the flatband potential, for MIS electrodes may be achieved through use of the so-called Mott-Schottky relationship, first developed for metal-semiconductor contacts. Given in the following equation, this relates the space charge capacitance of the semiconductor, C_{sc} , to band-bending, ΔV , in the space charge region [15].

$$\frac{1}{C_{sc}^2} = \frac{2 (\Delta V - \frac{kT}{q})}{N_0 \epsilon_0 \epsilon_s q} \quad (16)$$

where : a) N_0 , ϵ_s , ϵ_0 , and q have the same meanings as in Equation (15)

b) $\Delta V = V_{applied} - V_{fb}$

c) $\frac{kT}{q} = \frac{1}{\beta}$ is a term that arises from the contribution of the mobile carriers to the electric field in the semiconductor

Note the similarity between this equation and that for C_{sc} , given above in Equation (14). Assuming N_0 is constant throughout the depletion region,

Equation (16) predicts that C_{sc}^{-2} is a linear function of V . The intercept of this line with the voltage axis ($C_{sc}^{-2} = 0$) gives V_{fb} . As discussed above, the impedance of the MIS electrode is dominated by $C_e (= C_{ox} C_{sc} / (C_{ox} + C_{sc}))$ at sufficiently low frequencies. Under these conditions, the measured C_{eq} will be related to V_{fb} in a manner analogous to that given by the Mott-Schottky equation, Equation (16). Plots of C_{eq}^{-2} vs V may be used to obtain V_{fb} 's as a function of $[K^+]_{(aq)}$ for the MIS electrodes under consideration. Since C_{eq} rather than C_e is employed in the V_{fb} determination, resulting values for this parameter shall hereafter be referred to as apparent flatband potentials.

2.4 EXPERIMENTAL

Semiconductor electrodes were prepared from n-Si wafers, (100) face (Monsanto, 4-in. diameter) having a resistivity of 3 to 4 Ω -cm. This corresponds to a dopant concentration of about 10^{15} cm^{-3} (10^{21} m^{-3}) [15]. 500 Å of SiO_2 , followed in some cases by 500 Å of silicon nitride (nominally Si_3N_4), were deposited onto these wafers by chemical vapour deposition by Process Technology, Ltd. (Oronoco, New Brunswick, Canada). Insulating film on the back face was removed by application of etchant, either 5 min. of 10 % HF (Si/SiO_2) or 5 min. of 48 % HF ($\text{Si}/\text{SiO}_2/\text{Si}_3\text{N}_4$). Wafers were scribed to give $\sim 7\text{mm} \times 7 \text{ mm}$ pieces. Ohmic contact was made to the back face with Ga/In eutectic [23] and then Ag epoxy contacted the back face to a coiled copper wire. This assembly was cured (100°C , 3 h) and then cleaned in H_2O , CH_3OH , trichloroethylene, CH_3OH , and H_2O , followed by 30 s in 5 % HF. Electrodes were then insulated with epoxy (Clear, Hysol) to give exposed areas $\sim 3 \text{ mm} \times$

3 mm, cured 24 h at room temperature, and recleaned with H₂O, CH₃OH, trichloroethylene, CH₃OH, and H₂O. Under a tetrahydrofuran-saturated atmosphere, membranes were cast by evaporation of 1 to 4 drops of the following solution [24]: 3 mL of tetrahydrofuran (BDH, distilled from LiAlH₄ or K); 0.15 g of dioctyl adipate (Fluka); 0.075 g of poly(vinylchloride) (PVC) (Polysciences, chromatographic grade); 0.0015 g of valinomycin (Sigma); and 25 µg of potassium tetrphenylborate (KTPB) [25].

Impedance measurements and capacitance-voltage (C_{eq} -V) curves of MIS electrodes were made possible using the experimental set-up pictured in Figure 2.5. The electrochemical cell had a standard three-electrode configuration, with a saturated calomel electrode contained in a double junction filled with 0.1 M NH₄Cl serving as the reference electrode. The total capacitance of this cell is represented by

$$\frac{1}{C_{TOT}} = \frac{1}{C_{MIS}} + \frac{1}{C_H} + \frac{1}{C_{CE}} \quad (17)$$

where :

C_{TOT} = measured capacitance

C_{MIS} = MIS electrode capacitance

C_H = Helmholtz layer capacitance of MIS electrode

C_{CE} = capacitance of counter electrode

The relationship of C_{TOT} to the capacitance of the reference electrode is complex, and is not included in Equation (17). While reference electrode capacitance could potentially be a problem in a measurement of this kind, it was found that use of large area Ag/AgCl wires and commercial electrodes with and without double junctions caused no changes in C_{TOT} . Test solutions

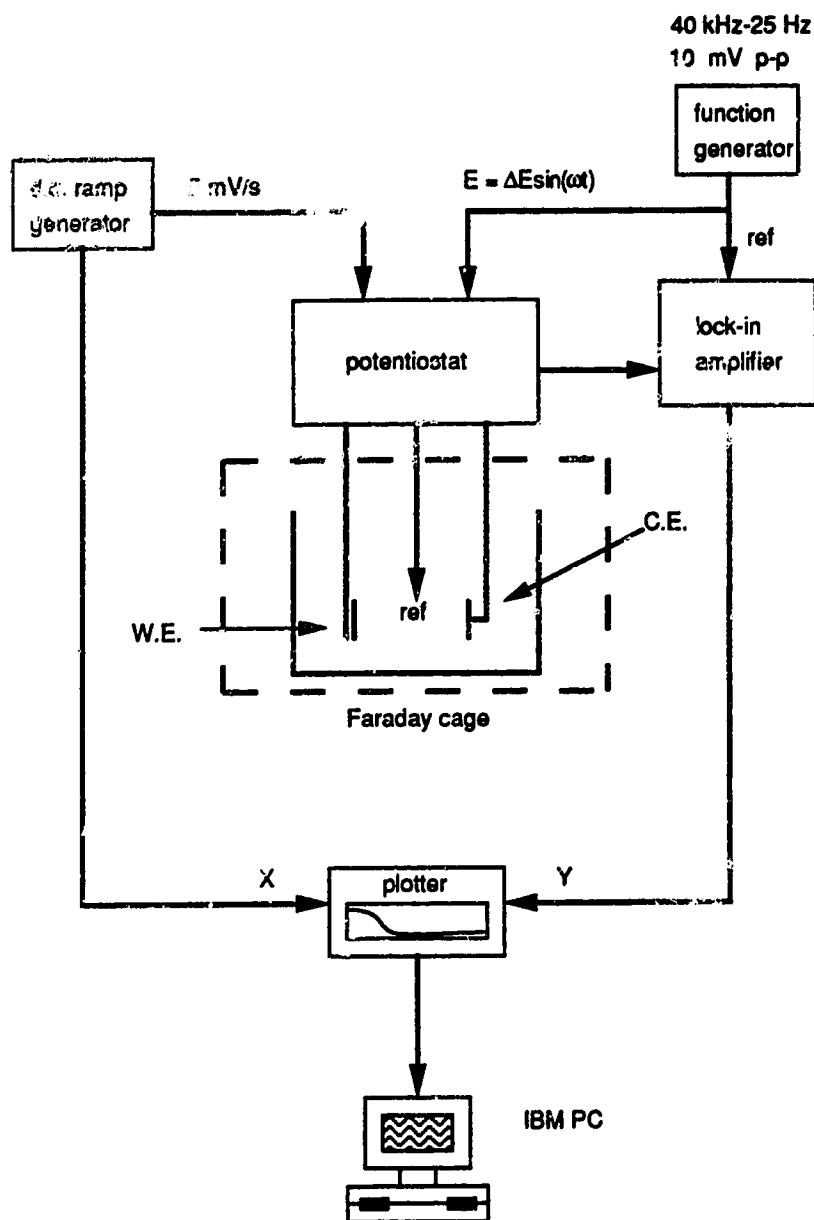


Figure 2.5 Instrumental set-up used in capacitance-voltage (C_{eq} -V) and impedance measurements.

were of varying KCl concentrations, maintained at a constant ionic strength of 0.1 by NaCl; with 0.1 M supporting electrolyte, $C_H \gg C_{MIS}$, so that C_H will have no effect on C_{TOT} . Use of a large-area Pt mesh (80 mesh) counter electrode ensured that $C_{CE} \gg C_{MIS}$. Therefore, neither the reference nor the counter electrodes affected the impedance measurements. As a result, observed impedance can be viewed as a cell resistance, R_s , in series with the MIS electrode impedance, which is modelled according to the equivalent circuit discussed above. As illustrated in Figure 2.5, the electrochemical cell was housed in a Faraday cage, both to keep the Si electrode in the dark so as to prevent production of photocurrent, and to prevent extraneous sources of noise from affecting the small-amplitude signal being monitored.

Potentiostatic control and current measurement for an AC experiment were provided by an Amel 521 potentiostat (Amel, Milan, Italy), modified to allow two external inputs to the summing point of the potentiostat control circuit. The potential applied to the MIS electrode was the sum of a DC potential and a small amplitude AC signal, described by $E_{AC} = E_0 \sin\omega t$, E_0 being about 5 mV. A Hi-tek PPRI waveform generator was the source of the DC potential, which in the case of C_{eq} -V measurements was slowly swept at 5 mV/s. An HP 200 AB audio oscillator provided the 10 mV peak-to-peak sine wave. The applied potential was then

$$E_{app} = E_{DC} + E_0 \sin\omega t \quad (18)$$

The resulting current flowing in the cell was fed into a PAR Model 5204 lock-in analyzer, which separated this current signal into in-phase (real) and out-of-phase (imaginary) components, with respect to the phase of the applied oscillation. The lock-in analyzer output signal was monitored with an HP

7090 A digital recorder/plotter, with the digitized signal being subsequently transferred to an IBM PC for data analysis.

Since it is i_{AC} that is being measured by the PAR 5204, and $i_{AC} = E_0/Z = E_0 \cdot Y$, where Y is admittance, the outputs being recorded by the HP are in effect real and imaginary admittances. The quadrature portion of the output is a direct measure of the MIS electrode's equivalent capacitance, C_{eq} , which at sufficiently low frequencies becomes proportional to C_e , as mentioned previously. Recording C_{eq} -V curves for MIS electrodes becomes a matter of simply acquiring the quadrature signal as a function of the applied DC ramp (5mV/s) and of frequency. However, in order to quantify the observed C_{eq} , the system's quadrature response must be calibrated to obtain the proportionality constant between Y_{im} and C_{eq} at each frequency used. This was done by replacing the cell with a number of capacitors varying from 2 pF to 80 nF, the expected range of capacitances to be measured for the MIS electrode, in series with a 100 Ω resistor, and measuring the magnitudes of the corresponding quadrature (Q) signals. The resulting Q-C calibration curves were linear over the entire range of capacitances used. At low frequencies, the direct proportionality between Y_{im} and C_e facilitated determination of apparent flatband voltages, V_{fb} , through the Mott-Schottky relation, Equation (16).

Impedance experiments for MIS electrodes were carried out by acquiring both real and imaginary admittances as a function of frequency, at a fixed DC potential and over frequencies ranging from 40 kHz to 25 Hz. It was found that the instrumental system itself introduced slight frequency-dependent phase shifts to the output signal. It was therefore necessary to compensate for these phase shifts by replacing the electrochemical cell with a

capacitor (between 10 pF and 40 nF) and adjusting the in-phase component of current to zero at each frequency, to develop a calibration curve of the changes in phase shifts as a function of frequency. This calibration curve was then used in subsequent impedance measurements. Once the real and imaginary admittances had been acquired and transferred to the IBM PC, they were converted to impedances through the transformations

$$Z_{im} = \frac{Y_{im}}{Y_{im}^2 + Y_r^2} \quad (18)$$

and

$$Z_r = \frac{Y_r}{Y_{im}^2 + Y_r^2} \quad (19)$$

The data was then presented as a Nyquist or impedance plane plot, in which Z_{im} was plotted versus Z_r ; MIS electrodes generally yielded plots of the form shown in Figure 2.6. Each point represents data acquired at a different frequency, with the frequency of the measurement decreasing as one moves from left to right on the plot. As predicted by Equations (8) and (9) for Z_r and Z_{im} , a semicircle due to the bulk membrane is observed in this plot at higher frequencies, with a rapidly rising tail due to the silicon electrode occurring at lower frequencies. R_g may be determined from a Nyquist plot by extrapolating the semicircle at the low frequency end to obtain the real axis intercept, as shown in Figure 2.6. C_g is subsequently evaluated by finding the frequency at which Z_{im} is a maximum in the semicircle, termed ω_{max} , and then employing the relation $\omega_{max} = 1/(R_g \cdot C_g)$.

However, since measured impedances rarely fell directly on the point at which Z_{im} was a maximum, an accurate estimate of ω_{max} was sometimes quite difficult to make. Determination of R_g and C_g may alternatively be

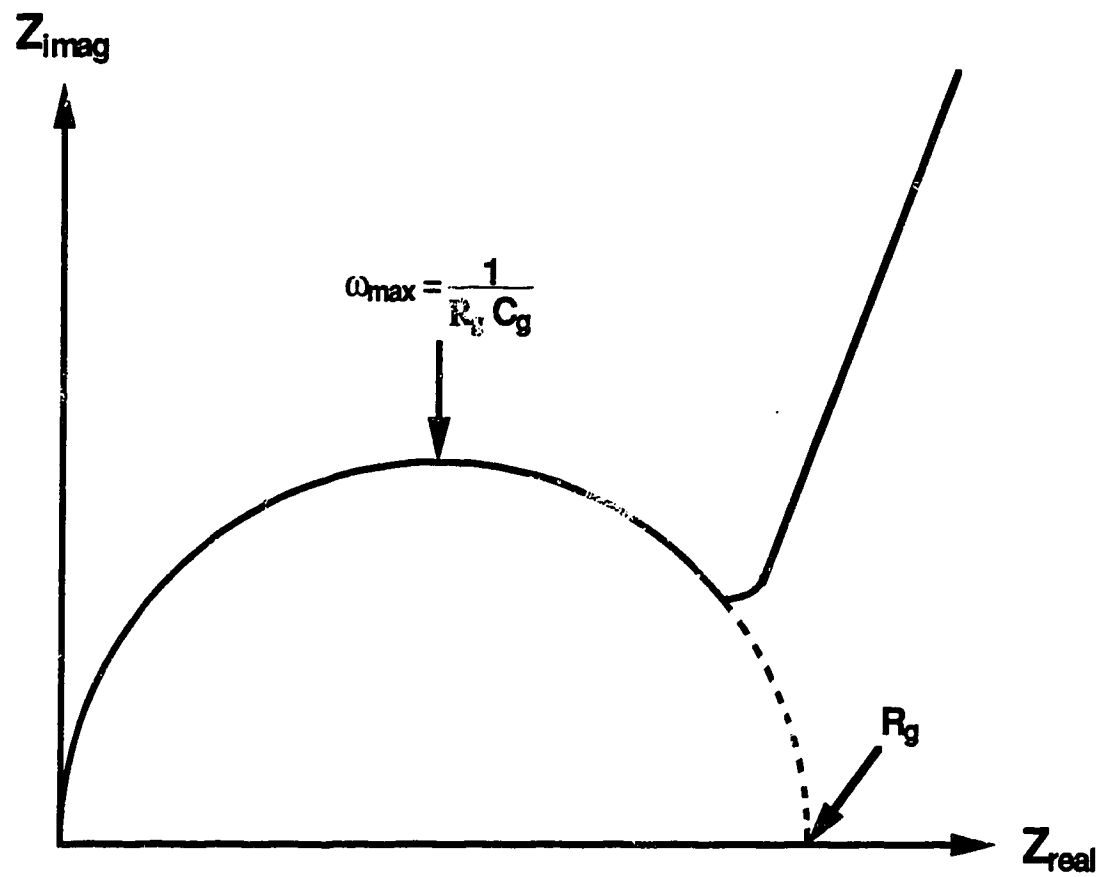


Figure 2.6 The type of Nyquist plot expected for the equivalent circuit of Fig. 2.4. The RC element due to the membrane solution interface is not observed over the frequency range employed for impedance measurements in this study.

accomplished by fitting impedance data comprising the semicircle of the Nyquist plot according to one of the following expressions

$$\frac{1}{Z_r} = \frac{1}{R_g} + R_g C_g^2 \omega^2 \quad (20)$$

or

$$\frac{\omega}{Z_{im}} = \frac{1}{C_g R_g^2} + C_g \omega^2 \quad (21)$$

Equations (20) and (21) predict that plots of Z_r^{-1} vs ω^2 or $\omega \cdot Z_{im}^{-1}$ vs ω^2 will yield straight lines, as indeed is found to be the case for the experimentally obtained data. Linear regression allows evaluation of R_g and C_g from the slope and intercept of either equation. This method proved to be more convenient than fitting impedance data to obtain C_g and R_g than the extrapolation method described above. The precision of R_g and C_g values measured by AC impedance analysis for MIS electrodes was determined by the instrumentation used for these experiments, and was about 1 to 2 % for R_g and about 5 % for C_g . Since stray capacitance within the instrumental system was estimated to be about 10 pF, 10 pF was subtracted from each experimentally determined C_g .

2.5 RESULTS AND DISCUSSION

Figure 2.7(a) shows a typical Nyquist plot of the impedance response of a MIS electrode in 0.1 M KCl, measured over a frequency range of 40000 Hz to 25 Hz. A single semicircle is observed at frequencies greater than 200 Hz, with a rapidly rising tail developed at lower frequencies, as predicted by equations (8) and (9). The Nyquist plot for a Pt electrode coated with a membrane of

similar thickness is given in Figure 2.8(a). Again, a single semicircle appears in this plot, but the tail at low frequencies is conspicuously absent. For both electrode configurations the values of R_g and C_g are functions of membrane thickness, with R_g increasing and C_g decreasing as thickness increases. Consequently, the RC element observed is assigned to the bulk membrane components C_g and R_g , in agreement with previous results [21, 26-28].

The corresponding Z_r^{-1} vs ω^2 plots of the data defining the semicircles in Figures 2.7(a) and 2.8(a) are given in Figures 2.7(b) and 2.8(b). From the slope and intercept of the plot in Figure 2.7(b), the R_g and C_g of the MIS electrode were found to be 1.02 M Ω and 52 pF, respectively. The time constant, τ , due to charging of the external space charge regions of the membrane coupled to membrane resistance, is thus 0.05 milliseconds, as calculated from the relation $\tau_{\text{mem}} = C_g R_g$. Extrapolation of Z_r^{-1} vs ω^2 over the 200 to 1500 Hz range for the membrane covering the Pt electrode yielded an R_g and C_g of 14.2 M Ω and 13 pF, respectively, in Figure 2.8(b). This is not in agreement with the low frequency intercept of the Nyquist plot in Figure 2.8(a). However, extrapolation of Z_r^{-1} vs ω^2 for this electrode over lower frequencies, from 25 to 400 Hz, yielded an R_g of 15.4 M Ω and a C_g of 22 pF. This latter value of R_g is close to that expected upon inspection of Figure 2.8(a). The dependence of R_g and C_g on the frequency range over which the data is extrapolated shows that the membrane is not a pure R-C network, but rather may consist of a series of R-C networks having very similar time constants [18]. τ_{mem} calculated for the Pt electrode at low frequencies is 0.34 ms. The fact that the two τ_{mem} 's are of similar magnitude is consistent with the above assignment of the observed RC element to the bulk membrane

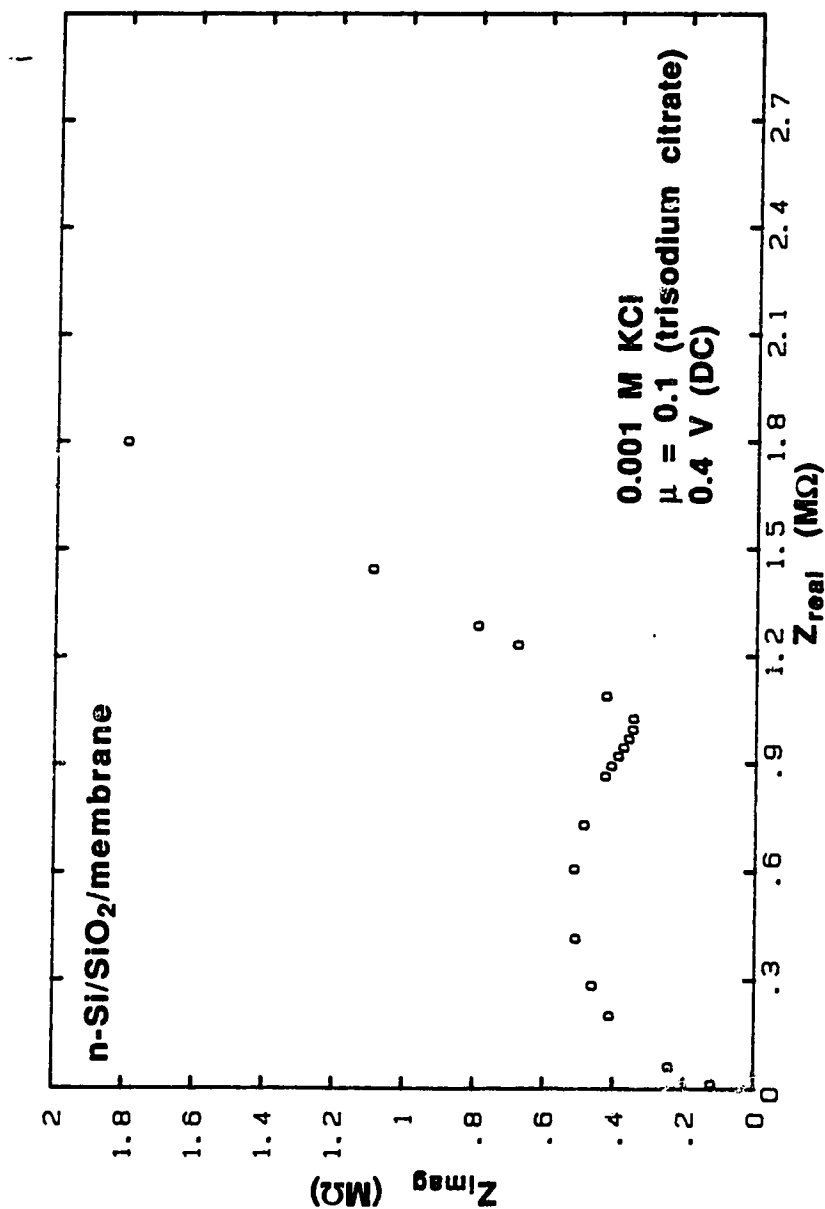


Figure 2.7(a): Nyquist plot of an n-Si/SiO₂/membrane electrode over a frequency range of 25 Hz to 40 kHz, measured in a solution containing 10⁻³ M KCl and buffered at pH 4.5 using 0.1 M trisodium citrate. A DC potential of 0.4 V vs SCE was applied, biasing the electrode into accumulation. This plot provides a good example of the type of Nyquist plot to be expected for MIS electrodes.

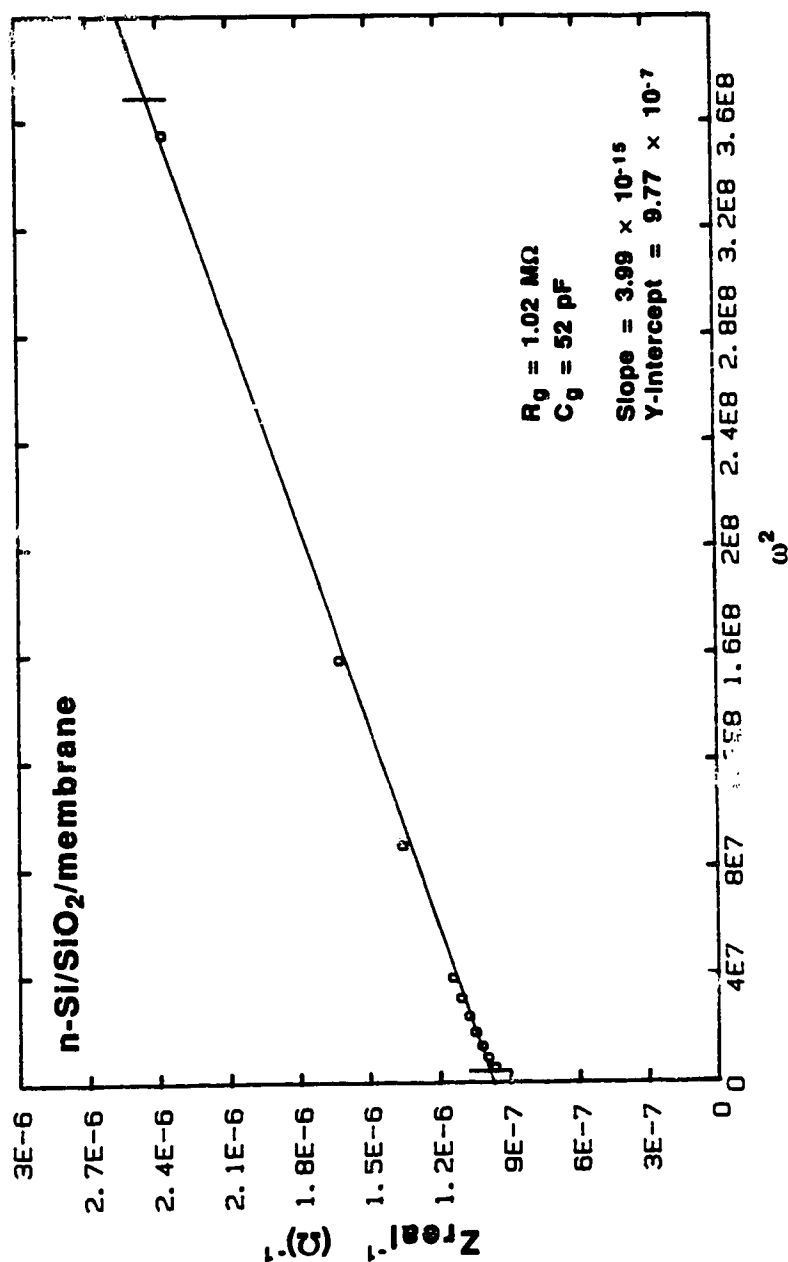


Figure 2.7(b) Plot of Z_{real}^{-1} vs ω^2 for the Nyquist plot of Figure 2.7(a). To evaluate R_g and C_g for the MIS electrode, data comprising the semicircle of Fig. 2.7(a) from its maximum to the point at which the rising tail begins to develop was considered. In this instance, linear regression is applied to the region of the Z_{real}^{-1} vs ω^2 curve corresponding to frequencies of 500 to 3000 Hz. From Equation (20), the slope and y-intercept of this best fit line yield an R_g of 1.02 M Ω and a C_g of 52 pF.

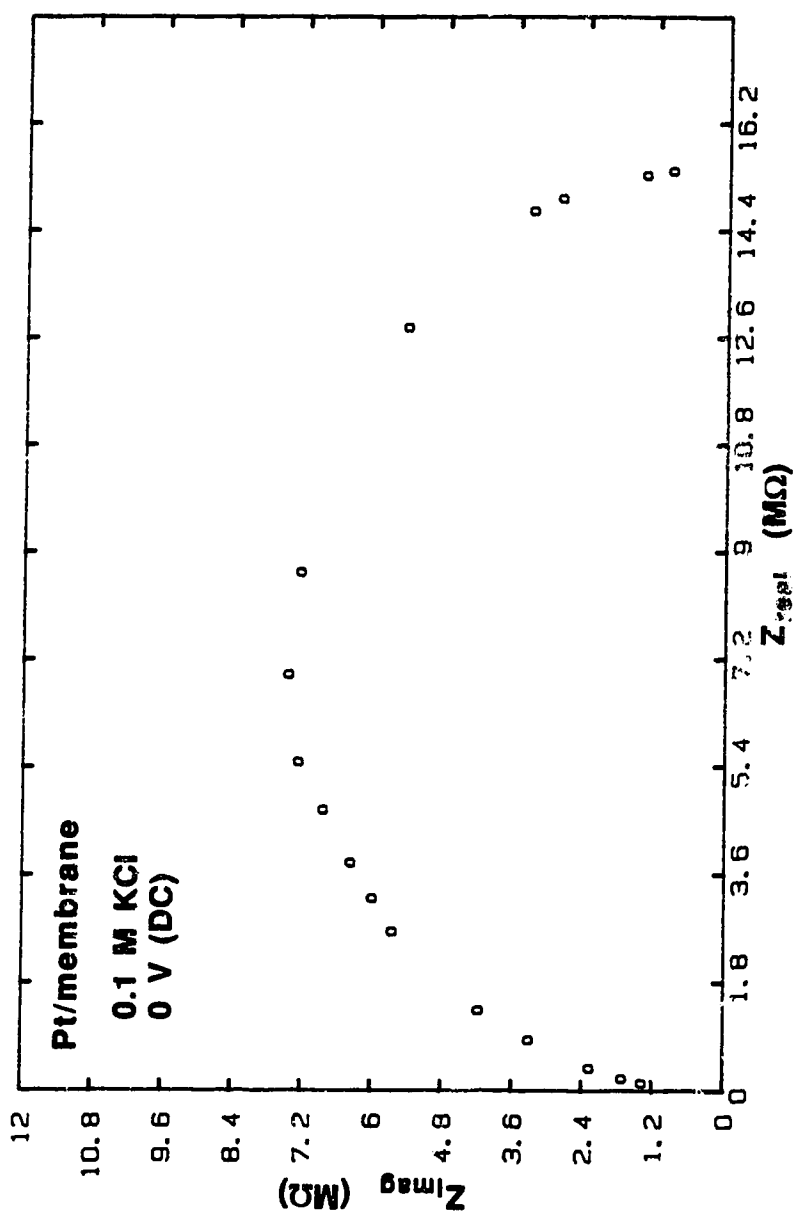


Figure 2.8(a) Nyquist plot of the membrane-coated Pt electrode over a frequency range of 25 Hz to 40 kHz, measured in 0.1M KCl. A DC potential of 0 V vs SCE was applied. The observed semi-circle is due to the RC element arising from the bulk membrane properties, R_g and C_g .

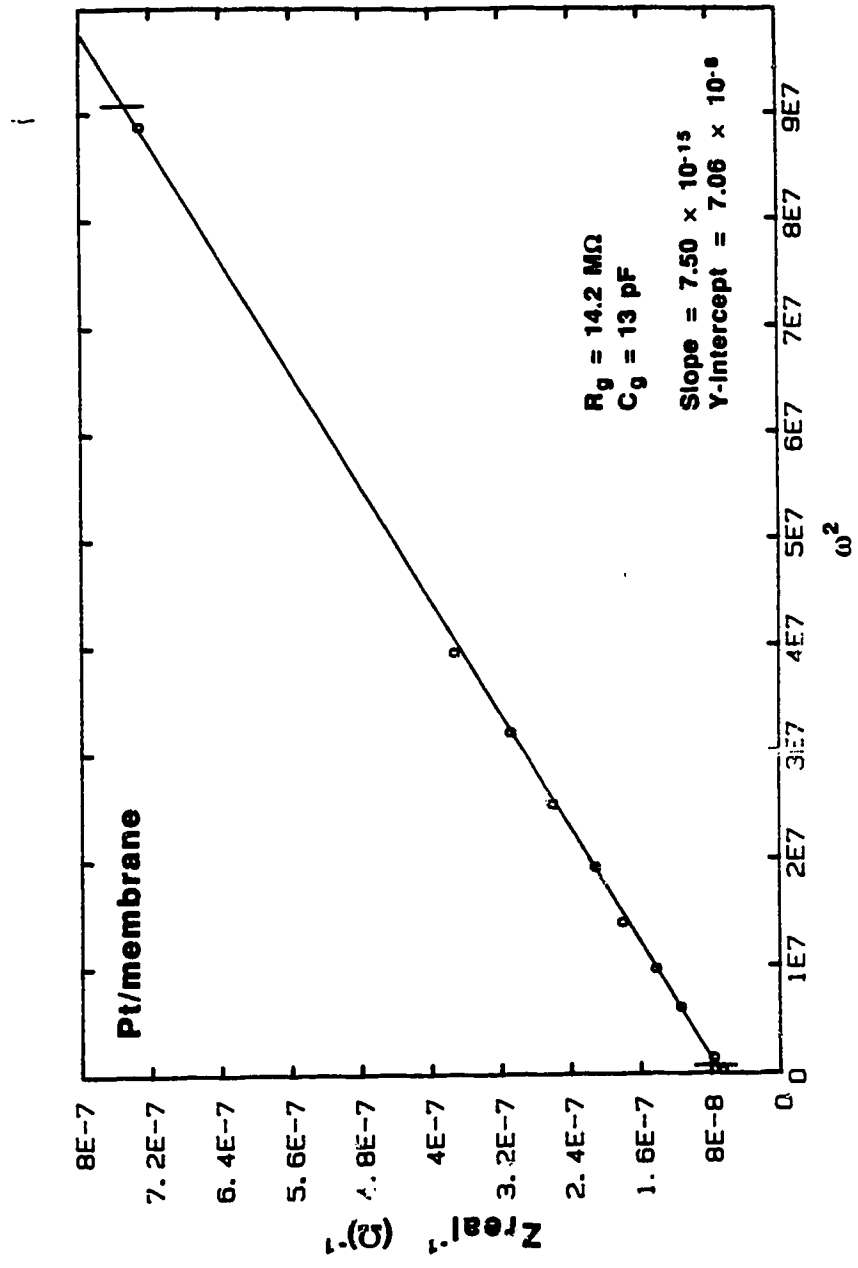


Figure 2.8(b) Plot of Z_{real}^{-1} vs ω^2 for the Nyquist plot of Fig. 2.8(a). To evaluate R_g and C_g for the Pt/membrane electrode, data comprising the semicircle from its maximum to the point of maximum Z_{real} are considered. In this instance, the region of the Z_{real}^{-1} vs ω^2 curve corresponding to the frequency range 200 to 1500 Hz was fitted by linear regression. From Equation (20) the slope and the y-intercept of this line yield an R_g of 14.2 M Ω and a C_g of 13 pF for the membrane coating the Pt electrode.

components R_g and C_g , but also shows the membrane to membrane variation that is often observed.

Figure 2.9(a) shows the C_{eq} - V curves recorded for an n-Si/SiO₂/membrane electrode at frequencies characteristic of the two frequency regimes of Figure 2.7(a). The horizontal axis in this figure is the voltage applied to the electrode with respect to the SCE reference electrode, with the flatband condition for the electrode falling in the region around 600 mV. At 10000 Hz, where the bulk membrane is predicted to dominate the impedance response, the C_{eq} - V curve shows only slight dependence on voltage. This is consistent with results on Pt/membrane electrodes or standard ISE's, for which the equivalent capacitance, C_{eq} , is independent of applied voltage over the frequency range encompassed by the membrane RC element above. At 100 Hz, where a tail develops for MIS electrodes in the Nyquist plot, the C_{eq} - V curve is strongly voltage dependent, and is consistent with observation of the semiconductor space charge capacitance, C_{sc} . The voltage range over which C_{eq} is at a maximum and appears to be levelling off corresponds to accumulation in the electrode. At more positive voltages, the decrease in C_{eq} mirrors the electrode capacitance, C_e , as it falls to its flatband value, and further to its eventual depletion value.

Figure 2.9(b) shows what the theoretical C_{eq} - V curves for the electrode of 2.9(a) look like, for R_g and C_g values extrapolated from the Nyquist plot for this electrode in 0.1 M KCl. The voltage axis for these curves is defined with respect to V_{fb} , with the origin occurring at $V=V_{fb}$. These values, as well as the values of R_s and C_{ox} used in the calculation, are given in the figure caption. The estimate of C_{ox} was obtained from the expression $C_{ox} = \epsilon_0 \epsilon_{ox} A/d$, where ϵ_{ox} , the insulator's dielectric constant, is about 3.9 for SiO₂ [9], d is about 500 Å,

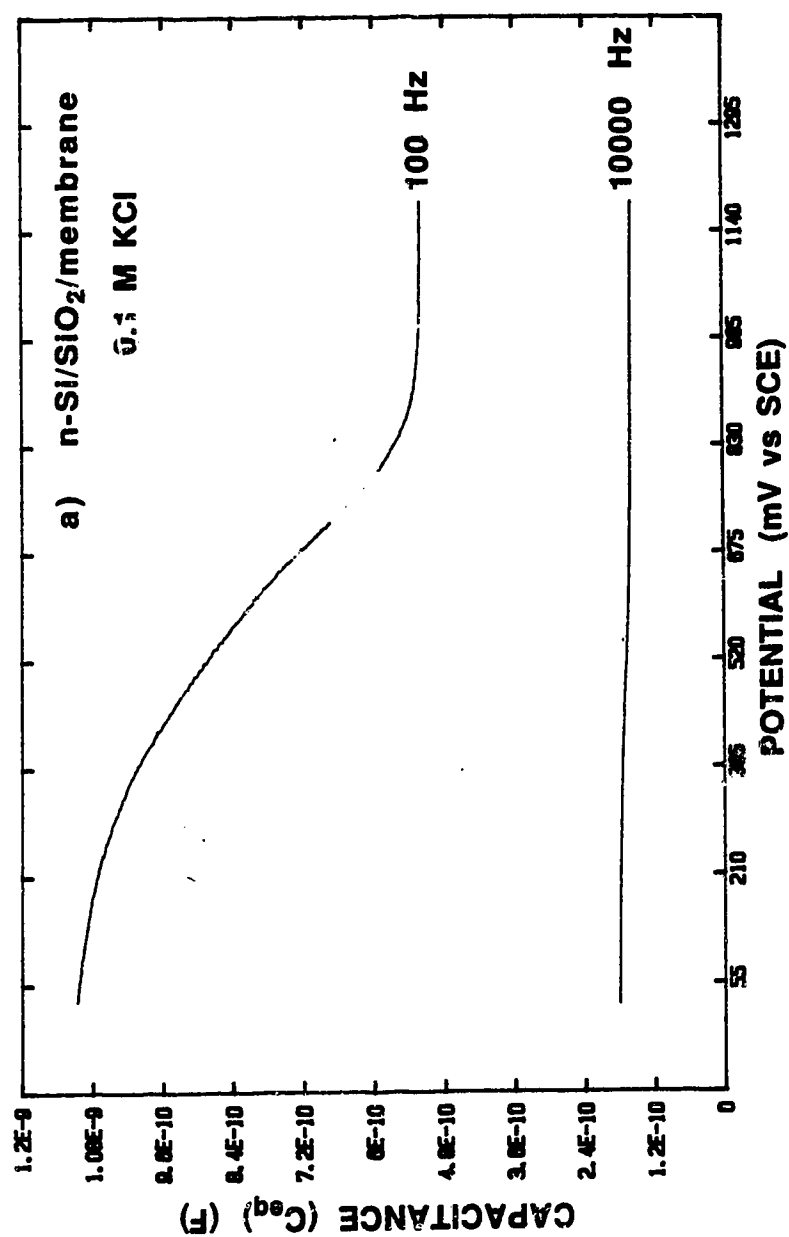


Figure 2.9(a) C_{eq} -V curves for an n-Si/SiO₂/membrane electrode obtained at 100 Hz and 10 kHz in 0.1 M KCl. The voltage dependence of C_{eq} at 100 Hz is consistent with the observation of the semiconductor space charge capacitance, C_{sc} . At 10 kHz, membrane capacitance, C_g , dominates the response, and C_{eq} is only slightly voltage-dependent.

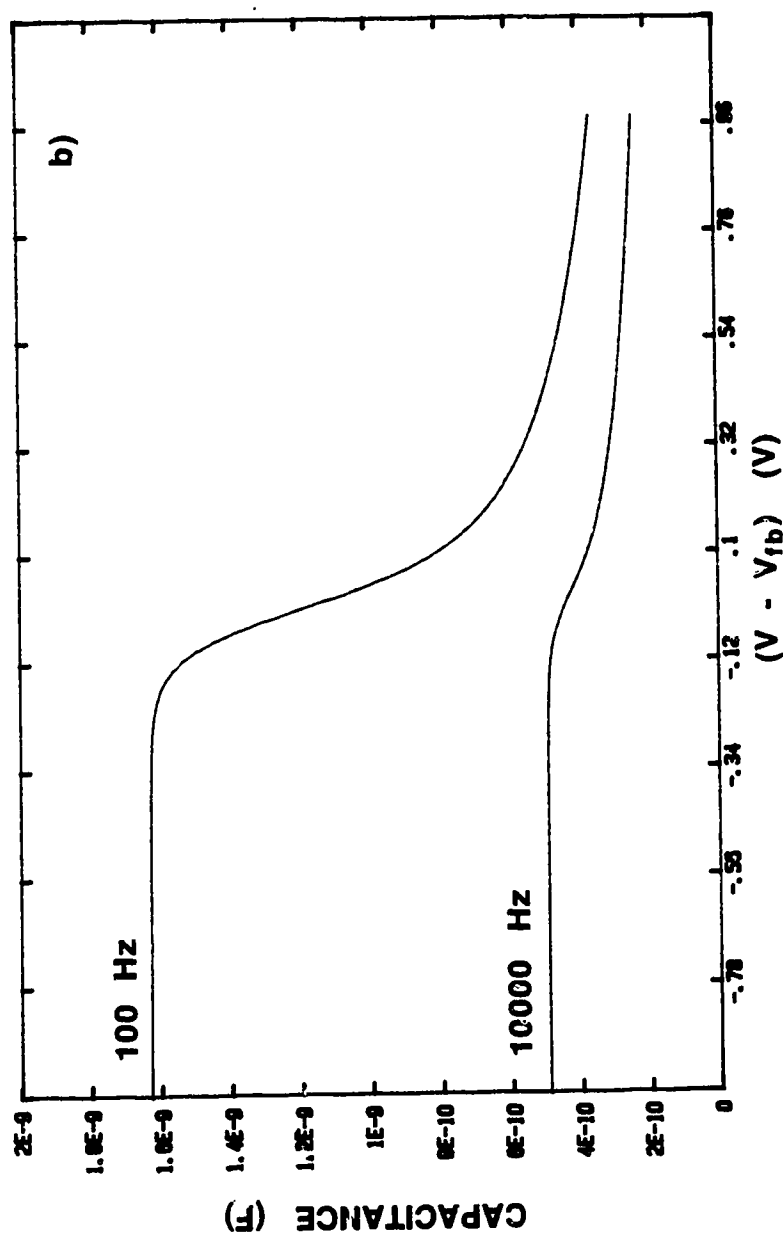


Figure 2.9(b) Model C_{eq} -V curves calculated for the MIS electrode of Figure 2.9(a) at 100 Hz and 10 kHz, using Equations (8)-(10). R_s was assigned a typical value of 100Ω . C_{ox} was calculated to be 1.7 nF. The values of R_g and C_g used in the calculation were $0.16 M\Omega$ and 700 pF, respectively, from the Nyquist plot of this electrode in 0.1 M KCl (not shown).

and electrode area estimated to be about $2.5 \times 10^{-2} \text{ cm}^2$ ($1.5 \text{ mm} \times 1.5 \text{ mm}$). These curves, calculated at 100 Hz and 10000 Hz demonstrate similar characteristics when compared to their experimental counterparts, so that the frequency dependence of the C_{eq} -V curves measured for MIS electrodes may be predicted using equations (8) and (9).

The curves presented in Figure 2.10(a), recorded for another n-Si/SiO₂/membrane electrode, document what happens to the C_{eq} -V curve of a MIS electrode at frequencies where both the membrane and the Si electrode contribute to Y_{im} in varying degrees. These curves were recorded at 25, 40, 50, and 100 Hz, and exhibit shapes that are intermediate between the high and low frequency cases of Figure 2.9(a). Note that while the C_{eq} behaviour of this MIS electrode was recorded at frequencies less than 100 Hz, limiting low frequency behaviour was not observed, unlike the MIS electrode of Figure 2.9(a). This is due to membrane R_g and C_g differing from one electrode to the other because membrane surface area and thickness differ. Though Y_{im} response was not calibrated for the C_{eq} -V curves of Figure 2.10(a), they were all recorded at the same instrumental settings. As a result, it can be concluded that the range of capacitances encompassing each curve increases as frequency decreases. This is in accordance with C_e playing an increasingly important role in determining Y_{im} . At 25 Hz, the C_{eq} of the electrode in Figure 2.10(a) falls off significantly with applied voltage toward the positive end of the voltage range. Even though the maximum C_{eq} at 25 Hz is not measured when the electrode is in accumulation, it appears that the curve is approaching low frequency limiting behaviour. As frequency increases, the smallest C_{eq} is measured at accumulation biases, and the curves become more sigmoidal again, although their shapes are the reverse of the curves acquired

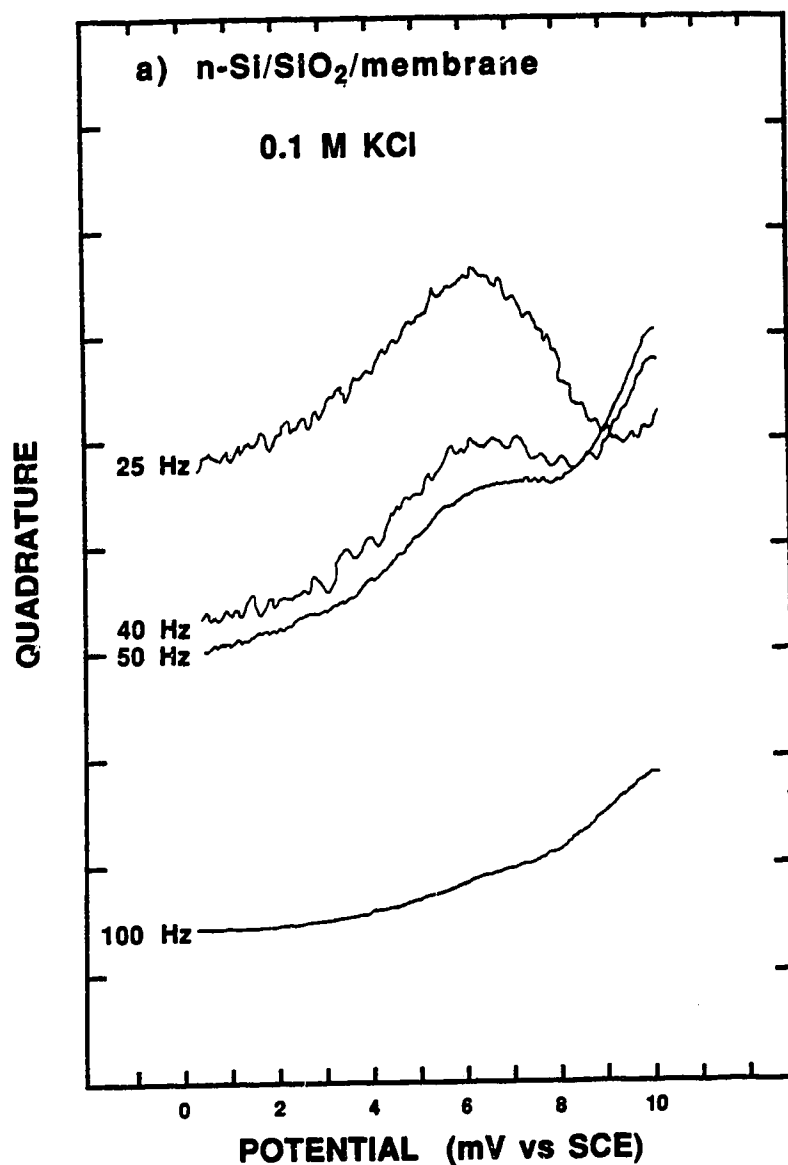


Figure 2.10(a) Quadrature-voltage curves for an n-Si/SiO₂/membrane electrode, obtained at 25, 40, 50, and 100 Hz in 0.1 M KCl. The quadrature response increases in an upward direction along the vertical axis. These curves document the C_{eq} -V behaviour of a MIS electrode when both the membrane and Si electrode contribute significantly to the Y_{im} response.

at low frequency. Though no experiments were executed at frequencies greater than 100 Hz, it is expected that the C_{eq} -V curves measured at higher frequencies would level off as the membrane contribution to Y_{im} became more important.

Figure 2.10(b) presents the theoretical C_{eq} -V curves for the electrode of 10(a), calculated according to Equations (8) and (9). No corresponding impedance experiment was done in conjunction with acquiring the curves of Figure 2.10(a). However, it was found that an R_g of 3 M Ω , a C_g of 20 pF, a C_e of 10 nF, and an R_s of 100 Ω yielded C_{eq} -V curves whose shapes mimicked those found experimentally at 25, 40, 50, and 100 Hz in Figure 2.10(a). Together, Figures 2.9 and 2.10 indicate that use of the equivalent circuit of Figure 2.4 is appropriate when describing the MIS electrode's impedance properties.

Since the strong voltage dependence of C_{eq} indicates that electrode capacitance, C_e , for the most part determines MIS electrode impedance response at low frequencies, C_{eq} -V curves measured at these frequencies may be used to evaluate apparent flatband voltages (V_{fb}) for the electrode. The Mott-Schottky (M-S) relationship between C_{eq}^{-2} and V, Equation (16), may be used to carry out this calculation, as discussed above. In order to verify that the MIS electrode responds by the same type of field effect mechanism as the ISFET, the C_{eq} -V curves of a number of functional MIS electrodes were measured as a function of K^+ concentration, and the resulting shifts in V_{fb} calculated. A functional MIS electrode is defined as one whose open circuit potential (V_{oc}) response varies in a Nernstian fashion with K^+ concentration. V_{oc} measurements for the MIS electrodes used in this study were made by Xizhong Li of our group. It was found that the selectivity coefficient of these electrodes for K^+ over Na^+ , $k_{K,Na}$, was 2×10^{-4} in the presence of 0.1 M Na^+ .

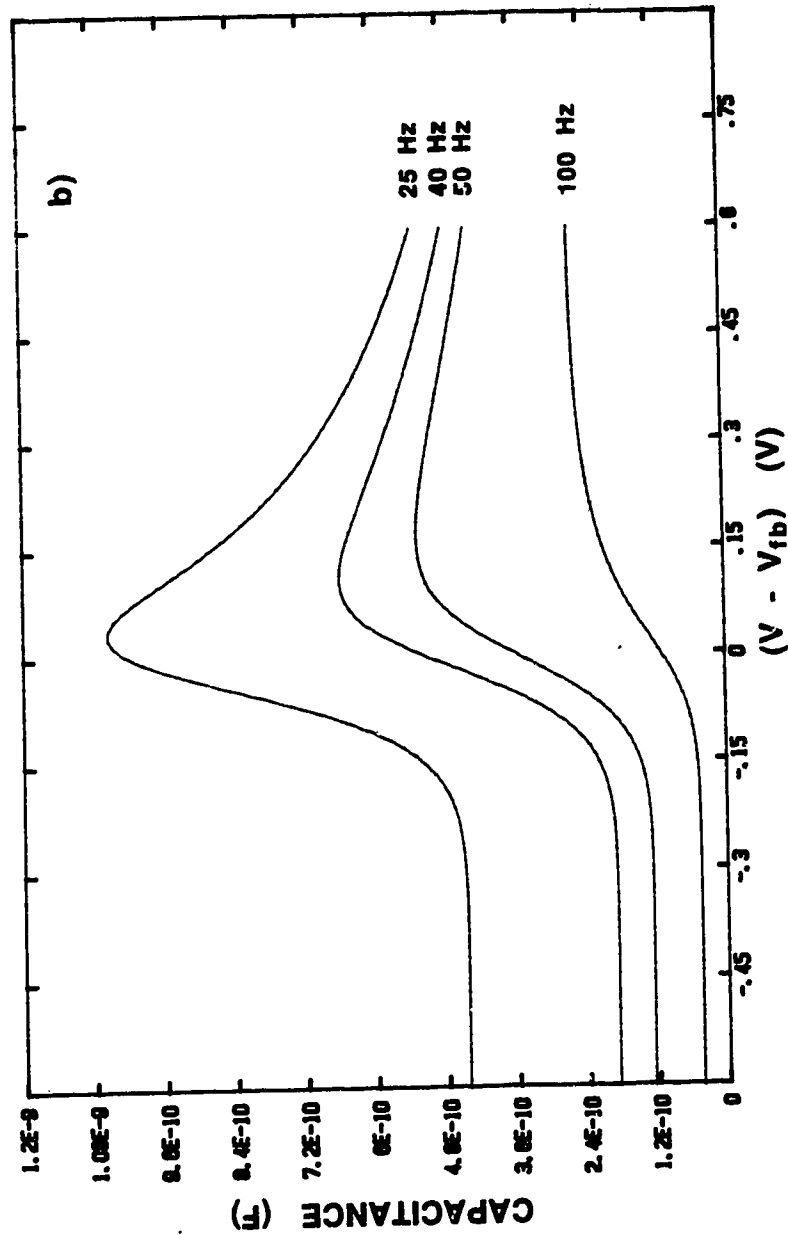


Figure 2.10(b) Model C_{eq} - V curves calculated for the MIS electrode of Figure 2.10(a) at 25, 40, 50, and 100 Hz from Equations (8)-(10). Values for equivalent circuit elements used in the calculation were: $R_g = 3 \text{ M}\Omega$, $C_g = 20 \text{ pF}$, $C_e = 10 \text{ nF}$, and $R_s = 100 \Omega$.

Figures 2.11(a) and 2.12(a) show the results of two C_{eq} - V measurements made as K^+ concentration was varied, for an n-Si/SiO₂/membrane electrode and an n-Si/SiO₂/Si₃N₄/membrane electrode, respectively. The C_{eq} - V curves in both figures shift in a positive direction along the voltage axis with increasing K^+ concentration, indicating a corresponding increase in measured V_{fb} . Figures 2.11(b) and 2.12(b) give the Mott-Schottky (M-S) plots of C_{eq}^{-2} versus V for C_{eq} - V data in Figures 2.11(a) and 2.12(a), respectively, and show how V_{fb} may be extrapolated from these plots. Values of V_{fb} for each electrode at each K^+ concentration considered are presented in Table 2.1. In both cases, the shift in V_{fb} is about 50 to 60 mV per decade change in K^+ concentration for 10^{-3} M to 10^{-1} M K^+ , which establishes that the membrane is coupled to the semiconductor substrate via a field effect. At concentrations less than 10^{-3} M K^+ , shifts in V_{fb} are less than 50 mV when 0.1 M Na^+ is present, as expected from the measured $k_{K,Na}$ for these electrodes. In the examples given in Figures 2.11(b) and 2.12(b), extrapolated portions of the M-S plots exhibit slopes which are very similar, reflecting the almost direct proportionality of the corresponding C_{eq} data to C_e . However, the observed value of V_{fb} will still be quite sensitive to the choice of data extrapolated. This is because small variations in the slope of the line being extrapolated can cause relatively large variations in the resulting intercept in determinations of this type. The precision of the V_{fb} measurement is therefore not as good as that of the V_{oc} determination.

In Figure 2.12(a), the C_{eq} of the electrode in the curves' accumulation region (negative voltages), corresponding to maximum values of C_e , appears to be decreasing with decreasing K^+ concentration. C_{eq} - V curves for bare semiconductor electrodes do not demonstrate such hysteresis over the time

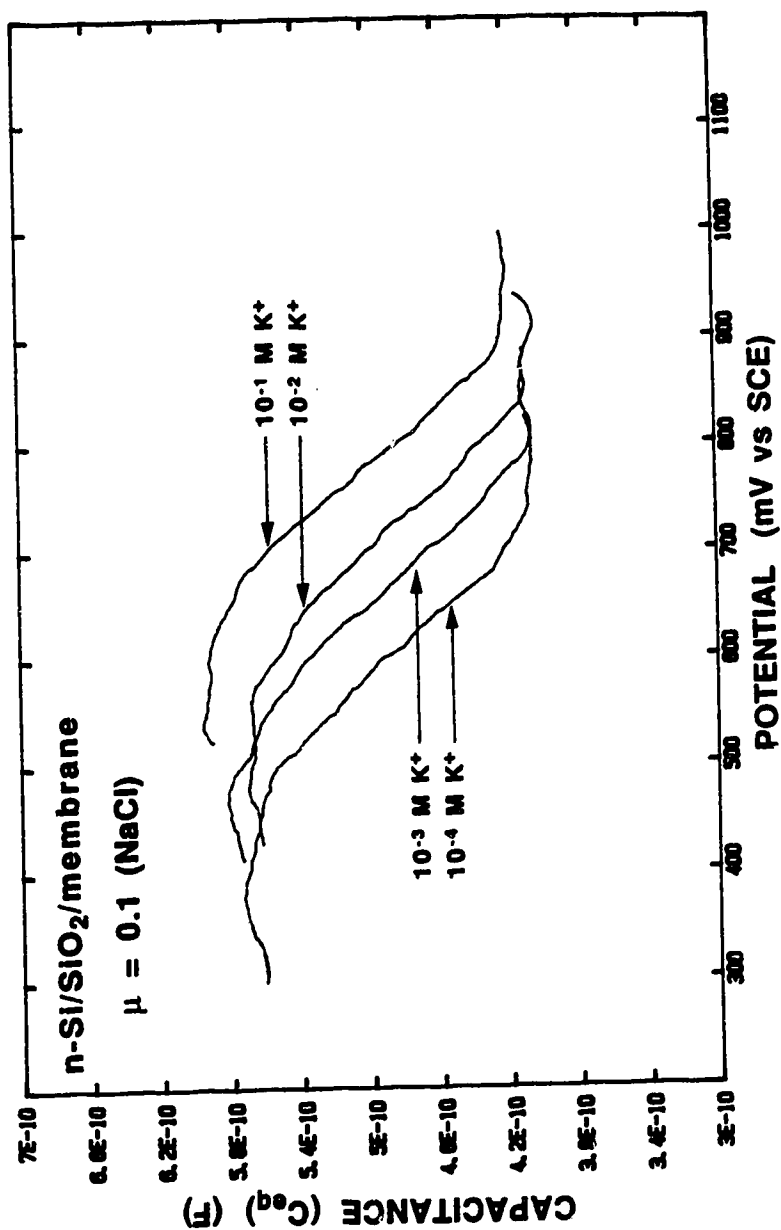


Figure 2.11(a) C_{eq} -V curves for an n-Si/SiO₂/membrane electrode acquired at 25 Hz as a function of K⁺ concentration. All solutions were maintained at constant μ of 0.1 by NaCl. Note that the curves shift in a positive direction along the V axis with increasing K⁺ concentration, indicating a corresponding increase in measured V_{fb} .

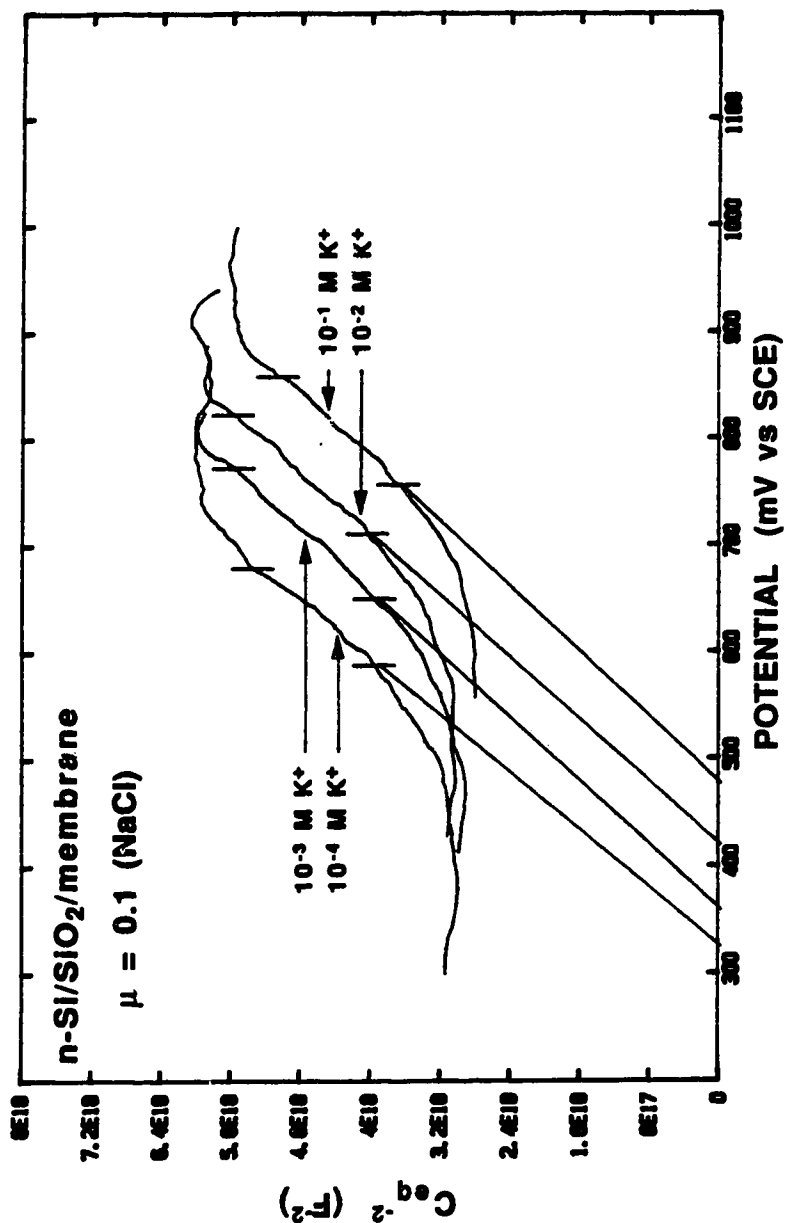


Figure 2.11(b) M-S plots of C_{eq}^{-2} vs V for the C_{eq} - V curves of Figure 2.11(a) acquired at 25 Hz. The linear portion of each curve has been extrapolated to the V axis to obtain a value of V_{fb} at each K^+ concentration. These values of V_{fb} are reported in Table 2.1.

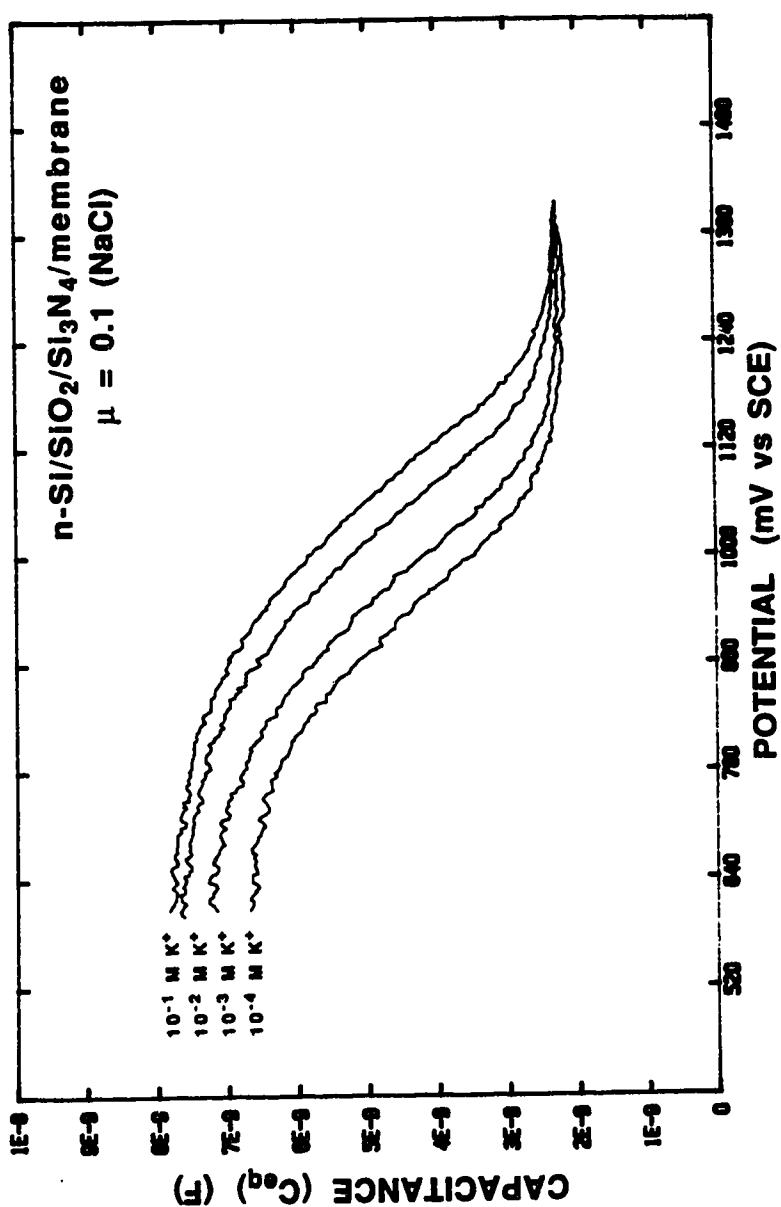


Figure 2.12(a) C_{eq} -V curves for an n-Si/SiO₂/Si₃N₄/membrane electrode acquired at 25 Hz as a function of K⁺ concentration. All solutions were maintained at constant μ of 0.1 by NaCl. Again, the curves shift in a positive direction along the V axis with increasing K⁺ concentration, indicating a corresponding increase in measured V_{fb} .

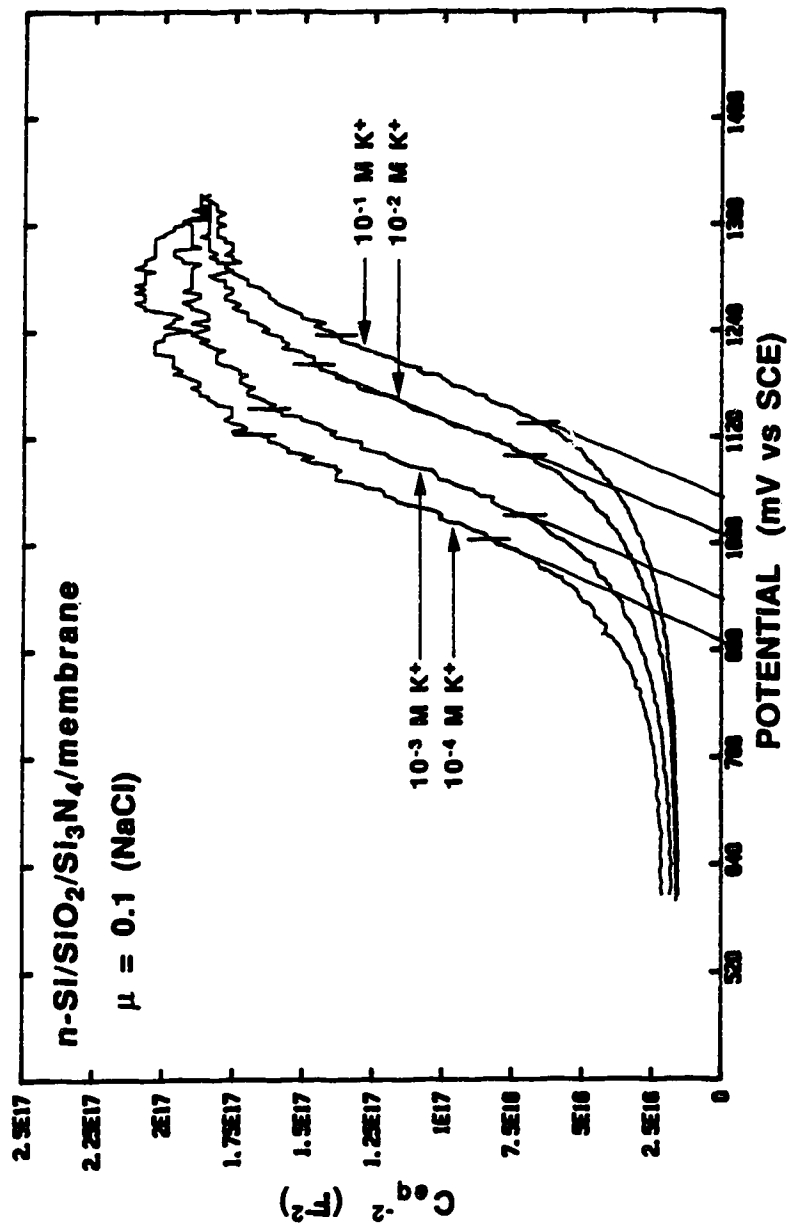


Figure 2.12(b) M-S plots of C_{eq}^{-2} vs V for the C_{eq} - V curves of Figure 2.12(a) acquired at 25 Hz. The linear portion of each curve has been extrapolated to the V axis to obtain a value of V_{fb} at each K^+ concentration. These values of V_{fb} are reported in Table 2.1.

TABLE 2.1: Flatband potentials, V_{fb} , and flatband shifts, ΔV_{fb} , determined as a function of KCl concentration for the MIS electrodes whose C_{eq} -V curves are given in Figures 2.11(a) and 2.12(a)

ELECTRODE	n-Si/SiO ₂ /mem		n-Si/SiO ₂ /Si ₃ N ₄ /mem		
	[KCl]	V_{fb} (V) a)	ΔV_{fb} (V)	V_{fb} (V) ^{a)}	ΔV_{fb} (V)
	10 ⁻¹	.47	.06	1.06	.05
	10 ⁻²	.41	.05	1.00	.06
	10 ⁻³	.36	.03	.95	.04
	10 ⁻⁴	.32		.90	

a) The precision of reported V_{fb} 's ranges from $\pm 1\%$ to $\pm 5\%$, as calculated by regression analysis of the linear portions of the M-S plots.

scale typical of this type of experiment (about 6 hours), since C_e , which is equal to oxide capacitance, C_{ox} , under accumulation, is for all practical purposes constant [7-9]. This suggests that there is some change occurring in the bulk membrane properties over the course of the measurements. However, the dependence of the electrode's impedance response on K^+ in Figure 2.12 still manifests itself primarily in the space charge layer of the Si electrode, with the 50 to 60 mV shift in V_{fb} per decade change in K^+ concentration.

The K^+ concentration dependence of C_{eq} at accumulation biases noted in Figure 2.12 was observed for several MIS electrodes. In some cases, the phenomenon extended into the depletion region of the C_{eq} -V curves, so that the electrode impedance response measured as a function of K^+ concentration was quite different from that illustrated in Figures 2.11 and 2.12. An example of this different impedance behaviour is given in Figure 2.13 for an n-Si/SiO₂/membrane electrode. The C_{eq} -V curves in this figure were measured sequentially in solutions ranging from 10⁻¹ M KCl down to 10⁻⁴ M KCl ($\mu = 0.1$ (NaCl)), and back up to 10⁻¹ M KCl, at a frequency of 100 Hz. Unlike the C_{eq} -V curves of Figures 2.11 and 2.12, these curves shift up to higher C_{eq} values as K^+ concentration in solution is increased, so that they appear to be stacked one above the other in Figure 2.13. In addition, the range of capacitances over which each curve is defined gets larger with increasing K^+ concentration. This causes the C_{eq} -V curves measured in concentrations of KCl less than 10⁻¹ M to look compressed with respect to the curve measured in 10⁻¹ M KCl. Altogether, the differences observed in these C_{eq} -V curves when compared to those shown in Figures 2.11 and 2.12 imply that the observed concentration

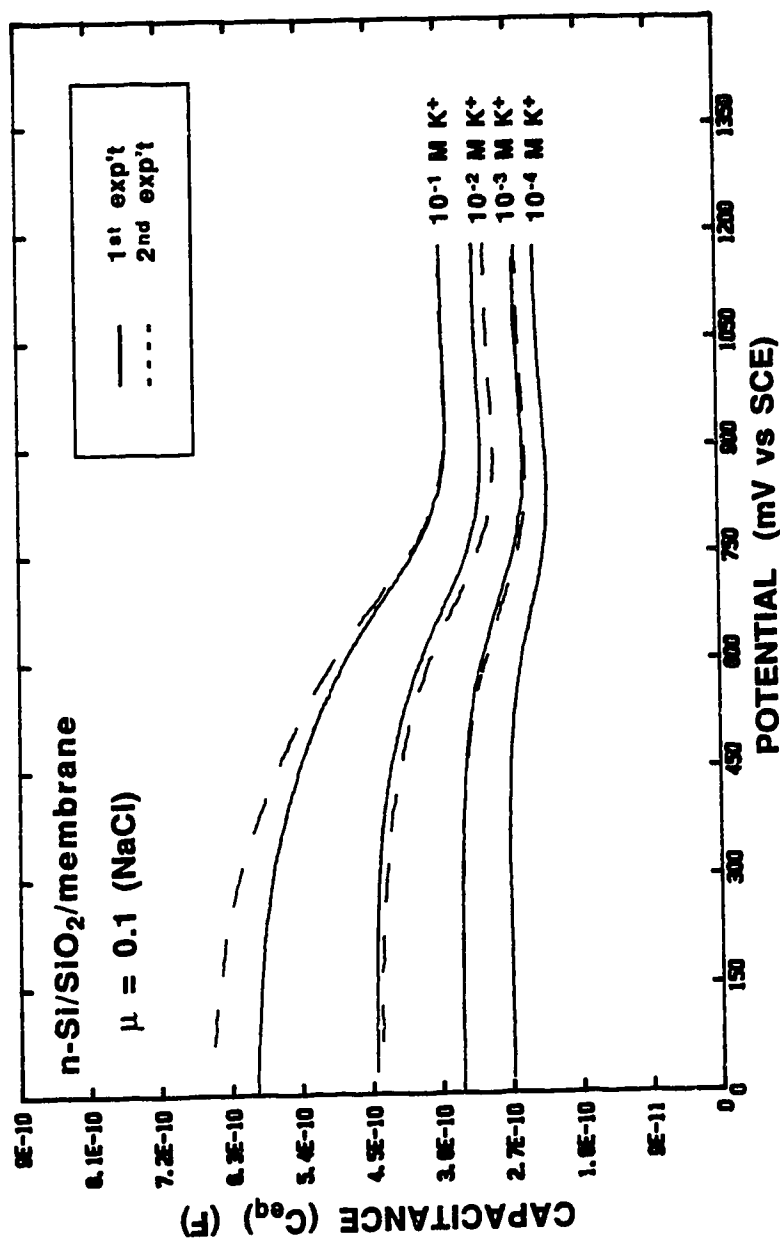


Figure 2.13 C_{eq} -V curves for an n-Si/SiO₂/membrane electrode acquired at 100 Hz as a function of K⁺ concentration. All solutions were maintained at a constant μ of 0.1 by NaCl. Curves were obtained sequentially from high (10⁻¹ M) to low (10⁻⁴) KCl concentrations (solid curves), and then remeasured from low (10⁻³ M) to high (10⁻¹ M) concentrations (dashed curves). The concentration-dependent shift of these curves along the V axis is obscured by the vertical shift to higher C_{eq} exhibited as a function of increasing K⁺ concentration, making the impedance response of this MIS electrode quite different from that shown in Figures 2.11(a) and 2.12(a).

dependent effect cannot be attributed solely to changes in the distribution of charge in the silicon space charge layer.

Nyquist plots were obtained in conjunction with each of the C_{eq} -V curves shown in Figure 2.13, making possible the determination of R_g and C_g at each K^+ concentration. The plots themselves are presented in Figure 2.14, with values of R_g and C_g given as a function of K^+ concentration in Table 2.2. Both parameters show a monotonic variation with K^+ concentration, R_g more so than C_g . R_g increases by about 100 % in going from 10^{-1} M KCl to 10^{-4} M KCl, while C_g only decreases by about 10 %. It seems, then, that the concentration dependence of the C_{eq} -V curves in Figure 2.13 may be correlated to changes in membrane bulk properties, particularly R_g .

To see if this correlation could be predicted by the equivalent circuit model proposed for the MIS electrode, C_{eq} -V curves calculated at a frequency of 100 Hz and as function of changing R_g were generated using Equations (8) and (9). The resulting curves are presented in Figure 2.15. R_g values listed in Table 2.2 were used to calculate these curves, so that they are meant to represent the four experimental curves in Figure 2.13, acquired at differing K^+ concentrations. The R_g values in Table 2.2 are the only concentration dependent variables used in the curve generation process, since shifts in the silicon electrode's V_{fb} have not been taken into account. Since the variation in C_g with K^+ concentration measured experimentally was not great, it was decided to hold this quantity constant at a value of 90 pF in the calculations. Each Nyquist plot in Figure 2.14 was recorded at an applied DC voltage of 0.64 V, which places the electrode's space charge region somewhere between the accumulation and depletion conditions, as deduced from Figure 2.13. Accordingly, C_e assumes a value of about 1 nF. It is evident from the curves

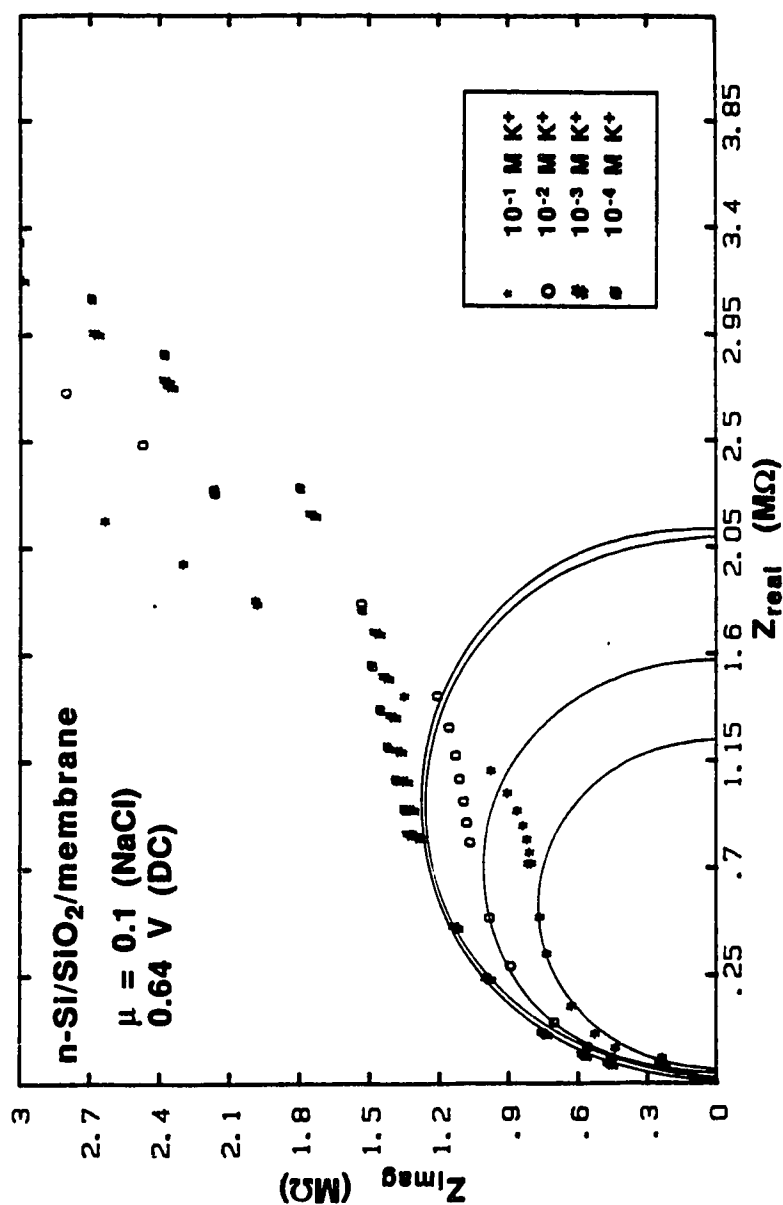


Figure 2.14: Nyquist plots for the MIS electrode of Figure 2.13 recorded over the frequency range 25 Hz to 20 kHz as a function of K⁺ concentration. All solutions were buffered to a μ of 0.1 by NaCl. A DC potential of 0.64 V vs SCE was applied, biasing the electrode to a near-flatband condition. As shown here, values of R_g extrapolated from the real axis intercept of the semicircle at low frequency increase as K⁺ concentration increases.

TABLE 2.2: R_g and C_g determined at each KCl concentration from the Nyquist plots shown in Figure 2.14 for a n-Si/SiO₂/membrane electrode

$[K^+]$	R_g (M Ω) ^{a)}	C_g (pF) ^{b)}
10 ⁻¹	1.23	93
10 ⁻²	1.57	88
10 ⁻³	2.06	83
10 ⁻⁴	2.12	82

- a) Measured R_g 's have a precision of ± 2 %.
- b) Measured C_g 's have a precision of ± 5 %.

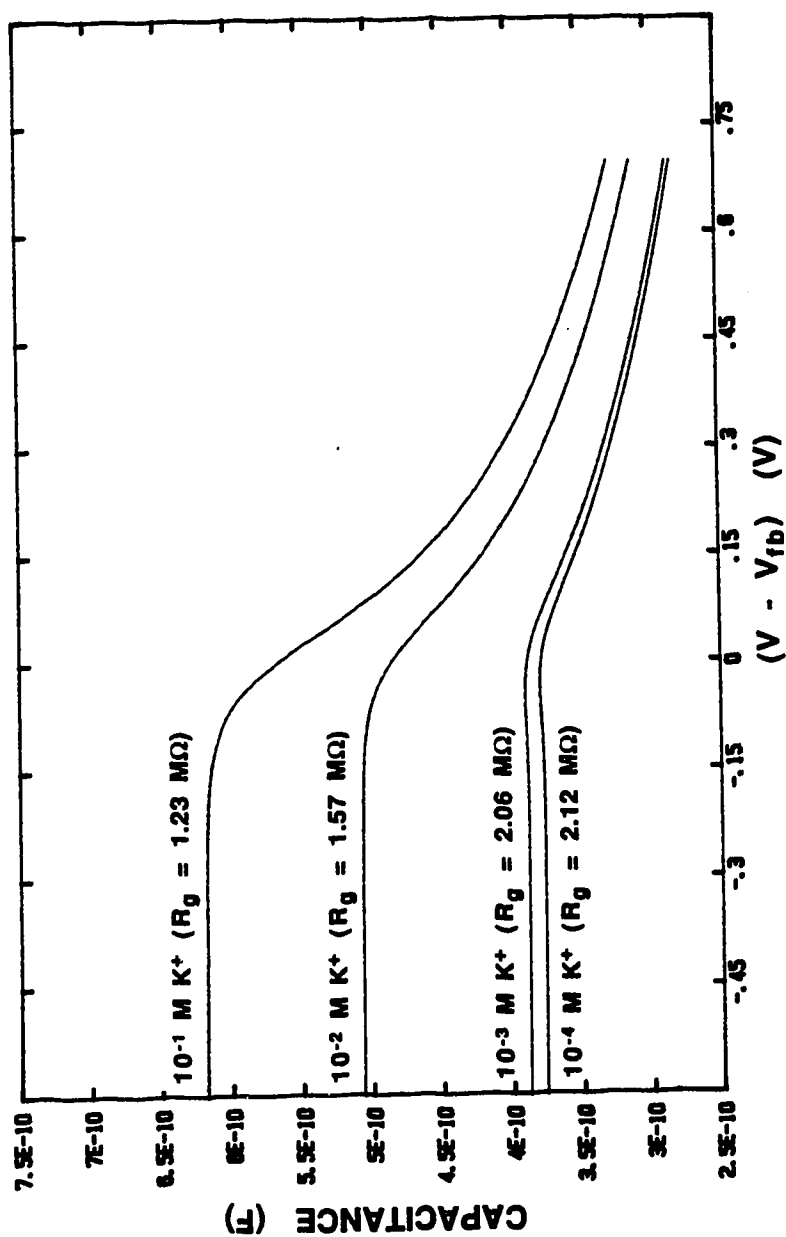


Figure 2.15 Theoretical C_{eq} - V curves calculated for the MIS electrode of Figure 2.13 as a function of R_g at a frequency of 100 Hz. Values of R_g used in the calculation are presented as a function of K^+ concentration in Table 2.2. C_g , R_s , and C_e were assigned values of 90 pF, 100 Ω , and 1 nF, respectively. These curves show the same type of K^+ -dependent behaviour as those in Figure 2.13.

in Figure 2.15 that varying R_g strongly influences the resulting C_{eq} -V curves, shifting them up to higher C_{eq} values as R_g is decreased. The range of capacitances defining each C_{eq} -V curve increases as R_g is decreased, so that the curves in Figure 2.15 show a compressed sigmoidal shape at R_g values corresponding to $[K^+] < 0.1$ M relative to the curve calculated for R_g at $[K^+] = 0.1$ M. Clearly, the theoretical C_{eq} -V curves of Figure 2.15 show an apparent K^+ concentration dependent behaviour similar to that found experimentally and shown in Figure 2.13, so that variations in R_g are at least partially responsible for the C_{eq} -V curves in Figure 2.13. This establishes that changes in the bulk membrane properties of a MIS electrode may be reflected in the corresponding C_{eq} -V curves.

Apparent V_{fb} 's were calculated from M-S plots of the C_{eq} -V data for the electrode of Figure 2.13. The M-S plots are shown in Figure 2.16, while values of V_{fb} are listed as a function of K^+ concentration in Table 2.3. In contrast to the M-S plots of Figures 2.11(b) and 2.12(b), the M-S plots of Figure 2.16 are seen to move to higher values of C_{eq}^{-2} as a function of decreasing K^+ concentration. This leads to the observation of some rather anomalous V_{fb} shifts which do not vary as an analytically useful function of K^+ concentration, as shown in Table 2.3. Moreover, they are all greater than the expected 50 to 60 mV per decade change in K^+ concentration. One of the reasons for these V_{fb} shifts deviating from Nernstian values lies in the nature of the M-S plots in Figure 2.16, as explained below.

Consider the M-S plots in Figure 2.16 calculated for data acquired at 10^{-1} and 10^{-2} M KCl. Assume first for the sake of this discussion that the curve for 10^{-2} M KCl was only shifted horizontally along the V axis with respect to the curve for 10^{-1} M KCl. The distance over which the curve for 10^{-2} M KCl

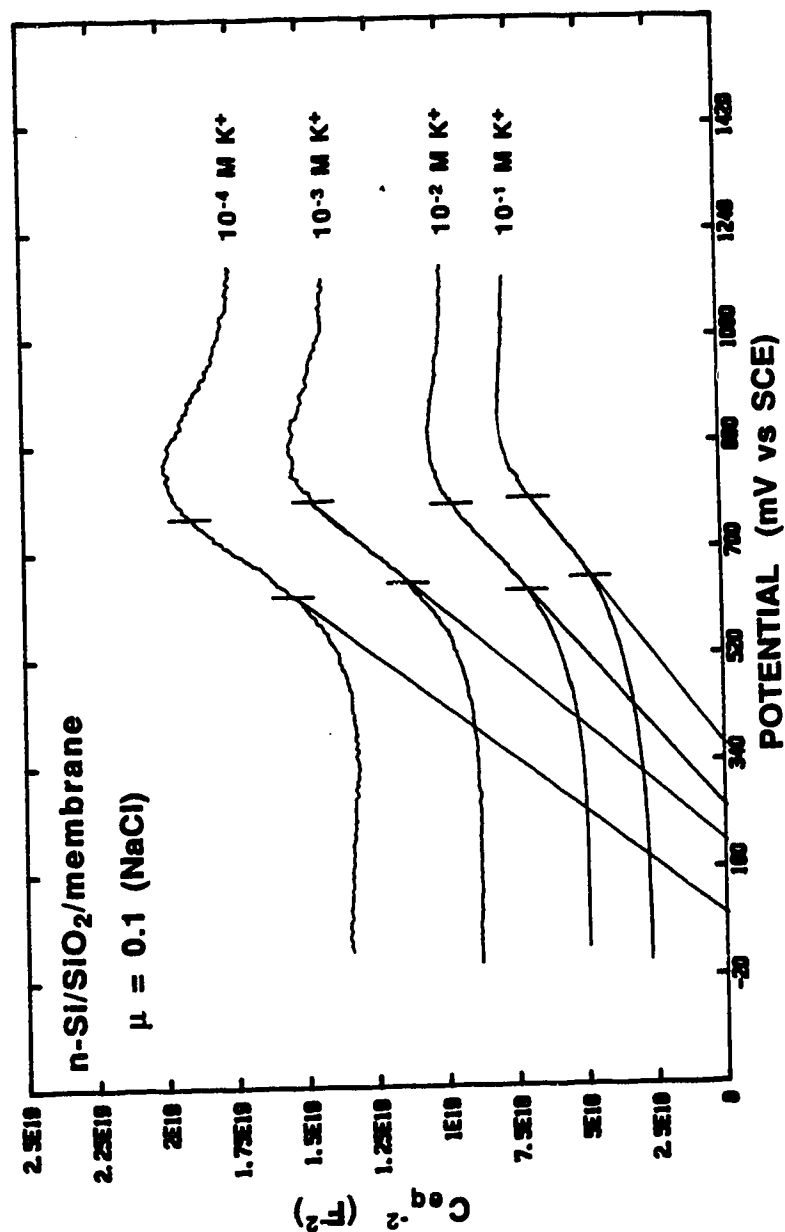


Figure 2.16 M-S plots of C_{eq}^{-2} vs V for the C_{eq} - V curves of Figure 2.13, recorded at 100 Hz. The linear portion of each curve has been extrapolated to the V axis to obtain a value of V_{fb} at each K^+ concentration. These values of V_{fb} are reported in Table 2.3. As with the C_{eq} - V curves of Figure 2.13, these M-S plots exhibit a K^+ -dependent behaviour quite unlike that of the MIS electrodes of Figures 2.11(b) and 12(b).

TABLE 2.3: Flatband potentials, V_{fb} , and flatband shifts, ΔV_{fb} , determined as a function of KCl concentration for the MIS electrode whose C_{eq} -V curves are given in Figure 2.13

[KCl]	V_{fb} (V) ^{a)}	ΔV_{fb} (V)
10^{-1}	.34	.08
10^{-2}	.27	.11
10^{-3}	.16	.09
10^{-4}	.06	

a) Values of V_{fb} have precisions ranging from $\pm 1\%$ to $\pm 5\%$.

would have to be extrapolated in order to obtain the apparent V_{fb} at 10^{-2} M KCl would be the same as that required to obtain the apparent V_{fb} at 10^{-1} M KCl. The apparent ΔV_{fb} determined in this manner would then be a true measure of the actual shift in the Si V_{fb} . In actual fact, however, the M-S plot in Figure 2.16 for 10^{-2} M KCl has been shifted vertically as well as horizontally with respect to the curve for 10^{-1} M KCl. The distance over which the former curve has to be extrapolated for the determination of the apparent V_{fb} at 10^{-2} M KCl will necessarily be larger than that required to obtain the V_{fb} at 10^{-1} M KCl. As a result, the V_{fb} evaluated for the C_{eq} -V measurement at 10^{-2} M will be lower than expected, leading to an apparent ΔV_{fb} that is larger than the 50 to 60 mV expected. The situation is complicated by the fact that the linear sections of the M-S plots in Figure 2.16 exhibit slopes which appear to vary slightly from one K^+ concentration to the next. Small variations in the slope of the line extrapolated may introduce relatively large variations in the magnitude of V_{fb} . Here, this phenomenon is exacerbated as the distance over which the curve is extrapolated increases.

From the foregoing discussion, it is clear that V_{fb} shifts in the Si substrate may be completely masked when C_{eq} -V curves exhibit the concentration dependent behaviour demonstrated in Figure 2.13. The possibility exists that apparent ΔV_{fb} shifts could be observed when no shift in Si V_{fb} has actually occurred. Unfortunately, because of the preliminary nature of these early impedance studies, no V_{oc} measurements were made with the MIS electrode of Figure 2.13. Since it could not be assumed that this electrode was responding to K^+ via a field effect, it was not possible to determine to what extent the observed ΔV_{fb} 's were influenced by factors such as changing membrane properties.

It was decided instead to examine the extent to which membrane properties could affect observed ΔV_{fb} 's through use of the equivalent circuit model. Calculations were carried out for a theoretical system at 100 Hz, in which R_g varied as a function of K^+ concentration by assuming values presented in Table 2.2. R_s , C_g , and C_e were maintained constant at 100 Ω , 100 pF, and 1 nF, respectively. C_{eq} -V data was generated for two cases. In the first case, it was assumed that no shift in Si V_{fb} occurred as a function of K^+ concentration. The resulting ΔV_{fb} 's, presented in Table 2.4, are then due only to changes in R_g . Also presented in Table 2.4 are ΔV_{fb} 's calculated for the second case, in which data was generated with the additional requirement that the V_{fb} of the system shifted 59.2 mV per decade change in K^+ concentration.

Two conclusions may be drawn from the data in Table 2.4. First of all, if significant changes in bulk membrane properties take place, no real shift in Si V_{fb} need occur for large ΔV_{fb} 's to be observed. Secondly, magnitudes of the apparent ΔV_{fb} 's do increase when Si V_{fb} shifts as well as concentration dependent R_g 's are included in the calculation of the C_{eq} -V curves. However, the calculated ΔV_{fb} 's in Table 2.4 for both cases show such variability that comparisons made between these and the experimentally determined ΔV_{fb} 's of Table 2.3 cannot lead to any firm conclusion regarding the functionality of the MIS electrode whose C_{eq} -V curves are given in Figure 2.13.

TABLE 2.4: Theoretical flatband potentials, V_{fb} , and flatband shifts, ΔV_{fb} , determined for R_s , C_g , and C_e values of 100 Ω , 100 pF, and 1 nF, respectively, with R_g varying as a function of concentration and assuming values given in Table 2.2; data was generated in one case assuming V_{fb} shifts in the silicon, in the other omitting V_{fb} shifts in the calculation

		V_{fb} included in cal'n		V_{fb} not included in cal'n	
R_g (M Ω)	[KCl]	V_{fb} (V)	ΔV_{fb} (V)	V_{fb} (V)	ΔV_{fb} (V)
1.23	10^{-1}	-.435	.187	-.435	.123
1.57	10^{-2}	-.622	.280	-.558	.260
2.06	10^{-3}	-.902	.076	-.818	.038
2.12	10^{-4}	-.978		-.856	

2.6 CONCLUSION

Properties of the bulk membrane coating of a MIS electrode are integral to the electrode's impedance response. Reasons why these properties, in particular R_g , may change under certain conditions may now be addressed. Returning to the C_{eq} - V curves for a functional MIS electrode in Figure 2.12, the apparent K^+ concentration dependent decrease in C_{eq} under accumulation is probably due to an increase in R_g . In this example, however, the observed phenomenon is most likely not related to K^+ concentration, but rather to the membrane slowly equilibrating with the aqueous phase. Experiments were carried out sequentially in solutions of 10^{-1} M KCl down to 10^{-4} M KCl, after the electrode had been conditioned for a couple of hours in 10^{-1} M KCl. It has since been ascertained that electrodes of this type require at least 24 hours of conditioning in aqueous solution to minimize drift in C_{eq} - V experiments. Studies show that as the membrane absorbs water, its resistance increases [28]. The rate at which this occurs is greater in the initial few hours of exposure - hence the gradual decrease in C_{eq} at accumulation voltages in Figure 2.12.

The observation that R_g increases with decreasing K^+ concentration for the MIS electrode in Figure 2.13 is more puzzling, however, because the electrode was properly conditioned before the experiments were carried out. This result is not supported by impedance studies of valinomycin-based membranes conducted in our laboratory. In these experiments, the membranes examined were either incorporated into an ISE, or mounted in specially designed cells, in which the composition of the solution to which a membrane is exposed may be controlled on both sides. Membranes studied in the ISE configuration yielded values of R_g which were invariant with K^+

concentration in solutions having an ionic strength of 0.1. The same conclusion was reached for more recent impedance studies carried out by A. Chan of our group on membranes which were symmetrically bathed in a cell. Moreover, these cell-mounted membranes, which have a surface area roughly five times that of membranes coated onto MIS electrodes, had C_g values ranging from 20 to 40 pF, results that are much smaller than and therefore inconsistent with the MIS electrode results given in Table 2.2. As with the R_g values measured for the membrane alone, these values of C_g did not show any significant dependence on the K^+ concentration of the solution to which the membrane was exposed. Given these ISE and cell studies which exclusively characterized the membrane itself, it seems that the behaviour of the membranes coated onto the MIS electrode of Figures 2.13 (and other electrodes exhibiting a similar K^+ concentration dependent impedance response) is somewhat incongruous. As mentioned earlier, no definite conclusions can be made as to the functionality of the electrode in Figure 2.13. However, functional electrodes have since been employed in impedance experiments to determine the dependence of the bulk membrane properties on K^+ concentration in solutions having an ionic strength of 0.1. These experiments, conducted by A. Demoz of our group, show that the membrane of a functional MIS electrode has an impedance response to K^+ concentration that is no different from membranes studied in either the cell or ISE configuration. This suggests that the membrane coating of the electrode in Figure 2.13 is showing signs of aging, or was not properly prepared in the first place. Films which have been improperly cast may be too thin, or may exhibit pinholes or bubbles, all of which pose potential problems with respect to electrode functionality. The large C_g 's measured for this electrode, which as

stated above are not typical of the plasticized membranes used in this study [18], may be caused by solution leaking through pinholes in the membrane coating, so that a second shunt capacitance appears in parallel with C_g in Figure 2.4. Future experiments should establish whether there is a firm connection between electrode response degradation and changes in membrane bulk properties. Should there be a correlation, measurement of bulk membrane properties would prove to be a good diagnostic tool in determining an electrode's (or ISFET's) degree of functionality, since it is likely that changes in R_g and C_g will appear before the V_{oc} for a MIS electrode, or the drain-source current of an ISFET device, begin to degrade significantly.

2.7 REFERENCES

- (1) Bergveld, P., *I.E.E.E. Trans. Biomed. Eng.*, 1972, BME-19, 342
- (2) Bergveld, P., Sibbald, A., *Analytical And Biomedical Applications Of Ion-Selective Field Effect Transistors*, Elsevier: Amsterdam, 1988
- (3) Janata, J., In "*Solid State Chemical Sensors*", Janata, J., Huber, R.J., Ed.; Academic: London, 1985
- (4) Fogt, E.J., Unterecker, D.F., Norenberg, M.S., Meyerhoff, M.E., *Anal. Chem.*, 1985, 57, 1995
- (5) Satchwill, T., Harrison, D.J., *J. Electroanal. Chem.*, 1986, 202, 75
- (6) Siu, W.M., Cobbold, R.S.C., *I.E.E.E. Trans. Electron Dev.*, 1976, ED-26, 1805
- (7) Lindner, R., *Bell Sys. Tech. J.*, 1962, 41, 803
- (8) Terman, L.M., *Solid-State Electron.*, 1962, 5, 285
- (9) Grove, A.S., Deal, B.E., Snow, E.H., Sah, L.T., *Solid-State Electron.*, 1965, 8, 145
- (10) Buck, R.P., Toth, K., Graf, E., Horvai, G., Pungor, E., *J. Electroanal. Chem.*, 1987, 223, 51
- (11) Buck, R.P., Hackleman, D.E., *Anal. Chem.*, 1977, 49, 2315
- (12) Janata, J., Huber, R.J., In *Ion-Selective Electrodes In Analytical Chemistry*, vol.2; Plenum Press, 1980
- (13) Lauks, I., *Sens. Actuators*, 1981, 1, 261
- (14) Reiss, H., *J. Phys. Chem.*, 1985, 89, 3783
- (15) Sze, S.M., *Physics of Semiconductor Devices*; Wiley-Interscience: New York, 1969
- (16) Buck, R.P., Toth, K., Graf, E., Horvai, G., Pungor, E., *J. Electroanal. Chem.*, 1987, 223, 51

- (17) Armstrong, R.D., Horvai, G., *Electrochim. Acta*, 1990, 35, 1
- (18) Lindner, E., Toth, K., Pungor, E., *Dynamic Characteristics Of Ion-Selective Electrodes*, C.R.C. Press: Boca Raton, Fla., 1988, p 4-10
- (19) Armstrong, R. D., Lockhart, J. C., Todd, M., *Electrochim.Acta*, 1986, 31, 591
- (20) Buck, R. D., *Ion Sel. Electrode Rev.*, 1982, 4, 3
- (21) Armstrong, R.D., Covington, A.K., Evans, G.P., *J. Electroanal. Chem. Interfacial Electrochem.*, 1983, 159, 33
- (22) Garrett, C.G.B., Brattain, W.H., *Phys. Rev.*, 1955, 99, 376
- (23) Legg, K.D., Ellis, A.B., Bolts, J.M., Wrighton, M.S., *Proc. Natl. Acad. Sci. U.S.A.*, 1977, 74, 4166
- (24) Band, D.M., Kratochvil, J., Treasure, T., *J. Physiol. (London)*, 1976, 265, 2P
- (25) Bassett, J., Denney, R. C., Jeffery, G. H., Mendham, J., *Vogel's Textbook of Quantitative Inorganic Analysis, 4th Ed.*; Longman: London, 1978
- (26) Armstrong, R.D., Nikitas, P., *Electrochim. Acta*, 1985, 30, 1627
- (27) Armstrong, R.D., Lockhart, J.C., Todd, M., *Electrochim. Acta*, 1986, 31, 591
- (28) Horvai, G., Graf, E., Toth, K., Pungor, E., Buck, R.P., *Anal. Chem.*, 1986, 58, 2735

CHAPTER 3

A CHARACTERIZATION OF NEUTRAL SPECIES INTERFERENCE AT THE ION-SENSITIVE MEMBRANE/SEMICONDUCTOR DEVICE INTERFACE

3.1 INTRODUCTION

Much of the research with regard to chemical sensors in recent years has focussed on ion-responsive semiconductor devices such as the ion-selective field effect transistor [1-3]. Like the conventional ion-selective electrode (ISE), it is the potentiometric response of these devices to the species of interest in solution that is monitored. However, because the internal membrane/solution interface of the ISE has been replaced by a membrane/insulator interface (usually silicon nitride), the ISFET has associated with it some unique problems not observed with the ISE. It has been reported by Fogt et. al. that ISFET's coated with a plasticized polyvinylchloride (PVC) K⁺-selective membrane are subject to a number of unexpected interferences [4]. Species such as CO₂, benzoic acid, and acetic acid, which show no interference at ISE's employing the same membrane, cause significant potential shifts at K⁺-membrane coated ISFET's. This phenomenon is thought to be due to the diffusion of the neutral species through the membrane to the membrane/nitride interface, where a shift in pH occurs as a result. In ISFET operation, the potential induced in the silicon substrate via a field effect mechanism is governed by the charge state at the membrane/nitride interface. This charge state, though constant at fixed K⁺

activity, is subject to change should the proton activity at the nitride surface be altered. In fact, the well-recognized pH-responsive nature of silicon nitride and silicon oxide surfaces has been exploited in the development of pH-FET's, that subset of ISFET's in which the insulator is left exposed for the purpose of measuring solution pH [3]. It is plausible to conclude, then, that the potential response of a membrane-coated ISFET is dependent on the history of the nitride surface, should the membrane prove to be permeable to acidic and basic species.

The reversible exchange of charge (in this case K^+) across the solution/membrane interface of the K^+ -sensitive ISFET ensures that a thermodynamically significant potential is established across this interface in response to variations in solution K^+ activity. The potential use of another type of electrochemically reversible "membrane", consisting of a metal coated with one of its insoluble inorganic salts, to impart ion sensitivity to the ISFET gate has been suggested by Buck and Hackleman [5]. In this study, they examined the open circuit voltage and impedance response of n-Si/SiO₂/AgBr/solution electrodes, and established that these electrodes respond to Ag^+ or halogen ions via the same field effect mechanism as the MIS electrodes described in Chapter 2. Whereas the MIS electrode's response is governed by the membrane/insulator interface, however, the potential induced in the Si substrate of these halogen-sensitive electrodes is due to the electric field generated by the charge on the conductive metal salt layer, making their response pH-independent. The very similar Ag/AgCl reference system has been successfully employed as a solid-state contact to replace the internal reference solution of a K^+ -sensitive ISE [6,7], so that interposition of a Ag/AgCl layer between the pH-responsive insulator and the K^+ -ISFET's membrane coating would seem to be a possible solution to the interference

problem observed by Fogt et. al. [4]. Simon has pointed out [7] that by including potassium tetrphenylborate (KTPB) in the PVC membrane, in addition to the other components, the Ag/AgCl/membrane/solution structure is unblocked to charge transfer at each interface and the thermodynamics are not dependent on charge stored at the interfaces. The incorporation of this additional reversible interface into the MIS electrode (and eventually, the ISFET) would thus lead to more reliable electrode (or ISFET) performance.

The aims of the study reported in this chapter are twofold. The first is to substantiate the postulated mechanism by which neutral species such as benzoic acid interfere with the potentiometric response of K⁺-sensitive ISFET's. MIS electrodes of the type characterized in Chapter 2 are employed as models of the ISFET, as they lend themselves well to both potentiometric and impedance methods of study. The second aim is to show that the interferences caused by neutral species at ISFET's may be eliminated through the introduction of a Ag/AgCl contact to the K⁺-sensitive membrane. A derivative of the MIS electrode, having a n-Si/insulator/Ag/AgCl/membrane structure, is used to this end, and shall hereafter be referred to as the MAgIS electrode.

3.2 EXPERIMENTAL

All semiconductor electrodes were prepared in basically the same way as described in Chapter 2. MAgIS electrodes were constructed using n-Si wafers similar to those used for MIS electrodes, but with Ag sputter deposited under vacuum to ~ 2000 Å thickness on the front, polished face. After

encapsulation with clear epoxy, Ag-coated electrodes were chloridized chemically by immersing in a 1 M NaCl, 16 % HNO₃ solution for 3 to 4 minutes. A white film was observed on the Ag surface following treatment. These electrodes were then coated as the MIS electrodes, using 1 to 4 drops of the following solution [8]: 3 mL of tetrahydrofuran (BDH, distilled from LiAlH₄ or K), 0.15 g of dioctyl adipate (DOA; Fluka), 0.075 g of poly(vinylchloride) (PVC) (Polysciences, chromatographic grade), 0.0015 g of valinomycin (Sigma), 25 µg of potassium tetrphenylborate (KTPB) [9].

Free-standing membranes contained PVC, DOA, valinomycin, and KTPB in the same ratio as membranes coated onto MIS electrodes. The first step in the preparation of these membranes involved weighing 205 mg of DOA and 2.1 mg of valinomycin into a 10 mL beaker, and dissolving in about 3 mL of tetrahydrofuran (BDH, distilled from potassium). 102 mg of PVC were next weighed out, and added to the DOA/THF solution with stirring so as to prevent the PVC from coagulating. The incorporation of 32 µg KTPB was accomplished through addition of an approximately 0.2 mL aliquot of a KTPB/THF solution prepared by dissolving 4 mg KTPB in 25.0 ml of THF. Membrane solutions were allowed to stir for 30 minutes, after which they were poured into circular PTFE moulds which were 4 cm in diameter and 1 cm deep. Pads of filter paper were placed over the moulds, and weighted down with weights having a flat surface. Crystallization dishes 4.5 to 5 cm in diameter were found to serve well in this capacity. Membranes were allowed to set for 24 hours or more, after which membrane thicknesses ranging typically between 0.1 and 0.2 mm were found. These thicknesses were determined by sandwiching a 6 mm diameter disc of membrane between two square metal plates, each about 2 cm² and 0.25 mm thick, and measuring the thickness of this assembly using a micrometer (Mitutoyo Manufacturing Co.,

Ltd., Tokyo, Japan). The contribution of the two plates to this overall thickness was then subtracted to yield the membrane thickness to the nearest 0.01 mm. When not in use, membranes were placed on glass plates and stored in plastic boxes at room temperature.

Series of membranes containing known amounts of benzoic acid (Terochem) were cast in groups of four, with one membrane in each series cast without added compound serving to act as a control. Stock solutions of benzoic acid in THF were made by dissolving about 15 to 30 mg in 25.0 mL of distilled THF. Subsequent THF solutions of lesser acid concentrations were prepared by dilution. To ensure that the normal membrane matrix was consistent over a series of membranes, a larger volume of membrane solution was prepared, and 2 to 3 mL portions of this delivered to each of four 10 mL beakers. Varying aliquots of THF solutions of the benzoic acid were then added to each of three beakers, and the total volume of membrane solution in all four beakers was brought to about 5 mL using distilled THF. After allowing to stir for 30 minutes or more, the mixtures were poured into PTFE moulds and allowed to set, as described above. After the curing process, membranes were weighed to the nearest 0.1 mg. To account for benzoic acid-containing membrane solution which inevitably remained behind in the beaker after casting, the 10 mL beakers used were weighed dry and again 24 hours after casting. The mass of "leftover" membrane thus determined was added to the mass of the corresponding cast membrane. Membrane concentrations of added benzoic acid could then be evaluated, since both the mass of acid and the total mass of membrane to which that compound was added were accurately known.

In order to confirm permeation of the membrane by benzoic acid, free-standing membranes were soaked for 90 hours in solutions with and without

benzoic acid and rinsed with doubly distilled H₂O. The UV spectra of these membranes were then obtained with an HP 8451A diode array spectrophotometer, with the membranes mounted on quartz cells. UV absorbance measurements of membranes containing known amounts of benzoic acid were obtained in the same way.

Open-circuit voltage measurements were made by using an Orion 701A ion-selective electrode meter and a sodium chloride saturated calomel electrode (SSCE). A glass electrode (Orion) was used to determine pH. K⁺ calibration curves were measured at fixed ionic strength by using 0.1 M NaCl as ionic buffer. Interference of acids was examined in 10⁻³ M KCl, 0.1 M trisodium citrate adjusted to the desired pH with HCl or NaOH. A 0.1 or 0.01 M KNO₃ solution was used to examine Cl⁻ interference by addition of KCl solution of equal concentration.

Impedance measurements and capacitance-voltage (C-V) curves were made using instrumentation previously described in Chapter 2, in solutions of constant ionic strength either 0.1 M in NaCl or 0.1 M in trisodium citrate buffer adjusted with HCl or NaOH. A SCE with a double junction filled with 0.1 M NH₄Cl served as reference electrode. The precision associated with measured bulk membrane resistances and capacitances was about ± 1 to 2 % for resistances and about ± 5 % for capacitances. Values of V_{fb} have precisions of ± 1 % to ± 5 %.

3.3 RESULTS AND DISCUSSION

The response of a number of K⁺-sensitive membrane coated semiconductor electrodes to K⁺ and the possible interferent species ascorbic,

benzoic, and carbonic acids [4] has been examined. Open circuit (V_{oc}) measurements of these electrodes with and without interferences present were made by X. Li of our group. The V_{oc} of the MIS electrodes used responds linearly to K^+ concentration over the range 10^{-1} to 10^{-4} M with a slope of 57.5 mV. With 0.1 M Na^+ present a selectivity coefficient, $k_{K,Na}$, of 2×10^{-4} is observed, which is somewhat poorer than the selectivity ($k_{K,Na} = 0.8 \times 10^{-4}$) of ion-selective electrodes with the standard solution/membrane/solution structure. The MAgIS electrodes used also show a Nernstian response to K^+ over the range 10^{-4} to 10^{-1} M K^+ ion with a slope of 58 mV, indicating the Ag/AgCl layer does not affect response of the assembly to K^+ .

The shift in potential response at K^+ -sensitive ISFET's observed by Fogt et. al. [4] when these devices are exposed to solutions containing acids that are neutral in their protonated form has been reproduced at MIS electrodes. Our findings show that ascorbic, benzoic, and carbonic acids all act as interferences at MIS electrodes at pH 4.5. The V_{oc} of a MIS electrode has been shown to shift positive by about 80 mV as the benzoic acid concentration increases from 0 to 30 mM in a 10^{-3} M K^+ , 0.1 M citrate, pH 4.5 solution [10]. At pH 4.5, about 33 % of the benzoic acid is in the neutral, protonated form. However, at pH 8.6, where the benzoate ion is the dominant form (>99.9 %), the same MIS electrode showed no change in V_{oc} with increasing benzoate concentration. In contrast, a naked n-Si/SiO₂/Si₃N₄ electrode didn't respond to benzoic acid at either pH, indicating the Si₃N₄ surface has no specific response to benzoic acid at a fixed, buffered pH. Exposure of a MIS electrode to bicarbonate and to ascorbic acid at pH 4.5 also caused significant positive shifts in the measured V_{oc} , whereas the same electrode showed no change in V_{oc} with increasing concentrations of either of these compounds at pH 8.6. The bicarbonate results parallel those reported previously [4] for K^+ -responsive ISFET's. Both ascorbic

and carbonic acid show a much stronger "memory" effect at MIS electrodes than does benzoic acid, although they generally induce a smaller shift in V_{oc} than does benzoic acid. Electrodes prepared with the interfacial structure n-Si/SiO₂/membrane also respond in a similar fashion to the neutral acids at low pH. Taken together, these results support the hypothesis developed in [4] that the neutral acid can enter the membrane, and that it is the ability of the acid to change the internal pH at the insulator/membrane interface that results in a potential response.

To obtain direct evidence that benzoic acid can actually permeate a plasticized membrane, a spectroscopic study was undertaken. Portions of K⁺-sensitive membrane were soaked for 90 hours in small amounts (~3 mL) of solution containing 0.1 M HCl, 0.1 M NaCl and 10⁻³ M KCl, which in some cases also contained 0.01 M benzoic acid. UV spectra obtained for two such samples are presented in Figure 3.1. While the absorbance spectrum measured for the membrane bathed in the control solution described above is featureless, a strong absorbance peak characteristic of benzoic acid is observed for the membrane bathed in 10 mM benzoic acid, centered at about 274 nm. Figure 3.1 clearly shows, then, that ingress of the acid into the membrane does occur when that acid is present in solution.

In order to determine the membrane acid concentration responsible for the spectrum in Figure 3.1, two series of PVC/DOA/valinomycin membranes containing known quantities of benzoic acid were cast, and their UV spectra recorded over the 250 to 350 nm range. The resulting calibration curve of absorbance change vs benzoic acid concentration in moles/L is given in Figure 3.2. The absorbance of each membrane at 274 nm was corrected by subtracting the absorbance of a control membrane at the same wavelength, resulting in the values for absorbance change plotted in Figure 3.2. Because

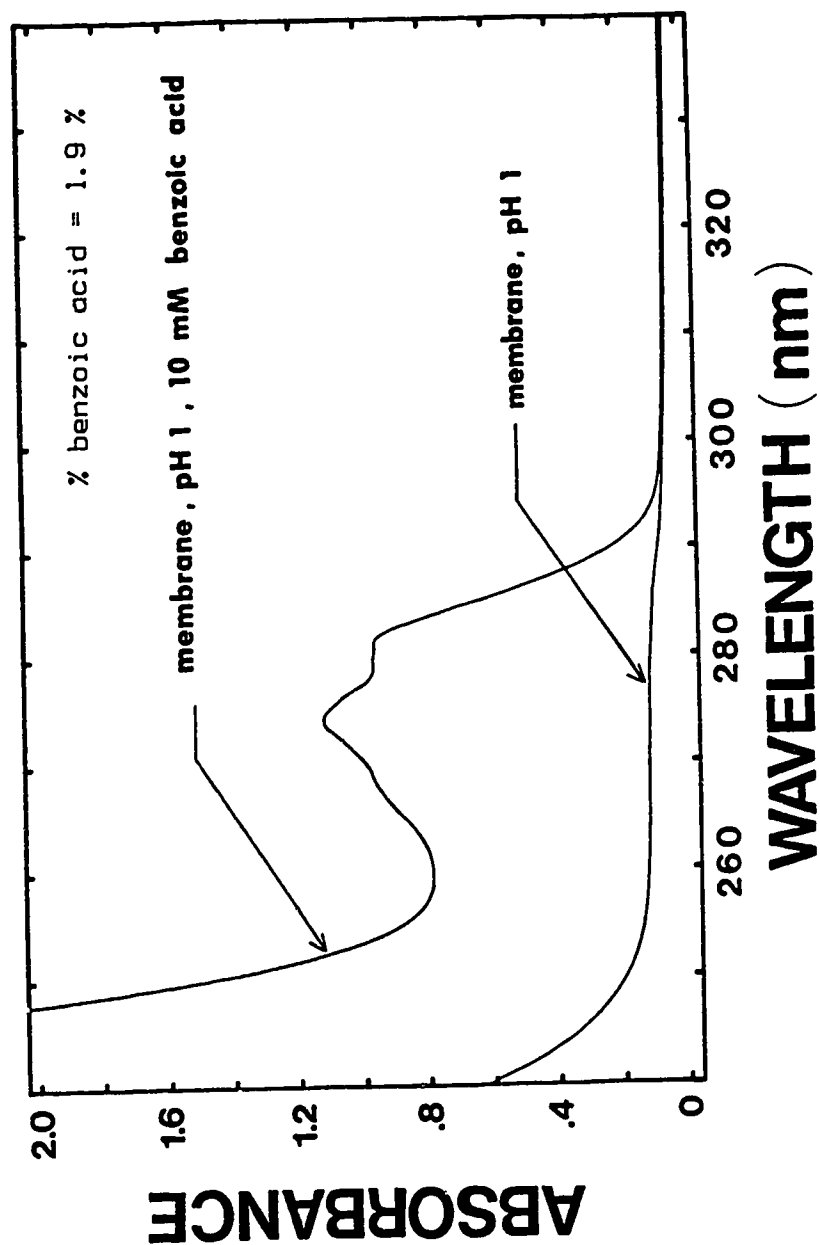


Figure 3.1: Absorbance spectra of K⁺ sensitive PVC membranes following a 90-h immersion in solutions containing 0.1 M HCl, 0.1 M NaCl, and 10⁻³ M KCl, both with and without 0.01 M benzoic acid present.

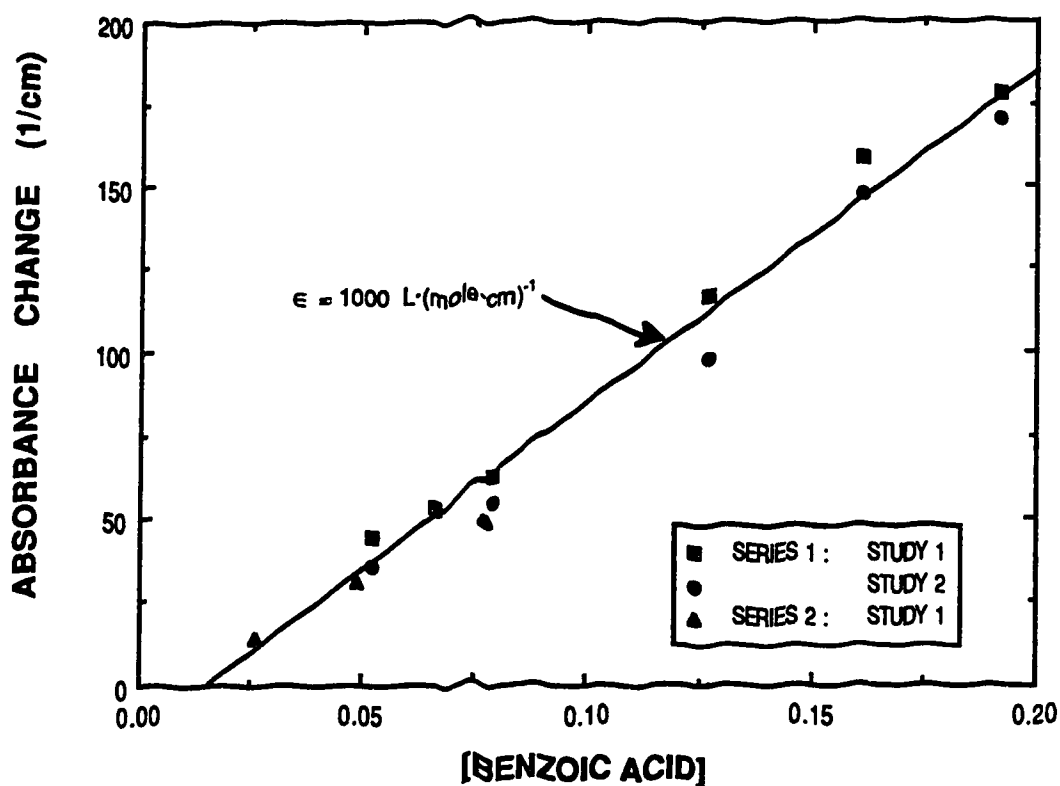


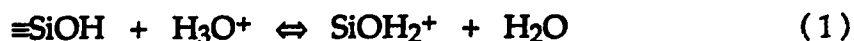
Figure 3.2: Calibration curve of absorbance change as a function of benzoic acid in the membrane, measured at 274 nm. Absorbances were normalized for membrane thickness. As a result, changes in this parameter are reported in cm^{-1} . Membranes in Series 1 and Series 2 differ in that they were cast from different membrane stock solutions. Measurements of the membranes in Series 1 were carried out twice, using different portions of membrane; results of both sets of measurements are presented, and are denoted as Study 1 and Study 2.

membrane portions varied in thickness, each value of absorbance change was divided by the thickness of the membrane used to measure it. This amounts to correcting absorbance values for varying "cell pathlengths", and is the reason for reporting absorbance changes in cm^{-1} . The molar absorptivity of benzoic acid in the membrane, then, is equal to the slope of the calibration curve, and has a value of $1000 \text{ L mole}^{-1}\text{cm}^{-1}$, which is approximately that observed for benzoic acid in DOA alone. From this curve, it is found that the membrane whose spectrum is presented in Figure 3.1 contained 0.11 M acid after 90 hours of soaking.

Membranes were also soaked in citric acid buffered solutions at pH 8.6 both with and without benzoate present, and very small differences in absorbance between membranes in the two solutions were observed. The spectroscopic evidence at high pH does not exclude the possibility of a small amount of benzoate permeating the membrane. However, from our results it is clear that the neutral acid is preferred by a factor of at least 50 over the conjugate base.

The conclusion that it is not solely permeation of the membrane by the neutral acid that causes the observed shift in V_{oc} at MIS electrodes is supported by the results of several potentiometric experiments carried out in our lab using K^+ -sensitive electrodes. Results of these experiments, in which the V_{oc} of an ISE was measured in the presence of varying concentrations of benzoic, carbonic, and ascorbic acids at both low and high pH's, show that the acids examined do not affect ISE response in any way. Shifts in V_{oc} for MIS electrodes exposed to the neutral acids appear to be due to a change at the insulator/membrane interface, since the membrane coated onto the insulator should behave no differently than in the ISE configuration.

It is well known that both Si_3N_4 and SiO_2 insulating layers have significant surface site densities associated with them, formed when the surface hydrolyzes in the presence of water to form silanol (SiOH) groups [11]. These groups can be protonated or deprotonated according to the following equations :



The pH at the insulator surface will determine whether the surface is positively charged, negatively charged, or neutral. Since the n-Si substrate is coupled to the oxide by means of a field effect, any change in the net oxide charge will be reflected as a change in the net charge at the n-Si/oxide interface. The introduction of a membrane onto the oxide simply means that now the n-Si substrate is coupled through the oxide to the membrane layer via the same field effect. The n-Si/insulator interface, and hence the insulator/membrane interface of a MIS electrode can be effectively studied by exploiting the dependence of the n-Si space charge layer capacitance on applied voltage. This is done by measuring the equivalent capacitance, C_{eq} , of MIS electrodes as a function of the applied voltage at low frequencies, where the response is dominated by the space charge layer of the semiconductor [10]. The apparent value of the flatband voltage, V_{fb} , the applied voltage at which the energy bands in the semiconductor are flat, can be determined from the resultant capacitance-voltage (C-V) curves through use of the Mott-Schottky relationship. The C-V curves may be analyzed by using the model developed to describe the impedance of metal/oxide/semiconductor and electrolyte/oxide/semiconductor devices [11-13]; a detailed discussion of this has already been presented in Chapter 2. We find that the apparent V_{fb} shifts

by ~50 to 60 mV per decade of K^+ concentration change for K^+ -sensitive MIS electrodes. The observed shift in the C-V curves with K^+ confirms that the electrodes prepared do operate by a field effect mechanism.

Presented in Figure 3.3 are C-V curves for a bare n-Si/SiO₂/Si₃N₄ electrode in solutions buffered at pH 4.5 and 8.6, with and without benzoate present. As with the V_{oc} measurements of bare electrodes, no shift in apparent V_{fb} is observed when benzoate is added to solution, indicating that benzoate does not undergo any specific interaction with the insulator surface. The V_{fb} measured at pH 4.5 is more positive, having a value of $0.46\text{ V} \pm 1\%$. This drops to a value of $0.31\text{ V} \pm 1\%$ at pH 8.6, which corresponds to a 40 mV change per decade change in H^+ concentration. Sub-Nernstian in magnitude, the response to pH change is comparable to the potentiometric response observed for pH field effect transistors, in which the insulator of the gate is exposed to solution [11]. It is generally accepted that the response of these devices is determined by surface silanol groups capable of undergoing acid-base chemistry, so that a variation in pH at the membrane/insulator interface of a MIS electrode is expected to manifest itself as a shift in V_{fb} .

The effect of exposure to benzoate at pH 4.5 and pH 8.6 on the C-V curves of a MIS electrode having a n-Si/SiO₂/Si₃N₄/membrane interfacial structure is shown in Figures 3.4(a) and 3.4(b), respectively. The curves of 3.4(a) are seen to shift to the right as the benzoic acid concentration increases, consistent with an increase in the apparent V_{fb} of the electrode. The corresponding ΔV_{fb} at pH 4.5 has a magnitude of 117 mV for an increase in benzoic acid concentration from 0 to 4 mM. This value of ΔV_{fb} is within the same order of magnitude as the ΔV_{oc} observed earlier, though it is somewhat larger than the shift observed in the V_{oc} measurement. For benzoic acid the observed shift is usually reversible, although up to two hours of soaking in

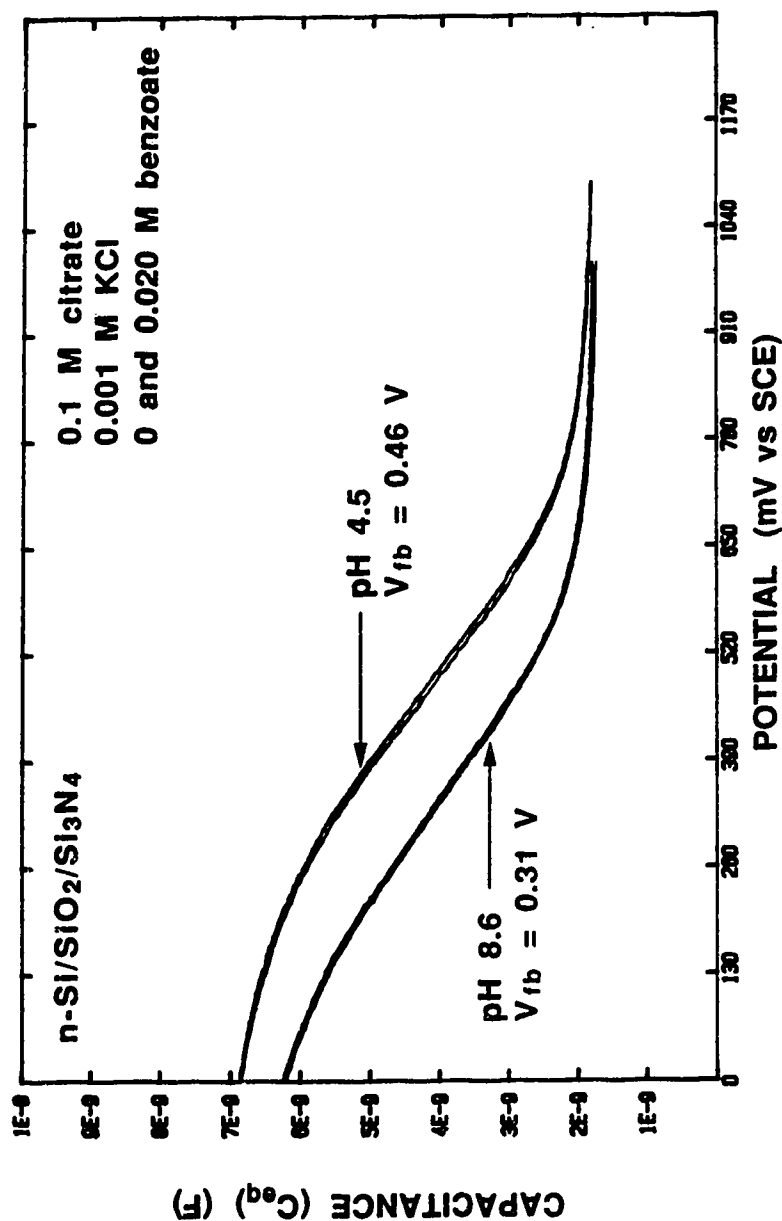


Figure 3.3: Effect of added benzoate on the capacitance-voltage (C-V) curves of a bare n-Si/SiO₂/Si₃N₄ electrode in solutions containing 10⁻³ M KCl and 0.1 M trisodium citrate adjusted to pH 4.5 and 8.6. Curves were recorded at 1000 Hz. Both the anodic and cathodic scans are shown. At each pH, the curve obtained in 0.020 M benzoate is indistinguishable from the curve obtained with no benzoate present.

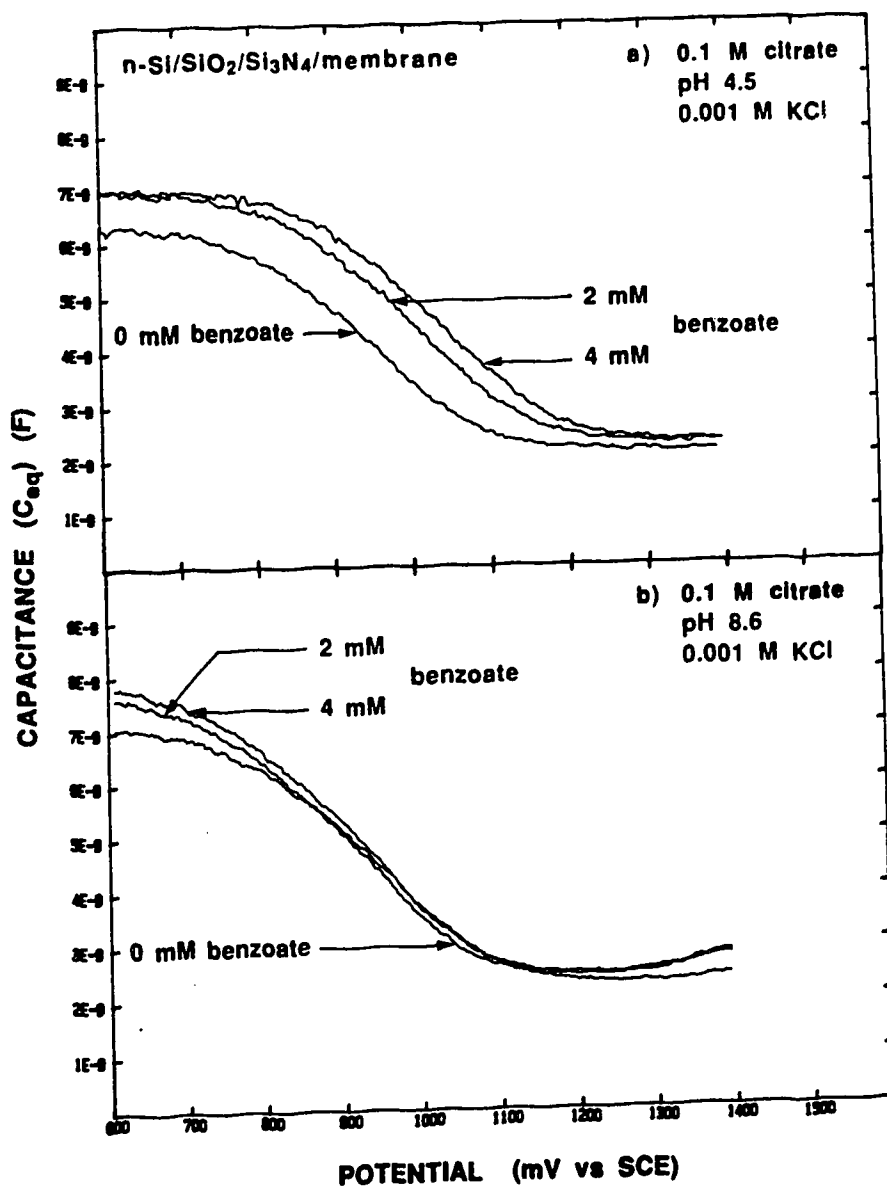


Figure 3.4: Effect of added benzoate on the capacitance-voltage (C-V) curves of a n-Si/SiO₂/Si₃N₄/K⁺-membrane electrode in solutions containing 10⁻³ M KCl and 0.1 M trisodium citrate adjusted to a) pH 4.5 or b) 8.6. Curves were measured at 25 Hz. At pH 4.5, curves shift in a positive direction along the V axis when benzoate is added, indicating an increase in V_{fb} .

benzoic acid free solution may be required to completely reverse the potential shift. In contrast, Figure 3.4(b) indicates that the C-V curves do not shift markedly in the presence of benzoate anion at pH 8.6, so that the change in apparent V_{fb} is much reduced. The ΔV_{fb} for the Si_3N_4 /membrane electrode of Figure 3.4(b) in going from 0 to 4 mM benzoate at pH 8.6 is -18 mV. Again, the smaller magnitude of the ΔV_{fb} observed at pH 8.6 is expected when one considers that no significant change in V_{oc} was observed for MIS electrodes in the presence of increasing benzoate concentrations at pH 8.6.

The other feature of the C-V curves to note in Figure 3.4 is that there is an increase in the maximum C_{eq} attained under accumulation conditions (negative potentials, forward bias) at both pH's when the benzoate concentration is increased. There is a smaller but measurable increase in minimum C_{eq} under depletion conditions (positive potentials, reverse bias) as well. This phenomenon is similar to that observed for certain MIS electrodes in solutions of increasing KCl concentration at an ionic strength of 0.1 (see Chapter 2). In the MIS electrode case, the observed variation in C-V curves was ascribed to changes in the membrane's electrical properties, particularly decreases in bulk membrane resistance, R_g . The same conclusion may be reached for the C-V curves of Figure 3.4, if the Nyquist plots of Figure 3.5 are taken into account. These impedance plane plots for the n-Si/ SiO_2 / Si_3N_4 /membrane electrode of Figure 3.4 show a single semicircle at frequencies greater than 100 Hz, which may be assigned to membrane capacitance, C_g , and resistance, R_g . Electrode capacitance governs electrode response at frequencies less than 100 Hz, giving rise to the largely capacitive behaviour observed at these frequencies in the form of a steeply rising tail. Since these experiments were carried out at an applied voltage of 0.6 V, which places the electrode in accumulation (see Figure 3.4), electrode capacitance in

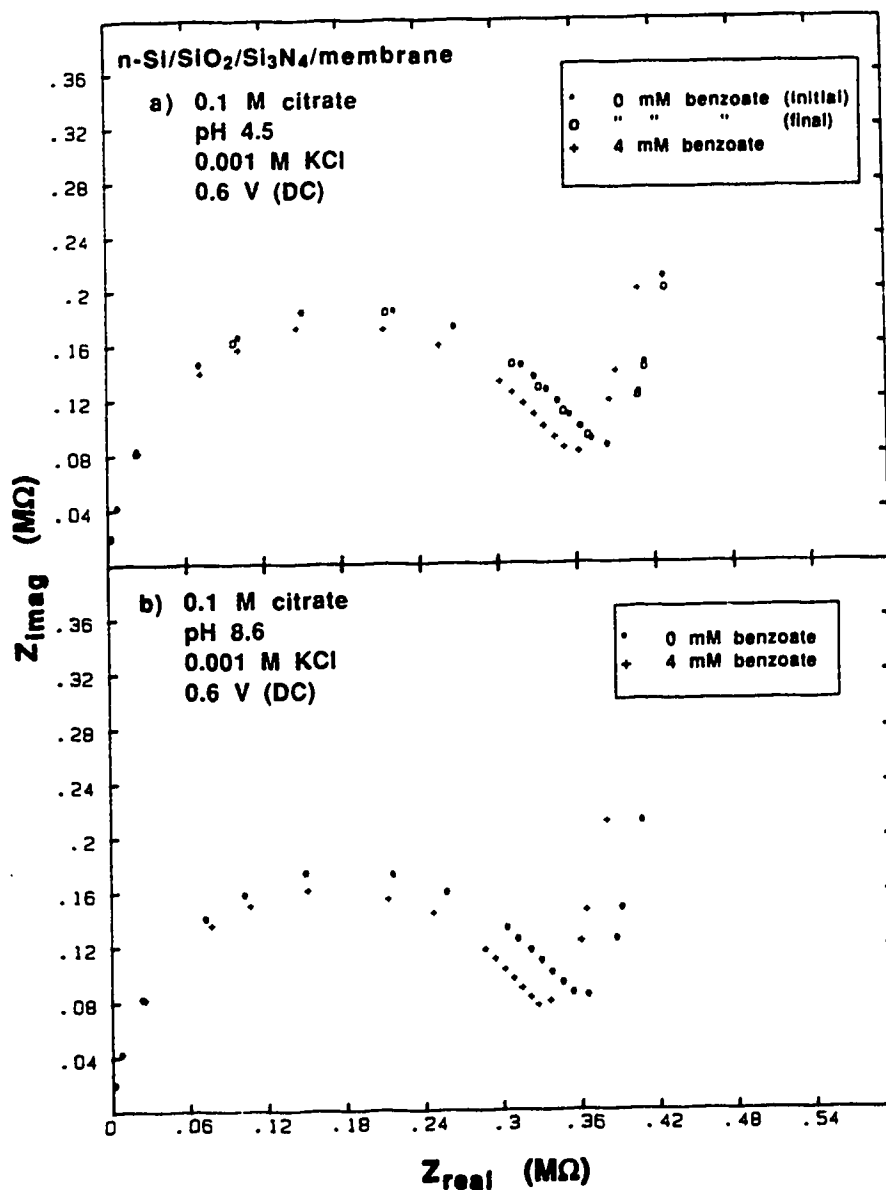


Figure 3.5: Nyquist plots recorded over frequencies ranging from 25 Hz to 40 kHz for the MIS electrode of Figure 3.4, showing the effect of added benzoate at a) pH 4.5 and b) pH 8.6. All solutions contained 0.1 M trisodium citrate and 10^{-3} M KCl. A DC potential of 0.6 V vs SCE was applied, biasing the electrode into accumulation. At both pH's, the addition of 4 mM benzoate (+) resulted in a reduction in R_g from the 0 mM benzoate case (*). The effect is shown to be reversible at pH 4.5, since re-immersion of the electrode in 0 mM benzoate for an hour after exposure to benzoate resulted in R_g returning to its original value (o).

these plots is determined mostly by the oxide capacitance, and the semicircle due to bulk membrane properties is well-defined. As benzoate is added to the test solution at both pH's R_g shows roughly a 5 to 7 % decrease, as indicated by the R_g values given in Table 3.1, obtained from the intercepts of the semicircles with the real axis at low frequency. This effect on membrane impedance appears to be totally reversible in the low pH experiment, as illustrated by Figure 3.5(a). The membrane resistance returns to its initial value after about 30 to 60 minutes of soaking in a benzoic acid-free solution at pH 4.5. Although no "recovery" experiment was carried out for this MIS electrode at pH 8.6, subsequent impedance experiments on these plasticized PVC membranes have shown that observed decreases in R_g are reversible at high pH's. The amount of soaking time required in benzoate-free solutions for the membrane to attain its initial resistance, however, may vary anywhere from 15 minutes to a couple of hours. The reversibility of the effect that exposure to benzoate at both pH's has on the Nyquist plots of a MIS electrode mirrors that observed for the shifts in V_{fb} discussed above in Figure 3.4. Overall, it is clear from Figure 3.5 that the increased C_{eq} measured at increased benzoate concentrations under accumulation and depletion conditions is at least partly attributable to measurable decreases in R_g . C_g appears not to affect C_{eq} to any significant extent, as these measured values all fall within the limits of precision for this parameter. Also of importance is the fact that impedance experiments at pH 8.6 point to permeation of the membrane by the benzoate anion, even though this permeation cannot be detected spectroscopically.

It should be noted at this point that changes in bulk membrane properties significant enough to affect the measured C-V curve of a MIS electrode may also cause an apparent change in the measured V_{fb} , even

TABLE 3.1: Changes in R_g and C_g as a function of added benzoate at pH 4.5 and pH 8.6, determined from the Nyquist plots in Figure 3.5 for a n-Si/SiO₂/Si₃N₄/membrane electrode; $E_{app} = 0.6$ V

[Benzoate] (mM)	pH	R_g (M Ω) ^{a)}	C_g (pF) ^{b)}
0 mM	4.5	0.378	179
2	"	0.361	184
4	"	0.358	186
0 mM	8.6	0.358	185
2	"	0.337	208
4	"	0.334	192

a) Measured R_g 's have a precision of ± 2 %.

b) Measured C_g 's have a precision of ± 5 %.

though no such change in V_{fb} has actually occurred. As discussed in Chapter 2, this is due to the corresponding Mott-Schottky plot of C^{-2} versus V being shifted vertically as well as horizontally, so that the distance over which the linear portion of the curve has to be extrapolated to obtain V_{fb} is increased. In light of corresponding V_{oc} measurements at pH 8.6, which predict little or no change in V_{fb} when benzoate is added to the solution, changes in bulk membrane properties, particularly R_g , may be largely responsible for the small but observable shifts in apparent V_{fb} measured for the MIS electrode of Figure 3.4(b) in the presence of benzoate. At pH 4.5 it is reasonable to conclude that the ΔV_{fb} 's due to added benzoate arise primarily at the insulator/membrane interface, given the correspondingly large ΔV_{oc} 's.

As suggested in the introduction, the vapour deposition of Ag onto the insulator surface, followed by partial chemical chloridation of the Ag layer, should protect the insulator surface sites from interaction with interferent species. To confirm this, several MAgIS electrodes were prepared and studied for their V_{oc} and impedance responses with and without benzoate present. Some of these electrodes were tested with regard to their response to Cl^- before deposition of a membrane coating was carried out. V_{oc} measurements, conducted by Xizhong Li of our group, yielded slopes typically of 30 to 40 mV per decade change in Cl^- concentration, indicating that the Ag/AgCl reference is less than ideal for such electrodes, but does nonetheless have a Cl^- response. This observation is corroborated by the C-V curves of Figure 3.6, measured at Cl^- concentrations ranging from 10^{-4} M to 10^{-1} M in solutions having an ionic strength of 0.1. This particular electrode, whose apparent V_{fb} values measured at 1000 Hz are presented as a function of Cl^- concentration in Table 3.2, produced a sub-Nernstian slope of -31.5 mV in V_{oc} measurements. The shifts in V_{fb} are also of a sub-Nernstian nature, and work

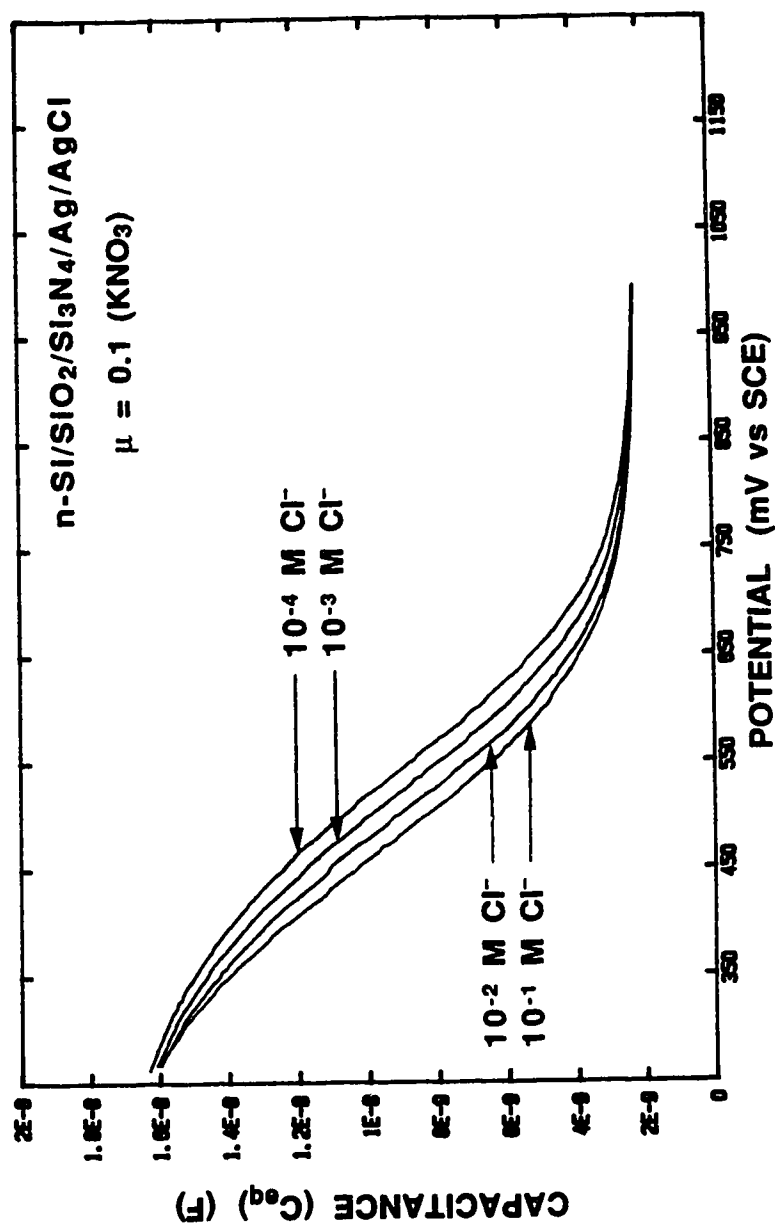


Figure 3.6: C_{eq} -V curves for a bare n-Si/SiO₂/Si₃N₄/Ag/AgCl electrode acquired at 1000 Hz as a function of Cl⁻ concentration. Cl⁻ concentration was varied by adding aliquots of 0.1 M KCl to 25.00 mL of 0.1 M KNO₃. The curves shift in a negative direction along the V axis with increasing concentration, reflecting the fact that the electrode is responding to an anionic species rather than a cationic species.

TABLE 3.2: Flatband potentials, V_{fb} , and flatband shifts, ΔV_{fb} , determined from the C-V curves in Figure 3.6, which were measured as a function of Cl^- concentration for a n-Si/SiO₂/Si₃N₄/Ag/AgCl electrode

[Cl ⁻]	V_{fb} (V) ^{a)}	ΔV_{fb} (V)
10 ⁻¹	.552	-0.018
10 ⁻²	.570	-0.027
10 ⁻³	.597	-0.018
10 ⁻⁴	.615	

- a) Values of V_{fb} have a precision of $\pm 1\%$, as calculated from the regression analysis of the linear portions of the M-S plots.

out to be about 20 mV per decade change in Cl^- concentration. As halogen sensitivity is not an objective here, and all that is required of the Ag/AgCl layer is that it form an electrochemically reversible interface with the K^+ -sensitive membrane, non-ideality of this metallic layer is not critical to its function in MAgIS electrodes unless it should prove to be sensitive to O_2 . This latter point is important, since O_2 can permeate the membrane, and Ag in the layer would readily form the oxide in the presence of O_2 if the Ag/AgCl were not of sufficiently good quality. This would lead to a degradation in the film's ability to act as an internal reference, and to maintain a stable potential across the Ag/AgCl/membrane interface. However, X. Li showed that very little change (only about 2 mV or so) in the V_{oc} of coated MAgIS electrodes occurs when solution O_2 is varied first by purging with N_2 and then with air, so that the Ag/AgCl layers as prepared were good enough to prevent oxide formation. He also found that coated MAgIS electrodes also show very limited V_{oc} response to Cl^- , as expected for K^+ -sensitive membranes of the type used in this study, which have been shown to be permselective enough to prevent the ingress of Cl^- to any great extent [14]. Despite the Cl^- sensitivity of the electrode's metallic layer, then, it appears that the membrane will not allow Cl^- to penetrate to the Ag/AgCl/membrane interface, and no Cl^- response is expected. The C-V curves as a function of K^+ concentration for the electrode of Figure 3.6 after it was coated with K^+ -sensitive membrane are presented in Figure 3.7. At this frequency of 25 Hz, the curves show a strong dependence on applied voltage, which is consistent with observation of the silicon space charge capacitance, C_{sc} , as in the MIS electrode case. The V_{fb} values listed in Table 3.3 vary in an expected manner as a function of K^+ concentration, given the Nernstian V_{oc} response to K^+ displayed by this

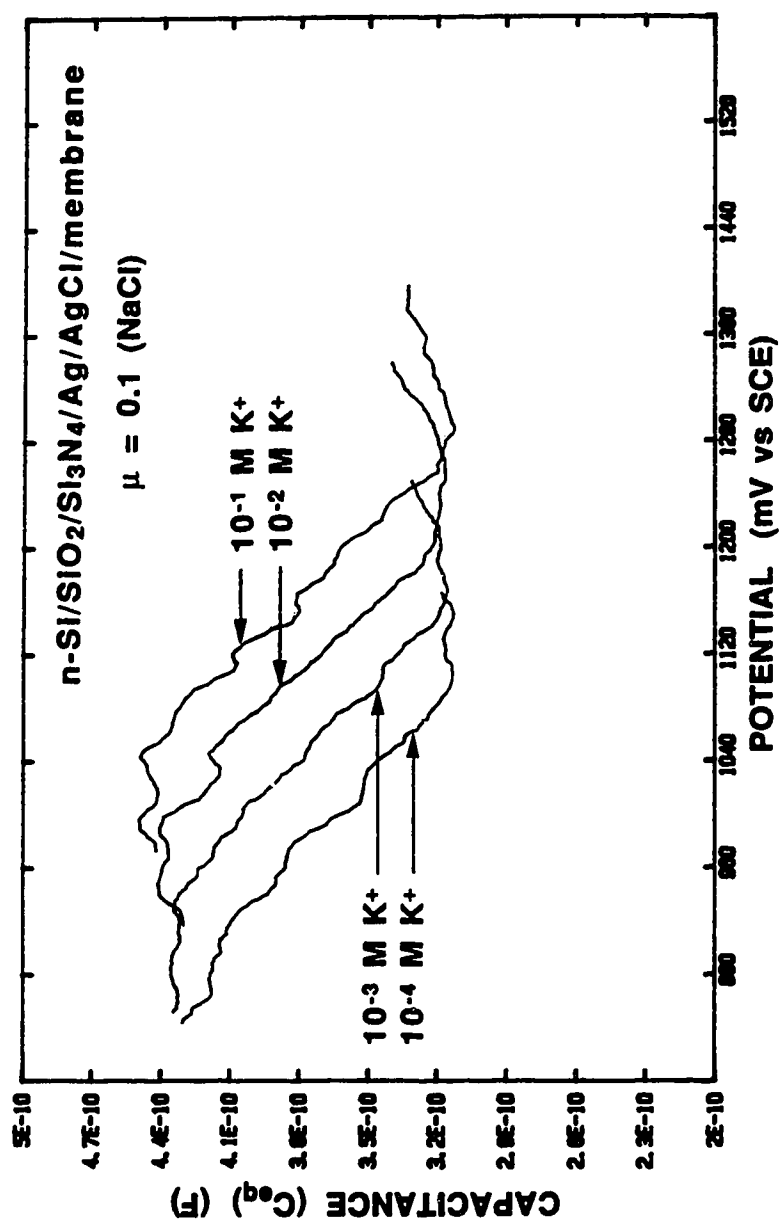


Figure 3.7: C_{eq} -V curves for an n-Si/SiO₂/Si₃N₄/Ag/AgCl/membrane electrode acquired at 25 Hz as a function of K⁺ concentration. All solutions were buffered at a μ of 0.1 by NaCl. The curves shift in a positive direction along the V axis with increasing K⁺ concentration, indicating a corresponding increase in V_{fb} .

TABLE 3.3: Flatband potentials, V_{fb} , and flatband shifts, ΔV_{fb} , determined from the C-V curves in Figure 3.7, which were measured as a function of K^+ concentration for a n-Si/SiO₂/Si₃N₄/Ag/AgCl/membrane electrode

[KCl]	V_{fb} (V) ^{a)}	ΔV_{fb} (V)
10 ⁻¹	.90	.05
10 ⁻²	.85	.07
10 ⁻³	.78	.06
10 ⁻⁴	.72	.06

a) Values of V_{fb} have precisions ranging from $\pm 1\%$ to $\pm 5\%$.

electrode. Therefore, functional MAgIS electrodes, which are derivatives of MIS electrodes, continue to respond to K^+ by a field-effect mechanism.

Having established that the MAgIS electrode is a viable alternative to the MIS electrode as far as response to K^+ is concerned, the effect of exposing this electrode to solutions containing neutral acid interferents was examined. V_{oc} results obtained by X. Li show that the open circuit voltage of MAgIS electrodes do not respond significantly to benzoic acid at pH 4.5, where MIS electrodes show up to an 80 mV shift. Similarly, neither HCO_3^- nor ascorbic acid show any sign of interference at MAgIS electrodes at low pH's. These statements hold true for MAgIS electrodes having either an insulator layer comprised of Si_3N_4 (500 Å) over SiO_2 (500 Å) or an insulator layer of just SiO_2 (500 Å), indicating that insulator composition is not imperative to electrode operation. At pH 8.6, no interference from any of the species considered is observed at MAgIS electrodes, which is in agreement with MIS electrode results.

The C-V curves as a function of added benzoate at pH 4.5 and 8.6 for the n-Si/ SiO_2 / Si_3N_4 /Ag/AgCl/membrane electrode of Figure 3.7 are given in Figure 3.8. Although an overall shifting up of these curves to higher C_{eq} values is observed at increased benzoate concentrations, they do not shift significantly towards more positive voltages upon exposure to benzoate at either pH. This implies that no significant shift in V_{fb} has occurred either, despite the apparent changes in this parameter that would result from calculations performed using the corresponding Mott-Schottky plots. The C-V curves of Figure 3.8 suggest that the observation of changing membrane properties caused by exposure to various acids is not restricted to MIS electrodes alone. The Nyquist plots in Figure 3.9 measured at the same time as the curves of Figure 3.8, along with the corresponding R_g data presented in

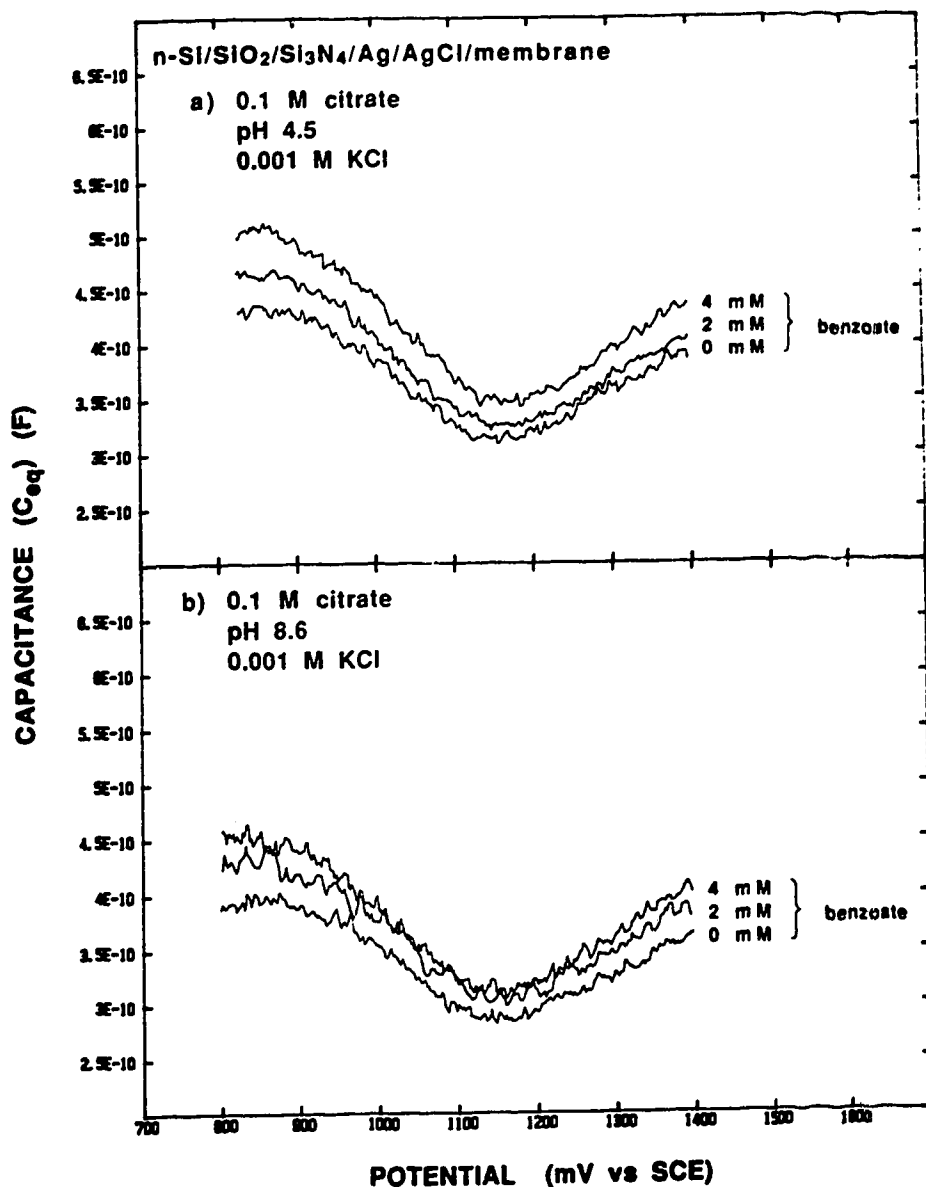


Figure 3.8: Effect of added benzoate on the capacitance-voltage (C-V) curves of an n-Si/SiO₂/Si₃N₄/K⁺-membrane electrode in solutions containing 10⁻³ M KCl and 0.1 M trisodium citrate adjusted to a) pH 4.5 or b) 8.6. Curves were measured at 25 Hz. At both pH's, the C_{eq} measured at any particular applied voltage increases as concentration of added benzoate increases.

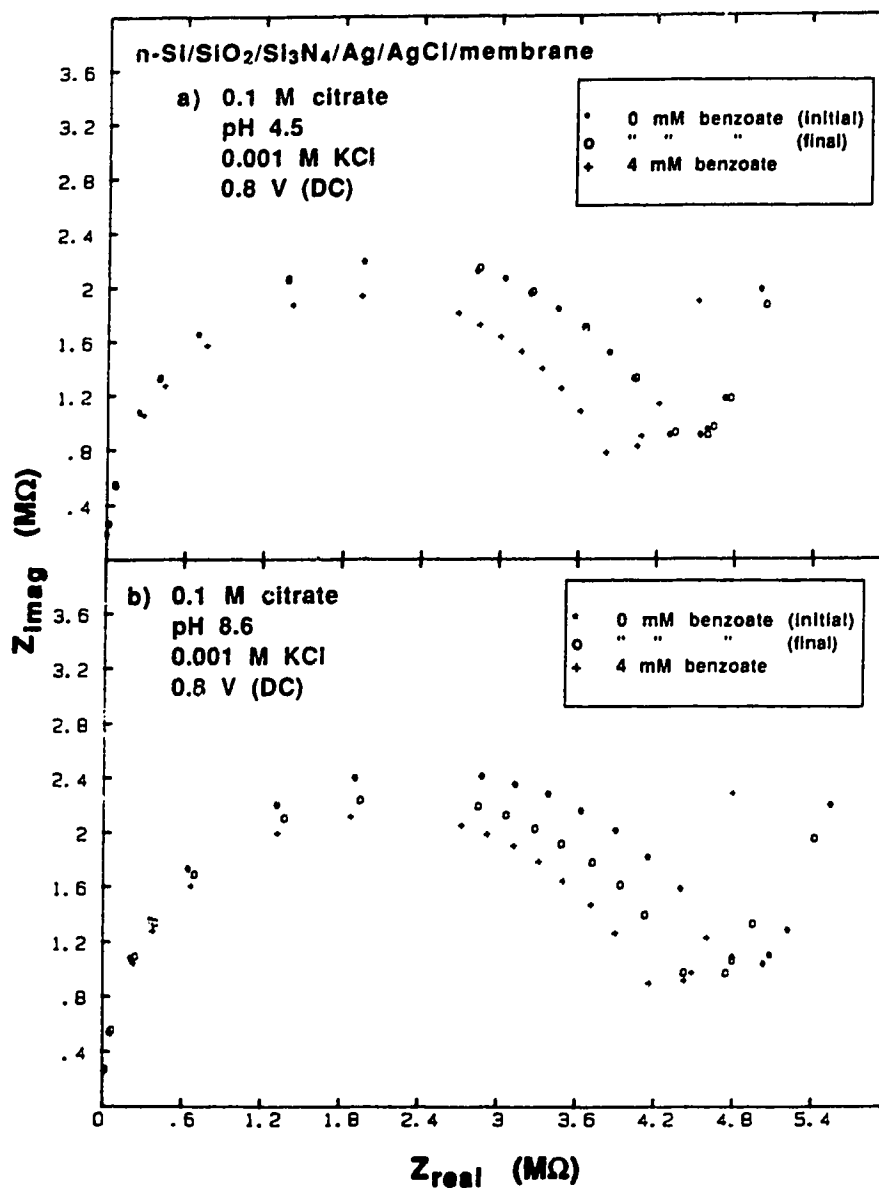


Figure 3.9: Nyquist plots recorded over frequencies ranging from 25 Hz to 40 kHz for the MIS electrode of Figure 3.4, showing the effect of added benzoate at a) pH 4.5 and b) pH 8.6. All solutions contained 0.1 M triscidium citrate and 10^{-3} M KCl. A DC potential of 0.8 V vs SCE was applied, biasing the electrode into accumulation. At both pH's, the addition of 4 mM benzoate (+) resulted in a reduction in R_g from the 0 mM benzoate case (*). The effect is shown to be reversible at pH 4.5, since re-immersion of the electrode in 0 mM benzoate for an hour after exposure to benzoate resulted in R_g returning to its original value (o). At pH 8.6, it appears that a longer soaking period in benzoate-free solution would be required for the membrane to return to its initial R_g .

TABLE 3.4: Changes in R_g and C_g measured as a function of added benzoate at pH 4.5 and pH 8.6, determined from the Nyquist plots in Figure 3.9 for a n-Si/SiO₂/Si₃N₄/Ag/AgCl/membrane electrode; $E_{app} = 0.8$ V

[Benzoate] (mM)	pH	R_g (M Ω) ^{a)}	C_g (pF) ^{b)}
0 mM	4.5	4.37	27
2	"	4.03	27
4	"	3.85	27
0 (2 nd x)	"	4.40	27
0 mM	8.6	4.88	27
2	"	4.49	28
4	"	4.19	28
0 (2 nd x)	"	4.65	27

a) Measured R_g 's have a precision of ± 2 %.

b) Measured C_g 's have a precision of ± 5 %.

Table 3.4, support this conclusion, as they clearly show reversible reductions in R_g at both pH's, ranging from 12 % at pH 4.5 to 14 % at pH 8.6. The fact that R_g is reduced for all types of membrane electrodes on exposure to benzoic acid, combined with the UV spectroscopic data at pH 1, provides strong evidence that benzoic acid permeates the PVC membrane. Though attention in this study has focussed primarily on permeation of the membrane by benzoic acid, a few experiments were carried out in the presence of carbonic and ascorbic acids. As with benzoic acid, reductions in R_g were observed upon exposure to these acids, which, when combined with the interference of these species at MIS electrodes, is also consistent with permeation of the membranes. Since these interferences have been eliminated at the MAgIS electrode, it appears that changes wrought by these species on membrane electrical properties, particularly conductivity, do not play a role in the observed interference to response in the MIS electrode case.

3.4 CONCLUSION

Interferences by CO_2 or ascorbic acid in the determination of K^+ ion in biological media could present a serious problem for membrane-coated ISFET's with a Si_3N_4 gate. The results presented in this chapter demonstrate that the presence of a Ag/AgCl overlayer on a gate subsequently coated with a permselective membrane would be an effective and simple means of avoiding such interferences. Importantly, procedures for deposition and preparation of Ag/AgCl films have been shown to be compatible with planar Si microlithographic technology [15,16]. Thus the approach presented here is readily incorporated into ISFET device fabrication. Further, since the Ag/AgCl

layer appears to adequately protect the underlying gate insulator, it may prove possible to eliminate the Si_3N_4 layer on the gate altogether, thus eliminating one photolithographic step in the fabrication of AgCl-coated gates.

The sensitivity to halogen ions that could arise as a complication is easily avoided with PVC membranes containing KTPB that are permselective for a cation such as K^+ [14,17]. Anions such as TPB^- are known to act as nearly fixed sites in the PVC matrix, providing Donnan exclusion of most anions from the membrane [18]. Interestingly enough, the results for both MIS and MAgIS electrodes presented here point to an increase in membrane conductivity upon exposure to solutions containing benzoate exclusively in its anionic form, indicating that species like benzoate, not known to be particularly lipophilic, are not totally excluded from the membrane phase. Permeation of the membrane by neutral acidic species also results in a such an increase, which suggests that these species undergo a further charge-generating process once inside the membrane. A more detailed study of the effect of pH and membrane composition on membrane impedance when exposed to lipophilic species is presented in Chapter 4.

Both spectroscopic data and impedance analysis of the PVC/DOA/valinomycin membrane system provide clear evidence that bulk membrane properties are influenced by species such as ascorbic, benzoic, and carbonic acids. It has been demonstrated that these neutral species can permeate the ion-responsive membrane in a reversible fashion, thus confirming the model suggested by Fogt et. al. [4] for interference at ISFET's. Finally, impedance analysis of ion-selective electrodes provides a much more sensitive probe than open circuit voltage measurements of the effect of lipophilic sample solutes on both membrane and silicon substrate characteristics.

3.5 REFERENCES

- (1) Janata, J. In *Solid State Chemical Sensors*; Janata, J. , Huber, R.J., Ed.: Academic, London, 1985
- (2) Wohltjen, H., *Anal. Chem.*, 1984, 56, 87A
- (3) Bergveld, P. Sibbald, A., *Analytical And Biomedical Applications of Ion-Selective Field Effect Transistors*; Elsevier: Amsterdam, 1988
- (4) Fogt, E.J., Untereker, B.F., Norenberg, M.S., Meyerhoff, M.E., *Anal. Chem.*, 1985, 57, 1995
- (5) Buck, R.P., Hackleman, D.E., *Anal. Chem.*, 1977, 49, 2315
- (6) Baucke, F.G.K., *J. Electroanal. Chem. Interfacial Electrochem.*, 1976, 67, 277
- (7) Ammann, D., Bissig, R., Cimerman, Z., Fiedler, U., Gugli, H., Morf, W.E., Oehme, M., Osswald, H., Pretsch, E., Simon, W., In *Ion And Enzyme Electrodes In Biology And Medicine*; Kessler, M., et al., Ed.; University Park Press: Baltimore, MD, 1976, p.22
- (8) Band, D.M., Kratochvil, J., Treasure, T., *J. Physiol. (London)*, 1976, 265, 2P
- (9) Bassett,J.,Denney, R. C., Jeffery, G. H., Mendham, J. *Vogel's Textbook of Quantitative Inorganic Analysis, 4th Ed.*; Longman: London,1978
- (10) Li,X., Verpoorte, E.M.J., Harrison, D.J., *Anal. Chem.*, 1988, 60, 493
- (11) Siu, W.M., Cobbold, R.S.C., *I.E.E.E. Trans. Electron Dev.*, 1976, ED-26, 1805
- (12) Lindner, R., *Bell Sys. Tech. J.*, 1962, 41, 803
- (13) Grove, A.S., Deal, B.E., Snow, E.H., Sah, C.T., *Solid-State Electron.*, 1965, 8, 145
- (14) Thoma, A.P., Viviani-Nauer, A., Arvanitis, S., Morf, W.E., Simon, W., *Anal. Chem.*, 1977, 49, 1567

- (15) Bousse, L.J., Bergveld, P., Gearaedts, H.J.M., *Sens. Actuators*, 1986, 9, 179
- (16) Koudelka, M., *Sens. Actuators*, 1986, 9, 249
- (17) Buck, R.P., Toth, K., Graf, E., Horvai, G., Pungor, E., *J. Electroanal. Chem.*, 1987, 223, 51
- (18) Lindner, E., Graf, E., Niegriesz, Z., Toth, K., Pungor, E., *Anal. Chem.*, 1988, 60, 295

CHAPTER 4

A STUDY OF MEMBRANE PERMEABILITY BY AC IMPEDANCE ANALYSIS

4.1 INTRODUCTION

Ion-selective liquid membrane electrodes (ISE) based on neutral carriers now find wide use in analytical chemistry in the determination of a range of ions such as K^+ , Na^+ , Ca^{2+} , and NH_4^+ . One commonly used K^+ -selective electrode has a liquid membrane which consists of 33 % polyvinylchloride (PVC) as a polymer matrix; 66 % dioctyladipate (DOA) as plasticizer and 1 % neutral carrier valinomycin, which gives the membrane its selectivity for K^+ . The response of these electrodes to K^+ is fully Nernstian when the potassium salt of a hydrophilic anion such as Cl^- or SO_4^{-2} is present in the test solution [1,2]. In order to more fully characterize the response of the liquid membrane on which the electrodes are based, potentiometric measurements have been supplemented by various mechanistic studies employing electro dialysis, radiotracer methods, and chronoamperometry, as well as several other techniques [3,4]. Results of these studies indicate that these membranes are electroneutral entities containing anionic sites capable of ion exchange. These sites are oil-soluble impurities associated primarily with the PVC matrix, and are thought to stem from the manufacturing process used to make this polymer. Though some sites will be relatively mobile within the membrane matrix, the majority are assumed to be fixed [3,5]. Site densities have been reported to range from 0.05 to 0.6 mM [5].

Existence of these sites within the membrane allows the membrane to be viewed as a low density, low capacity cation exchanger, with preferential extraction of K^+ from solution occurring because of the presence of valinomycin in the membrane. Donnan exclusion ensures that co-ions, in this case hydrophilic anions in the bathing solution, are not admitted into the membrane. The K^+ -selective membranes under consideration are therefore described as being permselective for cations, in reference to their ability to extract cations from solution while almost totally excluding hydrophilic anions.

The potential response of K^+ -selective liquid membrane electrodes has been shown to be adversely affected by a number of interfering species which are generally anionic and quite oil-soluble, or lipophilic. For instance, the presence of lipophilic anionic components in undiluted urine has been cited as the reason for K^+ concentrations being underestimated in this medium when liquid membrane based ISE's are employed for the analysis [6,7]. It has also been observed that the potentiometric response of K^+ -selective electrodes is subject to interference when measurements are made in test solutions of potassium salts of such lipophilic anions as thiocyanate (SCN^-) and picrate [5,8]. This interference manifests itself as a loss of membrane selectivity for K^+ . Nernstian response to K^+ is obtained only at the lowest bathing concentrations, with sub-Nernstian slopes being observed as salt activities increase. In some cases, this sub-Nernstian behaviour culminates in the potential response curve exhibiting a maximum, followed by a region of negative slope at the highest salt activities due to the electrode responding to the anion rather than to K^+ . This interference phenomenon is typically observed when ion exchangers undergo a process known as Donnan exclusion failure, and co-ions (anions in this case) as well as counterions are

admitted into the membrane [5]. A loss of membrane selectivity for K^+ in the presence of lipophilic anionic species can therefore be linked to a loss of membrane permselectivity for cations.

The effect of Donnan exclusion on the potential difference across a simple fixed site membrane was considered in detail in a theoretical treatment by Hills et al. [9]. Buck et al. extended this work to derive a theory of Donnan exclusion failure of low density, low capacity membranes containing neutral carriers, in which the neutral carrier concentration far outweighed the membrane site density [5]. The K^+ -selective liquid membranes under discussion satisfy this condition, as valinomycin is present at a concentration of approximately 10 mM, in contrast to the 0.05 to 0.6 mM concentration of sites. This theory predicts that interference of the type described above will be seen in the response of a K^+ -selective ISE in the presence of a lipophilic anion when the extracted anion concentration in the membrane exceeds the membrane site concentration. Furthermore, the aqueous salt activity at which this interference is demonstrated by the appearance of a maximum in the potentiometric response will be directly dependent on membrane site density, while showing a reciprocal dependence on the extraction coefficient of the salt into the membrane.

In the preceding chapter, it was shown that the presence of benzoate (Bz^-) at any pH in the bathing solution did not affect the potential response of a K^+ -sensitive membrane-coated silicon electrode, once the insulator surface of the electrode had been rendered inert to acid-base chemistry through the introduction of a Ag/AgCl layer between the insulator and the membrane. Yet, it was observed that both benzoic acid and benzoate can permeate the membrane. Direct evidence of the ingress of benzoic acid was obtained both through UV spectroscopic measurements and AC impedance analysis.

Though benzoate does not enter the membrane to a large enough extent to be determined spectroscopically, AC impedance analysis does indicate a decrease in membrane resistance if benzoate is one of the components in the bathing solution. In order to achieve a better characterization of membrane permeation by neutral species and non-lipophilic anions, a further study of this phenomenon was carried out using benzoic acid and benzoate as the permeating species of primary interest. Results of experiments, in which the effect of the lipophilic anion, ClO_4^- , on membrane properties was considered, are also presented. AC impedance analysis was chosen as the investigative technique, as earlier studies had proven it to be a sensitive method to monitor membrane permeability.

4.2 EXPERIMENTAL

The membranes typically contained 33 % (w/w) poly(vinylchloride) (PVC) (Polysciences, chromatographic grade), 66 % (w/w) dioctyladipate (DOA) (Fluka), and about 1 % valinomycin (Sigma). Potassium tetraphenylborate (KTPB) was also often included in the membrane at the 0.01 % (w/w) level. Membranes containing all four components will be referred to hereafter as "normal" membranes. KTPB was prepared according to a gravimetric method outlined in reference [11]. Membranes were cast following the method outlined in Chapter 3.

As will be described, bulk membrane resistances of normal membranes containing known amounts of potassium benzoate (KBz), sodium perchlorate (NaClO_4) and benzoic acid were measured. KBz was prepared by combining 1.6 g of benzoic acid (Terochem) and 0.8 g of KOH (Anachemia) in about 20 mL of ethanol (95 %), and filtering off the resulting KBz precipitate. The

product yield was about 1.7 g. Further purification was carried out through recrystallization from ethanol. Benzoic acid was recrystallized from cold water (doubly distilled from alkaline KMnO_4) before use. NaClO_4 (G. Frederick Smith Chemical Company, Columbus, Ohio) was used without further purification. Stock THF solutions of each compound were made by dissolving about 15 to 30 mg in 10 mL of distilled THF. For the KBz/THF stock solution, it was necessary to dissolve KBz in about 5 mL of methanol before diluting to the full 10 mL volume with THF. Subsequent THF solutions of lesser concentrations were prepared by dilution with distilled THF.

Series of normal membranes containing each compound were cast in groups of four, with one membrane in each series cast without added compound serving to act as a control. To ensure that the normal membrane matrix was consistent over a series of membranes, a larger volume of membrane solution was prepared, and 2 to 3 mL portions of this delivered to each of four 10 mL beakers. Varying aliquots of THF solutions of the compound were then added to each of three beakers, and the total volume of membrane solution in all four beakers was brought to about 5 mL using distilled THF. After allowing to stir for 30 minutes or more, the mixtures were poured into PTFE moulds and allowed to set, as described above. After the curing process, membranes were weighed to the nearest 0.1 mg. To account for compound-containing membrane solution which inevitably remained behind in the beaker after casting, the 10 mL beakers used were weighed dry and again 24 hours after casting. The mass of "leftover" membrane thus determined was added to the mass of the corresponding cast membrane. Membrane concentrations of added compound could then be evaluated, since both the mass of compound and the total mass of membrane to which that compound was added were accurately known.

Each ISE was constructed using a method outlined in reference [12]. A segment of glass tubing (4.5 mm O.D.) approximately 3 cm in length was pushed to a depth of about 3 mm into one end of a ~3 cm length of PVC tubing (6 mm O.D., 4.5 mm I.D.). A 6 mm diameter disc, cut from either a normal membrane or a PVC/DOA/valinomycin membrane, was mounted onto the other end of the PVC tubing, after this end had been allowed to moisten and swell for about 15 seconds in THF. To ensure that the disc was properly sealed to the PVC tubing, the outer edge of the disc was pressed down onto the tubing while it was still moist. After allowing the seal to dry, the electrode was filled with 0.1 M KCl internal solution, and a chloridized Ag wire was immersed into the solution to act as the internal reference. One end of this wire was pushed through a small septum, which was subsequently wired down over the end of the glass tubing to seal the electrode and prevent evaporation of the internal solution.

Potentiometric or open-circuit measurements of K⁺-ISE's were made using an Orion 701 A ion-selective electrode meter, with a sodium chloride saturated calomel electrode (SSCE) as reference electrode. Test solutions contained KCl (BDH), KBz, or KClO₄ at concentrations ranging from 10⁻⁴ M to 10⁻¹ M, buffered to an ionic strength of 0.1 by NaCl (BDH).

Impedance measurements of membranes were made with the membrane incorporated into an ISE or mounted in a specially designed cell. A diagram of the cell is given in Figure 4.1. This cell, made from PTFE, consists of two sections of equal length, each with a cylindrical central bore 0.6 cm in diameter. Three long narrow threaded rods are embedded at equal intervals in the inner face of one cell section. The other section has holes drilled lengthwise from one end to the other, at positions corresponding to the placement of the rods. A portion of membrane may be mounted by

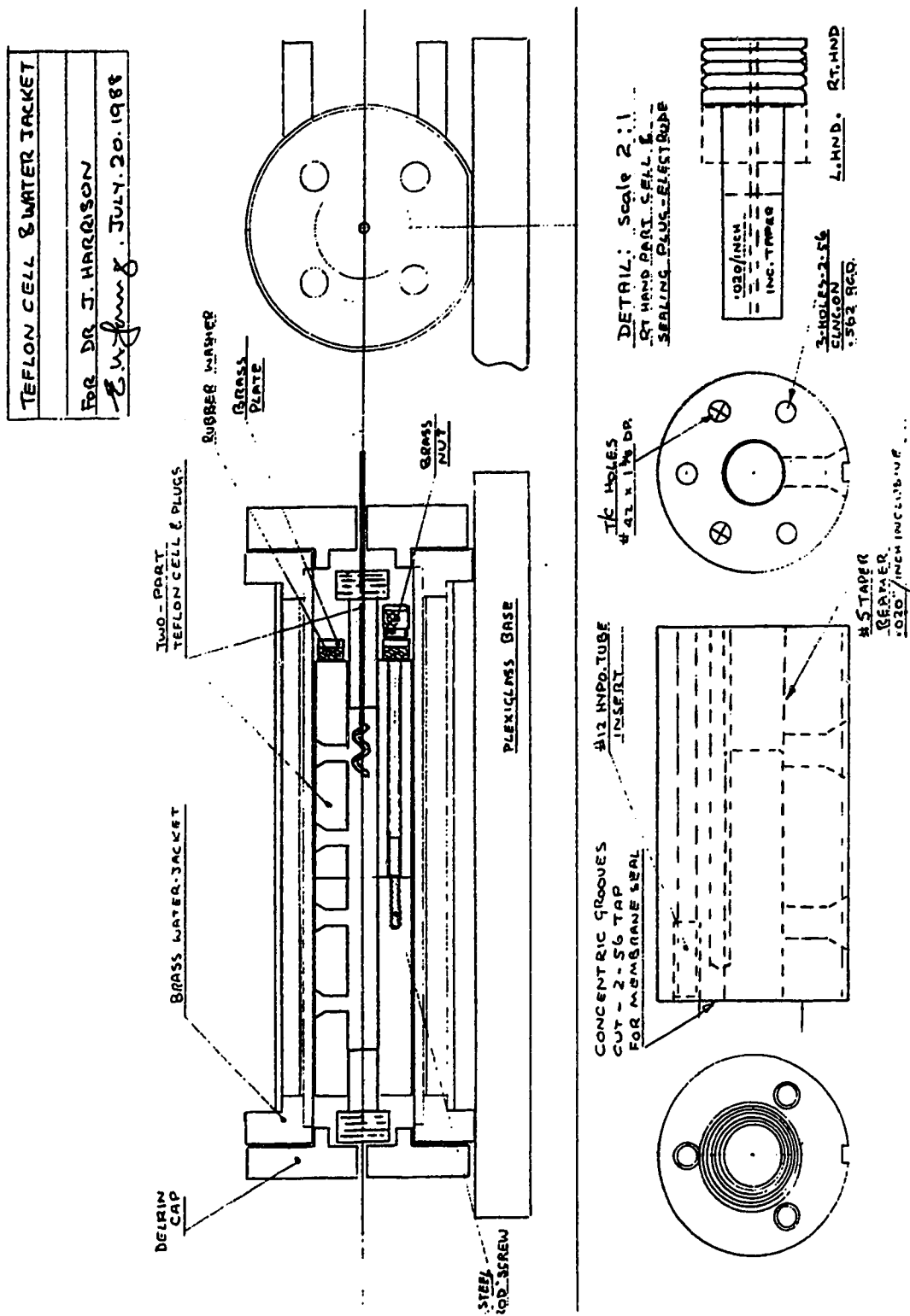


FIGURE 4.1 Side and end views of one half of the cell used in impedance measurements of free-standing membranes. The cell is shown in the water jacket in the top half of the diagram

placing it over the inner face of one section, and then fitting the section with holes onto the threaded rods of the other section, and pushing the two sections together. A thick rubber disc is then pushed over the ends of the rods, after which the cell is clamped together by screwing small nuts onto the threaded end of each rod. To ensure a proper membrane seal in the cell, concentric grooves are machined into the inner surface of one section, so that the membrane is prevented from sliding out of position when the cell is assembled. Two tapered Teflon plugs serve to seal the outer ends of the cell. Two chloridized Ag wires, wound at one end into corkscrew shapes, are pushed through these plugs, and act as the electrodes in this two-electrode system. A small diameter hole in the top of each section allowed for solution overflow from the cell when it was being filled. In this cell, the effective surface area of the membrane exposed to solution is 0.283 cm^2 . The temperature was maintained at $25.0 \text{ }^\circ\text{C}$ by fitting the cell into a brass water jacket, as shown in the top half of Figure 4.1. Water at the desired temperature was circulated through the outer compartment of this jacket from a Lauda K4R water bath (Westbury, N.Y.). Cells were placed in the jacket 30 minutes prior to a measurement, in order to allow them to attain a constant temperature. Monitoring of cell temperature was made possible through use of a thermocouple, positioned in a $\sim 2.5 \text{ cm}$ long shaft of narrow diameter, drilled into the cell wall along its length.

For measurements employing ISE's, the electrochemical cell had a standard three-electrode configuration, with a saturated calomel electrode contained in a double junction filled with $0.1 \text{ M NH}_4\text{Cl}$ serving as the reference electrode.

Impedance analyses of membranes were made possible using the experimental set-up shown in Figure 4.2. Potentiostatic control and current

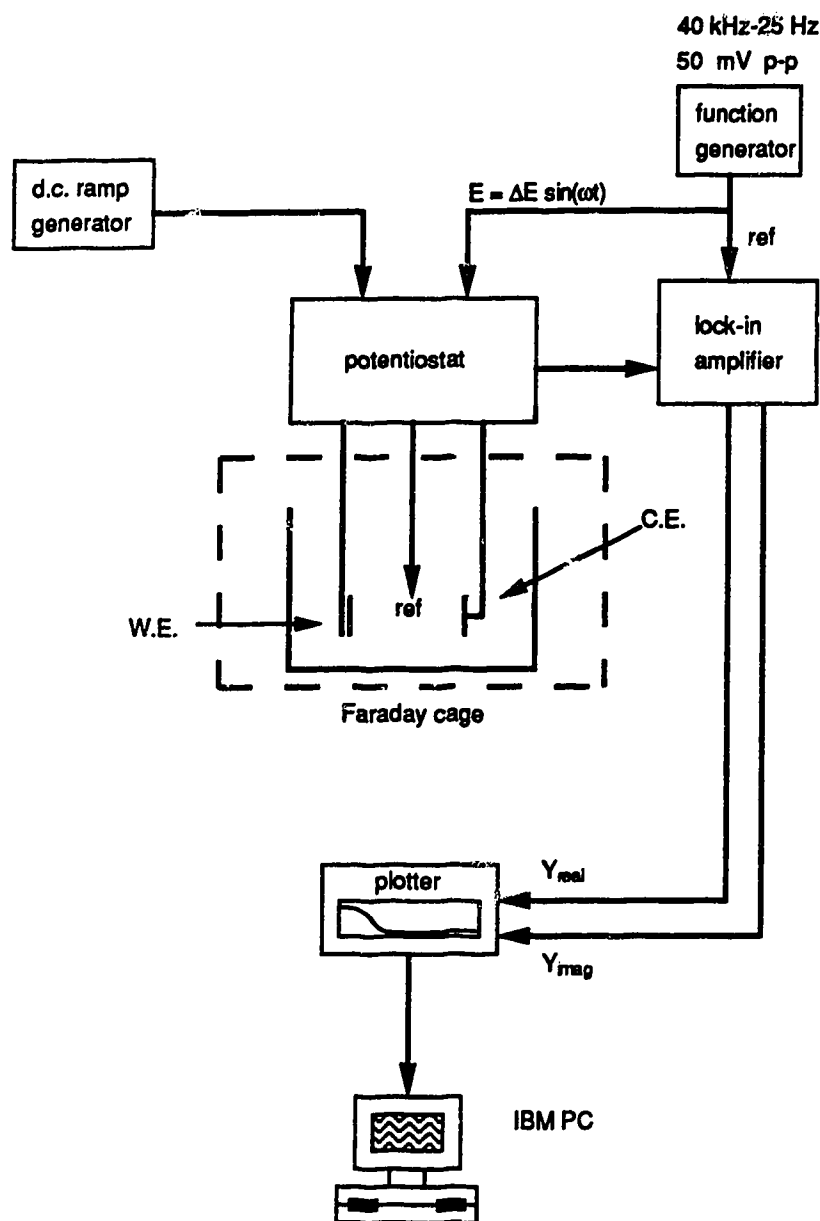


FIGURE 4.2 Experimental set-up used in impedance measurements. Though this is essentially the same as that described in Chapter 2, the source of the applied DC potential has been changed, as has the function generator used, as described in the text. This scheme indicates the other significant change which has been made, namely that the AC input signal had an amplitude of 50 mV p-p rather than 10 mV p-p for all the measurements carried out in this study.

measurement for an AC experiment were provided by an Amel 521 potentiostat (Amel, Milan, Italy), modified to allow two external inputs to the summing point of the potentiostat control circuit. The potential applied to the MIS electrode was the sum of a DC potential and a small amplitude AC signal, described by $E_{AC} = E_0 \sin \omega t$, E_0 being about 25 mV in these studies. A Hokuto Denko function generator was the source of the DC potential. A Wavetek Model 23 function generator provided the 50 mV peak-to-peak sine wave. The resulting current flowing in the cell was fed into a PAR Model 5204 lock-in analyzer, which separated this current signal into in-phase (real) and out-of-phase (imaginary) components, with respect to the phase of the applied oscillation. The lock-in analyzer output signal was monitored with an HP 7090 A digital recorder/plotter, with the digitized signal being subsequently transferred to an IBM PC for data analysis.

Impedance measurements were made in solutions of constant ionic strength either 0.1 M in NaCl or 0.1 M in trisodium citrate buffer adjusted with HCl or NaOH. The precision associated with measured bulk membrane resistances was $\pm 2\%$.

4.3 RESULTS AND DISCUSSION

The potentiometric response of electrodes made from membranes cast with and without KTPB was measured in solutions containing varying concentrations of KCl, KBz, and KClO₄ maintained at a constant ionic strength of 0.1 by addition of NaCl. Results of these experiments are presented in Table 4.1. All electrodes responded satisfactorily to KCl, giving E(mV) vs

TABLE 4.1: Results of potentiometric response measurements in KCl, KBz and KClO₄ solutions, maintained at a μ of 0.1.

Solutions		KCl		KBz		KClO ₄	
Elec.	%KTPB	Slope (mV)	Intcpt (mV)	Slope (mV)	Intcpt (mV)	Slope (mV)	Intcpt (mV)
D1 ^{a)}	0.01 %	56.5 ± .5	85.2 ± 1.3	56.9 ± .4	83.7 ± 1.3	53.9 ± .5	72.0 ± 2.2
D2 ^{a)}	0.01 %	56.0 ± .1	83.7 ± 0.4	56.5 ± .0	81.1 ± 0.1	52.7 ± .9	65.3 ± 3.1
V1 ^{b)}	0.01 %	57.0 ± .5	88.8 ± 1.3	56.2 ± .3	86.3 ± 0.8	—	—
V2 ^{b)}	0.01 %	57.1 ± .6	86.7 ± 1.7	56.0 ± .4	83.0 ± 1.0	—	—
1 ^{c)}	0 %	57.1 ± .4	87.2 ± 1.1	57.0 ± .2	86.3 ± 0.6	—	—
2 ^{c)}	0%	57.4 ± .6	86.0 ± 1.5	57.2 ± .3	85.0 ± 0.9	—	—

- a) Electrodes D1 and D2 were fresh (new) when these experiments were carried out; they had been made two days before, and were conditioned briefly in 0.1 M KCl before these measurements were made.
- b) Electrodes V1 and V2 were stored for 40 days in 1 mM KCl ($\mu = 0.1$ (NaCl)) before these experiments; they had been exposed to benzoate once before, during an impedance measurement two weeks prior to this set of measurements.
- c) Electrodes 1 and 2 had been soaked for two days beforehand in 1 mM KCl ($\mu = 0.1$ (NaCl))

$\log[K^+]$ plots that were linear over the 10^{-4} M to 10^{-1} M range, with near Nernstian slopes of 56.0 to 57.5 mV. Four of the electrodes containing KTPB, namely D1, D2, V1, and V2, were then tested for their response to KBz. Electrodes D1 and D2, which were new and had been conditioned a few hours in 0.1 M KCl, responded equally well to KBz as to KCl. The slightly higher slopes recorded for KBz, while not significantly different from those for KCl, may be due to the formation of a small junction potential at the saturated NaCl calomel electrode, as the mobility of benzoate in aqueous solutions is about half that of Cl^- [13]. Electrodes V1 and V2 produce slightly lower slopes when exposed to KBz, which indicates that the electrodes are in the early stages of an aging process that results in a loss of permselectivity, and have started to develop a susceptibility to the presence of anions whose extraction into the membrane may be slightly more favoured than Cl^- . However, the effect is not a strong one, considering that these electrodes had been soaked in 1 mM KCl ($\mu=0.1$) for a month and a half, and had previously been briefly exposed to benzoate-containing solutions.

Measurements in KBz were also made using electrodes constructed from membranes containing no KTPB. It has been noted that the addition of small amounts of this lipophilic salt leads to improved electrode response, through reduction of anionic interferences and membrane resistance [14,15]. It was thought that the deliberate exclusion of KTPB from the membrane might result in benzoate having a noticeable effect on electrode response, but this was not the case for electrodes 1 and 2. Studies in the literature [1] do report an interference by benzoate on the potential response of a K^+ -sensitive electrode, with the expected decrease in observed slope. However, the commercially available ORION 92-19 electrode, which is a neutral carrier electrode containing valinomycin dissolved in a nitro-type plasticizer, was used for

these measurements. The higher dielectric constant of such a plasticizer as compared to the long chain ester used in our membranes would account for the observed response of the ORION electrode to benzoate, as benzoate would be more easily solubilized in this matrix. The presence of benzoate in solution does not pose an interference problem for the type of membrane considered in this study.

The effect of exposing a KTPB-containing membrane electrode to KClO_4 is more remarkable, as shown for electrodes D1 and D2 in both Table 4.1 and Figure 4.3. Perchlorate in the bathing solution causes a compression of the region over which the potential response curve is linear, so that it covers a concentration range of only 10^{-4} to 10^{-3} M KClO_4 . A loss of membrane selectivity for K^+ is indicated even at these low concentrations, since the regions of linear response have slopes which are less than the expected 57 to 59 mV per decade change in K^+ concentration. At higher ClO_4^- concentrations, response deviates substantially from ideal Nernstian behaviour as it appears to level off. In fact, if KClO_4 were soluble at aqueous concentrations greater than 10^{-2} M, the response of these electrodes would be determined by ClO_4^- , not K^+ , and the $E(\text{mV})$ vs $\log[\text{K}^+]$ curves would in all likelihood show a maximum at about 10^{-2} M with a subsequent region of negative Nernstian response to ClO_4^- , similar to that reported for KSCN [5]. The manner in which ClO_4^- interferes with the potential response of electrodes D1 and D2 is consistent with the occurrence of Donnan exclusion failure in liquid membranes upon exposure to a hydrophobic anionic interferent. Observation of this phenomenon infers violation of membrane permselectivity resulting in the admission of ClO_4^- into the membrane. Establishment of a distinct concentration distribution of ClO_4^- in the membrane capable of partaking in ion diffusion processes is indicated.

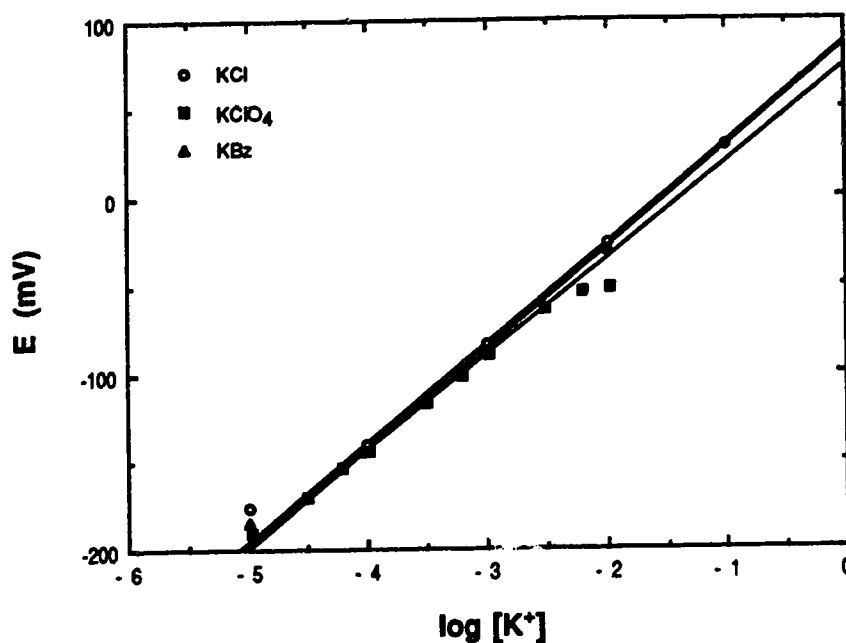


FIGURE 4.3 Potentiometric response of ISE D-1 as a function of K^+ concentration in solutions containing KCl, KBz, and $KClO_4$. This electrode is based on a PVC/DOA/KTPB/valinomycin membrane, and was briefly conditioned in 0.1 M KCl before these measurements were made. Curves for KCl and KBz were fitted over the 10^{-4} to 10^{-1} M K^+ range, and were found to have slopes of 56.3 and 56.9 mV, respectively. The curve for $KClO_4$ was fitted over the 10^{-4} M to 10^{-3} M range, and found to have a slightly reduced slope of 53.9 mV. Data for $KClO_4$ was not obtained at concentrations exceeding 10^{-2} M, as $KClO_4$ is not soluble in water at concentrations greater than 10^{-2} M.

That ClO_4^- affects electrode response even at submillimolar concentrations is apparent from Figure 4.4. This figure shows how the potentials of electrodes D1, D2, (from Table 4.1) and D3 change as NaClO_4 is gradually added to a 0.01 M KCl ($\mu=0.1$ (NaCl)) solution. The solution was allowed to stir for one minute after each addition of NaClO_4 -containing solution, followed by a one minute wait to allow stabilization of electrode readings before recording electrode potentials. It was found that even at a $[\text{NaClO}_4]=1 \times 10^{-5}$ M, following the first addition of NaClO_4 , the measured response showed a decrease, albeit a slight one. Subsequent additions of NaClO_4 served only to cause a further decrease in measured potential. For electrodes D1 and D2, which had been bathed in solutions of varying KClO_4 concentrations once before, the rate of potential change with $[\text{NaClO}_4]$ was greater than for the fresh electrode, D3. Exposure of electrodes to ClO_4^- a first time appears to condition them in some way, so that they respond more readily to the presence of ClO_4^- in following measurements. A similar phenomenon is observed for anion-selective ion exchange electrodes, which are typically loaded with salts in which the cation is a large lipophilic ion, such as a tetraalkylammonium ion [16]. These electrodes require several hours of use in aqueous media before their response to anions may be considered quantitative. While the electrodes under consideration in this study are not meant to respond to anions, it appears that the mechanism governing the observed effect of increased interference with increased exposure is perhaps related to the conditioning phenomenon noted for anion-sensitive electrodes.

In the potentiometric measurements above, Donnan exclusion failure manifests itself in the presence of KClO_4 for electrodes based on PVC/DOA/KTPB/valinomycin membranes. On the other hand, this

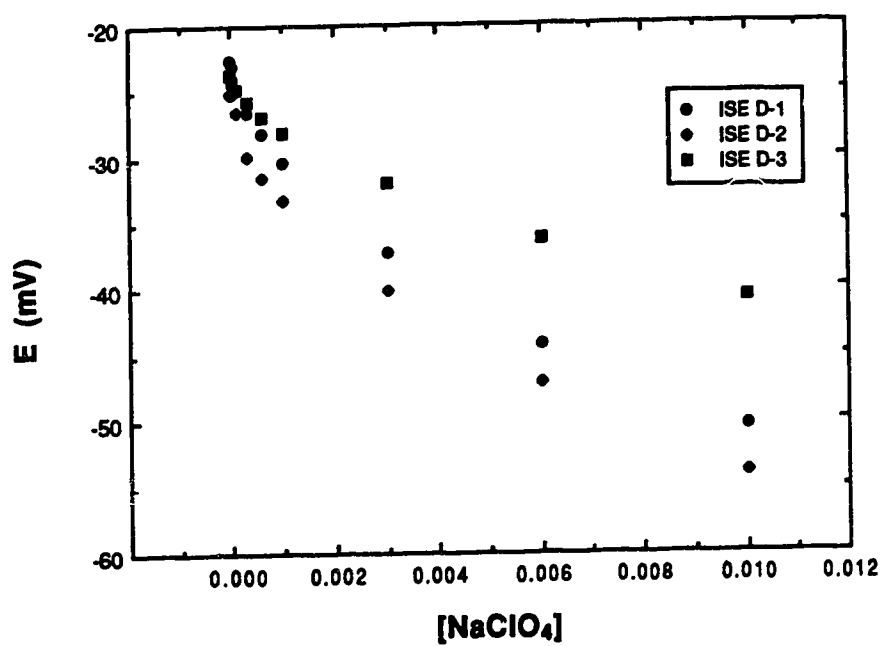


FIGURE 4.4 Effect of added ClO_4^- on the potentiometric response of ISE's D1, D2, and D3 in 0.01 M KCl at a constant μ of 0.1 (NaCl). All three electrodes were prepared from the same membrane. Electrodes D1 and D2 had been exposed once before to ClO_4^- -containing solutions.

interference phenomenon is not observed when K^+ determinations are carried out in KBz-containing solutions, even if the membranes on which the ISE's are based contain no KTPB to minimize anion interferences on electrode response. These experiments would suggest that membrane permselectivity is maintained in the presence of benzoate. However, AC impedance studies of K^+ -selective membrane coated silicon electrodes, reported in Chapter 3, showed that benzoate is capable of permeating the membrane both in its anionic and neutral (benzoic acid) form. This conclusion was drawn from the observation that bulk resistances (R_g) of the membrane coating dropped when these electrodes were exposed to solutions containing benzoate or benzoic acid. In order to better understand why changes in membrane properties wrought by benzoate or benzoic acid do not cause the interference to electrode potential response that ClO_4^- does, it was decided to examine more closely the response of the membrane itself to ClO_4^- and to benzoate at pH's of 1 and 8.6 to 9. AC impedance analysis was the method of choice for this investigation, as it is clear that the measurement of changes in bulk membrane properties in the presence of the various species of interest provides a direct and sensitive means of monitoring changing membrane permeability.

Figure 4.5 shows the results of impedance measurements conducted on a portion of normal membrane mounted and bathed symmetrically in a specially designed cell, described in the experimental section. This Nyquist plot illustrates the effect that changing the bathing solution from 0.1 mM KCl ($\mu=0.1$ (NaCl)) to 0.1 mM $KClO_4$ ($\mu=0.1$ (NaCl)) has on the R_g of a normal membrane, as measured from the intersection of each semicircle with the real axis. The result is dramatic : R_g drops from a value of 5.45 $M\Omega$ in 1 mM KCl ($\mu = 0.1$) to a value of 3.47 $M\Omega$ after being symmetrically bathed with the

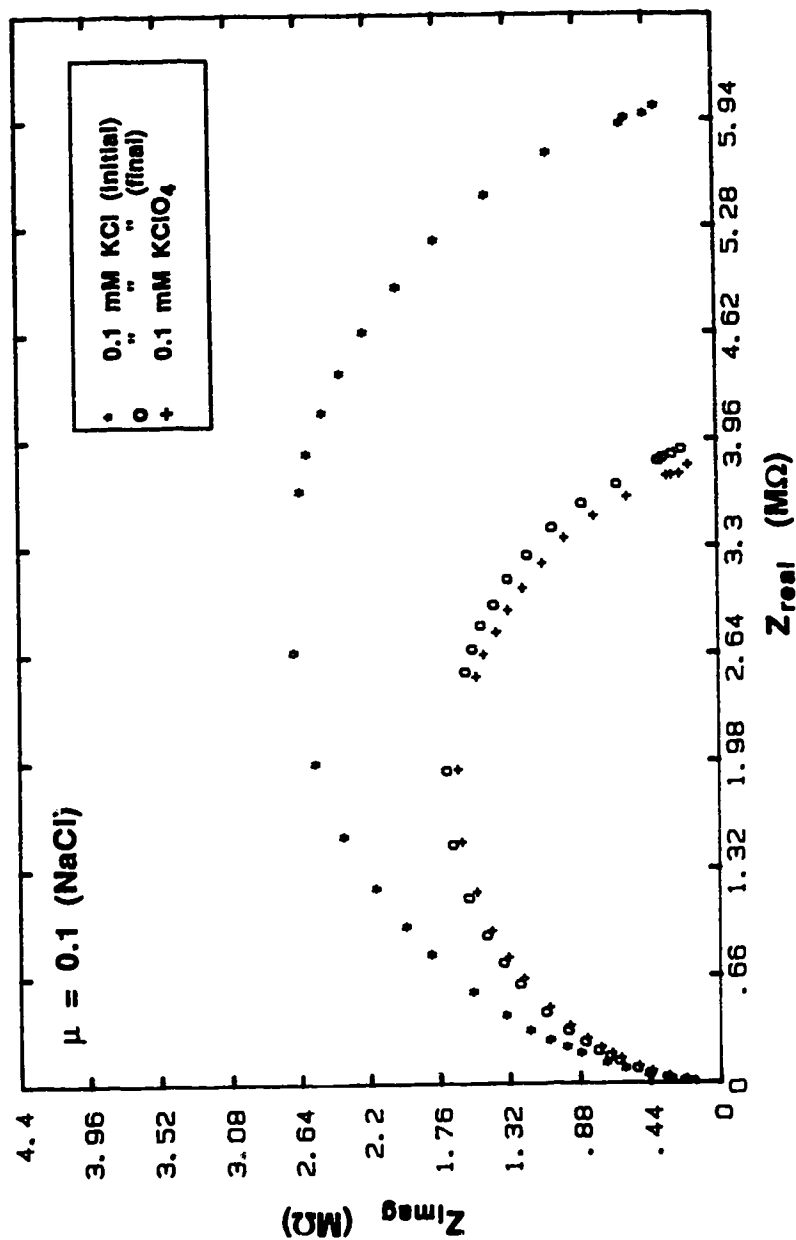


FIGURE 4.5 Nyquist plot for a portion of normal membrane over the frequency range 50 Hz to 40 kHz, showing the effect of added ClO_4^- on R_g . A 35% reduction is observed from the initial curve measured in 10^{-4} M KCl ($\mu = 0.1$ (NaCl)) (*) to that obtained after one hour in 10^{-4} M KClO_4 ($\mu = 0.1$ (NaCl)) (+). Soaking the membrane for 24 hours in 10^{-4} M KCl ($\mu = 0.1$ (NaCl)) does not restore the membrane's original resistance (o).

KClO₄ solution for an hour. This 35 % decrease in R_g can only be due to extraction of ClO₄⁻ into the membrane. The impedance result reported here in the presence of the lipophilic ClO₄⁻ is in keeping with impedance results reported for membranes exposed to the very lipophilic SCN⁻ ion [5], and is direct evidence for failure of Donnan exclusion caused by ClO₄⁻. The membrane showed no signs of recovery to its initial R_g after soaking overnight in 0.1 mM KCl ($\mu=0.1$ (NaCl)). The extraction of ClO₄⁻ into the membrane, presumably along with additional counterions, mostly K⁺, for charge neutrality, appears to be quite irreversible.

Impedance measurements studying the effect of exposing membranes to benzoate solutions at either pH 1 or pH 8.6 to 9 were made as described in the Experimental section, with membranes mounted in a cell or incorporated into a conventional home-made ISE. The benzoate solution concentration used in all cases was 0.01 M. Since the acid dissociation constant, K_a, of benzoic acid is 6.14×10^{-5} , benzoic acid will exist in its neutral form in solution at pH 1, and in its anionic form at pH 9. The membranes studied had not been previously exposed to solutions containing benzoic acid at any pH. The results are presented in Table 4.2, where % ΔR_g refers to the change in R_g in going from a solution at a particular pH to a solution containing 0.01 M benzoate at the same pH. The resistance values used to calculate this parameter, which are also reported in Table 4.2, were obtained only after the membrane had had an hour to equilibrate with the bathing solutions in question. R_g's measured for ISE membranes are generally two to three times larger than those measured for cell-mounted membranes. This is because the effective surface area of an ISE membrane exposed to solution is a factor of two to three times smaller than that of membranes studied in cells. A negative value for % ΔR_g indicates a decrease in membrane resistance.

TABLE 4.2: Bulk resistances, R_g , of membranes before and after a one hour exposure to a 0.01 M benzoate-containing solution, for membranes with and without KTPB

4.2(A) PVC/DOA/KTPB/valinomycin

Mem	Exp'tal Configuration	pH	R_g a) (0 M Bz^-) $M\Omega$	R_g b) (.01 M Bz^-) $M\Omega$	% ΔR_g c)	Conditioning
X2	cell	9.0	6.31	6.17	-2.3	-soaked 16 hrs bef. exp't in 1 mM KCl ($\mu=0.1$)
X3	"	"	6.76	6.66	-1.5	-soaked 3 hrs bef. exp't in 1 mM KCl ($\mu=0.1$)
V1	"	"	8.13	7.88	-3.5	-soaked 1 hr bef. exp't in 1 mM KCl ($\mu=0.1$)
V2	"	"	6.65	6.42	-1.3	- " " " "
V3	"	"	6.43	6.35	-3.1	- " " " "
Average % $\Delta R_g = -2.3 \% \pm 0.97 \%$						

a) solutions were 1 mM in KCl and 0.1 M in trisodium citrate buffer adjusted with HCl or NaOH to obtain the desired pH

b) solutions are the same as in a), but with 0.01 M sodium benzoate added

c) % $\Delta R_g = (R_g(10 \text{ mM } Bz^-) - R_g(0 \text{ mM } Bz^-)) / R_g(0 \text{ mM } Bz^-) \times 100$

4.2(B) PVC/DOA/valinomycin

Mem	Exp'tal Configuration	pH	R _g a) (0 M Bz ⁻) MΩ	R _g b) (.01 M Bz ⁻) MΩ	% ΔR _g c)	Conditioning
2	cell	9.0	29.1	27.9	-3.8	-soaked 15 hrs in 1 mM KCl (μ=0.1(NaCl))
1A	"	"	44.0	40.9	-7.3	-soaked 14 hrs in 1 mM KCl (μ=0.1)
1B	"	"	41.3	35.9	-12.8	-soaked 22 hrs in 1 mM KCl (μ=0.1)
Average % ΔR _g = -7.9 % ± 4.6 %						
1	cell	1.0	32.6	26.6	-17.3	-soaked 21 hrs in 1 mM KCl (μ=0.1(NaCl))
2	"	1.0	34.7	31.6	-9.2	-soaked 96 hrs in 1 mM KCl (μ=0.1)
S1	"	1.0	5.91	5.27	-10.3	-soaked 1 hr in 1 mM KCl (μ=0.1)
Average % ΔR _g = -12 % ± 4.4 %						

- a) solutions were 1 mM in KCl and 0.1 M in trisodium citrate buffer adjusted with HCl or NaOH to obtain the desired pH
- b) solutions are the same as in a), but with 0.01 M sodium benzoate added
- c) $\% \Delta R_g = (R_g(10 \text{ mM Bz}^-) - R_g(0 \text{ mM Bz}^-)) / R_g(0 \text{ mM Bz}^-) \times 100$

The values in Table 4.2(A) refer to results obtained for membranes containing 0.01 % (w/w) KTPB. Experiments carried out at pH's ranging from 8.6 to 9 yield an average % ΔR_g of -2.3 % for membranes mounted in a cell. At pH 1, this value is higher at -7.0 %, for experiments carried out using membranes both mounted in cells and incorporated into ISE's. The relatively large range of % ΔR_g 's measured, particularly at pH 1, reflects one of the problems associated with studying membranes of this type, that of membrane inhomogeneity. Other authors have encountered and commented on this as well [5,7]. Membrane characteristics appear to be very sensitive to the source and purity of their components. Buck has noted the presence of hydrophilic regions within given membranes which permit enhanced water uptake, and appear white and cloudy when immersed in solution because of water droplet formation; we have observed this phenomenon as well. Other groups in the field of plastics engineering describe the existence of "insoluble gels" within membranes of this type [17]. Often visible to the naked eye, these gels look like colourless strands, and are due to the PVC not being completely dissolved by the plasticizer. In any case, results for this type of experiment are often susceptible to what portion of the membrane has been sampled, and vary also from one membrane to the next. However, the trend is established: membrane resistances do decrease in the presence of benzoate at both pH's. At a pH of 9, the decrease in membrane resistance (and corresponding increase in membrane conductivity) is due to benzoate entering the membrane presumably along with an equivalent number of counterions to maintain electroneutrality. At pH 1 benzoic acid enters the membrane in its neutral form, as this is the only species in solution. Given the sizeable % ΔR_g at pH 1, it appears that once benzoic acid resides in the membrane, it undergoes a further charge-carrier producing process that results in increased membrane

conductivity. This process may be one of acid dissociation or of the neutral acid acting as some sort of complexing agent for K^+ or other cations.

Table 4.2(B) presents results for membranes cast without KTPB. At pH 9 the average % ΔR_g is -7.9 % which represents a significantly larger decrease in R_g than that observed for the so-called normal membranes, and is indicative of an increased benzoate concentration within the membrane. This means that the entry of benzoate into the membrane is made more facile in the absence of KTPB. It has been suggested [14,15] that incorporation of a salt like KTPB into the membrane leads to reduction of anionic interferences on potential measurements through introduction of additional negative sites, which serve to increase the membrane's ability to keep out anions from solution through more effective Donnan exclusion. The experimental results at pH 9 bear out this hypothesis, as they provide direct evidence that the presence of KTPB does curtail extraction of benzoate into the membrane phase.

At pH 1, the average % ΔR_g for membranes without KTPB is -12 %, which is slightly higher than that observed for normal membranes. However, given the range of results obtained for both types of membranes, it cannot be said that the presence of KTPB has any significant influence on the membrane's ability to exclude neutral species. This is consistent with permeation of the membrane by a neutral species being governed solely by the distribution of that species between the aqueous and membrane phases. The membrane's permselective nature, and the factors affecting it, appear not to exert any influence on this distribution, in contrast to the situation where distribution of an anionic species between the phases is of concern.

The length of time membranes were conditioned in 1 mM KCl ($\mu=0.1$ (NaCl)) before an experiment varied substantially as shown in Table 4.2, the

longest conditioning period having been 96 hours for membrane 2 before an experiment at pH 9 as indicated in Table 4.2(B). It has been shown that prolonged exposure of KTPB-containing membranes to NaCl solutions does result in loss of membrane permselectivity, probably due to TPB⁻ leaching out into the solution [18]. However, no such loss due to continual soaking in KCl/NaCl solutions over the period of a few days is indicated here, as the % ΔR_g 's evaluated do not imply that the amount of benzoate entering the membrane increases with the length of the conditioning time.

In order to determine the amount of each species required to produce the % ΔR_g values recorded in the impedance experiments above, several series of normal membranes containing known amounts of NaClO₄, KBz, and benzoic acid were cast, and their R_g 's measured after soaking in 1 mM KCl ($\mu=0.1$ (NaCl)) for an hour. The % ΔR_g values were calculated with respect to R_g values obtained for control membranes cast in each series. The resulting calibration curves of % ΔR_g vs concentration of additive are presented in Figures 4.6, 4.7 and 4.8.

It is apparent from Figure 4.6 that very little KBz need enter a normal membrane to cause the median 2.31 % decrease in R_g found for experiments at pH 9. A membrane concentration of less than 5 μM (the lowest standard concentration measured) is estimated, which supports earlier spectroscopic experiments that found the amount of benzoate entering the membrane to be in the sub-millimolar range, below the detection limit of the technique. Membranes lacking KTPB are permeated to a greater extent, to KBz concentrations lying somewhere between 5 μM and 200 μM (0.2 mM), in agreement with the larger % ΔR_g measured for these systems. This estimate, deduced from the calibration curve of Figure 4.6 for KBz in normal

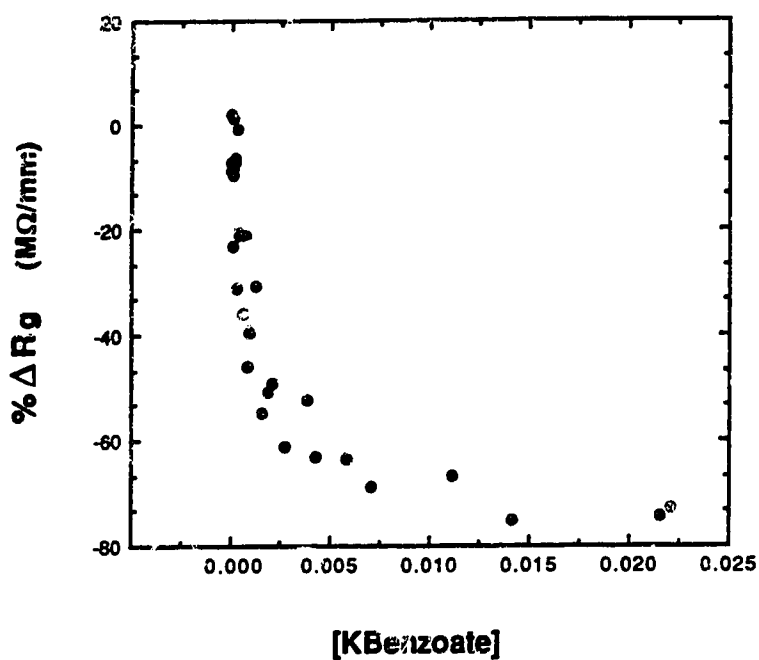


FIGURE 4.6 Calibration curve of % change in R_g ($\% \Delta R_g$) as a function of KBz concentration in a normal membrane matrix. Data for several sets of membranes, each cast from a different membrane stock solution, are presented in this figure. Negative values of $\% \Delta R_g$ indicate a decrease in R_g upon addition of KBz.

membranes, is based on the assumption that the effect of KBz concentration on R_g will not change with KTPB not present in the membrane.

Figure 4.7 is the % ΔR_g curve recorded for normal membranes containing NaClO_4 . As with Figure 4.6 for KBz, % ΔR_g is shown to be a rapidly changing function of concentration at NaClO_4 concentrations up to about 2 mM. This permits the membrane concentration of ClO_4^- responsible for the 35 % decrease in R_g observed in Figure 4.5 to be estimated at about 0.4 mM. Given that the concentration of ClO_4^- in the bathing solution was 0.1 mM initially for this experiment, as compared to an aqueous Bz^- concentration of 10 mM for the impedance experiments discussed above, it is clear that ClO_4^- enters the membrane far more readily than Bz^- .

According to Buck et al. [5] a membrane will exhibit Donnan exclusion failure upon exposure to a salt if the extracted anion concentration of the salt in the membrane exceeds the membrane site density. This hypothesis may be more closely examined using results of the impedance measurements discussed above. As mentioned earlier, the site density of a PVC/plasticizer membrane has been reported to range from 0.05 to 0.6 mM although the extent of ion pair formation is not known [5,19]. The addition of 0.01 % or 0.3 mM KTPB to the membrane will augment this number by about 0.1 mM, since KTPB is not fully dissociated in this matrix [20]. Generally speaking, site densities in normal membranes will not exceed 0.5 mM in most cases. It was found that the ClO_4^- concentration in a normal membrane was 0.4 mM after an hour's exposure to an aqueous KClO_4 concentration of 0.1 mM. In this instance, then, the membrane ClO_4^- concentration should be comparable to the membrane site density. Accordingly, establishment of ClO_4^- membrane concentrations that exceed the site density is expected at solution concentrations greater than 10^{-4} M, so that onset of Donnan exclusion failure

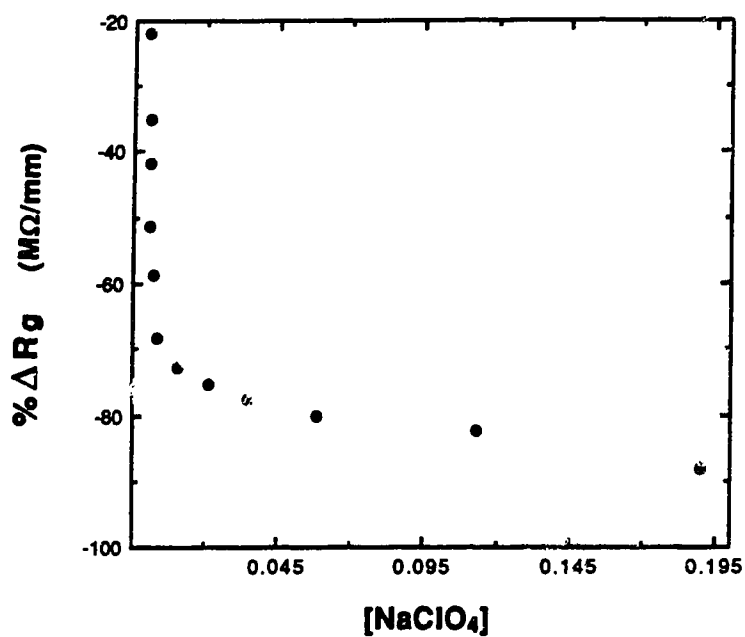


FIGURE 4.7 Calibration curve of % change in R_g ($\% \Delta R_g$) as a function of NaClO_4 concentration in a normal membrane matrix. Data for several sets of membranes, each cast from a different membrane stock solution, are presented in this figure. Negative values of $\% \Delta R_g$ indicate a decrease in R_g upon addition of NaClO_4 . Because of the lipophilicity of ClO_4^- , membrane concentrations of NaClO_4 up to about 0.2 M could be studied, in contrast to KBz .

in the membrane's potential response to K^+ should be observed at these higher concentrations. This in fact was found to be the case experimentally as demonstrated by potentiometric measurements discussed earlier, in which interference to K^+ ISE response was observed at $KClO_4$ concentrations of 10^{-3} and greater. In contrast, impedance analysis showed the Bz^- concentration in a normal membrane to be less than $5 \mu M$ at a corresponding bathing concentration of $0.010 M Bz^-$. Membrane concentrations of this anion therefore fall short of the membrane site density at KBz concentrations of $10^{-4} M$ to $10^{-2} M$. The observation that Bz^- did not interfere with ISE response over this range of concentrations when ISE's based on normal membranes were employed is then in agreement with the hypothesis put forth by Buck et al. [5]. Similarly, the Bz^- concentration found in membranes without KTPB upon exposure to $0.010 M Bz^-$ solution, though greater at $\sim 0.1 mM$ than that generally found in normal membranes, does not exceed the membrane site density. Corresponding potentiometric measurements using ISE's based on these membranes in $10^{-4} M$ to $10^{-2} M KBz$ solutions also showed no interference.

Figure 4.8 shows data for benzoic acid in normal membranes. From this curve, it can be deduced that benzoic acid must permeate the membrane to a concentration of between $8 mM$ and $15 mM$ to produce the $\% \Delta R_g$'s measured in the pH 1 experiments discussed above. Considering that the initial aqueous acid concentration was $10 mM$ in these experiments, it appears that this neutral species can enter the membrane with relative ease. This is born out by UV spectroscopic measurements reported in [2] and discussed in Chapter 3, where it was found that a normal membrane disc had a benzoic acid concentration of $0.11 M$ after 90 hours worth of soaking in a few mL's of $0.010 M$ benzoic acid solution buffered to pH 1.

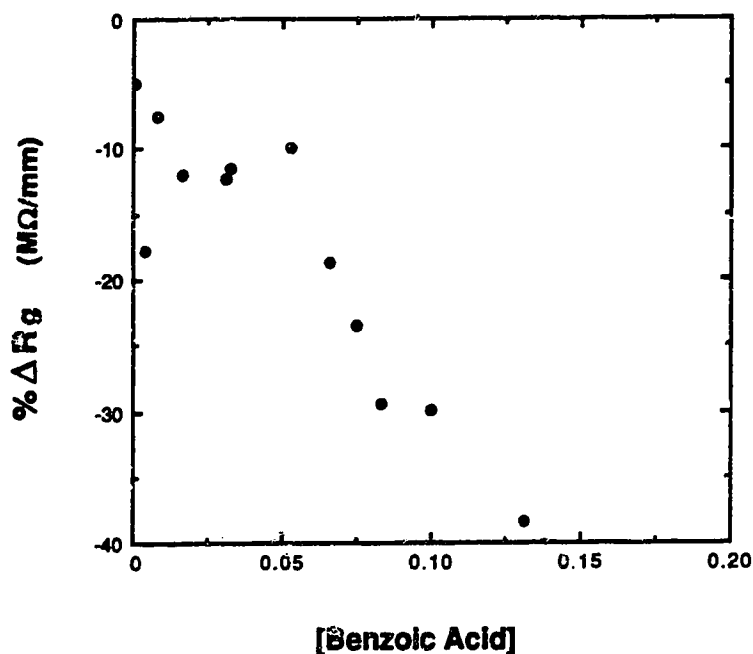


FIGURE 4.8 Calibration curve of % change in R_g ($\% \Delta R_g$) as a function of benzoic acid concentration in a normal membrane matrix. Data for several sets of membranes, each cast from a different membrane stock solution, are presented in this figure. Negative values of $\% \Delta R_g$ indicate a decrease in R_g upon addition of benzoic acid. The range of $\% \Delta R_g$ values measured for benzoic acid is smaller than for either KBz or NaClO_4 , with larger concentrations of acid being required to produce these values. For example, a 0.13 M concentration of benzoic acid produces the same $\% \Delta R_g$ value of about -40 % as does $\sim 10^{-3}$ M KBz.

A comparison of the curves in Figures 4.6 and 4.8 for benzoic acid and KBz leads to the conclusion that benzoic acid must be present in the membrane at much higher concentrations to produce measurable decreases in R_g . Because R_g shows an inverse dependence on membrane ion concentrations, this observation implies that the process by which benzoic acid adds to the charge-carrier concentration in the membrane must be less effective than the ion pair dissociation by which extracted salts contribute to membrane conductivity. No interference on ISE response has been reported when K^+ determinations are made in the presence of benzoic acid, suggesting whatever the charge generation process is, it does not produce enough anions to cause the type of interference that typifies Donnan exclusion failure.

Impedance measurements can provide information on membrane concentrations of a species of interest, even if the concentrations are quite small, as in the case of Bz^- . As a result, these measurements can be usefully employed to discuss species distribution between the aqueous and membrane phases through use of the distribution ratio, D , where

$$D = \frac{\text{solute conc'n in organic phase}}{\text{solute conc'n in aqueous phase}} \quad (1)$$

"Solute conc'n" refers to the total concentration of solute in all its forms in each phase, and disregards various association/dissociation equilibria that the solute may be involved in in either phase. Use of this parameter will allow the relative abilities of benzoic acid, ClO_4^- , and Bz^- to be extracted from the aqueous phase into the membrane phase to be compared more quantitatively.

A second expression for D in terms of the pertinent solute concentrations and volumes may be derived and is given in Equation (2)

$$D = \frac{[\text{sol}]_{\text{mem}} \cdot \text{Vol}_{\text{cell}}}{[\text{sol}]_i \cdot \text{Vol}_{\text{cell}} - [\text{sol}]_{\text{mem}} \cdot \text{Vol}_{\text{mem}}} \quad (2)$$

where $[\text{sol}]_i$ is the initial solute concentration in solution; $[\text{sol}]_{\text{mem}}$ is the solute concentration in the membrane; Vol_{cell} refers to the cell volume; and Vol_{mem} is the membrane volume.

An estimate of the D for ClO_4^- between the membrane and solution can be calculated using a membrane concentration of ClO_4^- estimated from impedance data above, given the following nominal values for cell and membrane parameters: cell volume = 3 mL; cell radius = $r = 0.3$ cm; average membrane thickness = $t = 0.015$ cm; membrane volume = $\pi r^2 t = 4.24 \times 10^{-3}$ mL. Then, from equation (2) and $[\text{ClO}_4^-]_{\text{mem}} = 0.4$ mM, $D \cong 4$. Similarly, for Bz^- extraction into a normal membrane (if $[\text{Bz}^-]_{\text{aq}} = 0.010$ M and $[\text{Bz}^-]_{\text{mem}} = 5 \times 10^{-6}$ M), $D = 5 \times 10^{-4}$. If KTPB is not present in the membrane, this ratio increases to 0.01, for a $[\text{Bz}^-]_{\text{mem}} = 0.1$ mM. These distribution ratios are only estimates of what the actual equilibrium values are, since an hour's exposure to a solution may not be enough for the membrane to be equilibrated with that solution. However, they do provide a useful measure of how much more easily ClO_4^- enters the membrane than Bz^- , and indicate that the extraction of ClO_4^- into the membrane must be governed by a much greater extraction coefficient than that of Bz^- . The ability of an anionic species to permeate the membrane in large part determines whether it will pose an interference problem to ISE response. Given the four order of magnitude difference between the D 's of ClO_4^- and Bz^- for distribution into a normal membrane, it is not surprising that ClO_4^- induces Donnan exclusion failure, whereas Bz^- does not. The benefit to be derived by including KTPB at the 0.3

mM level in the membrane is also obvious, as it leads to a substantial decrease in the amount of Bz^- entering the membrane, as indicated by the 20-fold decrease in D observed for the normal membrane versus the membrane without KTPB.

Using results from the UV spectroscopic measurement reported in [2], a D of 11 is calculated for benzoic acid. The membrane concentration of benzoic acid obtained from UV data was used in place of the value obtained from impedance data because the former result is truly an equilibrium value, having been measured after the membrane had soaked for 90 hours in the benzoic acid-containing solution. Because the pH of solutions with benzoic acid was 1, benzoic acid will have undergone very little dissociation in the aqueous phase. If it is assumed that dissociation of the acid is not a significant process in the low dielectric environment of the membrane, then the D observed for the acid can be regarded as the partition coefficient, P , for the acid between the membrane and solution, where P is in essence D corrected for association and dissociation equilibria. The P for partition of benzoic acid into ethyl benzoate, a less viscous solvent than DOA, has been reported as having a value of 30 [21]. The similar magnitudes of P for benzoic acid partitioning into the membrane and into ethyl benzoate indicate that the membrane's solvent character is determined primarily by the plasticizer, DOA.

4.4 CONCLUSION

The phenomenon which is commonly termed "Donnan exclusion failure" and manifests itself as non-ideal response behaviour of electrodes is caused by the extraction into the membrane of such salts as $KClO_4$ to concentrations exceeding the intrinsic site concentration of the membrane, as

predicted by the theory of Buck et al [5]. This is not to say that non-lipophilic anions such as benzoate that pose no interference problem are completely excluded from the membrane; however, the extraction of the potassium salt of this anion is not favoured enough for its membrane concentration to rival that of negative membrane sites, and a prerequisite for onset of Donnan exclusion failure is not satisfied.

The presence of KTPB has been shown to discourage ingress of benzoate into the membrane, but has no beneficial effect in the prevention of Donnan exclusion failure when lipophilic anions make up part of the bathing solution. The additional negative sites that KTPB contributes to the membrane will prolong the membrane's lifetime by warding off the loss of permselectivity that accompanies the aging process through improved Donnan exclusion of anions like benzoate. Some other change in membrane composition would have to be made, however, in order to minimize the interferences caused by lipophilic anions.

The AC impedance technique has provided direct evidence for membrane permeation by neutral species such as benzoic acid, and also indicated that this compound undergoes a subsequent charge-carrier producing process. A clarification of the role that such neutral species play in determining membrane characteristics might ultimately lead to a better understanding of the mechanism by which some neutral species in physiological fluids interfere with electrode response.

There is no doubt as to the sensitivity of the AC impedance technique, and its remarkable applicability to the study of membrane permeability. Very small changes in ion concentration within the membrane can be measured, so that membrane permeation can be studied at levels far below those required to affect electrode potentiometric response. AC impedance analysis is

therefore a valuable tool for studying the more subtle permeant effects that arise upon exposure to solutions containing neutral acids or non-lipophilic anions.

4.5 REFERENCES

- (1) Boles, J.H., Buck, R.P., *Anal. Chem.*, 1973, 45, 2057
- (2) Li, X., Verpoorte, E.M.J., Harrison, D.J., *Anal. Chem.*, 1988, 60, 493
- (3) Morf, W.E., Simon, W., *Helvetica Chim. Acta*, 1986, 69, 1120
- (4) Lindner, E., Toth, K., Pungor, E., *Dynamic Characteristics of Ion-Selective Electrodes*; CRC Press: Boca Raton, Fla, 1988
- (5) Buck, R.P., Toth, K., Graf, E., Horvai, G., Pungor, E., *J. Electroanal. Chem.*, 1987, 223, 51
- (6) Jenny, H.-B., Riess, C., Ammann, D., Magyar, B., Asper, R., Simon, W., *Mikrochim. Acta*, 1980, II, 309
- (7) Koch, D.D., Ladenson, J.H., *Anal. Chem.*, 1983, 55, 1809
- (8) Murinskaya, V.E., Stefanova, O.K., Maternova, E.A., Yukhno, D.A., *Elektrokhimiya*, 1980, 16, 320
- (9) Hills, G. J., Jacobs, P. W. M., Lakshminarayanaiah, N., *Proc. R. Soc.*, 1961, A262, 257
- (10) Band, D.M., Kratochvil, J., Treasure, T., *J. Physiol. (London)*, 1976, 265, 2P
- (11) Bassett, J., Denney, R. C., Jeffery, G. H., Mendham, J., *Vogel's Textbook of Quantitative Inorganic Analysis, 4th Ed.*; Longman: London, 1978
- (12) Craggs, A., Moody, G.J., Thomas, J.D.R., *J. Chem. Educ.*, 1974, 51, 541
- (13) Robinson, R.A., Stokes, R.H., *Electrolyte Solutions*; Butterworths Scientific Publications, London, 1955
- (14) Morf, W. E., Ammann, D., Simon, W., *Chimia*, 1974, 28, 65
- (15) Armstrong, R. D., Horvai, G., *Electrochim. Acta*, 1990, 35, 1
- (16) Mathis, D. E., Buck, R. P., *J. Memb. Sci.*, 1979, 4, 379
- (17) Sears, J. K., Darby, J. R., *The Technology of Plasticizers*; John Wiley and Sons: New York, 1982

- (18) Harrison, D. J., *J. Electroanal. Chem.*, 1990, 278, 193
- (19) Lindner, E., Graf., Niegreis, Z., Toth, K., Pungor, E., *Anal. Chem.*, 1988, 60, 295
- (20) Armstrong, R.D., Todd, M., *Electrochim. Acta*, 1987, 32, 155
- (21) Leo, A., Hansch, C., Elkins, D., *Chem. Rev.*, 1971, 71, 525

CHAPTER 5

BEHAVIOUR OF DISSOCIABLE SPECIES IN LIQUID ION-SELECTIVE MEMBRANES

5.1 INTRODUCTION

Ion-selective electrodes (ISE) constructed from plasticized poly(vinylchloride) (PVC) membranes based on neutral ion carriers have in recent years been introduced for the potentiometric measurement of such ions as K^+ , NH_4^+ , and Ca^{2+} , which were previously not determinable with glass electrodes or electrodes based on insoluble, conducting salts. Typically, these membranes consist of an approximately 2 : 1 mixture of plasticizer to PVC which has incorporated into it about 1 % (w/w) neutral carrier, where the plasticizer is often a high-boiling, long-chain ester, or else some other viscous, hydrophobic organic solvent. Commonly used carriers or ligands include nonactin, which preferentially complexes NH_4^+ , and valinomycin, which forms a stable complex with K^+ . The inclusion of a neutral ligand like those above in a PVC membrane will impart a high degree of selectivity to the membrane for the ion of interest. As in previous chapters, the membranes investigated in this study typically consist of 33 % PVC, 66 % dioctyladipate (DOA), with 1 % valinomycin and/or 0.01 % potassium tetraphenylborate (KTPB) being added if the situation warrants.

The potentiometric response of plasticized PVC membranes is not governed solely by what neutral carrier is present in the membrane phase. It has been shown in our laboratory and others (Chapter 1, ref. 8), for instance,

that ISE's based on PVC/DOA membranes containing no carrier respond to variations in K^+ concentration in solutions buffered to a constant ionic strength of 0.1 with NaCl, although the slopes of the resulting potential vs $\log[K^+]$ curves are, at ~ 30 mV/decade, sub-Nernstian. Generally speaking, plasticized PVC membranes can extract cations from solution, while excluding such hydrophilic anions as Cl^- . The ability to extract ions of one charge to the exclusion of ions of the opposite charge is known as permselectivity, and it can be said that the membranes in question are permselective for cations. The permselectivity of PVC/DOA membranes for cations is due to the presence of relatively immobile negative sites within the membrane, thought to be associated with the PVC matrix itself [1,3]. Evidence for this conclusion has been obtained through electroalytic measurements of PVC/DOA membranes, which show that K^+ enters the membrane to a far greater extent than Cl^- [2]. This deficit in Cl^- concentration in the membrane implies that there must be a significant concentration of negative sites in the membrane already, since the relatively thick (0.1 to 0.3 mm) PVC/DOA membranes under discussion are considered to be electroneutral [2,3].

As discussed in Chapter 4 and in references [1,4,5], a loss of membrane selectivity for K^+ is indicated when potentiometric measurements are made in test solutions containing lipophilic species such as ClO_4^- . Responses which are at least several mV less per decade change in $[K^+]$ than the expected 59 mV are observed, and the range over which the response is analytically useful is curtailed. These results show a correlation with the results of AC impedance measurements carried out in Chapter 4 on membranes of the same composition, in which significant decreases in bulk membrane resistance, R_g , upon exposure to solutions containing ClO_4^- implied significant permeation of the membranes by ClO_4^- . Membrane permeation by this anionic species

meant that the membrane had in effect lost much of its permselective character. Therefore, degradation of membrane selectivity is most likely to be related to a loss of membrane permselectivity. Several studies reported in the literature [1,4,5] come to this same conclusion. In particular, it has been shown that the addition of a small amount of a salt like KTPB, in which one ion is lipophilic (TPB⁻), the other hydrophilic (K⁺), improves membrane selectivity. This is due to the improved permselectivity that results when the additional negative sites, introduced when KTPB is added, enhance the membrane's ability to exclude anions.

In Chapter 4, the effect on R_g of exposing a membrane to solutions containing species which do not interfere with the potentiometric response of ISE's (benzoic acid and benzoate, in this case) was considered. As with ClO_4^- , it was found that both the anion and the neutral species permeated the membrane and caused decreases in R_g to be measured, though the effect was less pronounced in the benzoic acid/benzoate case. Chapter 4 addressed the reasons why a loss of membrane selectivity was observed in the ClO_4^- case but not in the benzoic acid/benzoate case, despite the apparent degradation in membrane permselectivity in both cases. No attempt was made, however, to quantify parameters associated with the behaviour of the various species once they had made their way into the membrane. That, then, is one of the goals of the study reported in this chapter.

AC impedance measurements of membranes cast with known amounts of various benzoate salts, NaClO_4 , or benzoic acid, carried out in this study, demonstrated the dependence of R_g on the concentration of added substance. In most cases, this dependence was straightforward, with R_g decreasing monotonically with increasing concentration. Decreases in R_g correspond to increases in membrane conductivity, σ , through the relations

$$\rho = \frac{Rg A}{l} \quad (\Omega \cdot \text{cm}) \quad (1)$$

$$\sigma = \frac{1}{\rho} = \sum q_i n_i u_i \quad (\Omega^{-1} \cdot \text{cm}^{-1}) \quad (2)$$

where ρ is membrane resistivity; A and l are the geometric parameters, membrane area and thickness, respectively; σ is the specific conductivity of the membrane; q_i , n_i , and u_i are the charge, the number present, and the mobility of the i^{th} charge carrying species, respectively. Rg is then a function of both ion concentration and ion mobility. Ion concentrations in membranes containing one or more solubilized salts or ionogens will depend on the degree of dissociation of ion pairs or neutral molecules, respectively, dissociation being a process which may be quantitatively described for each solute using the dissociation constant, K_d . If the species under consideration is a neutral acid such as benzoic acid, K_d becomes equivalent to the acid dissociation constant. Evaluation of this constant K_d for the various compounds examined was possible through use of the Fuoss equation of conductance (Λ) for associated electrolytes [6] (see also Chapter 1), where Λ is related to σ as follows :

$$\Lambda = \frac{\sigma \cdot 1000}{c} \quad (\text{cm}^2 \cdot \text{mole}^{-1} \cdot \Omega^{-1}) \quad (3)$$

where c is concentration of salt in moles/L, and the factor 1000 simply converts L to cm^3 . The other parameter whose evaluation may be accomplished through use of the Fuoss equation is Λ_0 , or the limiting conductance of the salt at infinite dilution. Λ_0 may be expressed as the sum of

the limiting ionic conductivities, λ_i , of the salt's component anion and cation, as follows :

$$\Lambda_0 = \lambda_{+}^{\circ} + \lambda_{-}^{\circ} \quad (4)$$

where the λ_i° , sometimes also referred to as limiting ion mobilities [7], may allow some conclusions to be drawn as to the relative magnitudes of ion mobilities within the membrane. Knowledge of K_d and Λ_0 can lead to a characterization, in part at least, of the transport properties of the bulk membrane. The conductivity of membranes containing benzoic acid was also studied as a function of temperature. This enabled a clearer description to be developed of the ion generation process taking place through the evaluation of an activation energy, E_a , for the process.

In using the Fuoss equation for conductance to find K_d and Λ_0 , we have assumed that membranes consisting of a 2 : 1 ratio of plasticizer to PVC are essentially very viscous liquid solutions, which is in agreement with other impedance and kinetic studies for these membranes reported in the literature [2,8]. A particularly compelling piece of evidence which firmly justifies regarding the membrane as a liquid may be found in the NMR study of Simon et al. [8], in which a PVC membrane plasticized with *o*-nitrophenyloctylether (NPOE) was probed spectroscopically. The linewidths of peaks in the ^{13}C NMR spectrum for NPOE are narrow enough that there is no doubt that NPOE is present in a liquid environment, albeit a viscous one, according to the broader linewidths of the corresponding ^1H NMR spectrum.

5.2 EXPERIMENTAL

The membranes used in determinations of K_a and Λ_o typically contained 33 % (w/w) poly(vinylchloride) (PVC) (Polysciences, chromatographic grade), 66 % (w/w) dioctyladipate (DOA) (Fluka), and about 1 % valinomycin (Sigma) [9]. Potassium tetraphenylborate (KTPB), prepared according to a gravimetric method outlined in reference [10], was also often included in the membrane at the 0.01 % (w/w) level. Membranes containing all four components will be referred to hereafter as "normal" membranes. Membranes used in temperature studies consisted either of PVC/DOA, or of PVC/DOA with 0.01 % KTPB.

As will be described, bulk membrane resistances of normal membranes containing known amounts of potassium benzoate (KBz), sodium benzoate (NaBz), tetraethylammonium benzoate (TEAB), sodium perchlorate (NaClO_4), methyl benzoate, and benzoic acid were measured. KBz was prepared by combining 1.6 g of benzoic acid (Terochem) and 0.8 g of KOH (Anachemia) in about 20 mL of ethanol (95 %), and filtering off the resulting KBz precipitate. The product yield was about 1.7 g. Further purification was carried out through recrystallization from ethanol. Benzoic acid (Terochem) was purified by recrystallization from cold water (doubly distilled from alkaline KMnO_4), followed by sublimation under vacuum. Methyl benzoate (Fisher Scientific) was purified through distillation. NaClO_4 (G.Frederick Smith Chemical Company, Columbus, Ohio) was used without further purification.

TEAB was prepared according to a procedure outlined in [11]. 1.0 g of NaOH (BDH) and 4.5 g of tetraethylammonium bromide (TEABr) were dissolved in 10 mL of water. 1.5 g of benzoic acid was dissolved in 10 mL of CHCl_3 . The two solutions were then shaken for 5 minutes in a separatory

funnel, after which the CHCl_3 layer was collected. This layer, which contained the TEAB product and some TEABr , was then extracted with three 10 mL portions of cold water, in order to separate TEAB, which is extremely hygroscopic, from the starting material, which is only slightly water soluble at room temperature. These three portions were collected, and the water evaporated off. The oily residue, TEAB, was extracted using ether and placed under vacuum for 48 hours to dry. NMR spectra of the resulting crystals showed that the compound of interest had been obtained.

Stock THF solutions of each compound were made by dissolving about 15 to 30 mg in 25.0 mL of distilled THF. For the KBz/THF stock solution, it was necessary to dissolve KBz in about 5 mL of methanol before diluting to the full 25.0 mL volume with THF. Four subsequent THF solutions of lesser concentrations were prepared by dilution with THF. It was noted that the solubility of KBz decreased as the percent THF increased in diluted solutions, making concentrations of the third, fourth, and fifth solutions in each series less reliable. In order to correct for this problem, three series of KBz/THF solutions were prepared in the usual way, using three KBz/THF/MeOH stock solutions of slightly different known concentrations. Three aliquots of each solution were then transferred to volumetric flasks of varying volumes, and the THF allowed to evaporate off. Aqueous solutions of the KBz residue in each flask were prepared by diluting to the mark with doubly distilled water. The absorbance of each solution was measured at 274 nm, along with a series of aqueous KBz standards, to obtain a calibration curve of measured versus expected KBz concentration for the KBz/THF solutions. This curve was subsequently employed to correct membrane concentrations of KBz.

Series of normal membranes containing each compound were cast in groups of four following the method outlined in Chapter 3, with one

membrane in each series cast without added compound serving to act as a blank. To ensure that the normal membrane matrix was consistent over a series of membranes, larger volumes of membrane solution was prepared and 2 to 3 mL portions of this delivered to each of four 10 mL beakers. Varying aliquots of THF solutions of the compound were then added to each of three beakers, and the total volume of membrane solution in all four beakers was brought to about 5 mL using distilled THF. After allowing to stir for 30 minutes or more, the mixtures were poured into PTFE moulds and allowed to set, as described above. After the curing process, membranes were weighed to the nearest 0.1 mg. To account for compound-containing membrane solution which inevitably remained behind in the beaker after casting, the 10 mL beakers used were weighed dry and again 24 hours after casting. The mass of "leftover" membrane thus determined was added to the mass of the corresponding cast membrane. Membrane concentrations of added compound could then be evaluated, since both the mass of compound and the total mass of membrane to which that compound was added were accurately known.

Impedance measurements were carried out with membranes mounted in a specially designed cell. Details of the instrumentation and the cell used are given in Chapter 4. For determinations of K_d and Λ_o , membranes were allowed to soak for an hour before the measurement was made, in a 1 mM KCl solution maintained at a constant ionic strength of 0.1 M by NaCl. Data was acquired with the membrane in the same solution. The frequencies employed for these experiments generally ranged from 40000 to 25 Hz. Membrane thicknesses were measured after each experiment, using the method described above. The active area of membrane exposed to solution

was in all cases 0.283 cm². The temperature was maintained at 25.0 °C by fitting the cell into a brass water jacket, as shown in Chapter 4.

In temperature studies of membrane σ , temperature was again maintained using the water jacket and the water bath. While data was acquired at 5° intervals, measurements were not made in order of increasing or decreasing temperature, but rather alternately at temperatures above and below 25 °C. Membranes were conditioned in 1 mM KCl ($\mu = 0.1$ (NaCl)) for about 24 hours prior to an experiment. Data was collected only after a cell had been equilibrated at the desired temperature for 30 minutes.

5.3 CALCULATION OF Λ_0 AND K_d

Λ_0 , the limiting conductance at infinite dilution, and K_d , the equilibrium constant describing either dissociation of ion pairs for salts or acid dissociation for neutral acids, were calculated using the Fuoss conductance equation for associated electrolytes, Equation (5) [6] :

$$\Lambda = \Lambda_0 - S\sqrt{c\alpha} + E c\alpha \log(c\alpha) + Jc\alpha - K_d \Lambda^2 c\alpha \quad (5)$$

In Equation (5), α refers to the degree of dissociation, while c is the total concentration of the compound of interest in solution (the solution in our case being the membrane). S , the so-called Onsager limiting slope, and E are both known functions of Λ_0 as well as the relative dielectric constant, ϵ , and viscosity, η , of the membrane. The coefficient J is also a function of these parameters, but has an additional and rather involved functional dependence on the ion size parameter, a , which is generally taken to represent the

separation between ions in ion pairs. The parameter a is often denoted as \tilde{a} , which is simply the ion size parameter expressed in units of Ångströms. The complete functional forms of S , E , and J are given in Chapter 1, and so will not be restated here. Though K_d does not actually appear in Equation (5), the ion pair association constant, K_a , does. K_d may be defined simply as the reciprocal of K_a .

There are essentially two methods in which Equation (5) may be manipulated in order to extract values of Λ_0 and K_d from a given set of Λ measurements for a solute. The first may be one of several graphical methods, developed by Fuoss [12], Fuoss and Shedlovsky [13], and Shedlovsky and Kay [14], among others. It has been noted, however, that these methods are very sensitive to the degree of precision in the data [15]. Because of the nature of the membrane systems being examined in this work, the precision of R_g 's measured as a function of additive concentration is generally not better than 10-15 % for different portions cut from the same membrane, especially at the lower concentrations. Our own experience has shown that a graphical method, based on a simpler equation for Λ [16] than that given in Equation (5), will not work for data sets obtained in our systems. Also of importance is the observation that the extrapolation of data to Λ_0 for weakly dissociated electrolytes is sometimes inaccurate [15]. The low dielectric constant of the membranes being examined should preclude the observation of large values of K_d for the salts or acid of interest, so that this would prove to be a problem as well.

The second method which may be used to evaluate Λ_0 and K_d , and the one eventually adopted in this study, is a least squares type of data analysis using Equation (5). First introduced by Kay [17], this iterative method is ideally suited for computer based analysis, and allows Λ data to be weighted using an

appropriate weighting function to account for such factors as reduced precision at the lower concentrations. Weighting of Λ data in our situation will be discussed at greater length below. A brief description of the method itself follows.

Each Λ_i in a data set may be written as a function of c_i (rearranging Equation (5)), to obtain :

$$\Lambda_i = \frac{\Lambda_o - S\sqrt{c_i\alpha} + E c_i\alpha \log(c_i\alpha) + Jc_i\alpha}{1 + K_a f^2 c_i\alpha} \quad (6)$$

This is the equation of condition; for n measured values of Λ at known c , there exist n equations of condition. This is obviously not a linear equation in the unknowns Λ_o and K_a , but it may be linearized by taking the total differential of Λ [18], resulting in an equation for $\Delta\Lambda$ which is linear in the unknowns $\Delta\Lambda_o$ and ΔK_a . This linearized version of Equation (6) is given below:

$$\Delta\Lambda_i = \frac{\partial\Lambda_i}{\partial\Lambda_o} \Delta\Lambda_o + \frac{\partial\Lambda_i}{\partial K_a} \Delta K_a \quad (7)$$

where $\Delta\Lambda_i = \Lambda_{i,obs} - \Lambda_{i,calc}$ ($\Lambda_{i,obs}$ being the experimentally observed value of Λ , and $\Lambda_{i,calc}$ being one which is calculated); $\Delta\Lambda_o = \Lambda_{o,i} - \Lambda_{o,i-1}$; and $\Delta K_a = K_{a,i} - K_{a,i-1}$. The two normal equations derived from equations having the form of Equation (7) should satisfy the relations that follow :

$$\frac{\partial \sum e_i^2}{\partial \Delta\Lambda_o} = 0 \quad (8)$$

$$\frac{\partial \sum e_i^2}{\partial \Delta K_a} = 0 \quad (9)$$

where e_i , the error being minimized, is :

$$e_i = \frac{\partial \Lambda_i}{\partial \Lambda_o} \Delta \Lambda_o + \frac{\partial \Lambda_i}{\partial K_a} \Delta K_a - (\Lambda_{i,obs} - \Lambda_{i,calc}) \quad (10)$$

Equation (8) then becomes :

$$\frac{\partial \sum e_i^2}{\partial \Delta \Lambda_o} = 2 \sum e_i \frac{\partial \sum e_i}{\partial \Delta \Lambda_o} = 0$$

where, from Equation (10),

$$\frac{\partial \sum e_i}{\partial \Delta \Lambda_o} = \frac{\partial \sum \Lambda_i}{\partial \Lambda_o}$$

Similarly, Equation (9) may be written as

$$\frac{\partial \sum e_i^2}{\partial \Delta K_a} = 2 \sum e_i \frac{\partial \sum e_i}{\partial \Delta K_a} = 0$$

where

$$\frac{\partial \sum e_i}{\partial \Delta K_a} = \frac{\partial \sum \Lambda_i}{\partial K_a}$$

Equation (8) then can be restated as :

$$\frac{\partial \sum e_i^2}{\partial \Delta \Lambda_o} = \left(\frac{\partial \sum \Lambda_i}{\partial \Lambda_o} \Delta \Lambda_o + \frac{\partial \sum \Lambda_i}{\partial K_a} \Delta K_a - \sum (\Lambda_{i,obs} - \Lambda_{i,calc}) \right) \times \frac{\partial \sum \Lambda_i}{\partial \Lambda_o} = 0$$

or

$$\left(\frac{\partial \sum \Lambda_i}{\partial \Lambda_o} \Delta \Lambda_o + \frac{\partial \sum \Lambda_i}{\partial K_a} \Delta K_a \right) \frac{\partial \sum \Lambda_i}{\partial \Lambda_o} = \frac{\partial \sum \Lambda_i}{\partial \Lambda_o} \sum (\Lambda_{i,obs} - \Lambda_{i,calc}) \quad (11)$$

and Equation (9) becomes

$$\frac{\partial \Sigma e_i^2}{\partial \Delta K_a} = \left(\frac{\partial \Sigma \Lambda_i}{\partial \Lambda_o} \Delta \Lambda_o + \frac{\partial \Sigma \Lambda_i}{\partial K_a} \Delta K_a - \Sigma(\Lambda_{i,obs} - \Lambda_{i,calc}) \right) \times \frac{\partial \Sigma \Lambda_i}{\partial K_a} = 0$$

or

$$\left(\frac{\partial \Sigma \Lambda_i}{\partial \Lambda_o} \Delta \Lambda_o + \frac{\partial \Sigma \Lambda_i}{\partial K_a} \Delta K_a \right) \frac{\partial \Sigma \Lambda_i}{\partial K_a} = \frac{\partial \Sigma \Lambda_i}{\partial K_a} \Sigma(\Lambda_{i,obs} - \Lambda_{i,calc}) \quad (12)$$

D, the matrix of coefficients, a_{ij} , of the normal equations, Equations (11) and (12), is then

$$D = \begin{bmatrix} \left(\frac{\partial \Sigma \Lambda_i}{\partial \Lambda_o} \right) \left(\frac{\partial \Sigma \Lambda_i}{\partial \Lambda_o} \right) & \left(\frac{\partial \Sigma \Lambda_i}{\partial \Lambda_o} \right) \left(\frac{\partial \Sigma \Lambda_i}{\partial K_a} \right) \\ \left(\frac{\partial \Sigma \Lambda_i}{\partial \Lambda_o} \right) \left(\frac{\partial \Sigma \Lambda_i}{\partial K_a} \right) & \left(\frac{\partial \Sigma \Lambda_i}{\partial K_a} \right) \left(\frac{\partial \Sigma \Lambda_i}{\partial K_a} \right) \end{bmatrix} \quad (13)$$

The matrix D is said to be axisymmetric, since a_{12} is equal to a_{21} . B, the matrix of constant terms, b_{ij} , is

$$B = \begin{bmatrix} \left(\frac{\partial \Sigma \Lambda_i}{\partial \Lambda_o} \right) \Sigma(\Lambda_{i,obs} - \Lambda_{i,calc}) \\ \left(\frac{\partial \Sigma \Lambda_i}{\partial K_a} \right) \Sigma(\Lambda_{i,obs} - \Lambda_{i,calc}) \end{bmatrix} \quad (14)$$

and Δ , the matrix of unknowns is

$$\Delta = \begin{bmatrix} \Delta \Lambda_o \\ \Delta K_a \end{bmatrix}$$

Solution of the system, $D \cdot \Delta = B$, gives the best values of the unknowns $\Delta \Lambda_o$ and ΔK_a . Equations (5) through (14), then, form the basis of the computer program written to calculate the values of Λ_o and K_d best fitting each set of experimentally measured Λ 's.

The computer calculation is started by selecting initial values for Λ_o and K_d , and calculating values for the various constants in the Fuoss

equation, using the following values for the solvent properties of the membrane : $\epsilon = 8$ (an average value calculated from the C_g 's of membranes of varying composition); $\eta = 2000$ Poise (obtained from an independent measurement); $T = 25$ °C. Calculation of the various derivatives and the $\Lambda_{i,calc}$ in Equations (11) and (12) are executed next, but not before values of α , the degree of dissociation, and hence f , the mean ion activity coefficient, have been obtained. This is done using an iterative procedure and the relationship between K_d and α , using Equation (15) :

$$\alpha = \frac{-K_d + \sqrt{K_d^2 + 4 K_d f^2 c}}{2 f^2 c} \quad (15)$$

To obtain an initial value for α (α_0), f is assumed to be either 1 (for the first point of a data set) or the last value of f calculated for the preceding point. Using α_0 , f is re-evaluated using the Debye-Hückel first approximation, and subsequently plugged into Equation (15) above to obtain α_1 , and so on.

Once two consecutive values of α have converged to within a set limit, a final f value is calculated, and the coefficients in the normal equations are evaluated. A determinantal method is then employed to solve for $\Delta\Lambda_0$ and ΔK_a . This method is based on a theorem known as "Cramer's Rule" for solving systems of linear equations [19], and involves use of the matrices D and B . D , as already stated, is the matrix of coefficients, a_{ij} , for the system of normal equations (11) and (12). Let $D_{\Delta\Lambda_0}$ denote the matrix obtained by replacing the first column of D with the column of constants in B . Similarly, $D_{\Delta K_a}$ is the matrix obtained by replacing the second column of D with B . Then, by Cramer's Rule,

$$\Delta\Lambda_o = \frac{|D_{\Delta\Lambda_o}|}{|D|} \quad (16)$$

and

$$\Delta K_a = \frac{|D_{\Delta K_a}|}{|D|} \quad (17)$$

where $|D_{\Delta\Lambda_o}|$, $|D_{\Delta K_a}|$, and $|D|$ represent the determinants of the corresponding matrices. The system $D \cdot \Delta = B$ has a unique solution provided $|D| \neq 0$. If the values of $\Delta\Lambda_o$ and ΔK_a found using this method do not satisfy a predetermined limit, they are added to the old values of Λ_o and K_a to obtain new estimates for these parameters. The entire calculation is then repeated, starting with the re-evaluation of the constants in the Fuoss equation. When both $\Delta\Lambda_o$ and ΔK_a have converged to within the set limits, the calculation process is ended.

Measurements of membranes containing no added salts or acid, hereafter to be referred to as blank membranes, showed that these membranes have associated with them a significant conductivity of their own. It was therefore decided to correct measured conductivities for membranes containing added salts or acid for the conductivity, $\sigma_{0\%}$, of the membrane matrix itself. This was done assuming that conductivities due to the matrix and the salt were additive, so that the σ contribution of the salt to each observed σ can be obtained by subtracting the σ of a corresponding blank membrane from the overall σ , as follows :

$$\sigma_{obs,i} - \sigma_{0\%} = \sigma_{cor,i} \quad (18)$$

where $\sigma_{obs,i}$ is the overall observed σ ; $\sigma_{0\%}$ is the conductivity of the blank membrane, and $\sigma_{cor,i}$ is the corrected σ , or the σ due to the added salt or acid. The basic assumption underlying this approach to correction of $\sigma_{obs,i}$ is that addition of a solute to the membrane does not result in any additional

chemical interactions between the species present. It was found that using uncorrected conductances, Λ , in the fitting program does have some effect on the magnitudes of both the resulting K_d and Λ_0 , the effect being larger in the latter case. Correction of observed conductances for contributions from the matrix is therefore appropriate.

As mentioned above, incorporation of a weighting factor into a least squares analysis is easily accomplished. Weighting the corrected Λ data measured in this study was necessary for two reasons. Firstly, concentrations of added salts were probably less reliable at lower concentrations because of the manner in which the membranes were prepared. As described in the Experimental section, THF solutions containing varying concentrations of the salts/acid to be added were made by dilution of stock solutions. Generally the third, fourth, and fifth dilutions were the solutions from which aliquots were taken and added to the membrane solutions. Because of the inherent dilution error, membranes cast using aliquots from a fifth dilution would have a less reliable concentration than those cast using a fourth dilution, and so on. Secondly, correction of observed Λ 's for the σ due to the membrane matrix will also result in uncertainty in the Λ_{cor} 's, especially at the lower concentrations. The smaller the difference between σ_{obs} and $\sigma_{0\%}$, as is the case at the lower concentrations, and the lower the concentration, the greater this uncertainty will be. In order to account for these factors contributing to the uncertainty of any given Λ_{cor} , the points were weighted by the product of two terms, the first being the square of the nominal concentration at which the point was measured, as suggested in [17], the second being the reciprocal of the relative standard deviation of the point [20]. The actual weighting process was easily accomplished by multiplying each equation of condition (Equation (7)) through by the square root of this product.

An expression for the relative standard deviation of each $\Lambda_{\text{cor},i}$ was derived by carrying out a propagation of errors analysis. It was assumed that the precision of actual impedance measurements due to instrumental considerations is the same for all membranes. A precision of 10 - 15 % was generally obtainable for a series of impedance experiments on several portions of one membrane, whereas thickness measurements could be carried out with a precision of 10 %. Then, from Equation (1),

$$\sigma_{\text{obs},i} = \frac{l_i(\pm 0.10 l_i)}{R_{g,i} (\pm 0.15 R_{g,i}) A} \quad (19)$$

and the relative standard deviation, $S_{(\sigma,\text{rel}),i}$ of the observed conductivity, $\sigma_{\text{obs},i}$, is

$$S_{(\sigma,\text{rel}),i} = \sqrt{\left(\frac{0.15 R_{g,i}}{R_{g,i}}\right)^2 + \left(\frac{0.10 l_i}{l_i}\right)^2} = 0.18 \quad (20)$$

The correction of $\sigma_{\text{obs},i}$, including expected absolute standard deviations, may be expressed as

$$\sigma_{\text{obs},i} (\pm 0.18 \sigma_{\text{obs},i}) - \sigma_0\% (\pm 0.18 \sigma_0\%) = \sigma_{\text{cor},i} (\pm S_{\sigma_{\text{cor},i}}) \quad (21)$$

The absolute standard deviation, $S_{\sigma_{\text{cor},i}}$, of the corrected conductivity, $\sigma_{\text{cor},i}$, is then

$$\begin{aligned} S_{\sigma_{\text{cor},i}} &= \sqrt{(0.18 \sigma_{\text{obs},i})^2 + (0.18 \sigma_0\%)^2} \\ &= 0.18 \sqrt{\sigma_{\text{obs},i}^2 + \sigma_0\%^2} \end{aligned} \quad (22)$$

where $\sigma_{0\%}$ is the conductivity of the blank membrane. The relative standard deviation of each $\sigma_{cor,i}$ is

$$S_{(rel,\sigma_{cor}),i} = \frac{0.18 \sqrt{\sigma_{obs,i}^2 + \sigma_{0\%}^2}}{\sigma_{cor,i}} \quad (23)$$

The weight assigned to each point is then

$$W_i = \frac{\sigma_{cor,i}}{0.18 \sqrt{\sigma_{obs,i}^2 + \sigma_{0\%}^2}} \times c^2 \quad (24)$$

Weighting of each $\Lambda_{cor,i}$ is easily accomplished by multiplying each equation of condition (Equation (7)) by the square root of Equation (24). The result of weighting with this function is that $\Lambda_{cor,i}$'s obtained at lower concentrations are generally weighted less than those obtained at higher concentrations, as expected.

Another advantage of using a least squares analysis to determine the most probable values of Λ_0 and K_a (K_d^{-1}) is that calculation of the standard deviations of these parameters is easily incorporated into the procedure. A brief description of how this was done will serve to complete the discussion of the method of data analysis used in this study.

Use can be made of the matrix D and cofactors of its various elements, a_{ij} , to determine the errors associated with Λ_0 and K_a [18]. The cofactor of a matrix element a_{ij} , denoted A_{ij} , is defined as [19]

$$A_{ij} = (-1)^{i+j} | M_{ij} | \quad (25)$$

The matrix M_{ij} is derived from D by deleting D 's i^{th} row and j^{th} column. The determinant $|M_{ij}|$, which appears in Equation (25), is called the minor of the element a_{ij} . The standard deviation for determination of the variable $\Delta\Lambda_0$, denoted by $S_{\Delta\Lambda_0}$, is then defined as

$$S_{\Delta\Lambda_0} = \sqrt{S^2 \frac{A_{11}}{|D|}} \quad (26)$$

where S is termed "the quadratic mean error to be feared in a determination whose weight is unity" [18]; $|D|$ is the determinant of the matrix of coefficients, D , given in Equation (13); and A_{11} , the cofactor of the element a_{11} in the matrix D , is equal to a_{22} , or $\left(\frac{\partial \sum \Lambda_i}{\partial K_a}\right)^2$. S^2 is further defined as

$$S^2 = \frac{[v^2]}{s - m} \quad (27)$$

where $[v^2]$ is the sum of the squares of the residuals; s is the number of data points; and m is the number of unknowns being considered (m is 2 in our case). If $\Delta\Lambda_0$ and ΔK_a are the most probable values of these parameters, found at the end of the last iteration of the calculation, then the residuals v_i may be expressed as

$$v_i = \frac{\partial \Lambda_i}{\partial \Lambda_0} \Delta\Lambda_0 + \frac{\partial \Lambda_i}{\partial K_a} \Delta K_a - (\Lambda_{i,\text{obs}} - \Lambda_{i,\text{calc}}) \quad (28)$$

To account for data points which are not of equal weight, each v_i is multiplied by the square root of the weight of the i^{th} point, using the square root of the expression for W in Equation (24).

Similarly, the standard deviation for determination of the variable ΔK_a , denoted by $S_{\Delta K_a}$, is defined by

$$S_{\Delta K_a} = \sqrt{S^2 \frac{A_{22}}{|D|}} \quad (29)$$

where A_{22} is the cofactor of the element a_{22} in the matrix D , and the other symbols have been defined above. A_{22} is equal to a_{11} , or $\left(\frac{\partial \sum \Lambda_i}{\partial \Lambda_o}\right)^2$.

In order to calculate the standard deviation of Λ_o itself, recall that

$$\Delta \Lambda_o = \Lambda_{o,i} - \Lambda_{o,i-1} \quad (30)$$

where $\Lambda_{o,i}$ is the last value of Λ_o evaluated, while $\Lambda_{o,i-1}$ is the last value but one for Λ_o . At the end of the calculation, $\Delta \Lambda_o$ is quite small, so that the absolute standard deviations of $\Lambda_{o,i}$ and $\Lambda_{o,i-1}$ may be assumed to be equal. If this deviation is denoted by S_{Λ_o} then

$$S_{\Delta \Lambda_o} = \sqrt{2 S_{\Lambda_o}^2}$$

so that

$$S_{\Lambda_o} = \frac{S_{\Delta \Lambda_o}}{\sqrt{2}} \quad (31)$$

Similarly, the standard deviation of K_a , S_{K_a} , is defined as

$$S_{K_a} = \frac{S_{\Delta K_a}}{\sqrt{2}} \quad (32)$$

Relative standard deviations of Λ_o , and K_a , $S_{\Lambda_o,rel}$ and $S_{K_a,rel}$, are found in the usual way. Due to the inverse relationship between K_d and K_a , the relative standard deviation of K_d , $S_{K_d,rel}$, will be the same as that of K_a . Values of $S_{\Lambda_o,rel}$ and $S_{K_d,rel}$ calculated for each data set will be included in the tabulation of results that will be presented below.

5.4 RESULTS AND DISCUSSION

5.4.1 Evaluation of Dissociation Constants (K_d) and Limiting Ionic Conductances (Λ_0) for Salts in the Membrane

The initial impetus for casting membranes containing known amounts of the various benzoate salts, NaClO_4 , and benzoic acid was to develop calibration curves of R_g as a function of added salt concentration, in order to be able to estimate the amounts of material required to permeate the membrane from solution to produce the decreases in R_g measured in Chapter 4. Because of the relationship between R_g and membrane conductivity, σ , however, it was also possible to utilize the impedance data obtained at known concentrations to describe more quantitatively the behaviour of the various salts and benzoic acid in the membrane phase itself. This was done through application of the Fuoss conductance equation for associated electrolytes, Equation (5), to the sets of impedance data to evaluate K_d and Λ_0 using the least squares method outlined above. These data sets, and the resulting values of K_d and Λ_0 , are presented in Tables 5.1 to 5.8.

Tables 5.1 to 5.5 give data for tetraethylammonium benzoate (TEAB), potassium benzoate (KBz), sodium benzoate (NaBz), and NaClO_4 in PVC/DOA/KTPB/valinomycin membranes (the so-called normal membranes), while Tables 5.6 and 5.7 present data for TEAB and KBz in the PVC/DOA matrix. The R_g results reported here are for the most part averages of two or three measurements carried out using different portions of a membrane, and have relative standard deviations ranging between 10 and 15 %. These values have been normalized for membrane thicknesses and

TABLE 5.1: R_g and Λ_{cor} data measured for TEAB in normal membranes, plotted in Figure 5.1 and used in least squares analysis; points which were used in the analysis have values of weight and $\Delta\Lambda$ included in the table.

[TEAB]	R_g ($M\Omega/mm$)	Λ_{cor} ($\Omega \text{ mole}^{-1} \text{ cm}^2$)	$\Delta\Lambda$	Weight (W)
0 M	21.4			
1.65×10^{-4}	18.3	.0211	.0168	2.03×10^{-8}
3.45×10^{-4}	22.5			
8.03×10^{-4}	18.2	.00443	.00222	4.90×10^{-7}
1.06×10^{-3}	20.8	.00106	-.00089	2.90×10^{-7}
1.63×10^{-3}	16.4	.00265	.00106	2.40×10^{-6}
3.83×10^{-3}	19.1	.000697	-.000335	8.59×10^{-6}
4.59×10^{-3}	17.1	.00106	.00012	2.11×10^{-5}
4.59×10^{-3}	12.8	.00257		
7.26×10^{-3}	18.3	.000481	-.000242	3.94×10^{-5}
1.18×10^{-2}	17.0	.000414		
1.39×10^{-2}	17.0	.000355		

TABLE 5.2: R_g and Λ_{cor} data measured for KBz in normal membranes (Series 1), plotted in Figure 5.2 and used in least squares analysis; points which were used in the analysis have values of weight and $\Delta\Lambda$ included in the table.

[KBz]	R_g ($M\Omega/mm$)	Λ_{cor} ($\Omega \text{ mole}^{-1} \text{ cm}^2$)	$\Delta\Lambda$	Weight (W)
0 M	24.3			
1.38×10^{-4}	18.7	.0319	.0058	1.95×10^{-8}
3.63×10^{-4}	16.7	.0182	-.0002	1.88×10^{-7}
8.37×10^{-4}	13.2	.0147	.0017	1.57×10^{-6}
1.58×10^{-3}	11.0	.0112	.0013	6.94×10^{-6}
2.74×10^{-3}	9.44	.00837	.00056	2.38×10^{-5}
4.26×10^{-3}	8.94	.00558	-.00062	5.99×10^{-5}

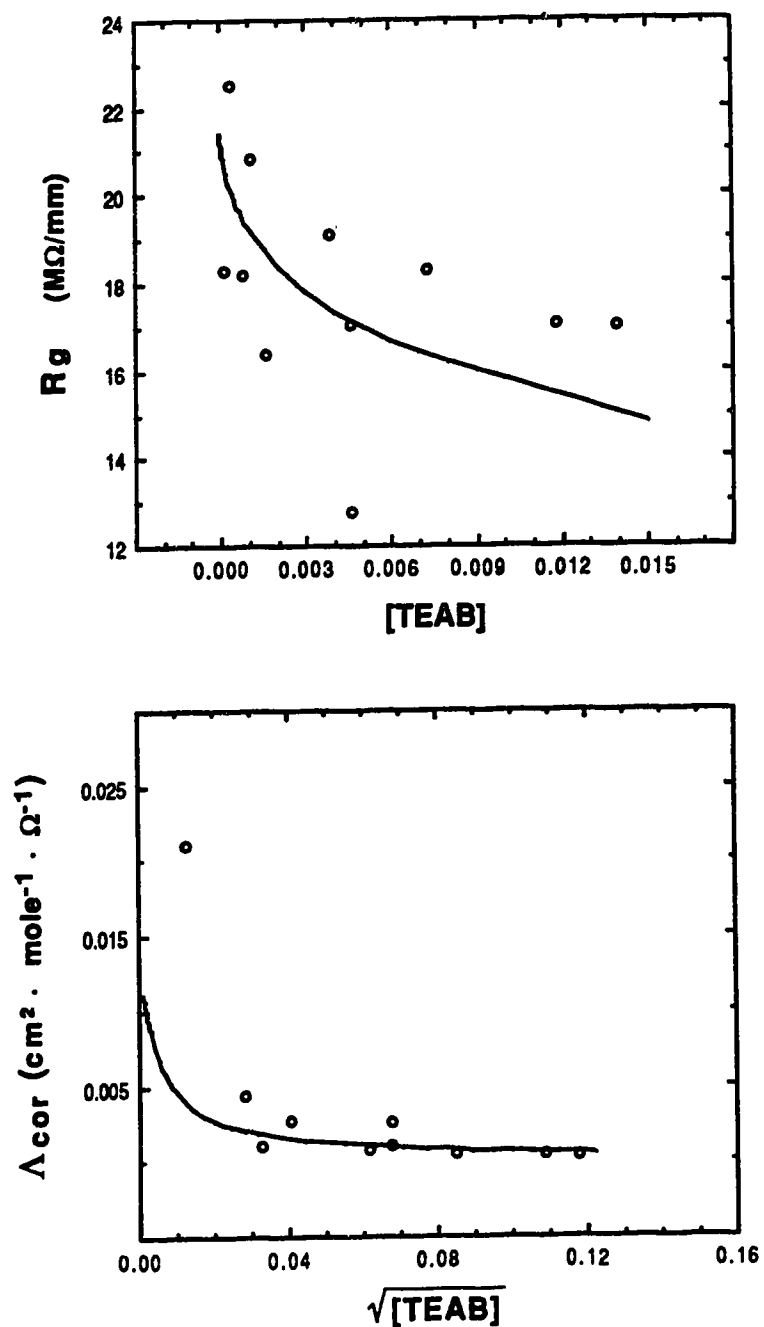


Figure 5.1 Curves of membrane resistance (R_g) vs concentration and corrected conductance (Λ_{cor}) vs the square root of concentration for TEAB in a normal membrane. Solid curves were calculated using, from Table 5.8, $K_d = 2.12 \times 10^{-5}$, $\Lambda_0 = 0.012$, and $\hat{a} = 5 \text{ \AA}$.

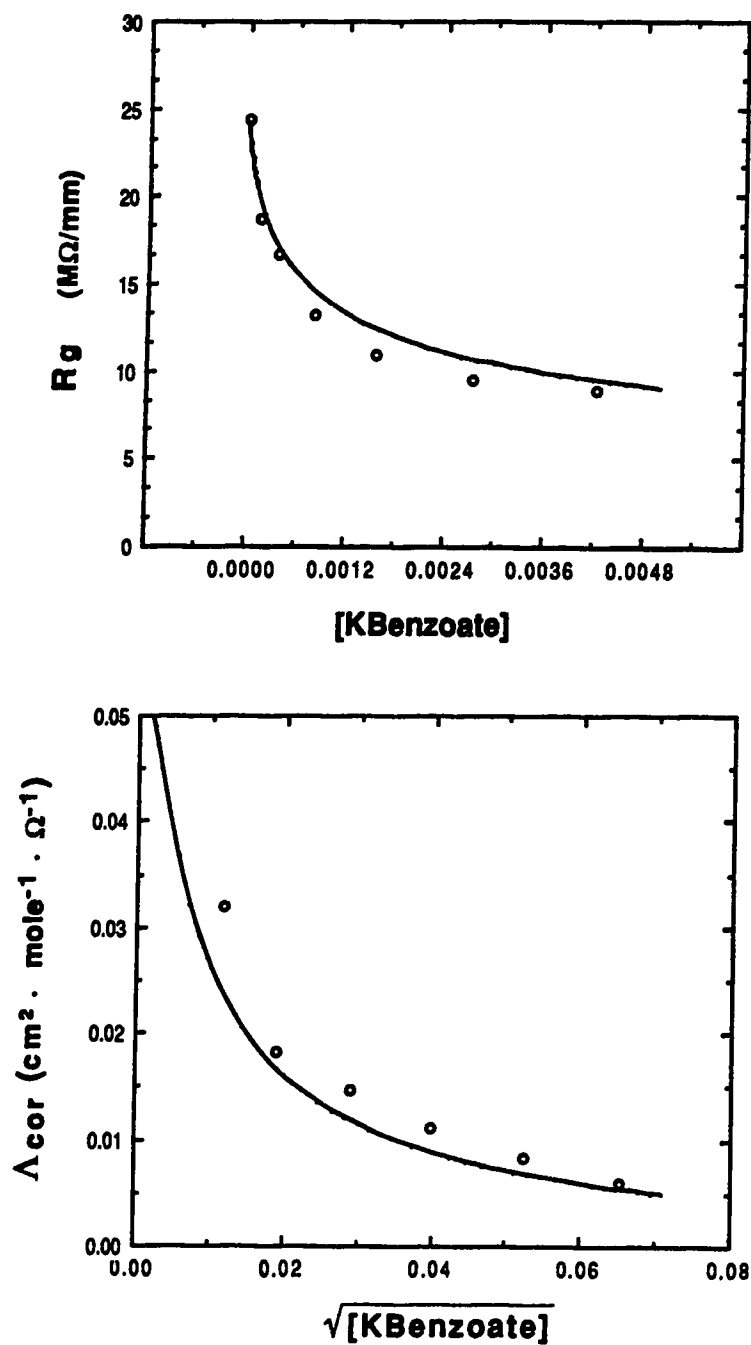


Figure 5.2 Curves of membrane resistance (R_g) vs concentration and corrected conductance (Δ_{cor}) vs the square root of concentration for a series of normal membranes containing KBz at concentrations up to 0.005 M (Series1 1). Solid curves were calculated using, from Table 5.8, $K_d = 3.51 \times 10^{-5}$, $\Lambda_0 = 0.056$, and $\dot{a} = 6 \text{ \AA}$.

TABLE 5.3: R_g and Λ_{cor} data measured for KBz in normal membranes (Series 2), plotted in Figure 5.3 and used in least squares analysis; points which were used in the analysis have values of weight and $\Delta\Lambda$ included in the table; this series of membranes differs from Series 1, considered in Table 5.2, in that a different membrane stock solution was used to prepare these membranes

[KBz]	R_g ($M\Omega/mm$)	Λ_{cor} ($\Omega \text{ mole}^{-1}cm^2$)	$\Delta\Lambda$	Weight (W)
0 M	19.6			
5.36×10^{-6}	18.1	.266	.239	8.57×10^{-12}
1.08×10^{-5}	19.9			
1.61×10^{-5}	17.9	.107	.084	9.22×10^{-11}
6.78×10^{-5}	17.9	.0247	.0096	1.59×10^{-9}
1.31×10^{-4}	17.7	.0149	.0029	6.89×10^{-9}
1.75×10^{-4}	18.3	.00706	-.00364	7.94×10^{-9}
2.03×10^{-4}	18.2	.00684	-.00325	1.20×10^{-8}
4.33×10^{-4}	15.4	.0112		
6.71×10^{-4}	12.5	.0151		
8.95×10^{-4}	11.8	.0133		
1.30×10^{-3}	13.6	.006163		
1.84×10^{-3}	9.64	.0101		

TABLE 5.4: R_g and Λ_{cor} data measured for NaBz in normal membranes, plotted in Figure 5.4 and used in least squares analysis; points which were used in the analysis have values of weight and $\Delta\Lambda$ included in the table.

[NaBz]	R_g ($M\Omega/mm$)	Λ_{cor} ($\Omega \text{ mole}^{-1}cm^2$)	$\Delta\Lambda$	Weight (W)
0 M	29.8			
1.46×10^{-4}	25.8	.0125	.0065	1.20×10^{-8}
3.19×10^{-4}	21.8	.0137	.0093	1.22×10^{-7}
4.58×10^{-4}	24.1	.00610	.00232	1.72×10^{-7}
1.66×10^{-3}	24.5	.00155	-.00049	2.09×10^{-6}
3.28×10^{-3}	23.5	.000970	-.000369	9.95×10^{-6}
3.74×10^{-3}	26.4	.000406		
5.07×10^{-3}	22.2	.000806		

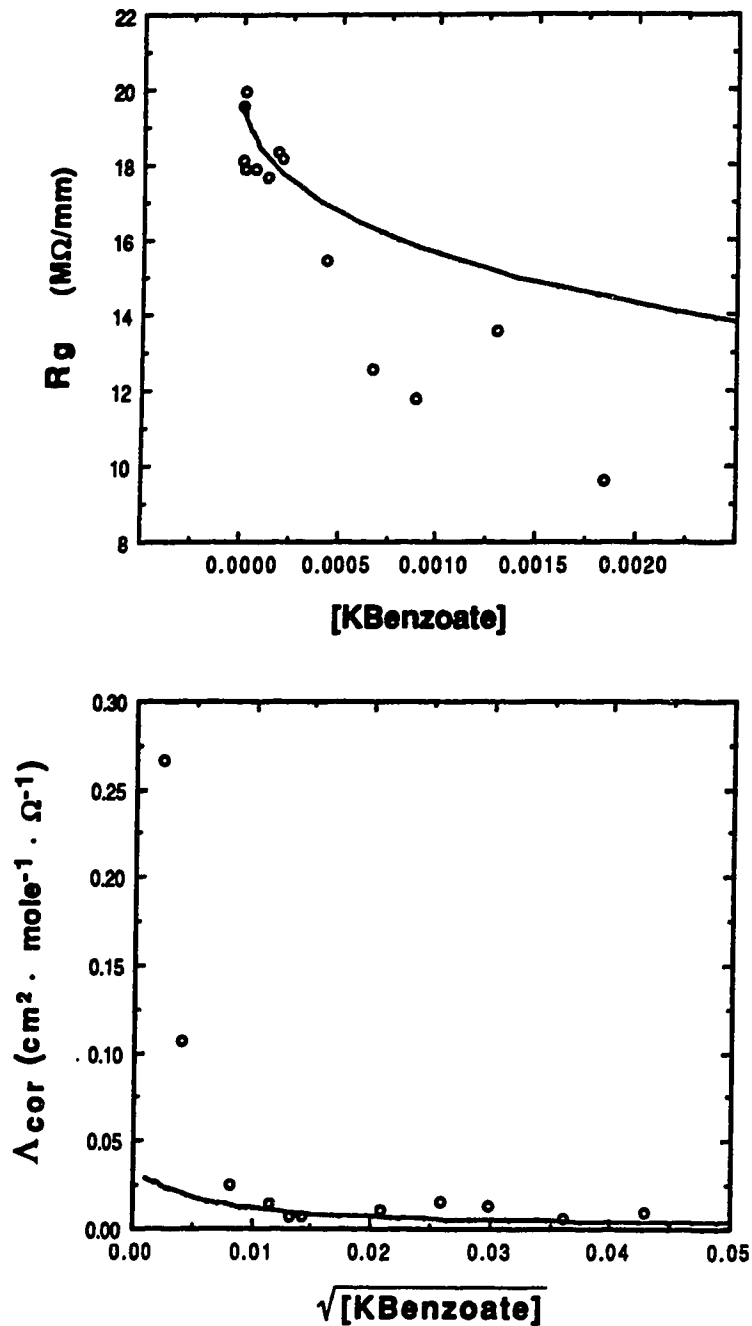


Figure 5.3

Curves of membrane resistance (R_g) vs concentration and corrected conductance (Δ_{cor}) vs the square root of concentration for a series of normal membranes containing KBz at concentrations up to 0.002 M (Series 2). Solid curves were calculated using, from Table 5.8, $K_d = 1.87 \times 10^{-5}$, $\Lambda_0 = 0.031$, and $\hat{a} = 6 \text{ \AA}$. This series of membranes was cast from a different membrane stock solution, and so is treated separately from Series 1.

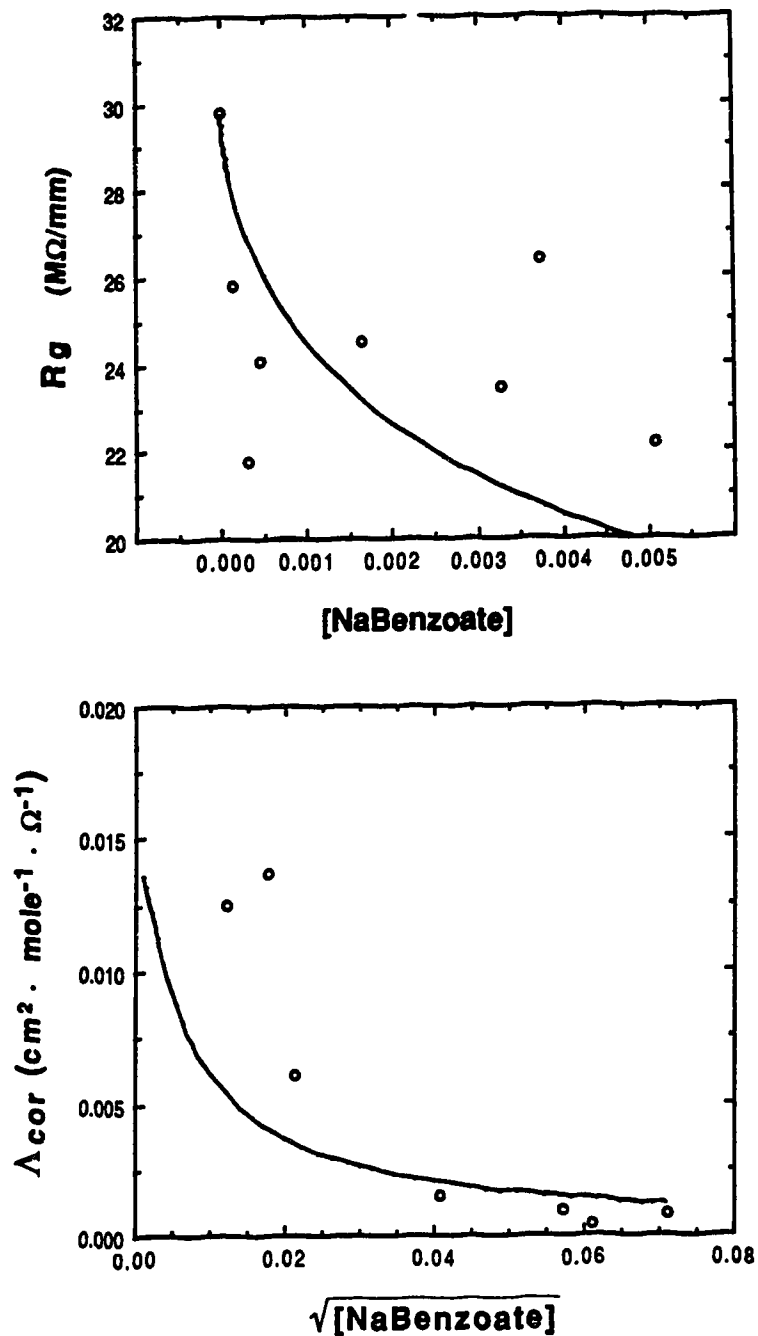


Figure 5.4 Curves of membrane resistance (R_g) vs concentration and corrected conductance (Λ_{cor}) vs the square root of concentration for a series of normal membranes containing NaBz. Solid curves were calculated using, from Table 5.8, $K_d = 2.73 \times 10^{-5}$, $\Lambda_0 = 0.014$, and $a = 4 \text{ \AA}$. The scatter in the resistance data infers a low solubility of NaBz in the membrane matrix.

TABLE 5.5: R_g and Λ_{cor} data measured for NaClO_4 in normal membranes, plotted in Figure 5.5 and used in least squares analysis; points which were used in the analysis have values of weight and $\Delta\Lambda$ included in the table.

[NaClO_4]	R_g ($M\Omega/\text{mm}$)	Λ_{cor} ($\Omega \text{ mole}^{-1}\text{cm}^2$)	$\Delta\Lambda$	Weight (W)
0 M	22.4			
1.94×10^{-4}	17.5	.0226	-.0094	3.59×10^{-8}
4.14×10^{-4}	14.5	.0207	-.0026	2.81×10^{-7}
5.80×10^{-4}	13.1	.0195	-.0005	6.74×10^{-7}
7.45×10^{-4}	10.9	.0224	.0047	1.43×10^{-6}
2.20×10^{-3}	9.24	.0102	-.0001	1.46×10^{-5}
3.78×10^{-3}	7.12	.00895		

TABLE 5.6: R_g and Λ_{cor} data measured for TEAB in PVC/DOA membranes, plotted in Figure 5.6 and used in least squares analysis; points which were used in the analysis have values of weight and $\Delta\Lambda$ included in the table.

[TEAB]	R_g ($M\Omega/\text{mm}$)	Λ_{cor} ($\Omega \text{ mole}^{-1}\text{cm}^2$)	$\Delta\Lambda$	Weight (W)
0 M	198			
9.92×10^{-6}	223			
1.93×10^{-5}	118	.0626	.0247	7.15×10^{-10}
2.87×10^{-5}	174	.00842	-.02646	4.10×10^{-10}
5.68×10^{-5}	131	.0159	-.0133	4.99×10^{-9}
7.84×10^{-5}	72.6	.0393	.0127	2.03×10^{-8}
1.17×10^{-4}	92.8	.0173	-.0062	3.62×10^{-8}
2.27×10^{-4}	48.7	.0241		
3.12×10^{-4}	33.1	.0284		
4.49×10^{-4}	28.0	.0341		

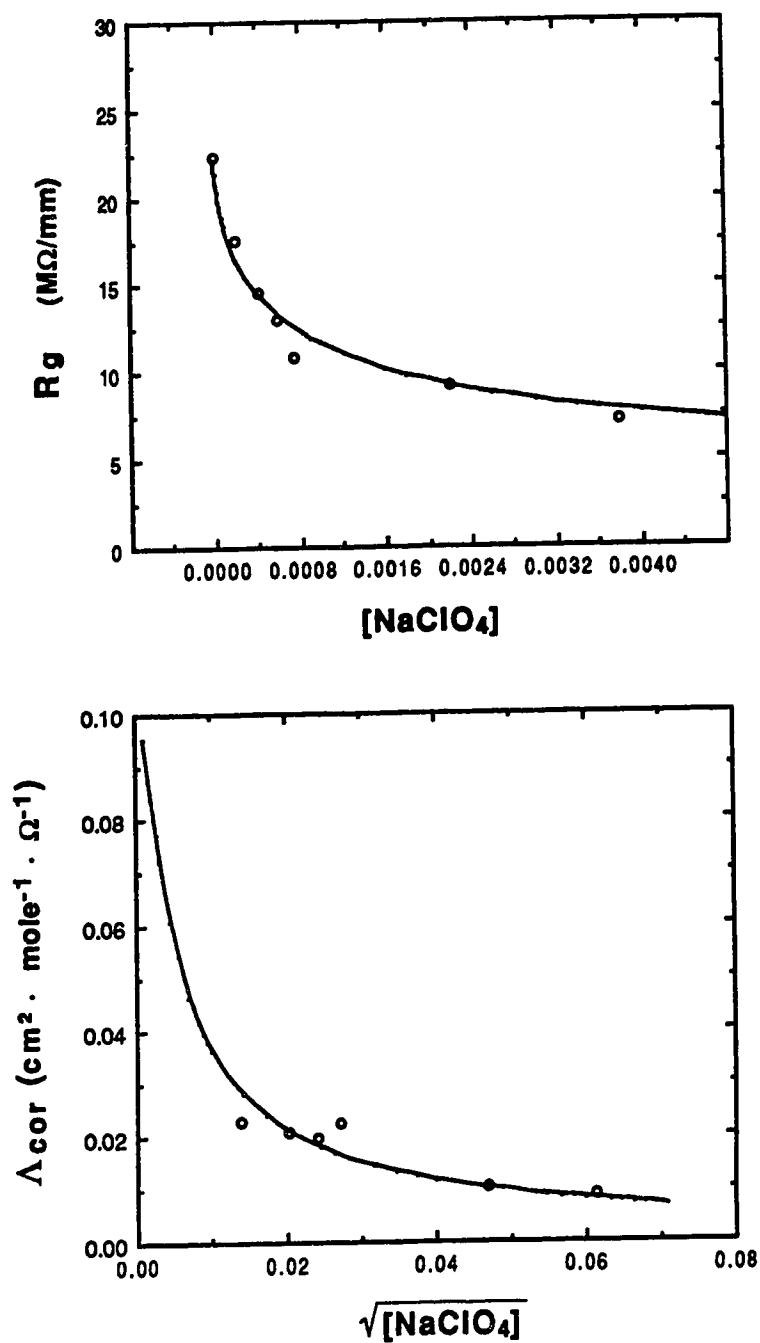


Figure 5.5

Curves of membrane resistance (R_g) vs concentration and corrected conductance (Δ_{cor}) vs the square root of concentration for a series of normal membranes containing $NaClO_4$. Solid curves were calculated using, from Table 5.8, $K_d = 1.66 \times 10^{-5}$, $\Lambda_0 = 0.10$, and $\hat{a} = 4 \text{ \AA}$.

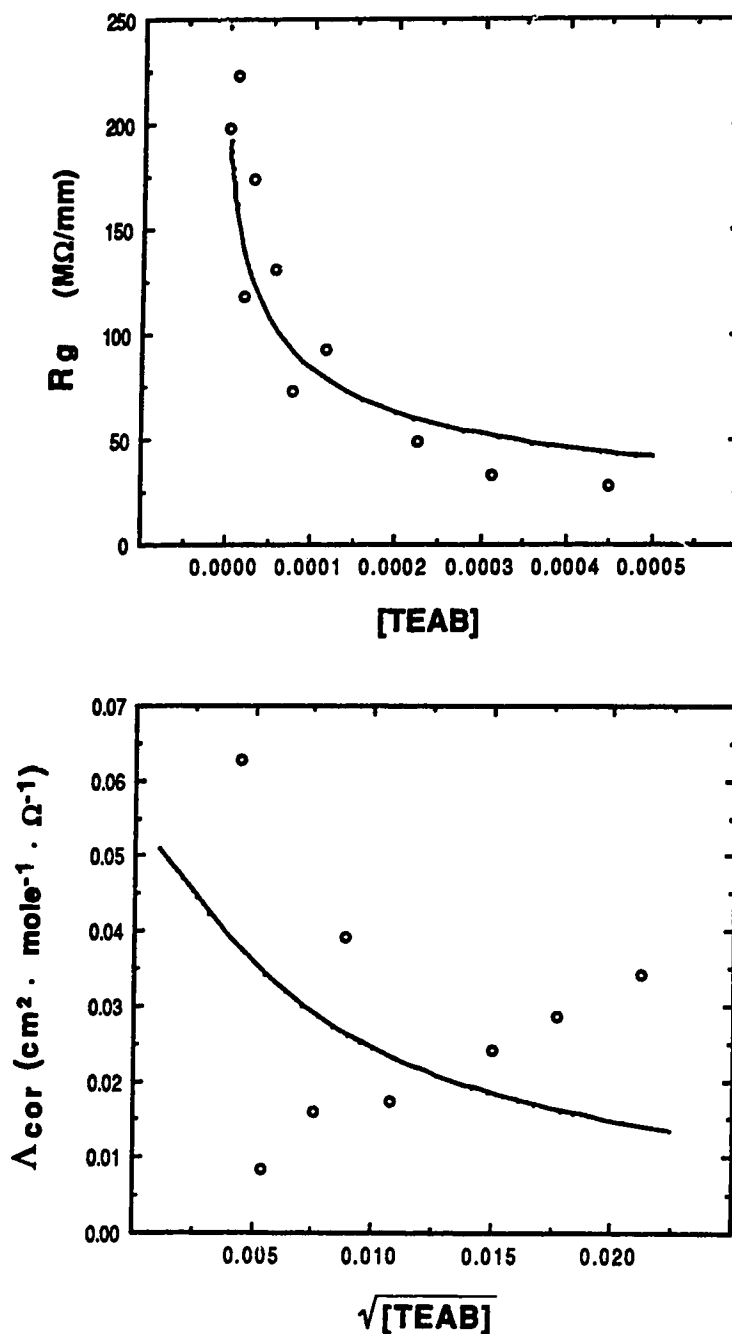


Figure 5.6 Curves of membrane resistance (R_g) vs concentration and corrected conductance (Λ_{cor}) vs the square root of concentration for a series of PVC/DOA membranes containing TEAB. Solid curves were calculated using, from Table 5.8, $K_d = 3.32 \times 10^{-5}$, $\Lambda_0 = 0.053$, and $\bar{a} = 8 \text{ \AA}$. While the measured resistances appear to be reasonable, the Λ_{cor} curve shows a great deal of scatter, indicating perhaps the extraction of TEAB into water within the membrane.

TABLE 5.7: R_g and Λ_{cor} data measured for KBz in PVC/DOA membranes, plotted in Figure 5.7 and used in least squares analysis; points which were used in the analysis have values of weight and $\Delta\Lambda$ included in the table.

[KBz]	R_g ($M\Omega/m.m$)	Λ_{cor} ($\Omega \text{ mole}^{-1} \text{ cm}^2$)	$\Delta\Lambda$	Weight (W)
0 M	243			
5.68×10^{-6}	198	.0580	.0515	2.56×10^{-11}
1.12×10^{-5}	239	.00186	-.00387	7.07×10^{-12}
1.86×10^{-5}	228	.00493	-.00021	8.31×10^{-11}
6.89×10^{-5}	255			
1.39×10^{-4}	180	.00362	.00085	2.22×10^{-8}
1.84×10^{-4}	214	.00107	-.00144	1.68×10^{-8}
3.41×10^{-4}	216	.000536		
4.29×10^{-4}	199	.000738		
7.13×10^{-4}	142	.00144		
9.37×10^{-4}	200	.000334		
1.37×10^{-3}	187	.000315		
1.84×10^{-3}	185	.000246		

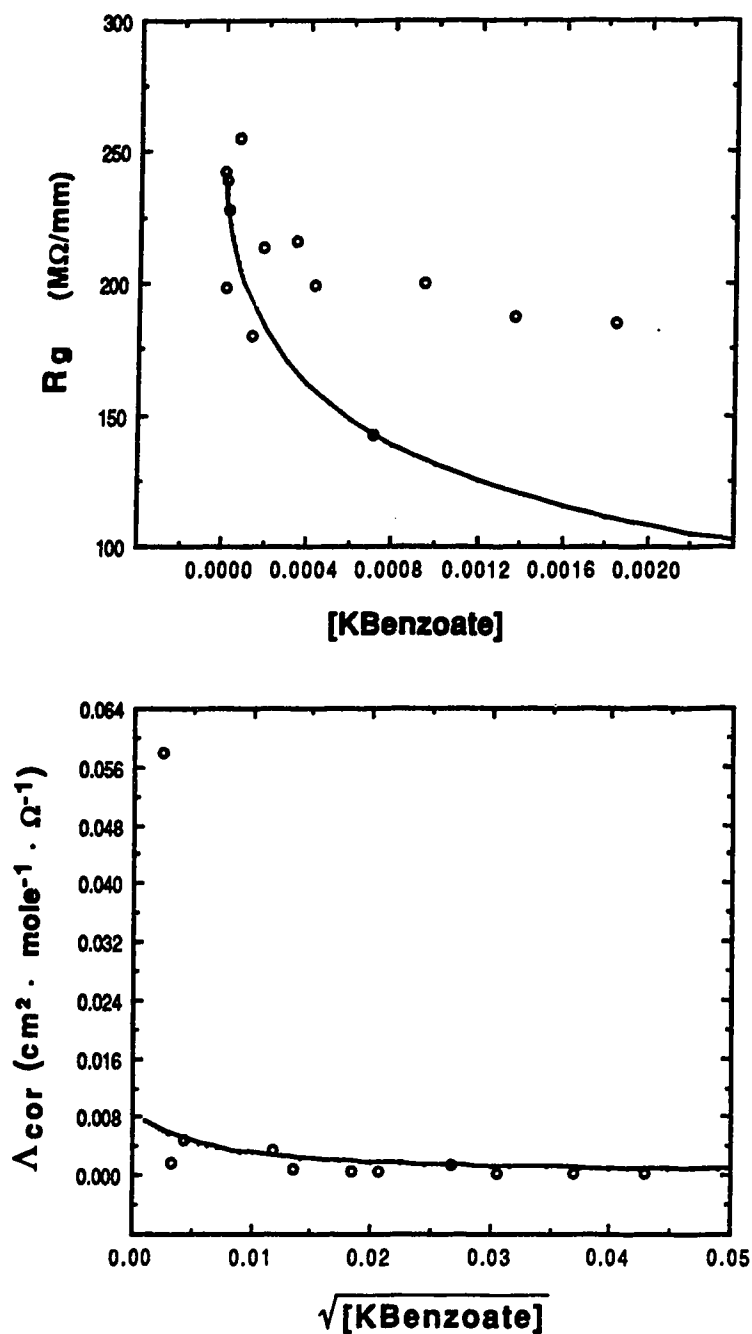


Figure 5.7 Curves of membrane resistance (R_g) vs concentration and corrected conductance (Λ_{cor}) vs the square root of concentration for a series of PVC/DOA membranes containing KBz. Solid curves were calculated using, from Table 5.8, $K_d = 2.15 \times 10^{-5}$, $\Lambda_0 = 0.008$, and $\dot{a} = 6 \text{ \AA}$.

TABLE 5.8: Results of Λ data analysis for data sets given in Tables 5.1 through 5.7

Compound	Matrix	λ (Å)	K_d	$S_{K_d,rel}$ (%)	Λ_0	$S_{\Lambda_0,rel}$ (%)
TEAB	normal	5	2.12×10^{-5}	10	.012	295
KBz (Ser 1)	normal	6	3.51×10^{-5}	4.8	.056	171
KBz (Ser 2)	normal	6	1.87×10^{-5}	15	.031	557
NaBz	normal	4	2.73×10^{-5}	14	.014	545
NaClO ₄	normal	4	1.66×10^{-5}	2.2	.10	59
KBz	PVC/DOA	6	2.15×10^{-5}	28	.008	1010
TEAB	PVC/DOA	8	3.32×10^{-5}	16	.053	632

therefore have units of $M\Omega/\text{mm}$. Included in the tables are values for the weighting function, W_i , calculated using R_g 's for blank membranes from Equation (24), as well as residuals, $\Delta\Lambda_i$, for each Λ_i used in the least squares analysis procedure. As expected, $\Delta\Lambda_i$ for points of lesser weight tend to be quite large relative to their Λ_i , exceeding these latter quantities in some cases and reflecting the greater uncertainty inherent in these points, as discussed above. In these latter cases, however, the amount by which the points are weighted is so much less that these data points will not strongly influence the resulting K_d and Λ_0 .

As indicated in Tables 5.1 through 5.7, not all the data points in each set were used to obtain K_a and L_0 , for several reasons. First of all, the Fuoss equation is applicable at ion concentrations satisfying the condition [21]

$$\kappa a \leq 0.2 \quad (32)$$

where κ , the Debye-Hückel term is defined as

$$\kappa = \sqrt{\frac{8 \pi e^2 N \mu}{1000 \epsilon k T}} \quad (33)$$

μ is equal to ionic strength in Equation (33) and all the other symbols have their usual meanings. Assuming a ϵ of 8 for the membrane and a typical ion size parameter, a , of 4×10^{-8} cm (4 Å), the maximum μ at which the Fuoss conductance function is applicable to these membrane systems is about 2 mM. Though the ion concentrations associated with nominal salt concentrations of 2 mM would be less than the maximum allowable 2 mM, due to significant ion-pairing occurring in the membrane (vide infra), salt concentrations

greater than this generally were not included in the data analysis. In some cases, the concentration ranges over which data sets were fitted to obtain Λ_0 and K_a had upper limits which fell short of 2 mM. In these instances, including all concentrations under the 2 mM limit resulted in the least squares calculation showing divergence of $\Delta\Lambda_0$ and ΔK_a to larger and larger values, or convergence of either K_d or Λ_0 to unrealistic, negative values. The difficulty in obtaining convergence is likely due in part to the solubility limits of the salts being surpassed, with precipitation occurring in the membrane as a consequence. This is consistent with the observation of crystalline precipitates in membranes cast with NaBz or KBz concentrations exceeding a few mM. Membranes exhibiting precipitation of the solute were not examined experimentally. TEAB and NaClO₄ proved to be soluble at higher concentrations in the membrane, due to the lipophilicity of the TEA⁺ and ClO₄⁻ ions.

Accompanying Tables 5.1 to 5.7 are a series of figures, Figures 5.1 to 5.7, for each data set; each figure includes a R_g vs concentration curve, along with a plot of Λ_{cor} vs (concentration)^{1/2}. Conductance and resistance curves calculated from best fit values of K_d and Λ_0 are given as solid lines. Results obtained for TEAB in both normal and PVC/DOA matrices, Figures 5.1 and 5.6, were disappointing. It had been expected that the observed solubility of this salt in the membrane would lead to the acquisition of impedance data sets exhibiting good reproducibility; unfortunately, this was not the case. The resistance curve of TEAB in Figure 5.1 shows a large degree of scatter, as does the conductance curve of Figure 5.6. The observed phenomenon is caused in all likelihood by the extreme hygroscopicity of TEAB. This may have led to TEAB leaching out of the membrane during the one hour soaking period before data acquisition. A second and stronger possibility is that TEAB was

extracted into water droplets in the membrane itself, effectively removing it from the organic phase to become immobilized in these droplets. This latter explanation is quite reasonable, since water is known to enter the membrane [1-3] and droplet formation is indicated by the growth of light scattering centres. Figures 5.2, 5.3, and 5.7 show data obtained for KBz in normal and PVC/DOA matrices. There is good agreement between calculated and experimental values of both R_g and Λ for KBz in the normal matrix over the entire concentration range in Figure 5.2. Calculated resistance curves of Figures 5.3 and 5.7 exhibit a large deviation from observed values at higher concentrations, due in part to the fact that only points at low concentrations were used to determine the K_d and Λ_0 values employed in the generation of these curves. However, the experimentally measured conductance curves in both Figures 5.3 and 5.7 are reasonably well behaved, leading to the conclusion that data in both cases is quite reliable. Calculated conductance curves in these figures show agreement with observed values except at the lowest concentrations, as a result of these points being weighted less in the data analysis. The resistance data for NaBz in the normal matrix, given in Figure 5.4, shows little real dependence on concentration. This is likely the result of the low solubility of NaBz in the membrane, as mentioned above. On the other hand, good agreement between calculated and experimental curves was obtained for NaClO_4 in the normal matrix, Figure 5.5. This was as expected, due to the fact that NaClO_4 was soluble up to relatively high concentrations in the membrane phase. Taken together, then, data reported here for KBz and NaClO_4 may be considered more reliable than that for TEAB and NaBz.

The conductance curves are included in the figures for a couple of reasons, the first being to emphasize the point that the compounds of interest

are indeed all behaving like weak electrolytes in the membrane, undergoing only partial dissociation. Had the opposite been true, a linear relationship between Λ and (concentration)^{1/2} would have been observed at low concentrations, in accordance with Kohlrausch's observation that strong electrolytes have Λ 's in dilute solutions which may be represented by the equation [6]

$$\Lambda = \Lambda_0 - A\sqrt{c} \quad (34)$$

The second reason for presenting these Λ - \sqrt{c} curves is to show that the scatter exhibited by the R_g - c curve is often dampened to a large degree when this data is viewed in terms of conductance. This is particularly true at the higher concentrations, where the Λ - \sqrt{c} curves abruptly level off and little if any variation in Λ is observed as a function of increasing concentration, in contrast with the initial portion of the curve. Because of this leveling off effect, fitting data at higher concentrations within the allowed concentration range to obtain K_d and especially Λ_0 becomes increasingly difficult, which is rather unfortunate as this data should be of higher precision. This may be another factor contributing to the lack of convergence observed when higher concentrations are included in the analysis of some data sets.

Values of K_d and Λ_0 determined from the data sets presented in Tables 5.1 to 5.7 are given in Table 5.8, along with the relative standard deviations calculated for each quantity during the fitting process. It becomes immediately apparent upon consideration of this table that dissociation constants may be worked out with a much higher degree of precision from the conductance data obtained for the various series of membranes than limiting conductances. In fact, the Λ_0 's determined in most cases are qualitative estimates only of this parameter. The reason for this discrepancy lies in the lack of measured Λ data for membranes having concentrations of the added

compounds dilute enough to fall into the concentration ranges over which the respective $\Lambda\text{-}\sqrt{c}$ curves are undergoing rapid change. Because K_d is the constant quantifying the equilibrium that determines the membrane ion concentration at each nominal salt concentration, it directly influences the magnitude of all the terms in the Fuoss Λ equation but one. As salt concentration increases so does the actual ion concentration, so that measured variations in Λ with concentration are a direct result of the K_d governing ion pair dissociation within the membrane. This is particularly true at higher salt concentrations, when observed Λ 's deviate significantly from the limiting behaviour expected at the more dilute concentrations. Λ_0 , on the other hand, only becomes a dominant contributor to measured Λ at the more dilute concentrations, at which data of sufficient precision is hard to obtain in the membrane systems considered in this study. A good example of the problems encountered in determination of Λ_0 's is illustrated by the the data set for KBz in PVC/DOA. Referring to Figure 5.7, it is clear that the low value of Λ_0 observed for KBz in this matrix when compared with the other KBz data sets is a result of the dilute region of the $\Lambda\text{-}\sqrt{c}$ curve being defined by only two points. It is not surprising, then, that the K_d for KBz in PVC/DOA was determined with far more confidence than Λ_0 , as indeed is the case for all compounds examined.

The magnitudes of \dot{a} , the ion size parameter in units of Ångstroms, used in the determination of K_d 's and Λ_0 's, are also presented in Table 5.8. This parameter is a measure of the separation between ions in ion pairs, and since ion pairs having small \dot{a} 's will dissociate less easily than those having larger \dot{a} 's, due to more extensive solvation of ions in the latter case, the value of K_d should depend on \dot{a} . Conductance measurements have been employed to deduce values of \dot{a} as well as K_d and Λ_0 for various salts in nonaqueous

media, using the same method of analysis as in this study [17]. However, fitting of this third variable in our case proved impossible. The choice of λ values was therefore of some concern, especially since the value of J is dependent on this parameter. The decision to use the λ values given in Table 5.8, derived from estimated crystallographic radii for the ions involved, was based on the observed low ϵ of the membrane ($\epsilon = 8$). The radii assumed for Na^+ and K^+ were 0.95 Å and 1.33 Å, respectively [22]. The tetraethylammonium ion (TEA^+) was assigned a radius of 4.0 Å, a value deduced from the various bond lengths and angles in the ion [7]. The value for the ClO_4^- ion is reported to be 2.5 Å [21]. Assigning a radius to the benzoate anion proved more difficult, as no literature source was found. However, the benzoate anion does have λ 's in several solvents which are equivalent to those measured for the TEA^+ ion [21]. Based on this, and on the strength of bond length arguments, a radius of 4 Å was assumed for benzoate. The λ 's used in the fitting procedure were simply the sum of the radii of the ions involved, rounded off to nearest integral values. NaBz and TEAB data acquired in normal membranes were analyzed using λ 's that were smaller than estimated, as these data sets did not show convergence when larger λ values were tried. A value of 8 Å estimated for the λ of TEAB was used successfully for PVC/DOA matrix data, as shown in Table 5.8.

The validity of employing the above radii in the analysis was tested by carrying out the determination of K_d and Λ_o for several data sets over a range of λ varying from a value of 3 Å to a maximum of 30 Å. Results of K_d and Λ_o obtained at several representative λ 's are given in Table 5.9. It was also possible to calculate predicted values of K_d over this range of λ , using the following expression derived by Fuoss [23]:

$$K_d^{-1} = (4000 \pi N a^3/3) \exp(|z_1 z_2| e^2/4 \pi \epsilon_0 \epsilon_r a k T) \quad (35)$$

where a is the ion size parameter in meters, ϵ_r is the relative dielectric constant of the membrane, and the other symbols have their usual significance (in SI units). The predicted K_d values that result when Equation (35) is evaluated at an ϵ_r of 8 and over a range of \hat{a} are shown in Table 5.10. The data in this table demonstrate that the magnitude assumed by \hat{a} is expected to strongly influence the dissociation of salts in the membrane, especially in the 3 Å to 6 Å range. The predicted value of K_d increases by approximately four orders of magnitude for a doubling of \hat{a} from 3 Å to 6 Å. In contrast, experimentally observed K_d 's increase by at most a factor of 3 over the 3 to 30 Å range. In particular, values of K_d determined for TEAB in PVC/DOA do not change much, which suggests that use of an \hat{a} which is smaller than the estimated 8 Å for normal membrane data of this salt should not result in a large error in the extrapolated value of K_d .

The fact that determination of experimental K_d 's is relatively unaffected by the choice of \hat{a} confirms that the J term acts primarily as a correction term in the Fuoss equation for Λ . Of the two terms that are first order in αc , $J\alpha c$ and $K_a \Lambda_{cor} f^2 \alpha c$, it can be shown that the term involving K_a (K_d^{-1}) is generally significantly larger than the J term at low concentrations in these membrane systems, with the result that separation of the two terms may prove difficult. Table 5.11 compares the relative magnitudes of the two terms calculated using the K_d and Λ_0 measured for the second normal membrane data set for KBz. \hat{a} was assigned a value of 6 Å, as estimated from the ionic radii of K^+ and Bz^- . At concentrations below 1×10^{-4} M, the K_a term is about an order of magnitude larger than the J term, so that the former dominates, and the value that \hat{a} assumes is relatively unimportant in analysis

TABLE 5.9: Variation of experimentally determined K_d 's and Λ_o 's with λ for KBz and TEAB in normal and PVC/DOA matrices

Cmpd	TEAB		KBz (Series 2)		KBz	
	PVC/DOA		normal		PVC/DOA	
λ (Å)	K_d	Λ_o	K_d	Λ_o	K_d	Λ_o
3	2.98×10^{-5}	.056	1.70×10^{-5}	.032	1.99×10^{-5}	.008
4	3.06×10^{-5}	.055	1.76×10^{-5}	.032	2.05×10^{-5}	.008
5	3.14×10^{-5}	.054	1.82×10^{-5}	.031	2.10×10^{-5}	.008
6	3.21×10^{-5}	.054	1.87×10^{-5}	.031	2.15×10^{-5}	.008
10	3.43×10^{-5}	.052	2.05×10^{-5}	.030	2.31×10^{-5}	.007
15	3.65×10^{-5}	.050	2.24×10^{-5}	.028	2.48×10^{-5}	.007
20	3.85×10^{-5}	.049	2.43×10^{-5}	.028	2.64×10^{-5}	.007
30	4.22×10^{-5}	.047	2.78×10^{-5}	.026	2.96×10^{-5}	.007

TABLE 5.10: Values of K_d predicted using Equation (35), at $\epsilon_r = 8$ for the membrane

\dot{a} (Å)	K_d
3	1.06×10^{-9}
4	1.53×10^{-7}
5	2.61×10^{-6}
6	1.56×10^{-5}
7	5.20×10^{-5}
8	1.22×10^{-4}
9	2.26×10^{-4}
10	3.59×10^{-4}
15	1.10×10^{-3}
20	1.49×10^{-3}
30	1.42×10^{-3}

TABLE 5.11: A comparison of the relative magnitudes of the $J\alpha c$ and $K_a\Lambda f^2\alpha c$ terms of the Fuoss equation over a range of concentrations. These were calculated using $K_d = 1.87 \times 10^{-5}$ and $\Lambda_0 = 0.0307$, found for the second series of normal membranes containing KBz. The full equation for J is given in Chapter 1. λ was assigned a value of 6 Å. Λ reported here is the calculated value.

Conc'n (mole/L)	Λ ($\text{cm}^2\text{mol}^{-1}\Omega^{-1}$)	f	α	$J\alpha c$	$K_a\Lambda f^2\alpha c$
.00002 M	.0191	.881	.650	.000504	.0103
.00004	.0158	.849	.544	.000844	.0133
.00006	.0139	.829	.484	.00113	.0148
.00008	.0126	.813	.444	.00138	.0158
.0001	.0116	.800	.414	.00161	.0164
.0002	.00902	.756	.331	.00257	.0183
.0004	.00687	.706	.263	.00408	.0193
.0006	.00583	.674	.230	.00535	.0195
.0008	.00517	.649	.209	.00648	.0195
.001	.00471	.629	.195	.00756	.0195

of the data. While the J term appears to become increasingly important at higher concentrations, the K_a term may be considered to be more significant over concentration ranges considered in this study. This weak dependence of the Fuoss conductance function on \hat{a} provides a partial explanation for the previous observation that obtaining a value for \hat{a} as well as for K_d and Λ_0 using the proposed fitting procedure proved impossible in our case. On the other hand, the expression for K_d given in Equation (35) shows a strong functional dependence on the parameters ϵ_r and \hat{a} , as shown in Table 5.10. Hence, experimental evaluation of K_d through the Fuoss conductance function and calculation of K_d via Equation (35) using estimated \hat{a} may be regarded as two independent routes to a value of K_d . Comparison of K_d 's obtained using both approaches show that K_d values predicted by Equation (35) fall within at least the same order of magnitude as those found experimentally, with closer agreement between measured and predicted values for several of the data sets. Exceptions to this are found for NaClO_4 and NaBz , whose data sets yield K_d 's which would require slightly larger \hat{a} values to be used in Equation (35) than those proposed through use of the crystallographic radii. However, use of crystallographic data for \hat{a} gives reasonable agreement between theoretical and experimental values of K_d . Application of the Fuoss conductance equation to impedance data measured for salts in PVC-based liquid membranes appears to yield realistic values of K_d for these systems.

The K_d 's of the four salts considered all fall in the 1×10^{-5} to 4×10^{-5} range for normal and PVC/DOA systems. The quality of the original impedance data precludes differentiation between these K_d values based on matrix effects or, in the case of the benzoate salts studied, on the identity of the cation involved. Nonetheless, it can be concluded that the factors

governing the dissociation process of all four salts are for all practical purposes the same, and that matrix composition has no effect on this. The experimentally observed K_d 's are of the same order of magnitude as those measured for certain salts in less viscous non-aqueous solvents having similar dielectric constants [21]. For instance, the tetraphenylborate salts of Na^+ , K^+ , and NBu_4^+ have K_d 's of 8.3×10^{-5} , 3.2×10^{-5} , and 4.3×10^{-5} , respectively, in THF, a solvent which has a ϵ of 7.6. The K_d 's measured in both membrane systems are consistent, then, for a solvent which has a low dielectric constant.

Not much information is available in the literature as to the dissociation behaviour of salts in PVC/plasticizer systems, the one exception being due to Armstrong et al. [24]. In this study, consideration was given to the behaviour of the tetraphenylborate salts of Na^+ , K^+ , and NBu_4^+ in 33 % PVC/66 % dioctylsebecate (DOS), a matrix purported to have a ϵ of 4.8 [25]. The K_d 's for these salts in this system are 2.3×10^{-3} , 5.0×10^{-4} , and 3.8×10^{-4} , respectively, and therefore are about one to two orders of magnitude larger than those measured in this study [24]. There was some suggestion in the case of NaTPB that the large K_d was attributable to PVC playing an active role in the solvation of the ion pair, leading to an estimated \hat{a} of 30 Å and allowing the ion pair to be described as a solvent separated rather than a contact pair [25]. Our data strongly implies, however, that the PVC component of the membrane does not participate in the solvation of ions, since \hat{a} values estimated from ionic radii to determine K_d experimentally and theoretically produced values of K_d that were similar. It is conceivable that the larger radius of the tetraphenylborate ion as compared to the benzoate ion, and the possible weak complexing capabilities of benzoate's carboxyl group, could lead to larger K_d 's being observed for tetraphenylborate salts.

A more plausible reason for the magnitude of these K_d 's reported by Armstrong et al. may well lie in the fact that they were estimated through use of the Ostwald dilution law, which relates Λ to concentration via the mass action law, assuming that α , the degree of dissociation, is equal to (Λ/Λ_0) , to obtain :

$$\frac{1}{\Lambda} = \frac{1}{\Lambda_0} + \frac{c\Lambda}{K\Lambda_0^2} \quad (36)$$

While Ostwald noted that this law was obeyed for a number of organic acids [26], it has long been recognized as being but an approximation for most other compounds, particularly under conditions other than that at the most dilute concentrations. Derivation of the law was based on the assumption that all of the observed change in Λ with concentration is due to a change in α . Ion-ion interactions, which would result in concentration dependent ion mobilities, were not taken into account. The Fuoss equation for associated electrolytes, Equation (5), is generally the equation of choice when probing the variation of Λ with concentration, particularly in non-aqueous systems.

As was the case with K_d , studies reporting values of Λ_0 for salts in plasticized membranes are very scarce. Again, one of the few sources available is the study mentioned above, in which the impedance of membranes containing the tetraphenylborate salts of Na^+ , K^+ , and NBu_4^+ was measured as a function of concentration in a 33 % PVC/66 % DOS matrix [24]. These researchers calculated the molar conductances, Λ_m , which could be expected if the salts were fully dissociated, using a type of Ostwald dilution law relation to first estimate α 's from observed R_g values, and then obtaining values of Λ_m through the relation $\alpha = \Lambda_{\text{obs}}/\Lambda_m$. Because conductance functions of this

sort do not take ion-ion interactions into account, the parameter Λ_m will not be completely analogous to Λ_o . However, values of Λ_m , reported to be 0.121, 0.090, and 0.049 $\text{cm}^2 \text{mol}^{-1} \Omega^{-1}$ for KTPB, NaTPB, and NBu₄TPB, respectively, are comparable to values of Λ_o given in Table 5.8, qualitative though these latter figures are. With the exception of the Λ_o measured for KBz in PVC/DOA, experimentally observed values in this work for Λ_o range from about 0.014 to 0.10, indicating that ions find themselves in a viscous environment. For example, KBz has a Λ_o in water ($\eta = 0.01$ Poise) of 105.9 [7], as compared to its value in the membrane of 0.043. Though no quantitative conclusions can be made about ion mobilities, it would seem upon consideration of data for the benzoate salts that the mobilities of the K⁺, Na⁺, and TEA⁺ cations are not radically different.

5.4.2 Dependence of Conductivity on Temperature

As noted in Chapter 4, ingress of benzoic acid in its neutral form into plasticized PVC/DOA membranes containing valinomycin caused a decrease in measured bulk membrane resistance, R_g . The magnitude of this decrease, in the order of 7 % to 11 %, was found to be no different in membranes containing the lipophilic salt, KTPB, than in membranes cast without this additive. Since conductivity in plasticized PVC membranes has been shown to be due to ionic charge carriers rather than to electrons [27], these results suggest that benzoic acid is acting in some way to increase the number of ions in the membrane, thereby increasing the observed conductivity. One obvious possibility is that the acid is undergoing acid dissociation within the membrane. The equilibrium constant governing this process would be expected to be very small, given that the membrane is a low dielectric

medium. In lieu of, or in addition to, the occurrence of acid dissociation, benzoic acid may be acting as a chelating agent to complex cations within the membrane, thought primarily to be K^+ or Na^+ . The presence of carboxyl groups in a molecule like ethylenediaminetetraacetic acid (EDTA) gives this well known chelating agent the ability to form stable complexes with a variety of cations. It is possible, then, that the benzoic acid, with its carboxyl group, could be involved in the formation of complexes with cations. It was of interest to us to determine which of the processes discussed above is predominantly responsible for increased conductivity in membranes containing benzoic acid, in the presence or absence of KTPB. To this end, a study of the temperature dependence of membrane conductivity was undertaken, in order to identify the charge generation process under various conditions, and to quantify the parameters characterizing it.

A general expression for conductivity, σ , is given in the following expression (already presented as Equation (2)) :

$$\sigma = \sum q_i n_i u_i \quad (37)$$

where q_i is the charge of the i^{th} charge carrying species; n_i is the number of the i^{th} species present; and u_i is the mobility of the i^{th} species. Measurements of σ as a function of temperature yielded results that conformed to an Arrhenius-type relationship between σ and T :

$$\sigma = \sigma_0 e^{(-E_a/kT)} \quad (38)$$

where E_a is an experimentally measurable activation energy, and k and T have their usual meanings. This relationship between σ and T has long been recognized for both polymers [28] and semiconducting organic substances [29], and has been employed to explain the observation of increased conductivity in these substances at elevated temperatures. Carmack and Freiser [27] found Equation (38) to be applicable to plasticized PVC membranes as well, using it

to describe the temperature dependence of the conductivity of various matrices containing Aliquat-Cl. The source of increased conductivity in the plasticized PVC membranes being considered is assumed to be both an increase in the number of ions in the membrane, and enhanced mobility of these ions at higher temperatures, in accordance with Equation (37). Since the number of ions within a membrane at a given temperature will be governed by a dissociation constant, K_d , the increase in this number with temperature follows an Arrhenius-type relationship with a positive activation energy. The increase in ion mobility, u , with temperature, which is dependent on decreasing membrane viscosity, may also be described by an exponential function, and is characterized by an activation energy. That this should be the case is supported by reports in the literature [30], which found that diffusion coefficients, D , for plasticizers and small molecules in plasticized PVC membranes may be well represented as a function of temperature using Equation (39), where

$$D = D_0 e^{(-E_D/kT)} \quad (39)$$

and E_D is the activation energy for the diffusion process. Given that D for an ion of valence z may be related to its mobility through the Nernst-Einstein formula (i.e. $D = (RT/zF) u$), it is reasonable that u should also vary with temperature in an Arrhenius-type manner. This, then, allows a reworking of Equation (38), to obtain Equation (40) [27]:

$$\sigma = q n_0 e^{(-E_c/2kT)} u_0 e^{(-E_u/kT)} \quad (40)$$

where n_0 represents the number of dissociable species initially present, E_c is the activation energy of carrier generation, and E_u is the activation energy of carrier mobility. The factor of 2 associated with E_c arises from the fact that two ions result from every dissociation.

Comparing Equation (38) with Equation (40), it is apparent that the experimentally measured E_a is actually comprised of two terms :

$$E_a = \frac{E_c + 2E_u}{2} \quad (41)$$

Therefore, characterization of the ion generation process by which benzoic acid increases the membrane σ should be possible through the evaluation of E_a , as long as E_u is not so large as to overwhelmingly determine the magnitude of E_a , thereby masking any significant variations in E_c .

The observed σ of membranes containing more than one dissociable entity may be described as a sum of the individual σ 's due to each component, based on the assumption that there is no chemical interaction between species. In this situation, Equation (38) assumes the following form :

$$\sigma = \sum \sigma_{0,i} e^{(-E_{a,i}/kT)} \quad (42)$$

The σ for a membrane with benzoic acid may be expressed as the sum of two terms, as discussed earlier, so that

$$\begin{aligned} \sigma_{obs} &= \sigma_{0\%} + \sigma_{HBz} \\ &= \sigma_{0,0\%} e^{(-E_{0\%}/kT)} + \sigma_{0,HBz} e^{(-E_{HBz}/kT)} \end{aligned} \quad (43)$$

The σ term subscripted by "0%" is due to the membrane itself, and arises from the presence of weakly dissociable sites and impurities within this matrix. The second term, subscripted using "HBz", represents the contribution to σ_{obs} by the acid.

The results for a temperature study carried out on portions of PVC/DOA membrane with and without benzoic acid are presented in Table 5.12. AC impedance experiments were carried out over a relatively narrow range of temperatures, from about 5 °C to 40 °C, a range over which K^+ -selective ISE's made from PVC/DOA membranes containing valinomycin are

TABLE 5.12: Conductivity as a function of temperature for benzoic acid in PVC/DOA

Temp. (°C)	σ_{obs} (0.0667 M Benzoic Acid)		$\sigma_{0\%}$ (Blank Membrane)		σ_{HBz}
	R _g (MΩ)	σ (Ω · cm) ⁻¹ (× 10 ⁹)	R _g (MΩ)	σ (Ω · cm) ⁻¹ (× 10 ⁹)	σ (Ω · cm) ⁻¹ (× 10 ⁹)
5.7	391	.180	248	.165	.015
12.6	239	.294	153	.268	.026
19.6	145	.485	93.5	.439	.046
25.1	111	.633	68.3	.601	.032
32.9	71.3	.987	44.5	.923	.064
39.6	47.3	1.49	30.8	1.33	.160
$E_{0\%} = .46 \text{ eV} \pm .05$ $\sigma_0 = .036 (\Omega \cdot \text{cm})^{-1}$					$E_{\text{HBz}} = 0.47 \text{ eV} \pm .07$ $\sigma_0 = .0052 (\Omega \cdot \text{cm})^{-1}$

functional. However, the effect of temperature on R_g even over this narrow range is quite dramatic, as shown by R_g values given in Table 5.12, and more clearly demonstrated by the Nyquist plot of Figure 5.8. This Nyquist plot of data obtained for the membrane containing 0.0667 M benzoic acid in Table 5.12 indicates that the R_g , can drop by more than 80 % from its value at 5 °C to its value at 40 °C.

Values of σ_{obs} , given in Table 5.12, were measured for a PVC/DOA membrane containing 0.0667 M benzoic acid. A second membrane, cast from the same membrane stock solution but with no acid added, served as the blank. Values of its impedance determined at different temperatures yielded the values of $\sigma_{0\%}$ given in Table 5.12. σ_{HBz} was obtained by subtraction of $\sigma_{0\%}$ from σ_{obs} , in agreement with Equation (43). Values of the E_a 's associated with the matrix and acid components of σ_{obs} , calculated from the $\ln \sigma$ vs $1/T$ plots corresponding to these data sets, are also presented. The plots themselves appear in Figure 5.9. Clearly there is a linear relationship between $\ln \sigma$ and $1/T$, indicating that Equation (38) is an appropriate description of the effect of temperature on membrane conductivity. The E_a 's measured for the PVC/DOA matrix and the acid are both around 0.5 eV, and are comparable to values reported by Carmack and Freiser [27] for PVC films loaded with the quaternary ammonium salt, Aliquat-Cl.

Before any firm conclusions can be drawn from the E_a values in Table 5.12, some consideration must be given to the relative contributions of the energy terms E_c and E_u to the overall E_a 's reported here. While a distinct differentiation of the two contributing energies is not possible, some comment can be made as to the approximate magnitude of E_u as compared to E_a . As mentioned earlier, an Arrhenius relationship similar to Equation (38) for σ has been shown to apply to diffusion of small molecules through

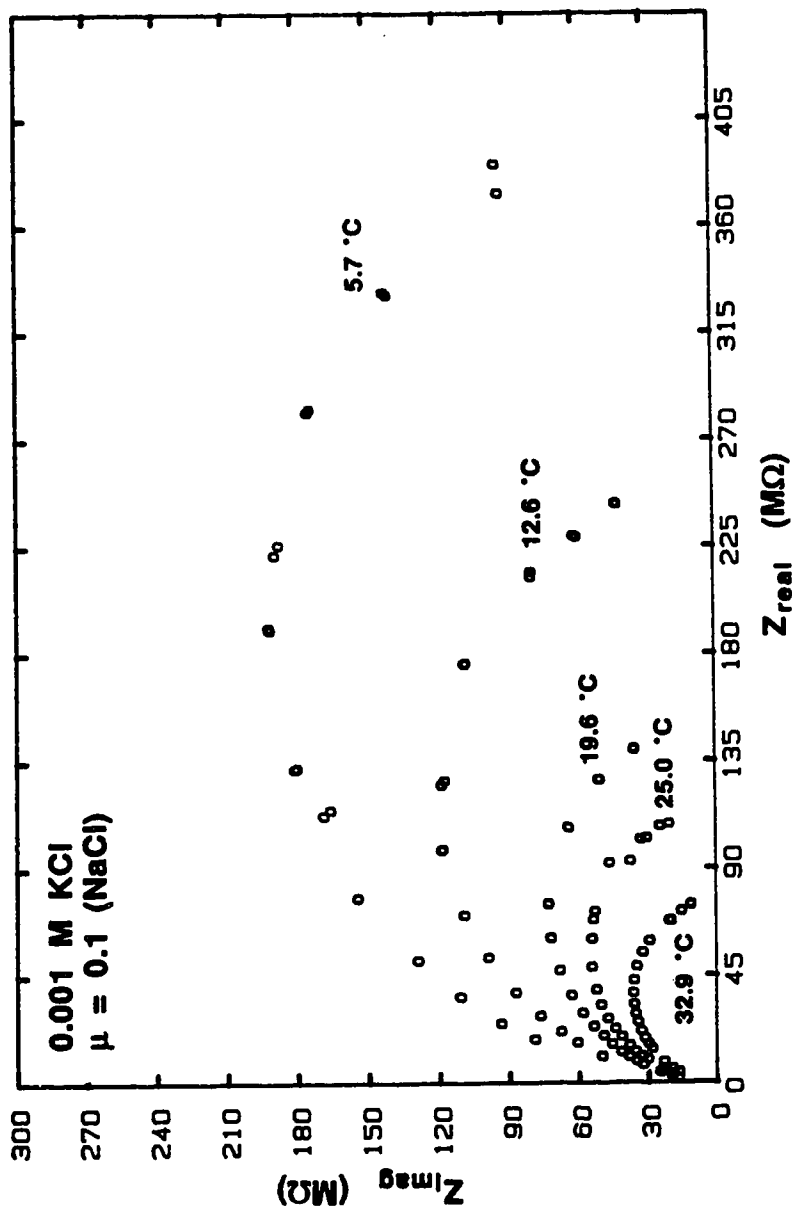


Figure 5.8

Nyquist plot showing the effect of temperature on membrane impedance in a 10^{-3} M KCl ($\mu = 0.1$ (NaCl)) for a PVC/DOA membrane containing 0.0667 M benzoic acid. Conductivity measured as a function of temperature for this membrane is given in Table 5.12. As temperature is decreased, R_g increases, and the frequency, ω_{max} , at which the semicircle has its maximum value, decreases, indicating a corresponding increase in the time constant, τ , associated with the membrane.

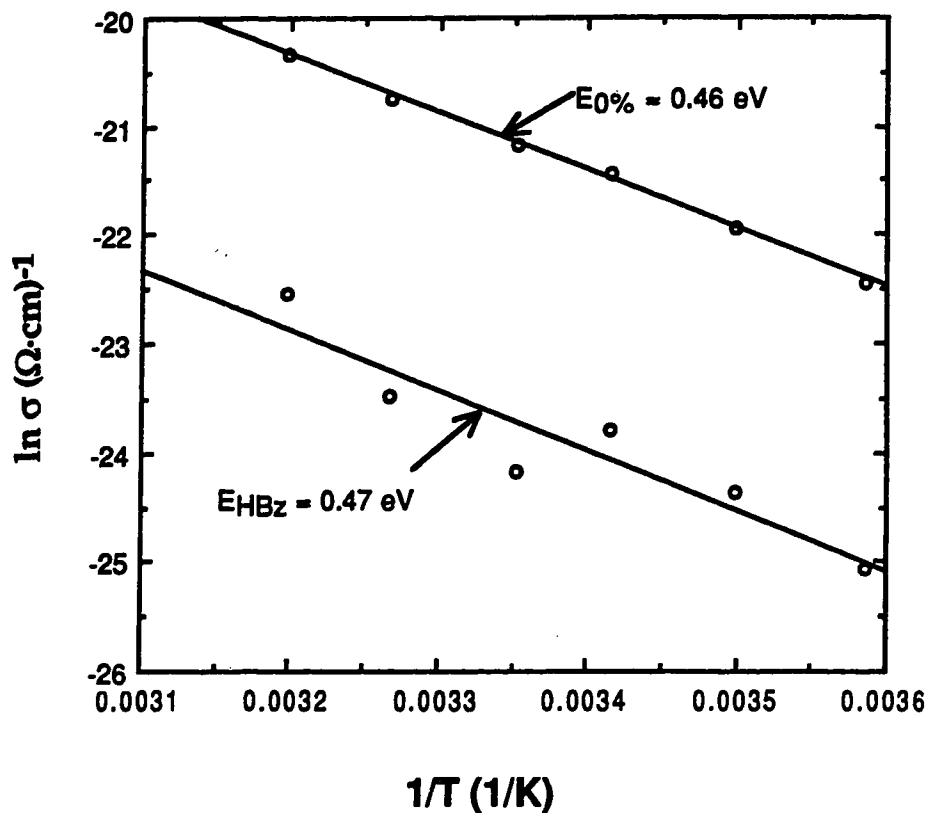


Figure 5.9 $\ln \sigma$ vs $1/T$ plots for the benzoic acid-containing PVC/DOA membrane of Figure 5.8 and the corresponding blank membrane. Activation energies $E_{0\%}$, for the membrane matrix, and E_{HBz} , for benzoic acid in the membrane, were found from the slopes of these curves to be the same within experimental error. The curve for HBz shows more scatter than that for the blank membrane, due to the fact that σ_{HBz} is not a directly measured quantity, whereas $\sigma_{0\%}$ is.

plasticized polymer films (see Equation (39)). Since the D and u of a species are closely related, and in fact the two quantities characterize the same process, it is expected that E_u and E_D will have very similar magnitudes. The results of measurements of diffusion coefficients, D , and the associated activation energies, E_D , calculated therefrom, have been reported for PVC membranes plasticized with dialkylphthalate plasticizers of the form $C_6H_4(COOC_nH_{2n+1})_2$, where n ranged from 4 to 10 [30]. As an example, membranes cast with 29 % to 50 % didecylphthalate (DDP) yield E_D values for diffusion of *n*-hexadecane which vary from 0.76 eV at 29 % DDP to 0.37 eV at 50 % DDP. D 's reported for various ions in plasticized PVC membranes having a 2 : 1 composition of plasticizer to PVC have values in the 10^{-8} to 10^{-7} cm^2/s range [2,25], comparable to D 's measured for the neutral species discussed above [30]. Therefore, it is reasonable to assume that E_u for the membranes in this study would have a magnitude similar to or less than that reported for membranes containing 50 % DDP. That being the case, it appears that E_u may be the major contributor to the E_a 's given in Table 5.12, with E_c having a smaller but still significant magnitude.

A comparison of the E_a values in Table 5.12 shows that these values are the same, within experimental error, for the membrane and benzoic acid in the membrane. This implies that the mechanism of ion generation in the blank PVC/DOA membrane is similar to that associated with the acid. The σ of blank membranes is due to ionic impurities whose charge is balanced by positive counterions, such as Na^+ . Increased dissociation of these weakly dissociable sites, and the correspondingly increased mobility of the resulting free counterions, accounts for the higher σ observed in blank PVC/DOA membranes at higher temperatures. The observation of an E_{HBz} which is equivalent to $E_{0\%}$ suggests that acid dissociation is the primary process by

which benzoic acid adds to membrane ionic strength. The addition of benzoic acid to the matrix may be regarded as simply augmenting the number of weakly dissociable "sites".

Studies of the temperature dependence of σ in PVC/DOA/KTPB membranes with and without benzoic acid or methyl benzoate were also carried out; the results are presented in Tables 5.13(a) and (b). Again, the blank membrane examined in each case was cast from the same membrane stock solution as the membrane containing additive. The KTPB concentration in these membranes is about 0.3 mM, in accordance with that of regular K^+ -selective membranes cast in our laboratory. The purpose of these experiments was to ascertain if the presence of KTPB in the matrix would cause benzoic acid to enhance ion generation in the membrane through chelation of K^+ as well as through acid dissociation. The decision to examine a membrane to which methyl benzoate rather than benzoic acid had been added is based primarily on the supposition that although methyl benzoate cannot undergo dissociation as benzoic acid does, the two species are potential chelating ligands for K^+ , the acid because of its carboxyl group, the ester because of its -COOR group. It was thought that methyl benzoate could perhaps associate with K^+ in a fashion similar to DOA, which imparts a slight selectivity for K^+ over Na^+ in membranes lacking valinomycin and KTPB. Addition of methyl benzoate also serves to test for the effect of additives on membrane viscosity, which would result in concentration-dependent diffusion coefficients.

Generally speaking, the σ 's of the PVC/DOA/KTPB membranes considered, whether blank or containing the acid or ester, are about an order of magnitude greater than that of the PVC/DOA membranes considered earlier. This is due to the presence of KTPB, which is itself undergoing dissociation, and is thereby increasing the membrane ion concentration

TABLE 5.13: Conductivity as a function of temperature for benzoic acid and methyl benzoate in PVC/DOA/KTPB

5.13 (a) Benzoic Acid

Temp. (°C)	σ_{obs} (0.0713 M Benzoic Acid)		$\sigma_{0\%}$ (Blank Membrane)		σ_{HBz}
	R_g (M Ω)	σ ($\Omega \cdot \text{cm}$) ⁻¹ ($\times 10^9$)	R_g (M Ω)	σ ($\Omega \cdot \text{cm}$) ⁻¹ ($\times 10^9$)	σ ($\Omega \cdot \text{cm}$) ⁻¹ ($\times 10^9$)
5.6	6.85	9.80	15.3	4.97	4.83
13.1	4.40	15.3	8.76	8.69	6.61
25.1	1.93	34.8	3.92	19.4	15.4
31.4	1.41	47.6	2.35	32.4	15.2
38.1	1.05	64.2	2.10	36.3	27.9
			$E_{0\%} = .47 \text{ eV} \pm .04$ $\sigma_0 = 1.6 (\Omega \cdot \text{cm})^{-1}$		$E_{HBz} = 0.39 \text{ eV} \pm .04$ $\sigma_0 = .058 (\Omega \cdot \text{cm})^{-1}$

TABLE 5.13: Conductivity as a function of temperature for benzoic acid and methyl benzoate in PVC/DOA/KTPB (cont'd)

5.13 (b) Methyl Benzoate

Temp. (°C)	σ_{obs} (0.0434 M Methyl Benzoate)		$\sigma_{0\%}$ (Blank Membrane)		σ_{MeBz}
	R_g (M Ω)	σ ($\Omega \cdot \text{cm}$) ⁻¹ ($\times 10^9$)	R_g (M Ω)	σ ($\Omega \cdot \text{cm}$) ⁻¹ ($\times 10^9$)	σ ($\Omega \cdot \text{cm}$) ⁻¹ ($\times 10^9$)
6.2	2.97	11.3	5.64	10.3	1.00
15.2	1.70	19.8	2.97	19.7	.100 a)
24.6	.721	46.6	1.40	41.8	4.80
31.1	.598	56.2	1.09	53.5	2.70
38.2	.394	85.4	.724	80.6	4.80
			$E_{0\%} = .47 \text{ eV} \pm .01$ $\sigma_0 = 3.1 (\Omega \cdot \text{cm})^{-1}$		$E_{\text{MeBz}} = 0.35 \text{ eV} \pm .14$ $\sigma_0 = .0021 (\Omega \cdot \text{cm})^{-1}$

a) This value of σ_{MeBz} was not used in the determination of E_{MeBz}

relative to a PVC/DOA membrane [24]. Again, the main observation that can be made about the E_a values in Table 5.13 is that the E_a values associated with the contributions of benzoic acid or methyl benzoate to overall σ are the same as that of the membrane matrix. Utilizing an argument similar to that presented above for the benzoic acid in PVC/DOA case, it does not appear that benzoic acid or methyl benzoate is acting as a chelating agent even when K^+ is already present in the membrane. The data then suggests that benzoic acid contributes to increased membrane σ primarily through acid dissociation. The fact that methyl benzoate does not appear to contribute to the ion generation process at all supports this assertion. It also appears that the variation of membrane viscosity with temperature may be described by the same E_u whether methyl benzoate is present or not, so that membrane viscosity is not significantly altered by the presence of additives.

5.4.3 Membrane Resistance as a Function of Benzoic Acid Concentration : Matrix Effects

In conjunction with the temperature study described above, the variation of R_g with concentration of benzoic acid was measured in different membrane matrices. Results for two such studies, one carried out in PVC/DOA/KTPB, the other in PVC/DOA/KTPB/valinomycin, are given in Tables 5.14 and 5.15, and in Figures 5.10 and 5.11, respectively. It is evident that R_g is not a monotonic function of acid concentration in either matrix, strongly suggesting that the dissociation of benzoic acid is effecting changes of some kind in the membrane over certain concentration ranges in the different matrices. In this section, the possible factors determining the

TABLE 5.14: Bulk membrane resistances measured for benzoic acid in PVC/DOA/KTPB

[Benzoic Acid]	R _g (MΩ/mm)
0 M	13.4
1.01 × 10 ⁻⁴	9.05
2.39 × 10 ⁻⁴	8.98
5.38 × 10 ⁻⁴	7.87
8.49 × 10 ⁻⁴	8.34
2.24 × 10 ⁻³	9.31
4.69 × 10 ⁻³	13.3
7.34 × 10 ⁻³	11.7
9.03 × 10 ⁻³	13.8
2.16 × 10 ⁻²	9.91
4.71 × 10 ⁻²	7.64
7.13 × 10 ⁻²	6.98
8.22 × 10 ⁻²	7.86

TABLE 5.15: Bulk membrane resistances measured for benzoic acid in two series of normal membranes; these two series differ because different membrane stock solutions were used in the preparation of each series

[Benzoic Acid] (Series 1)	R _g (MΩ/mm)	[Benzoic Acid] (Series 2)	R _g (MΩ/mm)
0 M	25.6	0 M	20.3
8.73 × 10 ⁻³	23.3	1.04 × 10 ⁻³	19.3
1.71 × 10 ⁻²	22.4	4.04 × 10 ⁻³	16.7
3.35 × 10 ⁻²	22.7	3.12 × 10 ⁻²	17.8
6.70 × 10 ⁻²	20.6	5.26 × 10 ⁻²	18.3
1.02 × 10 ⁻¹	17.9	7.49 × 10 ⁻²	15.5
1.34 × 10 ⁻¹	15.7	8.34 × 10 ⁻²	14.3

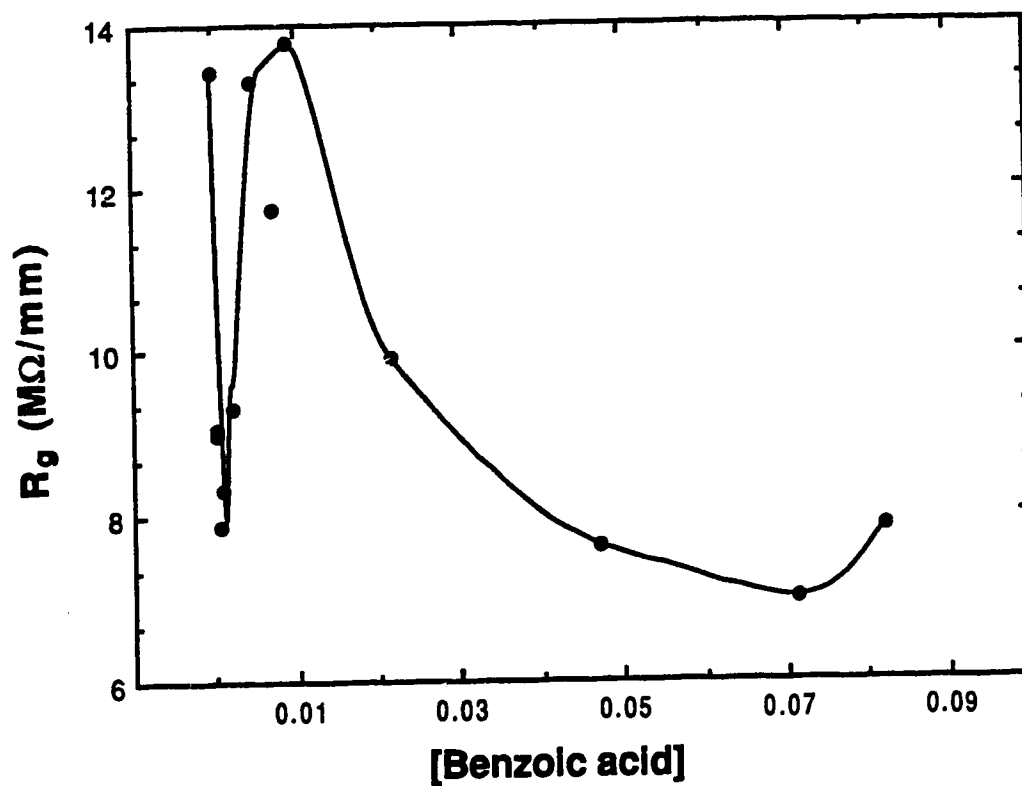


Figure 5.10 Plot of R_g vs concentration for benzoic acid in PVC/DOA/KTPB, showing the effect of benzoic acid on membrane impedance in this matrix. The solid curve in this plot is for clarity only.

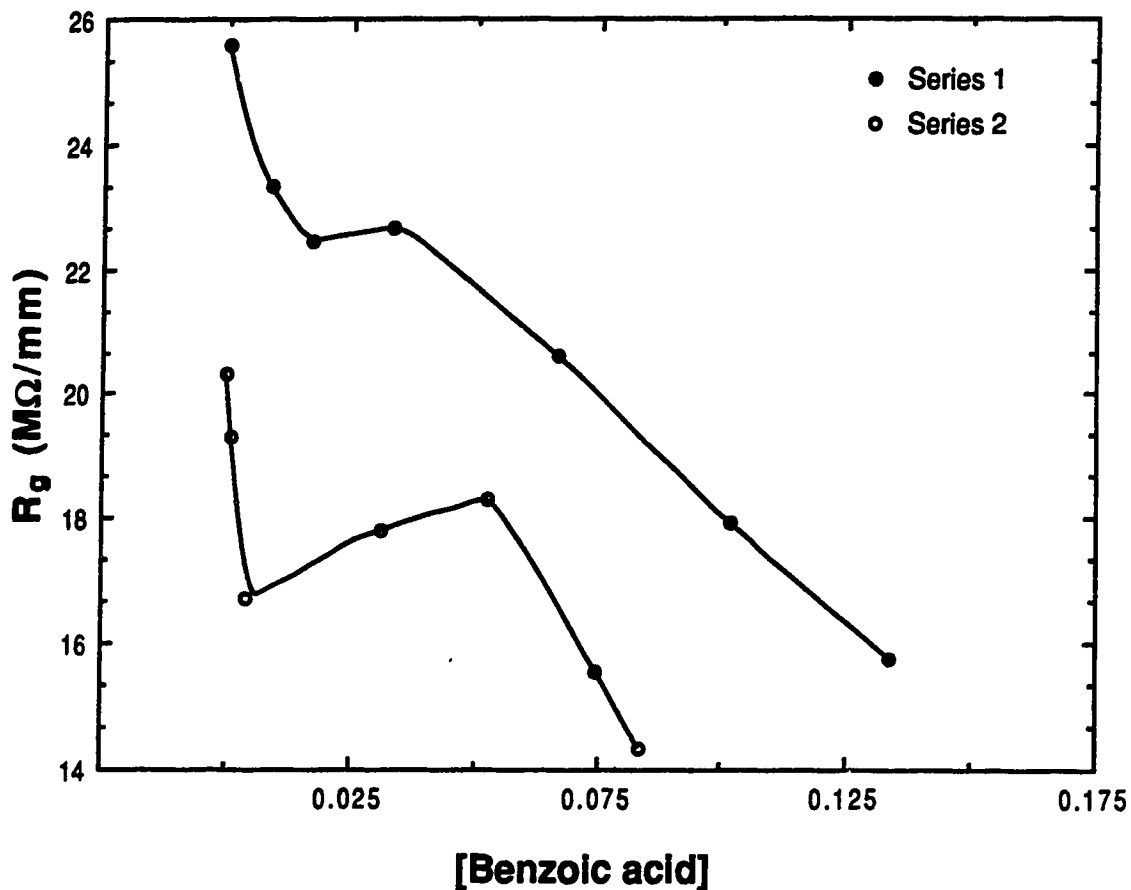
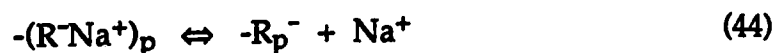


Figure 5.11 Plot of R_g vs concentration for benzoic acid in the normal matrix, showing the effect of benzoic acid on membrane impedance in this matrix. Results for two series of membranes is shown; these membranes differ in that different stock membrane solutions were used to prepare each series. Note that solid lines are for clarity only.

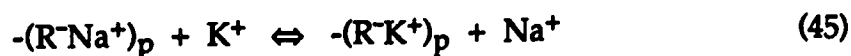
magnitude of R_g in the different regions of the various curves will be examined.

The R_g curve obtained for benzoic acid in the PVC/DOA/KTPB matrix exhibits an initial decrease, as might be expected upon addition of a weakly dissociable acid. At a concentration of about 1 mM, however, this quantity begins to increase with increasing acid concentration, and continues to do so up to a concentration of about 5 mM and an R_g which is roughly equivalent to that measured for the blank membrane. At this point the trend is reversed, and the curve undergoes a decline with concentration. The behaviour of R_g at concentrations less than 5 mM is unexpected, particularly since earlier studies have shown that ingress of benzoic acid from an aqueous solution into a membrane generally causes a decrease in this parameter.

As has been discussed previously, the membrane contains a measurable concentration of weakly dissociable ion exchange sites ranging from 0.05 mM to 0.6 mM [31,32]. These are thought to be mostly in the Na^+ form, as determined from atomic absorption studies [31]. Therefore, the σ of a PVC/DOA membrane is controlled by the equilibrium



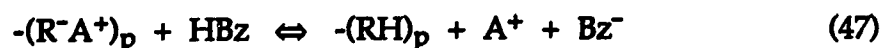
where the subscript p refers to the polymer. In a membrane containing KTPB as an additional component, a substantial contribution to membrane σ stems from the dissociation of this salt, as indicated by the approximately one order of magnitude increase in σ measured for membranes containing 0.3 mM KTPB as compared to the σ measured for blank PVC/DOA membranes. With K^+ present in the matrix, some competition will occur for the fixed ion exchange sites; this exchange may be expressed as shown below.



Inclusion of benzoic acid means that a third contribution to membrane σ should be accounted for, namely that due to dissociation of the acid i.e.



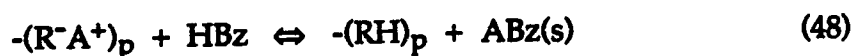
In addition, one can imagine an increased competition for ion exchange sites upon introduction of protons into the membrane, since these weakly acidic sites will have a relatively strong affinity for protons. This exchange may be pictured as follows:



where A^+ may be Na^+ or K^+ .

The equilibria given in Equations (44) and (46) depict processes which result in a net gain of ions. In the equilibrium of Equation (47), the extent of dissociation of the $(\text{RH})_p$ group is expected to be less than that of $(\text{R}^-\text{A}^+)_p$, due to the weakly acidic nature of the $(\text{RH})_p$ group. Whether the conductivity increases, decreases, or remains constant will depend on the relative dissociation equilibria of $(\text{R}^-\text{A}^+)_p$ and A^+Bz^- . Ion concentration is maintained in the process of Equation (45). As such, these equilibria provide a reasonable description of the PVC/DOA/KTPB membrane matrix for the initial region of the R_g curve given in Figure 5.10, over which R_g decreases as a function of benzoic acid concentration. At concentrations ranging from 1 mM to 5 mM, however, the observed increase in R_g implies a net loss of charge carriers. This requires the invocation of another process by which ions are removed from participation in current conduction. In the discussion concerning the behaviour of benzoate salts of Na^+ and K^+ , the low solubility of these compounds, particularly NaBz , in the membrane was noted. The process by which ion concentration is decreased in the membrane is then likely to be one of precipitation. As shown in Equation (47), Na^+ and K^+ ions are produced along with Bz^- in the protonation of ion exchange sites. At benzoic

K^+ ions are produced along with Bz^- in the protonation of ion exchange sites. At benzoic acid concentrations below 1 mM, the concentration of these ions is low enough that they remain mostly solubilized in the membrane. It is reasonable to assume, however, that at higher concentrations, the concentration of the benzoate salt produced by the equilibrium of Equation (47) will be such that the membrane cannot support it. Under this condition, Equation (47) may be restated as



where ABz is either NaBz or KBz. Equation (48) provides a representation of the phenomenon which is likely responsible for increasing R_g in the PVC/DOA/KTPB matrix at benzoic acid concentrations between 1 mM and 5 mM. The principle species contributing to σ in Equation (48) is $(R^-A^+)_p$, since its dissociation is reasonably expected to be greater than $(RH)_p$ and HBz. Consequently, as HBz protonates $(R^-)_p$ and ABz precipitates, the σ should decrease and R_g increase. Reactions in which one or more of the products is a sparingly soluble solid tend to proceed mostly in the forward direction. At benzoic acid concentrations exceeding 5 mM, then, most ion exchange sites will be protonated through Equation (48), with any additional benzoic acid contributing to increased membrane σ solely through the acid dissociation shown in Equation (46). The measurement of R_g 's which decrease as a function of increasing acid concentration at concentrations greater than 5 mM implies that acid dissociation dominates in the PVC/DOA/KTPB membrane under these conditions.

While the preceding discussion provides one explanation for the resistance curve of Figure 5.10, it is also possible that changes in water uptake with benzoic acid concentration and water's concomittant complex effects

Figure 5.11 shows results for R_g measurements of two series of normal membranes containing varying amounts of benzoic acid. The two curves represent data acquired for two series of membranes cast from different membrane stock solutions. These curves exhibit a similar type of behaviour to those obtained in the PVC/DOA/KTPB matrix, though the onset of the rise in R_g occurs much later, at a concentration of about 0.025 M, and R_g does not rise as steeply nor to a plateau value which is equivalent to that of the blank membrane. However, this effect is again probably caused by some kind of precipitation phenomenon. Addition of valinomycin to the membrane alters the concentration range over which this effect manifests itself. Valinomycin is present at a concentration of 10 mM, a large excess when compared to the 0.3 mM KTPB and the approximately 0.1 mM fixed site levels in the membrane. As a result, most of the K^+ and Na^+ exists as charged carrier complexes within the membrane [1], so that valinomycin will complicate the equilibria governing both membrane ion concentrations and competition of counterions for the negatively charged fixed sites in membranes lacking valinomycin. More specifically, complexation of Na^+ and K^+ by valinomycin should result in these salts being more soluble in the normal membrane matrix. This would be consistent with a higher membrane proton concentration being necessary for onset of precipitation of the $AvalBz$ to occur through a process analogous to Equation (48), where $Aval^+$ denotes the carrier complex of the cation. At an acid concentration of approximately 40 mM, the R_g curve in Figure 5.11 resumes its monotonic decrease with increasing concentration, presumably because dissociation of the acid becomes the predominant mechanism by which membrane σ is changed.

5.4.4 Evaluation of Λ Data for Benzoic Acid

Tables 5.16 and 5.17 give the impedance data used in the evaluation of K_d and Λ_0 for benzoic acid in PVC/DOA/KTPB and normal membrane matrices. Again, these tables include values for the weighting function as well as residuals for each Λ_j , $\Delta\Lambda_j$. Note that Table 5.16 reports two sets of Λ_{cor} . The set labelled $\Lambda_{cor}(1)$ has been calculated in the usual manner, as described by Equation (18), and has been used to develop the Λ plot presented in Figure 5.12. As shall be described below, the set labelled $\Lambda_{cor}(2)$ has been corrected differently using corrected concentrations. This latter set was used in the fitting procedure to obtain the K_d and Λ_0 of benzoic acid in this matrix. Values for these parameters in both matrices are given at the end of Tables 5.16 and 5.17.

Accompanying Tables 5.16 and 5.17 are Figures 5.12 and 5.13 of Λ versus (concentration)^{1/2} curves for each data set. There is little or no evidence of the non-monotonic dependence of R_g on acid concentration in the Λ curves, in contrast to the original R_g curves given in Figures 5.10 and 5.11. Careful consideration, then, should be given to measured impedances before any type of numerical analysis is carried out, since R_g proves to be a more sensitive indicator of changes in the membrane than does Λ . Both Λ curves exhibit only a narrow concentration range over which dilute solution behaviour is observed (i.e. the steeply rising portion of the curve) after which they both level off abruptly. Λ curves of this general shape are characteristic of carboxylic acids in solvents of low dielectric strength [15].

Summarized in Table 5.16 is data for benzoic acid in the PVC/DOA/KTPB matrix. As discussed above, the initial portion of the R_g curve for this data set, up to a concentration of about 5 mM, demonstrates

TABLE 5.16: R_g and Λ_{cor} data measured for benzoic acid in PVC/DOA/KTPB membranes, plotted in Figure 5.12 and used in least squares analysis; points which were used in the analysis have values of weight and $\Delta\Lambda$ included in the table. λ was assigned a value of 4 Å for the calculation

[Benzoic Acid]	R_g $\left(\frac{M\Omega}{nm}\right)$	$\Lambda_{cor(1)}$ $\left(\frac{cm^2}{\Omega mole}\right)$	[Benzoic acid] _{cor}	$\Lambda_{cor(2)}$ $\left(\frac{cm^2}{\Omega mole}\right)$	$\Delta\Lambda$	Weight (W)
0 M	13.4					
1.01×10^{-4}	9.05	.126				
2.39×10^{-4}	8.98	.0544				
5.38×10^{-4}	7.87	.0346				
8.49×10^{-4}	8.34	.0189				
2.24×10^{-3}	9.31	.00520				
4.69×10^{-3}	13.3	.0000524				
7.34×10^{-3}	11.7	.000516	2.34×10^{-3}	.00151	-.00032	2.69×10^{-6}
9.03×10^{-3}	13.8					
2.16×10^{-2}	9.91	.000432	1.66×10^{-2}	.000548	-.000132	3.15×10^{-4}
4.71×10^{-2}	7.64	.000424	4.21×10^{-2}	.000468	.000052	3.63×10^{-3}
7.13×10^{-2}	6.98	.000342	6.63×10^{-2}	.000364	.000042	1.03×10^{-2}
8.22×10^{-2}	7.86	.000227	7.72×10^{-2}	.000238	-.000056	1.17×10^{-2}
$K_d = 5.63 \times 10^{-7}$		$\Lambda_o = 0.088$				
$S_{K_d,rel} = 58 \%$		$S_{\Lambda_o,rel} = 79 \%$				

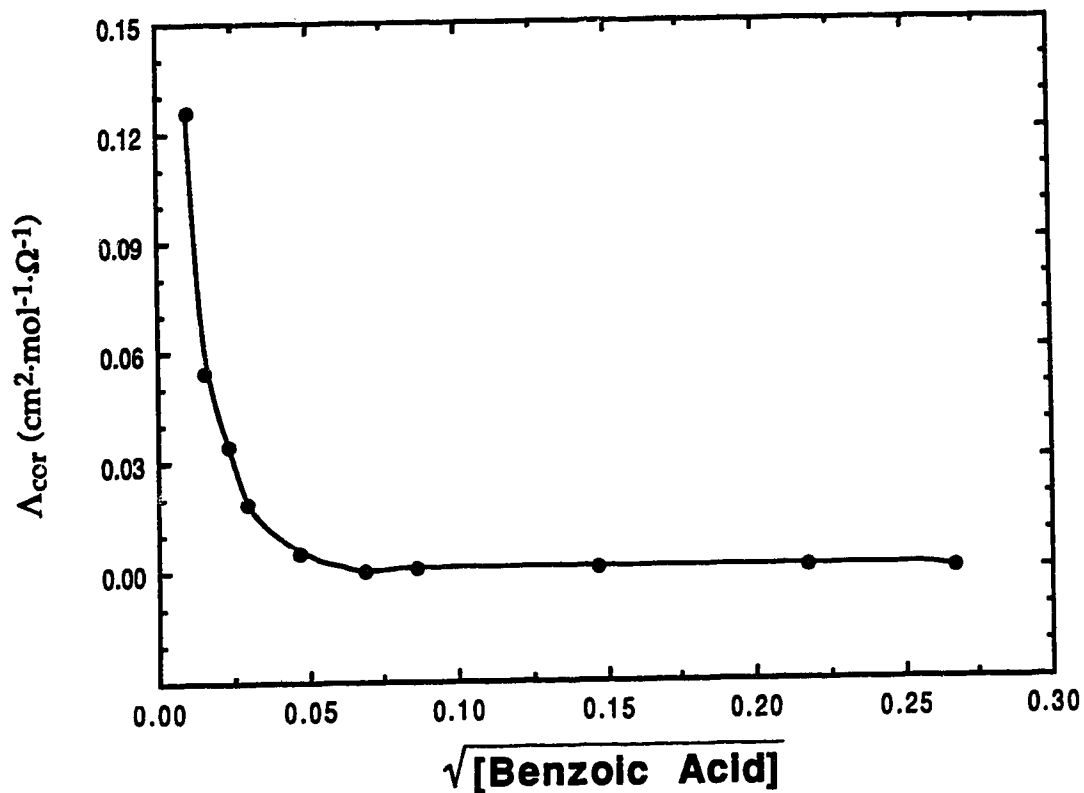


Figure 5.12 Plot of Λ_{cor} vs the square root of concentration for benzoic acid in PVC/DOA/KTPB for the R_g data of figure 5.10. The anomalous behaviour of the resistance curve at low concentrations is not apparent. The line shown is for clarity only.

TABLE 5.17: R_g and Λ_{cor} data measured for benzoic acid in normal membranes (Series 2), plotted in Figure 5.13 and used in least squares analysis; points which were used in the analysis have values of weight and $\Delta\Lambda$ included in the table. λ was assigned a value of 4 Å for the calculation

[Benzoic Acid] (Series 2)	R_g ($M\Omega/m^2$)	Λ_{cor} ($\Omega \text{ mole}^{-1} \text{ cm}^2$)	$\Delta\Lambda$	Weight (W)
0 M	20.3			
1.04×10^{-3}	19.3	.000874	-.000331	2.15×10^{-7}
4.04×10^{-3}	16.7	.000929	.000323	1.24×10^{-5}
3.12×10^{-2}	17.8	.0000787	-.0000295	5.00×10^{-4}
5.26×10^{-2}	18.3	.0000363	.0000255	1.12×10^{-3}
7.49×10^{-2}	15.5	.0000713	.00000357	5.81×10^{-3}
8.34×10^{-2}	14.3			
$K_d = 6.90 \times 10^{-6}$		$\Lambda_o = 0.012$		
$SK_{d,rel} = 0.43 \%$		$S\Lambda_{o,rel} = 33 \%$		

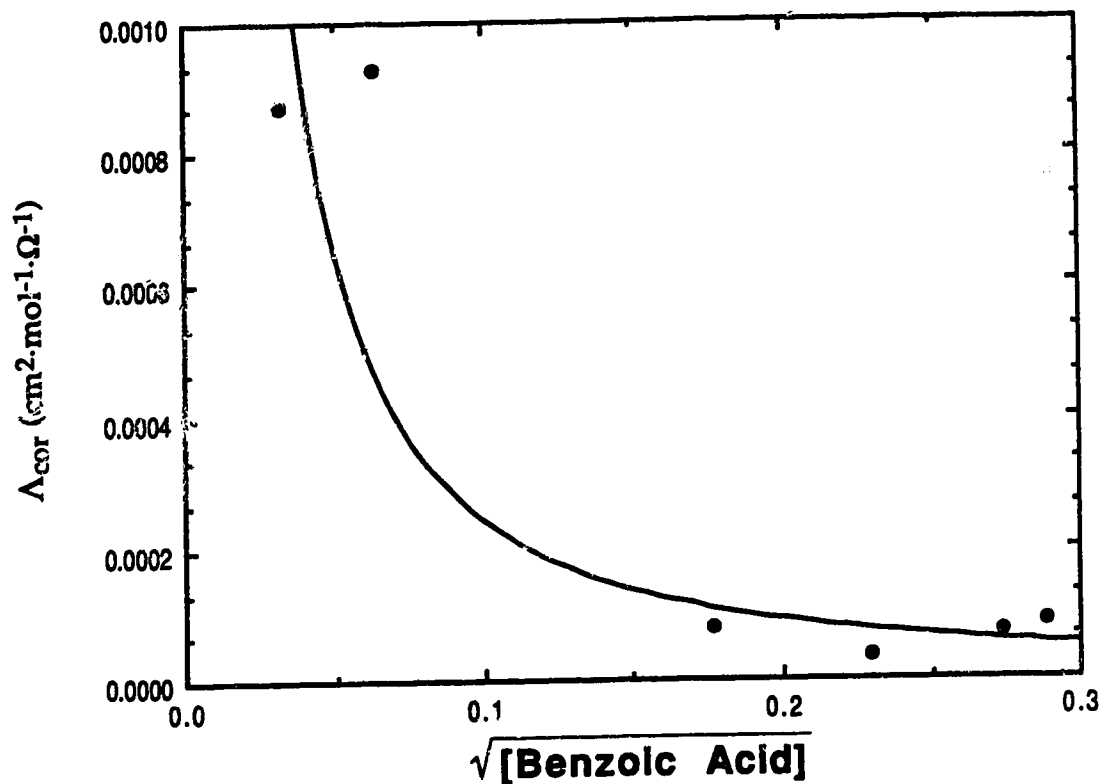


Figure 5.13 Plot of Λ_{cor} vs the square root of concentration for benzoic acid in the normal membranes for the R_g data of figure 5.11. Again, the anomalous behaviour of the resistance curve at low concentrations is not apparent. The line shown is for clarity only.

anomalous behaviour caused by what is considered to be some type of precipitation effect. As σ data in this region is affected not only by acid dissociation, but also by an ion exchange process whereby fixed sites are converted from a (R^-A^+) form to an (RH) form, it was decided to determine a K_d and Λ_0 for the acid in this matrix using points obtained at concentrations greater than 5 mM. The correction of σ for contributions from the matrix was carried out using as σ_0 the σ of a membrane whose acid concentration was about 5 mM. Benzoic acid concentrations for points obtained beyond the 5 mM mark were also corrected by subtracting 5 mM from the nominal concentrations of these membranes. This was done to take into account the postulated involvement of benzoic acid in processes besides simple dissociation at concentrations up to 5 mM. $\Lambda_{cor}(2)$ values were calculated from σ 's corrected as described above and corrected acid concentrations.

Table 5.17 presents the impedance data used in the determination of K_d and Λ_0 for benzoic acid in normal membranes. These points form a portion of the data set represented by curve 2 in Figure 5.11 for membranes of this type. In this case, σ 's were corrected in the usual manner, and nominal concentrations were used to calculate Λ_{cor} 's. This was because the observed behaviour at concentrations less than 40 mM was not as extreme as that observed for the PVC/DOA/KTPB matrix.

The values of K_d for benzoic acid in the PVC/DOA/KTPB and in the normal membrane matrix were found to be 5.6×10^{-7} and 6.9×10^{-6} , respectively. The latter value is of exceptionally good precision, when one compares this to the error associated with K_d 's measured for the salts and benzoic acid in PVC/DOA/KTPB. The difference in K_d values is likely not due to matrix effects, but to the experimental error associated with correction for the matrix σ and the complications induced by the complex concentration

dependence of R_g at low concentrations of benzoic acid. These values are remarkably high for a solution of such low dielectric strength, when one considers that pK_d values for benzoic acid generally range from 11 to 20 in non-aqueous solvents. Even in ethanol, a solvent having an ϵ of 24.3, the pK_d of benzoic acid has been found to be only 10.25 [33]. This is not surprising since the degree of reaction of benzoic acid with the solvent to yield benzoate and a protonated solvent molecule is expected to be less in ethanol than in water. However, the K_d values of benzoic acid in the membrane matrices above are at least 5 orders of magnitude greater than those found in most non-aqueous solvents, and not that much smaller than the acid's K_d in water, which is 6.31×10^{-5} [22]. Moreover, a comparison of values of K_d found for the various salts with the acid K_d 's above shows that the margin of difference between acid and salt values (which fall around 1×10^{-5} to 4×10^{-5}) is much less than expected. The dissociation of benzoic acid must therefore be occurring in the presence of water. Several authors have noted that water does enter the membrane [2,34-35]. Qualitative evidence for this is provided by membranes that have been soaked in aqueous solution, which appear cloudy to the eye presumably because of the presence of small water droplets [34]; this has been observed throughout the course of the various studies reported here and in preceding chapters as well. More quantitative spectroscopic measurements performed in this lab show the water level in the membrane to be approximately 1 % after equilibration with the bathing solution [35]. What form water takes once in the membrane, and what role or roles it may play in determining membrane properties, and ultimately membrane response characteristics, is still a matter of some speculation. These results for benzoic acid demonstrate that the presence of water in the

membrane can have a definite effect on the behaviour of neutral acidic species solubilized in this phase.

5.5 CONCLUSION

The studies presented in this chapter confirm the applicability of the AC impedance method to the characterization of liquid PVC-based membranes.

The behaviour in the membrane of benzoate salts of K^+ , Na^+ , and TEA^+ , as well as $NaClO_4$, was investigated. The Fuoss conductance function for associated electrolytes proved to be an appropriate means to analyze the resulting data. As expected, ion-pairing of these solutes is significant in this medium, as indicated by the observed K_d 's. The high viscosity of the matrix resulted in the determination of Λ_0 values which were generally 3 to 4 orders of magnitude less than those observed for the same salts in water. Comparison of the Λ_0 for $NaClO_4$ with the Λ_0 of $NaBz$ suggested that the mobility of ClO_4^- is substantially larger than that of Bz^- , making ClO_4^- a more active participant in the conduction of charge. This would account in part for the interference in the potentiometric response of ISE's observed when ClO_4^- is present in the test solutions.

Since successful employment of liquid membrane ISE's in the analysis of physiological fluids depends on the reduction of interferences caused by the neutral species present, the mechanism by which these species affect membrane response is of concern. As illustrated by the work presented in this chapter, AC impedance analysis provides a sensitive means by which the behaviour of neutral species in the membrane may be characterized.

Measurement of the σ of membranes containing benzoic acid as a function of temperature gave insight into the dissociation mechanism by which this neutral species influences the membrane's electrical properties, through determination of an E_a for this process. The relatively large K_d observed for benzoic acid provides clear evidence for the presence of water in the membrane. More importantly, the presence of water must be considered to affect the various chemical equilibria in the membrane for any ions that are strongly solvated by water. This means that use of equilibrium constants determined in pure, dry organic solvents in calculations for equilibria and selectivity coefficients in membranes may not yield viable results. It appears, then, that clarification of neutral species interference at ISE's will require a better understanding of the properties and function of water within the membrane.

5.6 REFERENCES

- (1) Buck, R.P., Toth, K., Graf, E., Horvai, G., Pungor, E., *J. Electroanal. Chem.*, 1987, 223, 51
- (2) Thoma, A.P., Viviani-Naner, A., Arvanitis, S., Morf, W.E., Simon, W., *Anal. Chem.*, 1977, 49, 1567
- (3) Morf, W.E., Simon, W., *Helvetica Chim. Acta*, 1986, 69, 1120
- (4) Boles, J.H., Buck, R.P., *Anal. Chem.*, 1973, 45, 2057
- (5) Yurinskaya, V.E., Stefanova, O.K., Maternova, E.A., Yukhno, O.A., *Elektrokhimiya*, 1980, 16, 320
- (6) Fuoss, R.M., Accascina, F., "Electrolytic Conductance", Interscience Pub., New York, 1959
- (7) Robinson, R.A., Stokes, R.H., *Electrolyte Solutions*, Butterworths Scientific Publications, London, 1955
- (8) Büchi, R., Pretsch, E., Simon, W., *Helvetica Chim. Acta*, 1976, 59, 2327
- (9) Band, D.M., Kratochvil, J., Treasure, T., *J. Physiol. (London)*, 1976, 265, 2P
- (10) Bassett, J., Denney, R. C., Jeffery, G. H., Mendham, J., *Vogel's Textbook of Quantitative Inorganic Analysis, 4th Ed.*; Longman: London, 1978
- (11) Brandstrom, A., Berntsson, P., Carlsson, Djurhuus, A., Gustavii, K., Junggren, U., Lamm, B., Samuelsson, B., *Acta Chem. Scand.*, 1969, 23, 2202
- (12) Fuoss, R.M., *J. Am. Chem. Soc.*, 1957, 79, 3301
- (13) Fuoss, R.M., Shedlovsky, T., *J. Am. Chem. Soc.*, 1949, 71, 496
- (14) Shedlovsky, T., Kay, R.L., *J. Phys. Chem.*, 1956, 60, 151
- (15) Kortum, G., Wenck, H., *Ber. Bunsenges. Physik. Chem.*, 1966, 70, 435
- (16) Fuoss, R.M., Kraus, C.A., *J. Am. Chem. Soc.*, 1933, 55, 476
- (17) Kay, R.L., *J. Am. Chem. Soc.*, 1960, 82, 2099

- (18) Whittaker, E.T., Robinson, G., "*The Calculus Of Observations*" (3rd Ed.), Blackie and Son Ltd., London, 1940
- (19) Lipschutz, S., "*Theory And Problems Of Linear Algebra*" (Schaum's Outline Series), McGraw-Hill Book Co., New York, 1968
- (20) Kratochvil, J., Harris, W.E., "*An Introduction To Chemical Analysis*", Saunders College Pub., Philadelphia, 1981
- (21) Kratochvil, B., Yeager, H., *Topics in Current Chemistry*, 1972, 27, 1
- (22) *C.R.C. Handbook Of Chemistry And Physics*, 64th Ed., Weast, R.C., Ed., C.R.C. Press, Boca Raton, Fla, 1983
- (23) Fuoss, R.M., *J. Am. Chem. Soc.*, 1958, 80, 5059
- (24) Armstrong, R.D., Todd, M., *Electrochim. Acta*, 1987, 32, 155
- (25) Armstrong, R.D., Covington, A.K., Proud. W.G., *J. Electroanal. Chem.*, 1988, 257, 155
- (26) Ostwald, W., *Z. Physik. Chem.*, 1888, 2, 36
- (27) Carmack, G.D., Freiser, H., *Anal. Chem.*, 1975, 47, 2249
- (28) Kallweit, J.-H., *J. Polym. Sci. Pt. A-1*, 1966, 4, 337
- (29) Rosenberg, B., Bhowniik, B.B., Harder, H.C., Postow, E., *J. Chem. Phys.*, 1968, 49, 4108
- (30) Griffiths, P.J.F., Krikor, K.G., Park, G.S., In "*Polymer Additives*", Kresta, J.E., Ed., Plenum Press, New York, 1982, 249
- (31) Lindner, E., Graf, E., Niegreis, Z., Toth, K., Pungor, E., *Anal. Chem.*, 1988, 60, 295
- (32) van den Berg, A., van der Wal, P. D., Skowronska-Ptasinska, M., Sudhölter, E. J. R., Reinhoudt, D. N., Bergveld, P., *Anal. Chem.*, 1987, 59, 2827
- (33) Bates, R. G., *Determination of pH*; John Wiley and Sons: New York, 1964, p. 195

- (34) Horvai, G., Graf, E., Toth, K., Pungor, E., Buck, R. P., *Anal. Chem.*, 1986, 58, 2735
- (35) Li, X., Petrovic, S., Harrison, D. J., *Sens. Actuators*, 1990, B1, 275

CHAPTER 6

CONCLUSIONS

As stated in the introduction, the fundamental objective of this thesis was to obtain a better understanding of the response properties of a liquid K^+ -selective membrane which has found wide application in both ion-selective electrodes (ISE) and ion-sensitive field-effect transistors (ISFET). Of particular interest were the interference phenomena observed at ISE's and ISFET's in the presence of lipophilic anionic species and neutral acidic species (in the latter case) in solution. The main purpose of this concluding chapter is to summarize the progress made in this thesis towards achieving a clearer characterization of the membrane of interest. Also presented are some suggestions for future work in this general vein, inspired by various aspects of the studies carried out during the course of this research.

6.1 SUMMARY OF PROGRESS

Interferences to ISFET response generally arise at the membrane-coated gate of the device. A knowledge of the changes that occur in this region when response is affected is therefore required, if such interference problems are to be eliminated. To facilitate studies of liquid membrane-based ISFET response, a membrane-coated silicon electrode was proposed as a model for the ISFET gate; in this instance, the membrane contained the neutral carrier, valinomycin, making it selective for K^+ . Capacitance-voltage measurements showed that the electrode responded to K^+ via the same field effect mechanism as the ISFET, thereby confirming its use as an appropriate

representation of the ISFET. Characterization of the impedance response of this electrode was made possible through an equivalent circuit model consisting of simple circuit elements, as shown in Chapter 2. This allows utilization of the AC impedance technique to gain valuable information about the response properties of the membrane/insulator/silicon structure of the ISFET gate. Practical considerations such as ease of preparation and handling in a laboratory situation also make the use of membrane-coated silicon electrodes advantageous in ISFET studies.

A study examining the interference of neutral acids such as benzoic acid at K^+ -selective ISFET's demonstrated the usefulness of the silicon electrode discussed above. Results of capacitance-voltage and UV spectroscopic measurements verified the hypothesis that these neutral acids were capable of permeating the membrane and undergoing acid-base chemistry at the insulator surface, causing a change in the charge state at this interface. Having established the mechanism of the interference, it became clear that the problem could be eliminated by passivation of the insulator surface. This was accomplished through interposition of a Ag/AgCl layer between the membrane and the insulator, thereby rendering the insulator surface inert to acid/base chemistry. The response of electrodes having an n-Si/insulator/Ag/AgCl/membrane structure was found to be unaffected by the presence of benzoic acid in test solutions. This represents a significant step forward in the development of a K^+ -ISFET which may be employed in assays of K^+ in whole blood, since the presence of neutral species such as benzoic, ascorbic, and carbonic acids in blood has restricted the effectiveness with which these devices may be used in this medium.

Another interesting result of this study was the observation that, while only benzoic acid in its neutral form affected ISFET response, both benzoic

acid and benzoate were shown by AC impedance analysis to be capable of permeating the membrane. Though the potentiometric response of K^+ -ISE's suffers from interference by lipophilic anions such as picrate, thiocyanate, and perchlorate through a phenomenon known as Donnan exclusion failure, K^+ may be safely assayed using these electrodes in the presence of both benzoic acid and benzoate. The mechanisms underlying the induction of Donnan exclusion failure in certain instances were examined by contrasting membrane permeability to perchlorate and to benzoate/benzoic acid. Theoretical treatments of Donnan exclusion failure predict that this phenomenon will be observed when the fixed site concentration in the membrane is exceeded by the concentration of the interfering species. In agreement with theory, membrane concentrations of perchlorate were found by AC impedance measurements to be greater than site concentrations after only short soaking times, whereas benzoate entered the membrane to a far lesser extent. In this way, AC impedance analysis allowed a direct substantiation of the theoretical description of Donnan exclusion failure not possible through potentiometric measurements alone. The utility of the technique in the investigation of membrane permeability to neutral species was also demonstrated. While benzoic acid was observed to be extracted into the membrane more readily than perchlorate, its effect on membrane properties was less notable than that of either perchlorate or benzoate.

Studies of membrane permeability established a link between membrane conductivity and concentrations of extracted salts and neutral species. Behaviour of these species within the membrane could then be considered by exploiting the well-known relationship between conductance and concentration. A detailed analysis of membrane conductance as a function of concentration enabled the determination of values of dissociation

constants, K_d , and limiting conductance, Λ_0 , for various benzoate salts, NaClO_4 , and benzoic acid. The relatively large K_d of benzoic acid in the membrane clearly indicated the presence of water in the membrane. Further, it was apparent that the effect of water on membrane properties and on chemical equilibria with this phase should not be underestimated.

6.2 DIRECTIONS FOR FUTURE WORK

AC impedance analysis has been shown to be a powerful tool for investigating membrane permeability in the studies presented in this thesis. Attention has been focussed primarily on a liquid K^+ -selective membrane based on the neutral ion-carrier, valinomycin. However, plasticized polymer membranes incorporating ion exchangers have found wide application in the field of ion-selective electrode technology. Numerous examples of such systems are given in the review of ref. [1]. The salts of large quaternary ammonium ions have been found to serve particularly well as anion exchangers in these membranes [2,3], since the hydrophobicity of the ammonium cation ensures that it remains in the organic phase to provide exchange sites for the transfer of anions between aqueous and membrane phases. Liquid anion exchange electrodes based on these salts have proven to be quite useful in the determination of a wide variety of inorganic and surfactant anions. However, this versatility is generally accompanied by an increased susceptibility to interference from anions other than the species of interest. Many electrode systems are also characterized by anomalous behaviour in the initial hours of use, which manifests itself as a noisy, drifting response. Quantitative measurements often cannot be made until the

electrode in question has been exposed to aqueous solutions of the ion being determined for several hours. This conditioning phenomenon implies that the process by which anions permeate the membrane is affected by changes in membrane properties brought about by exposure to aqueous solution. While studies employing AC impedance analysis to examine the response properties of liquid membranes have become more common over the past number of years, most have considered membranes based on neutral carriers only. Some research using impedance measurements has been conducted on the behaviour of ion exchange salts in membranes [2,4], but many questions remain as to the response of these membranes to various interferences, as well as the conditioning phenomenon often observed [5]. A natural extension of the work carried out in this thesis, then, would see AC impedance analysis being used in conjunction with other electrochemical techniques to more clearly define the response mechanisms of anion exchanger-based membranes.

Neutral species interference at the K^+ -selective membrane/insulator interface of an ISFET gate was considered in Chapter 3, with particular attention being paid to benzoic acid. The successful utilization of capacitance-voltage and impedance measurements to describe the mechanism of this interference may spawn some additional projects looking at other neutral interferences to ISFET response. The ubiquitous nature of CO_2 requires that the interference caused by this gas [6] be thoroughly characterized, if reliable ISFET devices are to be developed. Also of interest would be a study of the effect of salicylic acid and its derivatives on ISFET operation, since these benzoic acid-related compounds will be commonly present in blood. The ability to monitor permeation of the membrane by neutral acidic species provided by impedance measurements suggests that the technique might well be

technique might well be applicable to the study of other non-classical interferences to both K^+ -selective electrodes and ISFET's stemming from the complex matrices of biological samples such as urine and blood [7,8]. Little as yet is known concerning the eventual degradation in ion-selective electrode response that is observed in the presence of matrix components such as proteins and phospholipids [9].

It became increasingly apparent during the course of the work reported in this thesis that water functions in a complicated manner to affect chemical equilibria within the liquid membranes in question. As a result, the membrane cannot be regarded as a pure dry organic phase when exposed to aqueous solutions. Clarification of the role that water plays in determining membrane properties and equilibria would prove beneficial in understanding membrane response behaviour. This could conceivably be achieved in part through the use of spectroscopic techniques such as NMR and IR.

As discussed in Chapter 3, the application of liquid ion-selective membrane technology to ISFET's can result in some unique interferences arising at the membrane/insulator interface, due to the permeability of the membrane to certain neutral species [6]. Passivation of the insulator surface with an Ag/AgCl layer was proposed as one method of eliminating this problem. While this proved to be an effective solution in this case, use of an Ag/AgCl layer may not always be appropriate, since the presence of a pool of anions is required if the membrane/AgCl interface is to be maintained at a constant potential. Hence, it would be of interest to investigate further the possible use of other materials as underlying solid-state contacts. One suggestion has been to deploy a layer of buffered hydrogel [10] between the membrane and insulator. Hydrogels saturated with certain salts could be expected to stabilize the local pH at the insulator surface, while at the same

constant through the presence of a fixed activity of K^+ (in the case of K^+ -selective membranes) or some other species, depending on the nature of the membrane deposited over the hydrogel. Though in theory the introduction of a layer of hydrogel or some other material over the insulator seems ideal, practical considerations, such as deposition of the membrane over the material, stress developed due to swelling characteristics, and loss of ions from the hydrogel phase may be difficult to address. AC impedance methods could prove particularly useful in evaluating the fundamental behavior of these more complicated structures.

6.3 REFERENCES

- (1) Arnold, M. A., Meyerhoff, M. E., *Anal. Chem.*, 1984, 56, 22R
- (2) Mathis, D. E., Buck, R. P., *J. Memb. Sci.*, 1979, 4, 379
- (3) Dowle, C. J., Cooksey, B. G., Ottaway, J. M., Campbell, W. L., *Analyst*, 1987, 112, 1299
- (4) Mathis, D. E., Stiver, F. S., Buck, R. P., *J. Memb. Sci.*, 1979, 4, 395
- (5) Morf, W. E., Simon, W., *Helvet. Chim. Acta*, 1986, 69, 1120
- (6) Fogt, E. J., Untereker, D. F., Norenberg, M. S., Meyerhoff, M. E., *Anal. Chem.*, 1985, 57, 1995
- (7) Jenny, H. B., Riess, C., Ammann, D., Magyar, B., Asper, R., Simon, W., *Mikrochim. Acta*, 1980, II, 309
- (8) Koch, D.D., Ladenson, J.H., *Anal. Chem.*, 1983, 55, 1809
- (9) Harrison, D. J., *J. Electroanal. Chem.*, 1990, 278, 193
- (10) Bergveld, P., Sibbald, A., *Analytical And Biomedical Applications Of Ion-Selective Field Effect Transistors*, Elsevier: Amsterdam, 1988